THE INFLUENCE OF AGITATOR TYPE ON FLUID DYNAMICS AND OXYGEN MASS TRANSFER IN A PILOT SCALE MIXING VESSEL

by

MICHAEL KEITH DAWSON

A thesis submitted to the Faculty of Engineering of the University of Birmingham for the Degree of DOCTOR OF PHILOSOPHY.

School of Chemical Engineering

University of Birmingham

Birmingham

B15 2TT

England

January 1992.

ABSTRACT

The power consumption (gassed and ungassed), bulk and local impeller fluid dynamics, gassed hold-up and oxygen mass transfer characteristics of a variety of industrially significant agitator types have been investigated using a pilot-scale mixing vessel. The purpose built perspex vessel of 0.72 m diameter was operated at both H/T=1 (V=0.293 m^3) and H/T=2 (V=0.586 m^3). Agitators tested were the Ekato InterMIG^R, Lightnin' A315 hydrofoil, Rushton disc turbine, pipe-section disc turbine and mixed flow impeller, with the latter in both upward and downward pumping modes. Test fluids were deionised water and solutions of non-Newtonian, shear-thinning sodium carboxymethylcellulose, giving a viscosity range of from 0.001 Pa.s to 0.4 Pa.s. Gas flowrates of up to 1.5 vvm and gassed power inputs of up to 5 kWm^{-3} were used.

A novel steady-state oxygen mass transfer measurement technique was developed and used to determine the volumetric oxygen mass transfer coefficient (k_La). The technique utilizes the continuous generation of oxygen in the liquid phase by the degradation of hydrogen peroxide in the presence of the enzyme catalase. The oxygen produced in this manner is stripped from the liquid phase by the continuously flowing gas phase until steady-state conditions are achieved. The technique proved to be easy to use, provided reproducible results and was independent of peroxide concentration over a wide range and catalase concentration over a more restricted range. It avoids potential problems associated with tiny bubble hold-up and gas phase mixing encountered when using dynamic techniques in viscous liquids.

At constant P/V and v_s in water, inter-impeller k_La and hold-up variation was low. The k_La and ε_G dependence on P/V was similar irrespective of impeller, but dependence on v_s was not. Low viscosity CMC solutions provided equal or greater k_La and hold-up than water due to coalescence suppression. Higher viscosity solutions provided greatly

reduced k_La and hold-up. Inter-impeller k_La and hold-up variation rose with increased shear-thinning viscosity. Low power number agitators (InterMIG, A315) consistently provided enhanced k_La at constant power input and gas velocity in CMC. Correlation of k_La data for various impellers in CMC was achieved with the inclusion of an apparent viscosity term. Low power number impellers ran at higher speed and hence lower apparent viscosity at a given power input, supporting the use of the Metzner and Otto[4] shear-rate determination method for viscosity dependent k_La correlation.

TO LOUISE

ACKNOWLEDGEMENTS

Primarily, I would like to thank Professor A.W.Nienow for his unstinting support and encouragement throughout the duration of this work.

Secondly, I am extremely grateful for the technical expertise and bonhomie provided by John Homer, Sid Chatwin and Bob Sharpe, aswell as the organizational talents of Bob Badham.

I also greatly appreciate the interest and advice of fellow members of the School of Chemical Engineering Mixing Group, especially Waldek Bujalski, Gul Ozcan-Taskin, Shaliza Ibrahim, Dave Weale, Caroline McFarlane and Noboru Otomo.

My profuse thanks to Wendy Keil and Val Walker for typing, not to mention Suze Dawson for her production of figures and diagrams.

Finally, I gratefully acknowledge the financial support of the National Engineering Laboratory aswell as the advice of Alan Hickman, George Moody and Debbie Crozier.

CONTENTS.

		Page No.
CHAPTER 1	**INTRODUCTION.**	1
1.1	MOTIVATION AND AREAS OF INTEREST.	1
1.2	LAYOUT OF THESIS.	4
CHAPTER 2	**BACKGROUND AND LITERATURE.**	6
2.1	INTRODUCTION.	6
2.2	RHEOLOGY.	6
2.3	DIMENSIONLESS NUMBERS.	10
2.4	UNAERATED POWER.	13
2.5	AERATED POWER.	17
2.6	GASSED HOLD-UP.	27
2.7	OXYGEN MASS TRANSFER.	30
2.8	$k_L a$ MEASUREMENT METHODS.	34
2.9	CHOICE OF $k_L a$ MEASUREMENT TECHNIQUES.	44
CHAPTER 3	**EXPERIMENTAL EQUIPMENT AND TECHNIQUES.**	46
3.1	INTRODUCTION.	46
3.2	MIXING VESSELS AND ANCILLARY EQUIPMENT.	46
3.3	POWER MEASUREMENT.	51
3.4	BULK FLOW AND LOCAL IMPELLER FLUID DYNAMICS.	52
3.5	GASSED HOLD-UP.	54
3.6	$k_L a$ MEASUREMENT: THE NEL/HICKMAN TECHNIQUE.	55
3.7	TEST FLUIDS.	63
CHAPTER 4	**INTERMIG POWER AND FLUID DYNAMICS.**	67
4.1	INTRODUCTION.	67
4.2	FLOW PATTERNS AND SURFACE AERATION.	72
4.3	UNAERATED POWER CHARACTERISTICS.	75

4.4 AERATED POWER CHARACTERISTICS IN WATER. 83

4.5 AERATED POWER CHARACTARISTICS IN CMC. 104

4.6 VESSEL VIBRATION. 111

4.7 CONCLUSIONS. 112

CHAPTER 5 THE POWER AND FLUID DYNAMICS OF OTHER IMPELLERS TESTED.

5.1 INTRODUCTION. 115

5.2 FLOWPATTERNS. 121

5.3 UNAERATED POWER DRAW. 125

5.4 AERATED POWER AND BULK FLOW CHARACTERISTICS. 134

5.5 DISCUSSION AND CONCLUSIONS. 151

CHAPTER 6 GASSED HOLD-UP. 155

6.1 INTRODUCTION. 155

6.2 HOLD-UP RESULTS IN WATER. 155

6.3 HOLD-UP IN NON-NEWTONIAN CMC. 166

6.4 EFFECT OF VISCOSITY ON HOLD-UP IN CMC. 182

6.5 COMPARISON OF HOLD-UP RESULTS WITH THE LITERATURE. 187

6.6 CONCLUSIONS. 191

CHAPTER 7 OXYGEN MASS TRANSFER RESULTS. 193

7.1 INTRODUCTION. 193

7.2 OXYGEN MASS TRANSFER RESULTS IN WATER. 194

7.3 OXYGEN MASS TRANSFER RESULTS IN 0.07% CMC. 203

7.4 OXYGEN MASS TRANSFER RESULTS IN 0.4% CMC. 209

7.5 OXYGEN MASS TRANSFER RESULTS IN 0.8% CMC. 214

7.6 INFLUENCE OF APPARENT VISCOSITY ON k_La. 222

7.7 GAS PHASE POWER INPUT AND MIXING MODEL SIGNIFICANCE. 230

7.8 COMPARISON OF k_La RESULTS WITH THOSE FROM LITERATURE. 233

CHAPTER 8 CONCLUSIONS AND FURTHER WORK. 244

8.1 CONCLUSIONS. 244

8.2 FURTHER WORK. 248

APPENDIX I INTERMIG AND MIG LITERATURE SURVEY. 250

1. INTRODUCTION. 250

2. DIMENSIONS. 252

3. FLOW PATTERNS. 253

4. VELOCITY FIELDS. 254

5. UNAERATED POWER CHARACTERISTICS. 256

6. AERATED POWER CHARACTERISTICS. 263

7. SPARGERS. 271

8. VESSEL VIBRATION. 272

9. MASS TRANSFER. 275

10. FERMENTATION. 277

APPENDIX II MASS TRANSFER IN AERATED AGITATED VESSELS: ASSESSMENT OF THE NEL/HICKMAN STEADY-STATE METHOD. 279

APPENDIX III NEL/HICKMAN TECHNIQUE. 288

1. CATALASE CONCENTRATION AND INTERBATCH REPRODUCIBILITY. 288

2. HYDROGEN PEROXIDE CONCENTRATION. 294

3. MULTIPLE DISSOLVED OXYGEN PROBES. 298

4. CALCULATION OF $k_L a$ FROM EXPERIMENTAL DATA. 300

5. ESTIMATION OF ERRORS. 306

NOMENCLATURE. 310

REFERENCES. 314

1. INTRODUCTION

1.1 MOTIVATION AND AREAS OF INTEREST

Many commercially important chemical and biochemical operations rely on gas-liquid contacting. These may involve adsorption or desorption of the gas followed by chemical reaction or utilization by micro-organism. The processes concerned include reactions such as oxidations, hydrogenations, chlorinations etc. as well as biochemical operations such as aerobic fermentation and waste-water treatment. Devices used for gas-liquid contacting vary considerably in design depending on process requirements. Typically a high interfacial area for mass transfer is achieved by passing the liquid over a solid support of high surface area or by sparging the gas into the liquid. In the latter case mechanical agitators are often used to promote liquid turbulence, break-up gas bubbles, circulate the two phase mixture and increase homogeneity. Mass and heat transfer are thereby enhanced but installation and power consumption costs for agitation are considerable, necessitating careful optimization on economic grounds.

This study focuses on the transfer of oxygen from air to aqueous solutions in gas sparged and agitated vessels, a situation commonly found in the fermentation industry. Applications include the production of biomass (yeast or single cell protein), metabolites (e.g. antibiotics) and macromolecular enzymes or polysaccharides. Oxygen utilization by aerobic micro-organisms is primarily to provide energy for growth and product formation via respiration. Oxygen is taken up from the liquid phase where it is only sparingly soluble, making continuous supply from the gas phase necessary. Should aeration fail, the dissolved oxygen in a fermentation broth is likely to last a matter of seconds only. Shortage of oxygen may reduce cell growth and product yield, cause the formation of unwanted by-products and possibly cell death. Oxygen transfer is

therefore rate limiting in many commercial fermentations.

Fermentation broths are usually more viscous than water and often of non-Newtonian rheology (see Section 2.2). Factors that may influence the rheology include high substrate concentration (e.g. glucose), product formation (e.g. Xanthan or Alginate) and cell morphology (e.g. fungal mycelia). The liquid rheological properties can have a significant effect on the process performance. Turbulence is reduced with increasing viscosity (at constant stirrer speed) in turn reducing heat and mass transfer rates. Mixing times also tend to increase with viscosity leading to the formation of concentration gradients for oxygen and substrate. Many broths exhibit non-Newtonian shear-thinning behaviour which causes a rapid reduction in shear rate away from the turbulent impeller region. This results in stagnant or near-stagnant zones around the periphery of the vessel, particularly behind baffles or other vessel internals such as heat exchange coils. The coalescence of bubbles is commonly inhibited in fermentation broths when compared with pure water due to the presence of media components, electrolytes for pH control, anti-foams and micro-organisms. The degree of coalescence affects gas-liquid interfacial area and hence mass transfer rate.

The rheological and coalescence properties of fermentation broths often vary with time, making identification of their respective influences on oxygen transfer extremely difficult. The variation of micro-organism growth characteristics also tends to make reproducing fermentations for experimental purposes problematic. Additionally fermentations on the pilot or larger scale are very expensive. For these reasons, a common research approach is to use model fluids, generally in the absence of micro-organisms, enabling rheological properties to be more precisely controlled. Model fluids include electrolyte solutions, viscous Newtonian liquids (e.g. glucose, glycerol or Versicol) and non-Newtonian liquids (e.g. CMC, Natrasol and Carbopol) to model polysaccharide fermentations or

fibrous materials (e.g. paper pulp) to model mycelial fermentations.

The optimization of bioreactor performance requires an understanding of the influences of agitator type, geometry, power input, speed, gassing rate, liquid properties and vessel configuration on oxygen transfer rates. Most industrial fermenters do not feature accurate measurement of agitator power input, so that design data must be acquired from experimentation using purpose built mixing vessels equipped with accurate torque measurement instruments. Although the unaerated power draw of some commonly used impeller types (e.g. Rushton turbines) can be accurately predicted from empirically derived correlations, this is not the case with aerated power draw despite much research. In order to obtain a better understanding, observations of the gas-liquid dispersion in transparent walled vessels have been used to link impeller and bulk fluid dynamics to aerated power draw.

The research effort into mixing and mass transfer in aerated, agitated vessels has been considerable in recent years, due in part to a desire to identify impeller designs which offer improvements over the very widely used Rushton turbine. Many impeller manufacturers claim enhanced performance for their products, yet independent data on the proprietary impellers is scarce, particularly with respect to mass transfer. Significant advances have, however, been made towards the basic understanding of mixing in fermenters but with certain important limitations. These are:

1) Multi-impeller, high aspect ratio vessel configurations typical in industrial practice have seldom been used.

2) The scale of operation at which accurate power and mass transfer measurements have been carried out has generally been rather small.

3) Oxygen mass transfer measurement methods developed for use in air-water systems cannot easily be applied to rheologically complex fluids.

This study sets out to address some of the aforementioned

deficiencies in the current understanding of mixing and mass transfer in agitated, aerated vessels. To this end a purpose built perspex vessel of 0.72 m diameter and a 2:1 aspect ratio was employed (Chapt.3) in order to provide data with the high degree of accuracy usually associated with small scale studies. Both water and various concentrations of non-Newtonian shear-thinning CMC were used as test fluids. The principal agitator tested was the InterMIG, a proprietary design from Ekato G.m.b.h. for which only the manufacturers data is generally available (Appendix I). The other impellers tested in a comparative fashion provide a cross-section of the commonly used industrial types, both traditional and new e.g. Rushton turbine, concave turbine, pitched-blade turbine (mixed-flow) and hydrofoil. Established techniques for torque and hold-up measurement as well as bulk flow and local impeller flow visualisation were used. A novel steady-state oxygen mass transfer measurement technique was developed. This technique is potentially simple, low cost and applicable to rheologically-complex systems.

1.2 LAYOUT OF THESIS

The thesis is divided into three main areas: 1) background and literature 2) experimental equipment and techniques and 3) experimental results and discussion. Firstly background and literature are covered in Chapter 2 and Appendix I, the latter comprises a detailed literature survey on the MIG and InterMIG impellers. This is included in the Appendices as it discusses the MIG impeller which is not investigated in the main thesis. Chapter 2 details the background and literature on rheology, dimensionless numbers, unaerated and aerated impeller power characteristics and gassed hold-up. This chapter also outlines oxygen mass transfer theory, $k_L a$ measurement methods and the problems associated with them.

The second main part of the thesis covers experimental equipment,

techniques used and their development. Details of the development of the steady-state technique and the correction of errors concerning its use in the literature are located in Appendices II and III. Equipment used and finalised techniques are described in Chapter 3.

The third and principal area of the thesis presents and discusses experimental findings. The aerated and unaerated power and fluid dynamics of the InterMIG are covered in Chapter 4 and those of the other agitators in Chapter 5. Relative impeller gassed hold-up and k_La results are described in Chapters 6 and 7 respectively, where comparisons with the literature are also made. In Chapter 8, overall conclusions are drawn and areas for future investigation discussed.

2. BACKGROUND AND LITERATURE

2.1 INTRODUCTION

In this chapter, the background to the subsequent experimental sections is described. Firstly relevant rheological theory is given in Section 2.2, followed by a description of the dimensionless numbers used in mixing studies. The next section outlines studies on ungassed agitator power consumption and the factors affecting Po. A detailed description of the aerated power characteristics of the agitators of interest is given in Section 2.5. Gassed hold-up theory and studies are summarised in Section 2.6 whilst oxygen mass-transfer theory is outlined in Section 2.7. The penultimate section comprises a literature survey on techniques used for oxygen mass transfer measurement in agitated vessels. Finally the advantages and disadvantages of the various techniques are compared and a technique chosen. Literature $k_L a$ results are detailed in Chapter 7 where comparisons are made with data from this work.

2.2 RHEOLOGY

The theoretical and practical aspects of rheology are the subject of standard texts[1], this section deals only with the parts of the subject which are of direct relevance to the work carried out. Fluids can be divided into two main rheological classes: Newtonian and non-Newtonian.

2.2.1 Newtonian

Newtonian fluids are defined as exhibiting direct proportionality between applied shear stress, τ, and the resultant shear rate, $\dot{\gamma}$. Therefore:

$$\frac{\tau}{\dot{\gamma}} = \mu = \text{a constant} \qquad (2.1)$$

The parameter μ is termed the 'coefficient of viscosity' or 'viscosity' of the fluid. Newtonian viscosity is dependent on temperature and pressure but independent of shear rate.

2.2.2 Non-Newtonian

Generally non-Newtonian fluids have variable coefficients of viscosity, termed 'apparent viscosity', μ_a. The apparent viscosity (at constant T and P) may depend on the rate of shear, the time of shearing and previous shear history. By analogy with Newtonian fluids,

$$\frac{\tau}{\dot{\gamma}} = \mu_a = \text{a variable} \qquad (2.2)$$

The apparent viscosity is therefore the ratio of shear stress to shear rate at a given value of shear rate.

2.2.2.1 Shear Thinning (Pseudoplastic).

Shear-thinning fluids are those in which apparent viscosity decreases with increasing shear rate (Figs. 2.1 and 2.2) and are typified by many fermentation broths. As Fig. 2.2 shows, at very high and very low shear rates Newtonian behaviour is approximated whereas at intermediate shear rates shear thinning behaviour occurs. This is thought to be due to the changing orientation of large asymmetric molecules within the liquid. At low shear rates the shear effects which tend to organise the tangled molecules are overcome by the random motion of the molecules, hence high resistance to shear and high μ_a. Increasing shear progressively organises and aligns the molecules in the flow direction, causing μ_a to fall. At high shear rates the molecules are thought to become completely aligned and μ_a becomes independent of shear rate. In the region of falling μ_a, a double logarithmic plot of τ versus $\dot{\gamma}$ is often linear over a wide range of shear rates. Where this is the case, the power law equation can be used.

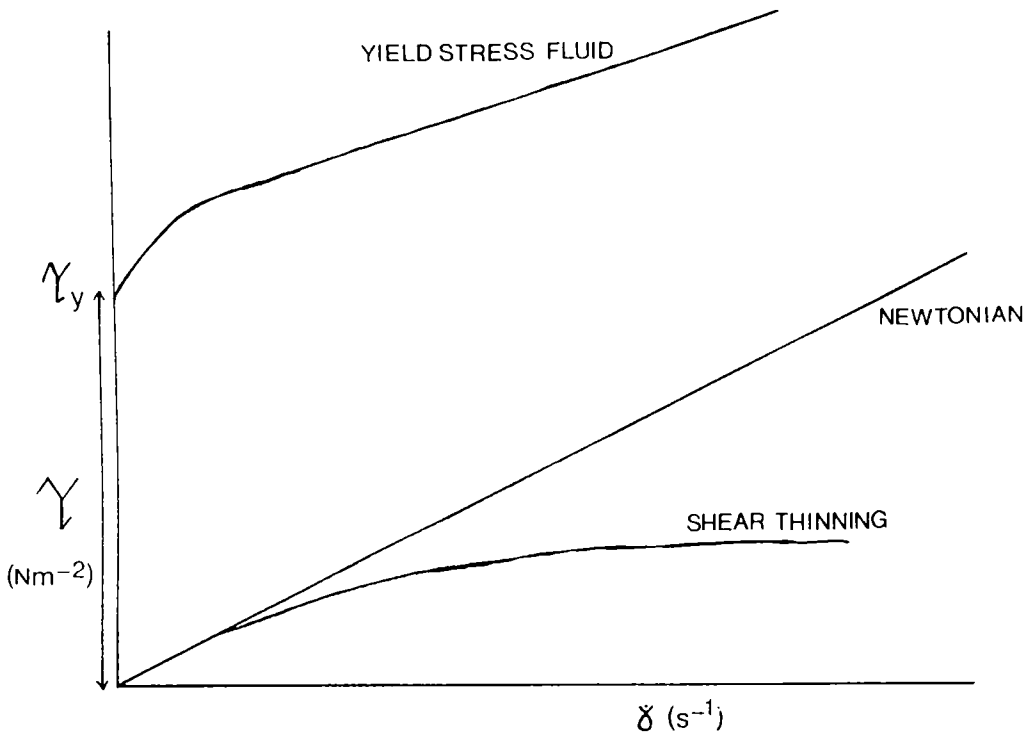

Figure 2.1 Examples of Rheograms.

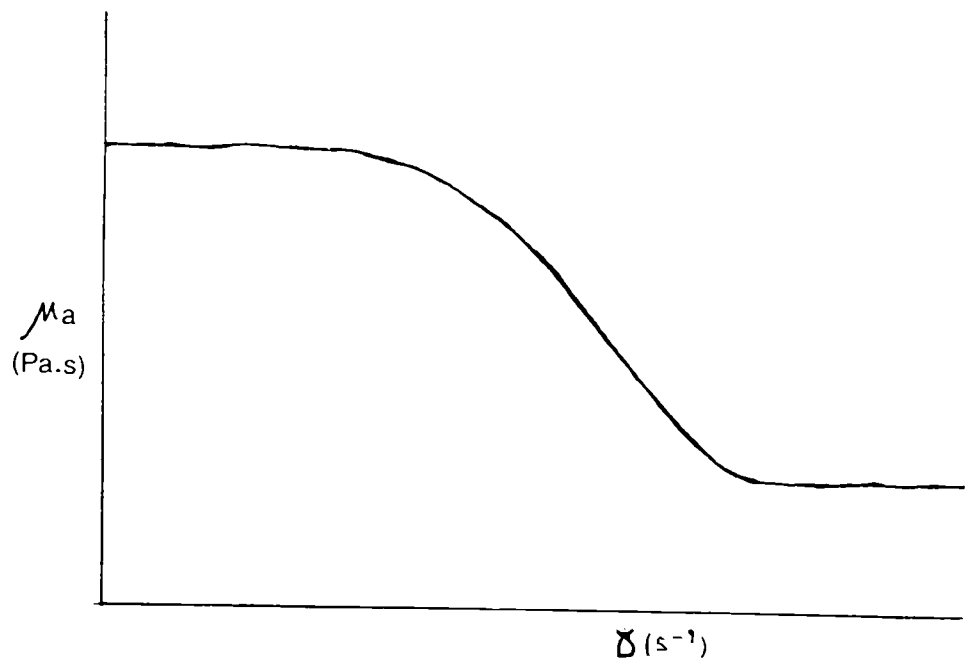

Figure 2.2 Flow Curve for Shear-thinning Fluid.

This takes the form:

$$\tau = K \dot{\gamma}^{n} \qquad , \; n < 1 \text{ for shear-thinning fluids} \tag{2.3}$$

Combining Eqns. 2.2 and 2.3 gives:

$$\mu_a = K \dot{\gamma}^{n-1} \tag{2.4}$$

Where K, ($Ns^n m^{-1}$), is the consistency index and n, (-), is the flow behaviour index. The consistency index, K, is a measure of viscosity at a given rate of shear. The dimensions of K are dependent on the value of n, making comparison of results for different n values difficult. The smaller the value of n, the more rapid the decrease in viscosity with increasing shear rate, making the shear-thinning effects on transport phenomena more pronounced.

Eqn. 2.3 does not accommodate the regions of Newtonian behaviour shown in Fig. 2.2 and is also dimensionally unsound. Other models have been developed[1], although none is completely satisfactory for all shear thinning fluids over the whole shear rate range. The power law model has therefore been used throughout this work.

When agitating a shear-thinning fluid in a stirred vessel the shear rates in the impeller region are typically high, leading to a low apparent viscosity in that region. As the distance from the impeller increases, shear rates fall and μ_a increases. If the shear-thinning fluid also exhibits a yield stress, (Fig. 2.1), i.e. requires a minimum shear stress before fluid flows, a well mixed cavern region is formed around the impeller. Outside this cavern region little or no flow occurs. None of the test fluids used in this work exhibited a yield stress.

2.2.2.2 Viscoelasticity.

Typically highly shear-thinning liquids also exhibit viscoelastic properties. Viscoelastic fluids can be classified as somewhere between Hookean elastic solids and Newtonian viscous liquids[1]. They will flow when subjected to a shear stress, but part of their deformation is recovered upon removal of that stress. The viscoelastic properties of agitated fluids may manifest themselves in the occurrence of unusual phenomena such as reverse flow[2,3,18] or the Weissenberg Effect[1]. These are caused by forces normal to the plane of shear, in the former case reversing the direction of the discharge stream from a turbine and in the latter causing liquid to climb a rotating shaft. Single phase mixing may therefore be affected by alteration of flow patterns whereas two-phase mixing may be affected by changing cavity shape[3].

2.3 DIMENSIONLESS NUMBERS

2.3.1 Determination of Apparent Viscosity

The determination of some of the dimensionless numbers used requires a value for the liquid viscosity. As outlined in Section 2.2, viscosity in non-Newtonian liquids is dependent upon shear rate which varies with position in the vessel. An average value of shear rate, $\dot{\gamma}_{AV}$, must therefore be determined.

Metzner and Otto[4] measured agitator power input (using constant geometry, impeller speed etc.) in the laminar flow regime using Newtonian and non-Newtonian liquids. It was assumed that since viscous forces determine power consumption in this flow regime, power curves (Po v Re) for the differing liquids should be identical. By matching non-Newtonian and Newtonian Power numbers, equivalent Reynolds numbers for non-Newtonian liquids could be determined. Thus, an apparent viscosity for a given stirrer speed could be arrived at. By defining the average shear rate as,

$$\dot{\gamma}_{AV} = \tau / \mu_a \qquad (2.5)$$

they found that $\dot{\gamma}_{AV}$ was linearly related to impeller speed,

$$\dot{\gamma}_{AV} = k_s N \qquad (2.6)$$

where k_s is the Metzner-Otto constant. The value of k_s was found to be dependent upon agitator type[5]. By assigning a value to k_s the apparent viscosity may be found by combining Eqns. 2.4 and 2.6, to give for power law fluids:

$$\mu_a = K (k_s N)^{n-1} \qquad (2.7)$$

Metzner et.al.[5] determined values of k_s using various impeller types and non-Newtonian liquids. They found $k_s = 11.5 \pm 10\%$ for disc turbines, $k_s = 10.0 \pm 10\%$ for propellers and $k_s = 13.0 \pm 15\%$ for pitched blade turbines. Ducla et.al.[6] found k_s to be constant in shear-thinning inelastic liquids but k_s was reduced in viscoelastic liquids. In 1% and 1.25% CMC solutions they found $k_s = 6.1$ to 7.1, depending upon agitator type.

2.3.2 Reynolds Number

In agitated vessels Reynolds number (Re) takes the form:

$$Re = \frac{\rho N D^2}{\mu} \qquad (2.8)$$

where $\mu = \mu_a$ for non-Newtonian liquids. Re represents the ratio of inertial to viscous forces which determine whether the fluid flow is laminar, transitional or turbulent. Both ρ and μ are based on liquid

properties even in gas-liquid dispersions. For a power law fluid Reynolds number can be evaluated by combining Eqns. 2.7 and 2.8:

$$Re = \frac{\rho N^{2-n} D^2}{K k_s^{n-1}} \qquad (2.9)$$

The k_s values used for the various impellers studied are given in Section 3.2.4..

2.3.3 Power Number

The power number, (Po), represents the ratio of the pressure differences producing flow to the inertial forces and is analogous to a friction factor or drag coefficient. Po is usually based on the power input by the impeller for agitated vessels and takes the form:

$$Po = \frac{P}{\rho N^3 D^5} \qquad (2.10)$$

2.3.4 Froude Number

The Froude number represents the ratio of inertial to gravitational forces and takes the form:

$$Fr = \frac{N^2 D}{g} \qquad (2.11)$$

For fully baffled vessels, with no central vortex formation and no aeration, Froude number is generally considered to be unimportant.

2.3.5 Gas Flow Number

The gas flow number (Fl_G) represents the ratio of gas flow rate to a

quantity proportional to the impeller pumping rate and is given by:

$$Fl_G = \frac{Q_G}{ND^3} \qquad (2.12)$$

2.3.6 Galilei Number

The Galilei number is represented as:

$$Ga = \frac{Re^2}{Fr} = \frac{g\ D^3 \rho^2}{\mu^2} \qquad (2.13)$$

Ga has the advantage that the impeller speed, N, is removed from the dimensionless number. This enables the variation of Po due to other parameters such as viscosity to be analysed independently[7].

2.4 UNAERATED POWER

Accurate prediction of the power consumed by a rotating agitator is fundamental in the economic design of mixing processes. Mass transfer rates are often related to specific power inputs so that mixer design begins with this requirement. A motor and drive system should only be specified once a power requirement has been determined and scale-up is often conducted on the basis of constant power. The power consumption of a mixer also contributes significantly to the operating costs.

Agitator power draw and the parameters that influence it have therefore been widely researched. The majority of the work has considered the Rushton turbine (6DT) in vessels of standard geometry (Fig. 2.3). Novel impellers such as the InterMIG (IM), Lightnin' A315 hydrofoil (A315), concave turbine (6PSDT) and to a lesser extent the mixed flow turbine (6MF) have been investigated sparingly.

This section summarises the factors (other than agitator type) that influence unaerated power draw, these have generally been identified using the 6DT.

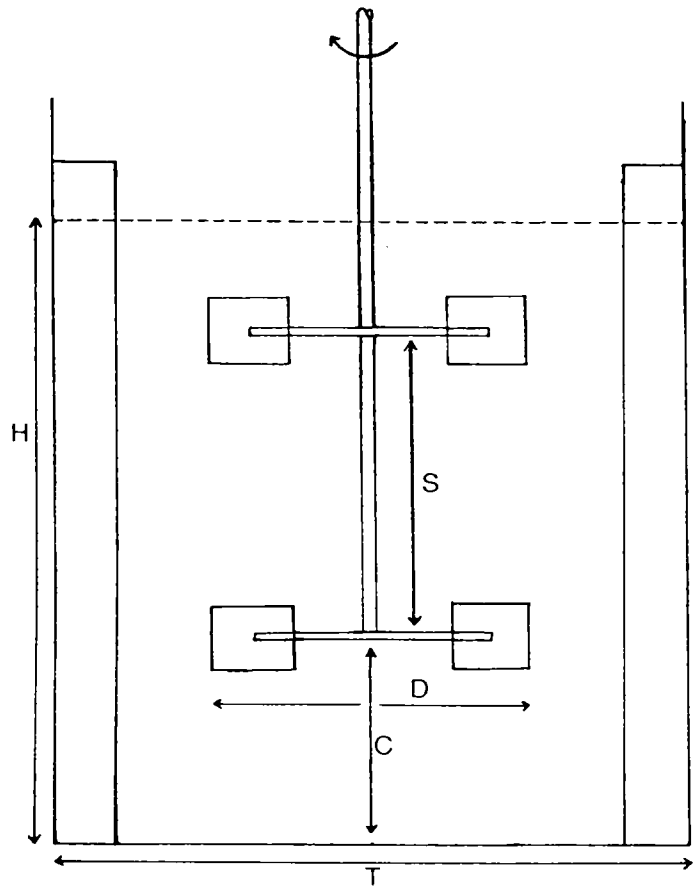

Figure 2.3 Standard Geometry Vessel.

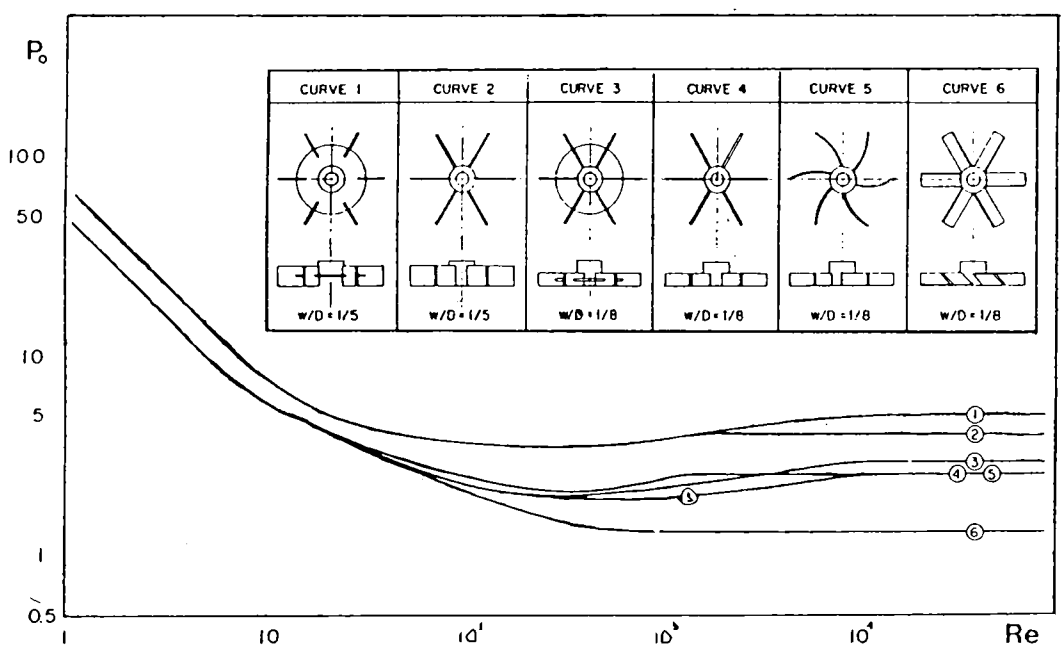

Figure 2.4 Power Curves in Newtonian Fluids for various Turbine Impellers[10].

The unaerated power data in the literature for the impeller types investigated in this study are described elsewhere. IM (and MIG) agitator studies are located in Appendix I, also relevant IM literature results are compared with this work in Chapter 4. 6DT, 6PSDT, 6MF and A315 impeller literature results are compared in Chapter 5.

2.4.1 Power Curves

The power consumed in an agitated vessel may be determined by measuring the torque (M) on the impeller shaft and the rotational speed (N). The power consumption is then given by:

$$P = 2\,\pi.M.N \qquad (2.14)$$

By substituting the measured power (P) and speed (N) in Eqn. 2.10 the power number (Po) may be determined for a given system. The results of studies of power consumption in unaerated mixing are usually presented in terms of the dimensionless groups: Re, Po and Fr. However when geometric similarity is maintained and the vessel is fully baffled, then:

$$Po = f\,(Re)$$

Rushton et.al[8]. and Bates et.al.[9] produced Po versus Re curves (power curves) for unaerated Newtonian liquids using a variety of agitator and vessel geometries. In the laminar flow regime ($Re < 10$) they found:

$$Po = C\,Re^{-1} \qquad (2.15)$$

where C was dependent on system geometry. In the turbulent flow regime ($Re > 10^4$) the power number was found to be constant:

$$Po = A \qquad (2.16)$$

where A was dependent upon agitator type. In the transitional flow regime ($10 < Re < 10^4$) the power number varied non-linearly with Re and the power curve was difficult to characterize.

2.4.2 Influences on Po in the Turbulent Regime

For $Re > 10^4$, A becomes independent of Re but remains dependent upon impeller type. Power curves obtained in Newtonian liquids are shown in Fig. 2.4 for various impeller types[10], wide variation in A can be seen. Nienow and Miles[11] found that, using 6DT, smaller A values were found in smaller vessels and lower A values were found for both small D/T and small C/T ratios. Bujalski[12] confirmed an effect of vessel scale and also showed that the thickness of 6DT blades and disc influenced A. Cronin[13] showed an effect of vessel base shape on Po, again using 6DT.

Variation of A with geometrical changes has frequently been related to the unaerated flow pattern developed[12,13]. The flow patterns developed by agitators used in this study are described in Sections AI.3, 4.2 and 5.2 and the effect of geometrical changes on unaerated power related to them where relevant.

2.4.3 Multiple Impeller Po in the Turbulent Regime

Many industrial mixing applications require that more than one impeller be used because of the vessel geometry (H/T > 1). The separation of and type ofmultiple impeller stages has been shown to influence A[13-16]. Typically maximum power draw is only achieved when the separation is such that the flow patterns from each stage do not interfere with each other. For 6DT agitators in a low viscosity broth, maximum power is drawn at S/T = 0.5 for D/T = 0.33[14,15], S/T = 0.7 for D/T = 0.4[16] and S/T = 1.0 for D/T = 0.5[13]. Increasing S/T above these values will not increase power draw

whereas decreasing S/T reduces power draw. Assuming an impeller spacing of at least one vessel diameter (D/T = 0.5), the power number for n impellers, $(Po)_n$, is approximated by:

$$(Po)_n = n\ Po \qquad (2.17)$$

2.4.4 Viscous Non-Newtonian Fluids

The effect of non-Newtonian behaviour on the unaerated power curve has been commented on by various workers[3,5,7,17-20]. When using the 6DT impeller in inelastic shear-thinning fluids, Po exhibits a sharp minimum in the transitional regime[3,5,18]. Ranade and Ulbrecht[3] found that when using viscoelastic shear-thinning fluids no minimum was apparent and Po was lower than for Newtonian or inelastic shear-thinning fluids in this regime. Hockers[7] findings were similar. Other workers[17,18,20] have found shallow minima when using mildly viscoelastic shear thinning fluids which extend the region of reduced power consumption to higher Re. This has been attributed to the drag reducing tendency of viscoelastic fluids[18]. In the turbulent flow regime slightly shear-thinning CMC solutions have been found to give similar Po values to Newtonian fluids under identical conditions[18].

2.5 AERATED POWER

2.5.1 Introduction

Power drawn in a 6DT agitated vessel falls when gas is introduced. The degree of power reduction has been linked to the aerated bulk flow pattern within the vessel and the shape and size of gas filled cavities which form behind the impeller blades[21]. The variation of gassed power and its relation to the physical phenomena mentioned has been studied extensively using the 6DT but to a lesser extent using the 6MF, 6PSDT

A315, and IM. In the first sub-section the fundamentals of aerated power draw and data presentation will be discussed, referring to the 6DT. Subsequently the literature concerning the aerated power characteristics of the other agitators studied will be discussed with emphasis on differences from the 6DT case. The effect of viscous, non-Newtonian fluids on aerated power draw is described in Section 2.5.7.

Detailed comparisons with results from this work are made in Chapters 4 and 5, whilst the IM and MIG literature is detailed in Appendix I.

2.5.2 6DT

The gas-liquid flow phenomena in the agitator region which determine the gassed power consumption are often complex. This has led to considerable difficulty in the development of empirical correlations to predict the gassed power, P_g. The data obtained using small scale equipment cannot be applied to industrial-scale vessels without detailed understanding of the gas-filled cavities and their role in determining bulk and local flow phenomena.

In systems where the liquid phase has low viscosity, P_g depends on the gassing rate, Q_G. It is conventional to plot the gassed Power Number, Po_g, (or Po_g/Po, which is equivalent to P_g/P) as the dependent variable against the Flow Number, Fl_G. The resultant curves may then be related to both the bulk two-phase flow and the local impeller hydrodynamics determined by cavities. The independent variable, Fl_G, may be varied by either changing Q_G at constant N or changing N at constant Q_G. Each method results in quite different Po_g-Fl_G curve shapes which are not easy to relate to each other. If Q_G is maintained constant and N altered, as in the work of Nienow et al.,[22] the Po_g - Fl_G curve can be related easily to the bulk flow regimes. If N is constant and Q_G altered, as in the work of Smith and Warmoeskerken[23], the Po_g - Fl_G curve can be related more easily to local impeller hydrodynamics (cavities).

The range of bulk flow patterns observed using a 6DT in a cylindrical vessel of H/T = 1 with varying N is shown in Fig. 2.5. From N = 0 to N = N_F (Fig. 2.5a) the flow pattern is dominated by the rising gas i.e. the impeller is flooded. From N_F to N_{CD} (Fig. 2.5b) the gas is discharged horizontally by the agitator i.e. the impeller is loaded. From N_{CD} to N_R (Fig. 2.5c), gas is completely dispersed throughout the vessel. Increasing Q_G at constant N reverses the sequence of bulk flow patterns.

Po_g - Fl_G curves at constant Q_G have been thoroughly discussed by Nienow et.al.[22]. A typical curve for the 6DT is shown in Fig. 2.6. The minimum which occurs as N is increased from zero corresponds to N_{CD}. Further N increase leads to a maximum associated with gross recirculation, N_R. Correlations have been established in order to predict N_F, N_{CD} and N_R for a wide range of D, T, D/T and Q_G[22,24,25]. N_F has been defined as the minimum speed required for vessel design purposes.

The series of cavities observed with changing operating conditions (N or Q_G) are depicted in Fig. 2.7. In the unaerated system strong vortices have been observed behind the blades of the 6DT[26]. Under aerated conditions gas is drawn into these vortices causing a reduction in the pressure drop over the blade. As a consequence drag, power draw and pumping capacity also fall. Increasing Q_G at constant N leads to the sequence of cavities shown in Fig. 2.7. The power drawn generally decreases as cavity structure changes with increasing Q_G, until flooding occurs (ragged cavities). When cavities reach their maximum size the impeller pumping capacity and hence power drawn is a minimum (3-3 cavities). The connection between 6DT cavity form and distribution, and the fall in P_g/P with increasing N has been intensively studied and will not be reviewed further here.

2.5.3 Scaba SRGT, 6PSDT and ICI Gasfoil

van't Riet[28] first showed that if the 6 flat plates of the Rushton

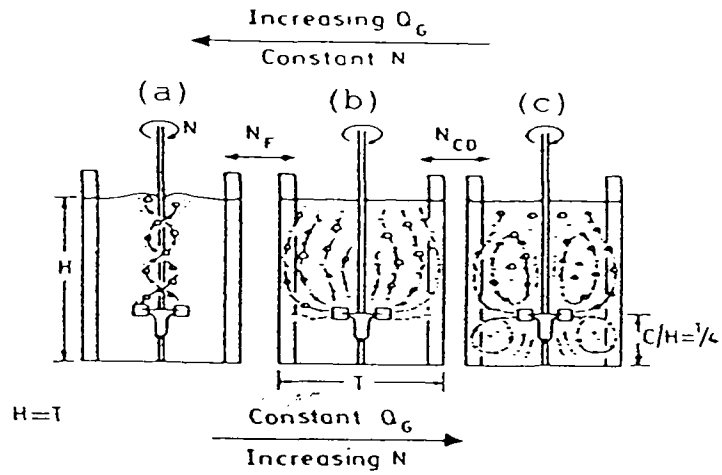

Figure 2.5 Gas-Liquid Bulk Flow Patterns for the 6DT.

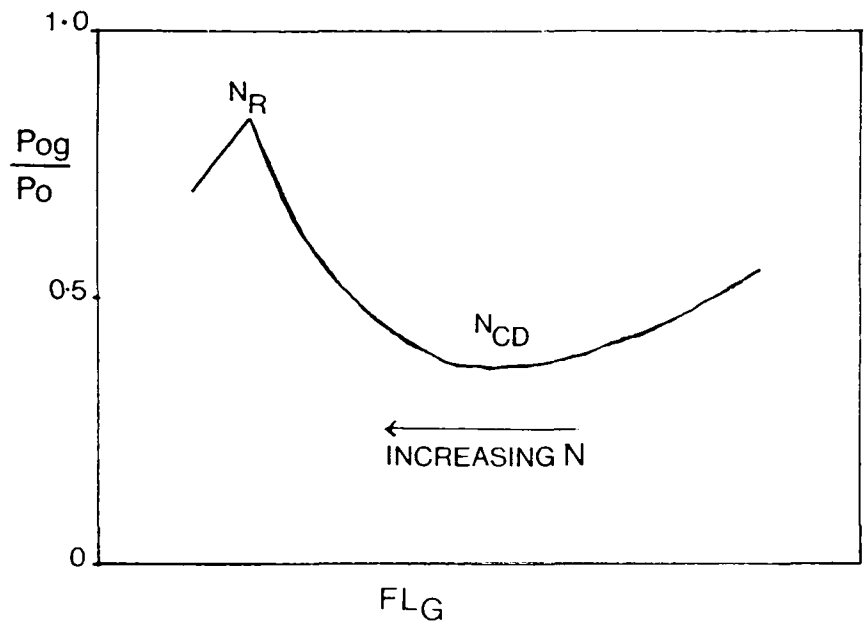

Figure 2.6 Pog/Po v Fl_G at constant Q_G for the 6DT.

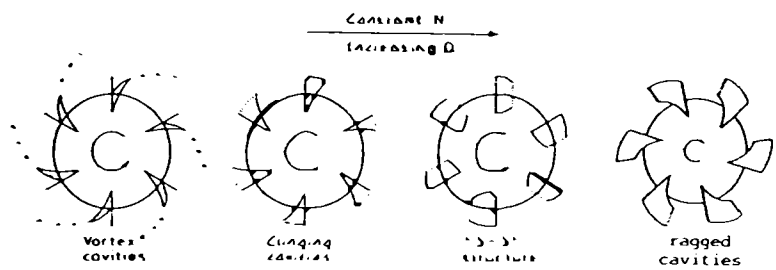

Figure 2.7 Gas Cavity Types for the 6DT.

turbine were replaced by segments of pipe concave to the direction of rotation, (6PSDT), the power reduction on aeration was less. This was because the transition to larger cavities was delayed and occured at higher gas rates[29]. Flooding also occured at higher gas rates than with the 6DT.

One advantage highlighted by these findings is that greater aerated power is drawn with 6PSDT than with 6DT at equal D/T when using the same speed and hence motor and gearbox. Commercial designs such as the ICI Gasfoil[30] and Scaba SRGT[31] have used this concept. In the former case gassed power falls to 0.9 of the ungassed in water whilst the latter's power draw does not fall at all on aeration. This is due to vortex cavities being present up to the point of flooding. Flooding with SRGT occurs at roughly three times the Q_G required to flood an identical D/T Rushton at equivalent unaerated power draw. Overall these impeller types offer considerable potential benefits over the 6DT in low viscosity systems.

2.5.4 Mixed Flow Impellers

This section is intended as a resume of the salient features of the 6MF, whilst direct comparison of literature results with this work is made in Chapter 5. Under aerated conditions the pumping direction of these combined axial/radial flow impellers significantly effects power draw, gas dispersion and torque stability. The downward pumping mode (DPM) will be discussed first.

Mixed flow impellers pumping downwards (6MFD) against the gas-liquid plume from the sparger may exhibit significant bulk flow pattern instabilities. These instabilities are linked to the direct loading-indirect loading transition[32]. For a particular Q_G, from N = 0 to a certain critical value air enters the agitator directly from the sparger (direct loading). Above the critical speed air is driven away from the

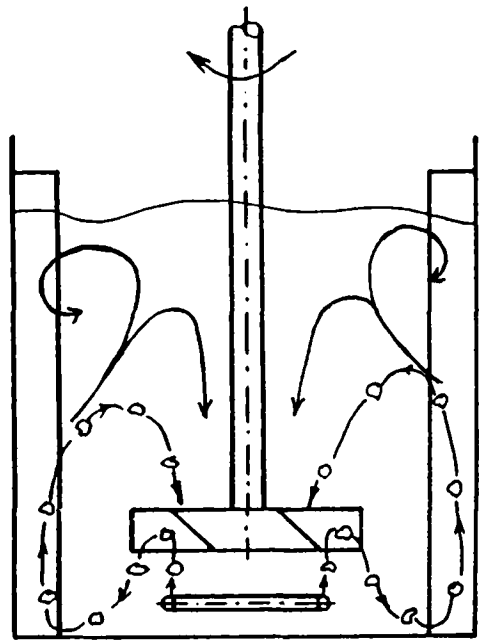

a) direct loading

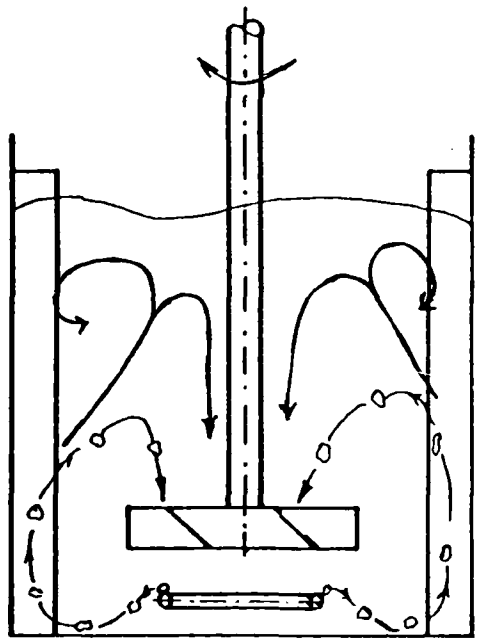

b) indirect loading

Figure 2.8 Gas Loading Regimes for the 6MFD[12].

agitator and only enters by recirculation (indirect loading) (Fig. 2.8).

In the region of the direct-indirect loading transition considerable torque instability and fluctuation occurs. The direct-indirect loading transition has also been linked[12,33] to the transition from large cavities to clinging cavities (Fig. 2.9). Instabilities have been shown to be reduced by adopting a 6-bladed as opposed to 4-bladed 45° pitch turbine and by increasing D/T from 0.33 to 0.5. A ring sparger of D_s/D = 0.8 has also been shown to reduce instability with the 6MFD when compared to a point sparger. This is achieved by removing the influent gas stream from a region of upward to a region of downward flow[12,33].

Mixed flow impellers pumping upwards (6MFU) completely disperse gas at lower speeds than the 6MFD and show greatly reduced instability. The optimum configuration is D/T = 0.5, 6 blades and a D_s/D = 0.8 ring sparger[12,33]. The power reduction on gassing is much smaller in the UPM.[34] Above N_{CD} clinging cavities are present except at the very highest speeds and gassing rates.

2.5.5 Hydrofoil Agitators

The class of agitators referred to as 'hydrofoil' produces more predominantly axial flow than pitched blade turbines[35,36]. A number of proprietary designs have become available over the last few years. Principal types used for gas dispersion and bulk blending are the 4-bladed Lightnin' A315 (Mixing Equipment Co. Inc., USA) and the 5-bladed Prochem Maxflo T hydrofoil (Prochem Mixing Equipment Ltd., Canada). Both of these types should be operated in the DPM (according to the manufacturers) and have high solidity ratios. The solidity ratio[37] refers to the fraction of the area of a circle of diameter = D, occupied by the agitator blades.

Similarities between the gassed behaviour of hydrofoils and mixed flow impellers have been reported. Flow and torque instabilities associated with the direct-indirect loading transition have been seen for

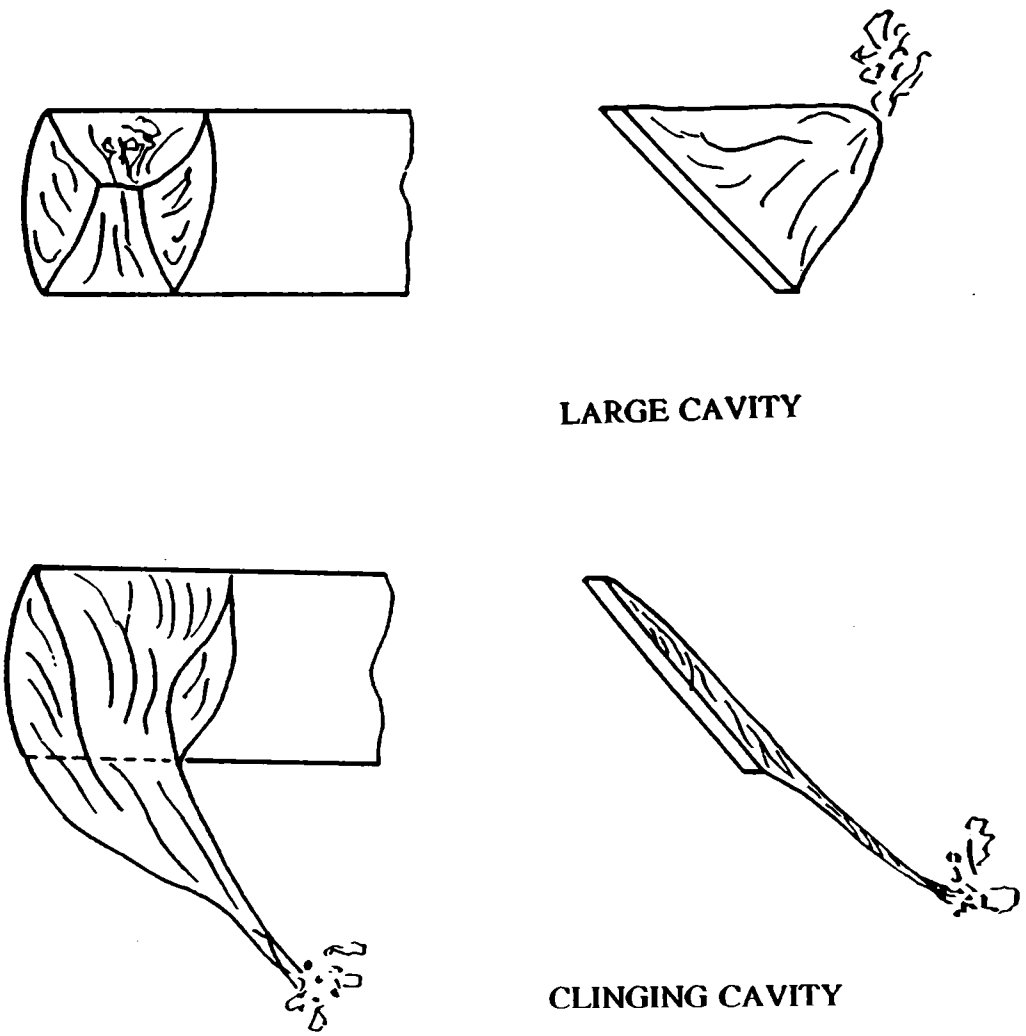

Figure 2.9 Gas Cavity Types for the 6MFD[12].

Prochem[36,38] and A315[36] in the DPM. At the transition the downward liquid velocity is not sufficient to overcome the upward momentum of gas continually. Hydrofoil performance has been found to be sensitive to both sparger geometry and clearance. As usual, power draw is linked to cavity size and type, the types of cavity found are shown in Fig. 2.10[36]. As with the mixed flow impellers, the hydrofoils have been found to be more stable in the UPM (even though not recommended by the manufacturers). Both the A315 and Prochem Maxflo T draw higher relative power on aeration than the Rushton at equal unaerated power input[36].

2.5.6 InterMIG.

A detailed survey of InterMIG literature is given in Appendix I, including that concerning aerated power data.

2.5.7 Viscous, Non-Newtonian Fluids.

Studies on gas dispersion in non-Newtonian fluids have generally been conducted using Rushton turbines and have spanned a range of $1 < Re < 10^5$. Gas dispersion applications generally require $Re > \sim 50$[39]. In the turbulent flow regime ($Re > 10^4$) non-Newtonian fluids exhibit very similar gassed power characteristics to those found for Newtonian fluids.

In the transitional flow regime ($10 < Re < \sim 10^4$) the gassed power behaviour of the 6DT varies with fluid rheology. The dependence of Po_g on fluid rheology is complex with shear thinning viscosity, yield stress and viscoelasticity all possibly affecting cavity size and shape when present.

Over the transitional flow regime 6DT Po_g falls and then rises producing a minimum. This minimum was found to be sharper for viscoelastic fluids than for non-elastic ones[7,18].

At constant N, the aeration rate (Q_G) has been found not to effect Po_g, cavity size or shape at $Re < 900$[3,18,41]. The effect of non-Newtonian

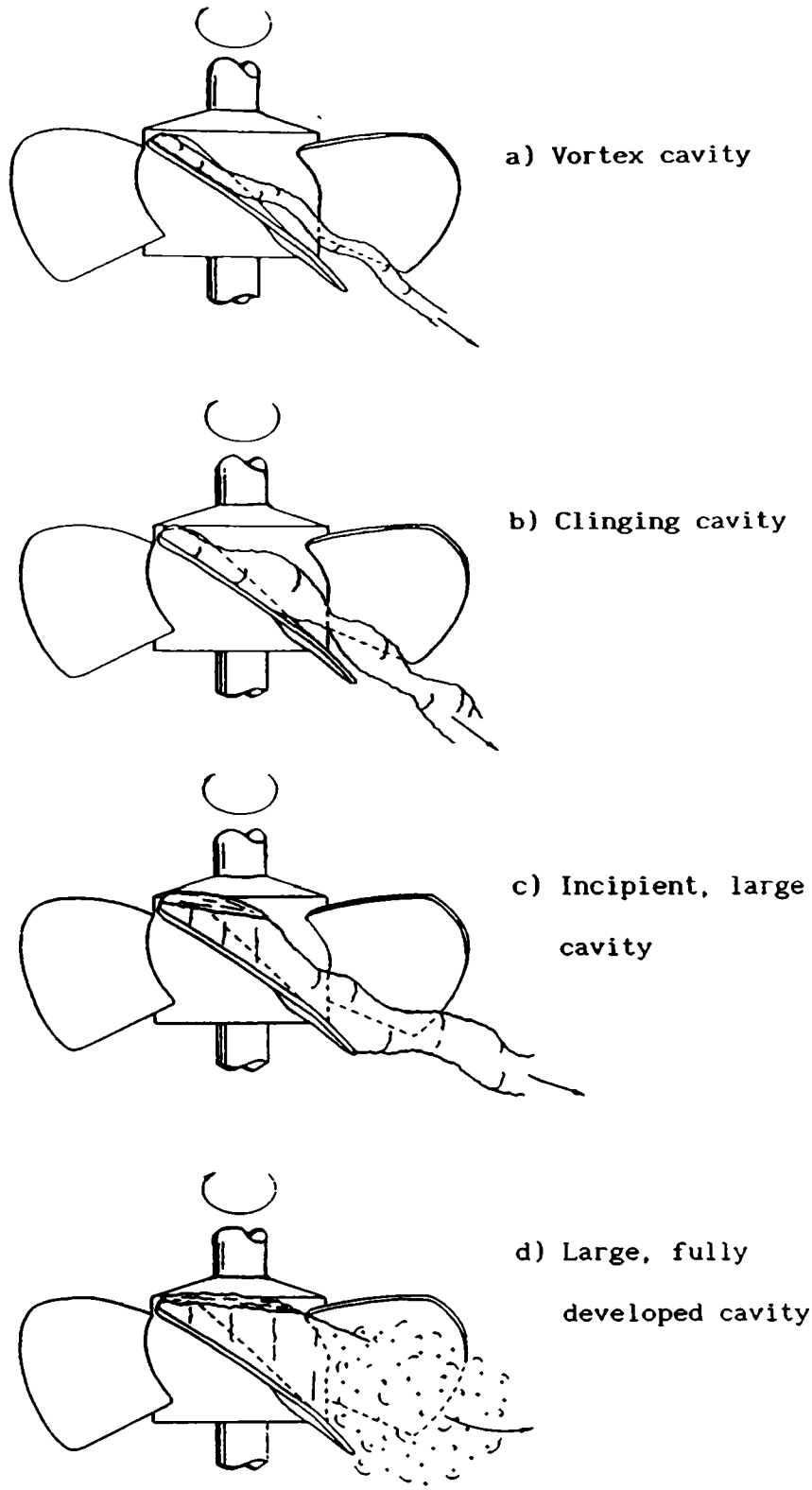

Figure 2.10 Gas Cavity Types for a Hydrofoil Impeller[36].

rheology on the gassed power of agitators other than the 6DT has been sparsely investigated. Hocker[7] found the dependence of Po_g on Q_G diminished with increased viscosity for both 6DT and MIG in Newtonian and inelastic shear thinning fluids. In viscoelastic polyacrylamide (PAA) solutions Po_g was higher in the transitional regime than for inelastic fluids when using MIG.

Increasing viscosity tends to stabilize cavities, reducing the effect of Q_G on Po_g. Cavities often remain attached to the agitator blades after the cessation of aeration in viscous fluids[18]. Cavity stability would appear to be greater in viscoelastic as opposed to inelastic non-Newtonian fluids, enhancing the above mentioned effects.

The influence of enhanced viscosity on Po_g is best represented by data in the form of Po_g v Re with the unaerated power curve for comparison.

2.6 GASSED HOLD-UP

2.6.1 Theory

A principal requirement of gas-liquid mixing vessels is to create a large interfacial area, a, for mass transfer. Direct measurement of a is problematic and therefore gas hold-up has been frequently used as a guide to interfacial area variation in agitated-aerated vessels. The gas hold-up, ε_G, is defined as follows:

$$\varepsilon_G = \frac{\text{Gas volume}}{\text{Gas volume + liquid volume}} \qquad (2.18)$$

In practice, ε_G is obtained by measuring the increase in fluid level due to gas introduction.

$$\varepsilon_G = \frac{H_g - H}{H_g} \qquad (2.19)$$

Where H is the unaerated liquid level and H_g is the level of the gas-liquid mixture. The hold-up, thus defined, is an overall value. Local hold-up values may vary considerably within the vessel[22]. For small spherical bubbles the specific interfacial area, a, can be calculated from the idealised relationship[42] between bubble size and hold-up given below.

$$a = 6\ \varepsilon_G / d_s \qquad (2.20)$$

where d_s is the Sauter bubble diameter[43] defined as:

$$d_s = \frac{\sum f_i\ d_i^{\,3}}{\sum f_i\ d_i^{\,2}} \qquad (2.21)$$

where f_i is the bubble frequency with diameter d_i. For freely rising evenly distributed bubbles the gas hold-up is given by:

$$\varepsilon_G = v_s / v_{bs} \qquad (2.22)$$

where v_s = superficial gas velocity and v_{bs} = single bubble rise velocity. The bubble rise velocity in water depends upon bubble size and water purity. In water bubble sizes tend to be in the range 4-6 mm[44] and rise velocities have been reported as v_{bs} = 0.215 ms^{-1} and 0.235 ms^{-1} by van't Riet[28] and Dean et.al.[44]

In agitated mixing vessels, ε_G may be affected by fluid properties (coalescence, rheology), impeller design (local and bulk hydrodynamics), recirculation of gas, sparger design and scale of operation. The interaction of these factors makes the development of correlations for hold-up in agitated vessels difficult.

Typically the effect of impeller type on hold-up has been assessed in terms of specific power input and superficial gas velocity[45] e.g.,

$$\varepsilon_G = K\ (P/V)^{\alpha}\ (v_s)^{\beta} \qquad (2.23)$$

Values of α and of β range from 0.2 to 0.7 with α tending to be higher for non-coalescing systems. Hold-up is controlled by bubble size and the quantity of gas rising and recirculating, all of which are functions of P/V and/or v_s for a given system, indicating that the basic form of the correlation is sound.[45] Attempts to correlate hold-up using Q_G [vvm] at different scales and aspect ratios have been found to be unsatisfactory.[12] As the power drawn by an impeller is a function of gassing rate a more explicit relationship may be obtained if ε_G is correlated with N. This form of relationship is more predictive for a given vessel scale and agitator type but is likely to produce worse results when combining data from differing scales and/or agitator types with different power numbers[12]. Hold-up data in this work has therefore been correlated using Eqn. 2.23.

2.6.2 Hold-Up Studies

Gas hold-up has been shown to be influenced strongly by liquid properties such as coalescence phenomena[46] and rheology. In deionised water bubbles coalesce more frequently and easily than in electrolyte solutions, leading to a larger mean bubble size in the former[47]. Hold-up in electrolyte solutions is enhanced when compared with deionised water due to lower rise velocities of the smaller bubbles and greater recirculation into the impeller zone. A significant change in coalescence behaviour occurs over a relatively narrow concentration range of electrolytes or organic chemicals[47,48], enabling systems to be defined as either coalescing or non-coalescing.

In viscous non-Newtonian fluids, such as CMC, a roughly bimodal bubble size distribution exists[42,49]. This comprises many tiny (< 1mm) bubbles with practically zero rise velocity and fewer large slug-like bubbles which rise more rapidly through the liquid. As shear thinning viscosity increases, hold-up is reduced[49,50]. The reduction in hold-up has been ascribed to a changing proportion of large and small bubble hold-up. Phillip[49] (loop reactor) and Machon[50] (stirred vessel) suggested increased large and reduced small bubble hold-up.

The gas-filled cavities behind 6DT impeller blades have been linked to hold-up in water[51-53] and CMC solutions. In the transitional regime, the 6DT aerated power curve goes through a minimum in CMC, this has been related to the largest cavities and the maximum hold-up in both the impeller region and overall. As N increased cavities shrunk and hold-up decreased in spite of greater recirculation of tiny bubbles.

Mann[54] reviewed a range of correlations for predicting hold-up in agitated vessels using a variety of fluids. The results of various hold-up studies are compared with those from this work in Section 6.5.

2.7 OXYGEN MASS TRANSFER

2.7.1 Theory

This section is concerned with the mass transfer problem of a sparingly soluble gas (oxygen) being transferred from a source (rising air bubble) into a liquid or visa versa. The oxygen must pass through a series of transport resistances of variable relative magnitude shown diagrammatically in Fig. 2.11 (p.45). These consist of:-

a) Diffusion from bulk gas to the gas-liquid interface.

b) Movement through the gas-liquid interface.

c) Diffusion through liquid film to bulk liquid.

For sparingly soluble species such as oxygen in water, the

equilibriated interfacial concentrations p_i and c_i on the gas and liquid sides may be related through a linear partition-law relationship e.g. Henry's Law[55]:

$$Hc_i = p_i \tag{2.24}$$

where H is the Henry's Law Constant.

The rate, r, of mass transfer across the gas-liquid interface is given by the mass transfer coefficient, k_G, for the gas phase and k_L for the liquid phase multiplied by the area of transfer, A', and the concentration gradient available as a driving force,[56] or

$$r = k_G A' (p_G - p_i) = k_L A' (c_i - c_L) \tag{2.25}$$

The interfacial concentrations are not usually measurable and may be eliminated by combining equations 2.24 and 2.25

$$r = A' (p_G/H - C_L) \left[\frac{1}{k_L} + \frac{1}{H k_G}\right]^{-1} \tag{2.26}$$

Since oxygen follows Henry's Law closely and H is independent of concentration of the transferring species:

$$p_G/H = C^* \tag{2.27}$$

where C* is the liquid phase concentration in equilibrium with the gas phase. For sparingly soluble species, H is much larger than unity,[55] also k_G is typically considerably larger than k_L[55,61] therefore:

$$\frac{1}{k_L} >> \frac{1}{H k_G} \tag{2.28}$$

and

$$\frac{1}{k_L} \simeq \left[\frac{1}{k_L} + \frac{1}{H\, k_G} \right] \qquad (2.29)$$

From the above equations 2.26 to 2.29 the following rate equation may be written:

$$r = k_L A' \, (C^* - C_L) \qquad (2.30)$$

Equation 2.30 applies to situations where all the resistance to mass transfer can be considered to lie on the liquid film side.

The conventional picture of absorption of a gas into an agitated liquid where the resistance to transfer lies on the liquid side is that there exists a stagnant 'film' of liquid at the interface.[57] The concentration in the bulk liquid is kept uniform by turbulent mixing whilst the interface surface concentration has the value C*. The film theory described above is considered to be unrealistic[57] as it seems probable that in many situations turbulence will extend to the interface. For many practical purposes this is unimportant as measured absorption rates conform to the film theory[58]:

$$k_L = D_L/\delta \qquad (2.31)$$

where D_L = diffusivity

δ = film thickness

The film theory is simple to use, particularly where the reaction process is complex, involving several absorbing, desorbing species and chemical reaction[58].

The classical penetration theory is considered more realistic than the film theory as it accounts for transient mass transfer conditions where the surface is continually being replaced with fresh liquid.[57] The

penetration theory gives a more accurate answer for the absorption rates when the diffusivities of all reacting species are unequal.[59]. The penetration theory leads to:

$$k_L = 2\sqrt{D_L/\pi\ t_c} \qquad (2.32)$$

t_c = time constant.

When the reaction process is complex, an analytical evaluation of the absorption rate by penetration theory may become too involved for practical use[58]. Both film and penetration theories neglect convective mass transfer at the gas-liquid interface. Generally in agitated, aerated contactors involving chemical or biochemical reaction, the film theory is used due to its simplicity. Increased turbulence in the bulk liquid will increase k_L irrespective of theory type due to reduction of stagnant film thickness or increase in surface renewal rate (decrease in t_c). The oxygen transfer rate per unit reactor volume is given by:

$$Qo_2 = k_L\ (C^* - C_L)\ A'/V = k_La\ (C^* - C_L) \qquad (2.33)$$

where a is the specific interfacial area (A'/V) in units [m^2m^{-3}] and V is the volume of the system of interest (usually liquid volume but in some cases liquid + gas hold-up volume[55]). From the above, Qo_2 is defined as a local volumetric oxygen absorption/desorption rate. The average volumetric rate of oxygen absorption/desorption in the total liquid volume V is given by[55]:

$$\bar{Q}o_2 = 1/V \int_o^V Qo_2\ dV \qquad (2.34)$$

If the hydrodynamic conditions, interfacial area/volume and oxygen concentrations are uniform throughout the vessel then $\bar{Q}o_2$ is equal to Qo_2.

The factors which affect mass transfer in gas-liquid dispersions include[59] the physical properties of the gas and liquid, type and characteristics of gas distributor, dimensions of vessel, characteristics of mechanical agitator, energy input and velocity of agitator, gas flow rate, presence of chemical reaction and presence of solid particles. For a given system the dependent parameters include power input, bubble size distribution, gas hold-up and bubble relative slip velocity.

The main parameters of interest in determining the overall mass transfer rate for design purposes are k_L and a which may be determined separately or, as is more commonly the case, in combined form as k_La (the volumetric mass transfer coefficient).

2.8 k_La MEASUREMENT METHODS

2.8.1 Introduction.

Oxygen mass transfer measurement techniques may be categorised according to the system to which they are applied. Ideally oxygen transfer rates should be measured in biological reactors which include the nutrient broth and cell populations of interest, these are termed 'direct methods'[60]. Direct methods require considerable attention and expense in order to prepare and operate the fermentation of interest aseptically. Fermentations tend to be both difficult to reproduce and exhibit variation in liquid phase properties with time. Consequently synthetic systems are a common feature of mass transfer study which approximate bioreactor conditions without the complication of a living culture, these are termed 'indirect methods'. The usefulness of synthetic systems depends upon the degree of similarity between the rheology, coalescence, O_2 solubility, O_2 diffusivity and interfacial resistance of the synthetic medium and the fermentation of interest.

In this work indirect methods were used and hence will be discussed

in detail with cursory reference to direct methods. Indirect methods may be further divided into separate determination, chemical, dynamic and steady state methods. These categories are not mutually exclusive and many techniques fall into more than one. Some measurement methods may also be applied to both synthetic and real systems.

2.8.2 Seperate Determination of k_L and a.

Considerable research effort has been directed towards the individual determination of k_L and a, in order to obtain a more comprehensive understanding of the effect of system parameters on mass transfer.

The liquid mass transfer coefficient, k_L, may be determined using methods suited to dissolved gas diffusivity measurement, however the usual equipment (laminar jet or laminar film) provides data that is difficult to adapt to practical systems. To overcome this both stirred cells and single bubble measurements have been employed. In these measurements either a constant known contact area must be achieved or both k_La and a measured in order to arrive at k_L values.

Various authors investigated k_L by measuring k_La and a in stirred vessels. Calderbank[61] used a range of vessel sizes and types whilst measuring both k_L and a for water, alcohols, glycol and glycerol solutions. k_L was found to be independent of bubble size, velocity and degree of agitation (questionable) but dependent upon viscosity. They also found $1/k_G$ to be negligibly small.

Mehta and Sharma[62] measured k_La and a in agitated vessels using chemical methods (CO_2 absorption with slow chemical reaction into sodium carbonate/bicarbonate buffer and O_2 absorption into acidic cuprous chloride).

Robinson and Wilke[63] used concurrent chemical pseudo steady-state absorption of CO_2 with reaction and unsteady state desorption of O_2 in aqueous solutions of ionic solutes to evaluate k_La and a. k_L was found to

decrease with increased P/V and decreased d_b, the results contradicting those of Calderbank[61].

Joshi and Kale[64] used O_2 absorption into aqueous alkaline sodium dithionite to measure a and lean CO_2 absorption into sodium carbonate-bicarbonate buffers to measure k_La in a vessel equipped with a gas inducing agitator. Drag reducing agents such as polyethylene oxide, guar gum and CMC were tested for effect on k_La. k_L was found to decrease with increasing additive concentration whilst a increased substantially leading to slight increases in k_La.

As well as the chemical methods mentioned above for the determination of a, light transmission, photographic and bubble extraction by capillary suction techniques have been used. Light transmission techniques provide local values of a and were pioneered by Vermeulen[65] and subsequently used by Calderbank[43], Lee and Meyrick[66], Lockett and Safekourdi.[67] The earlier workers[43,65] found that a variation with probe position in the vessel was dependent on agitation intensity. Electrolytes were found to increase interfacial area considerably[66]. Sridhar and Potter[68] developed a fibre optic probe which allowed higher values of a to be determined.

Kawecki[69] used the pumping action of the impeller to transport bubbles out of the vessel and into a liquid filled column for photographic area determination. Reith and Beek[70] used a method based on that of Kawacki[69] and compared it with sulphite oxidation. The results of the former offered more straighforward calculation but it was very time consuming to conduct and could only handle low air flow rates.

Comparison of a chemical method and two physical (photography, light attenuation) methods was made by Landau et.al.[70] Conclusions were that the chemical method (sulphite oxidation) was useful as a standard but was time consuming and system specific due to the chemical addition. The photographic technique provided information on bubble shape, shape factor, size distribution etc. but was again time consuming. Light attenuation

provided a large body of data due to its speed of use and simplicity and with improvements was able to handle large interfacial areas.

In general, photographic methods provide information about conditions near the vessel wall. If bubbles are removed from the vessel[69], coalescence may occur during removal with high gas hold-up situations. Bubble suction into a capillary can also lead to difficulties due to unrepresentative samples. The photographic method does not yield a directly but requires hold-up measurement as well. Therefore if bubble sizes are underestimated the interfacial area will be overestimated. This is often postulated to be the case due to a thin curtain of small bubbles present at the vessel wall[68].

The light scattering technique has been limited by the phenomenon of multiple scattering at high interfacial areas[43]. However reduction in pathlength by better probe design[68] permits higher values of a to be determined and the reduction in probe size[68] enables local areas to be investigated. Reliable values are only obtained if the probe does not interfere with the flow pattern in the vessel and if a representative sample is included in the light path.

Chemical methods of interfacial area determination are the most widely reported in the literature. Sridhar and Potter[71] showed that the chemical method yields higher values of interfacial area in a stirred vessel. Chemical techniques do however provide overall values of a unlike photographic or light scattering techniques.

2.8.3 Chemical Methods for $k_L a$ Determination.

As can be seen from the previous section chemical methods have been widely used for mass transfer coefficient determination. The methods described are generally steady state i.e. C_L is constant. A chemical reaction in the bulk liquid at a sufficiently high rate reduces $C_L \simeq 0$ and the reaction rate is equal to $k_L a\ C^*$.

The most commonly reported technique is that of the oxidation of sodium sulphite to sulphate in the presence of a cobalt or copper ion catalyst[72]. This technique has been reviewed by a number of authors[54,55,60,73]. It has been noted that the reaction may proceed so rapidly that significant oxidation takes place at the gas-liquid interface, leading to $k_L a$ enhancement[55,74]. An enhancement factor ε has been calculated to account for the degree of film reaction, provided reaction order, rate constant and boundary conditions are known[55]. The reaction rate constant and order must be determined for every set of experiments due to the sensitivity of the rate to small changes in catalyst concentration, type, pH, sodium sulphite purity and other additions to the system[72,75]. The reaction kinetics are difficult to determine accurately due to their complexity[73].

A serious drawback of the sulphite oxidation technique is that high ionic concentrations are required which alter the coalescence properties of the system compared with water[73] or viscous media[76]. Therefore results obtained with the technique are only applicable to one particular liquid and can only be used to compare system properties (agitator, sparger, vessel geometry etc.) with great care taken to maintain identical conditions.

Another chemical method of $k_L a$ determination is that of CO_2 absorption into sodium carbonate/bicarbonate buffer[62,73] or sodium hydroxide[63]. Robinson and Wilke[63] combined CO_2 absorption with dynamic gassing out to obtain a steady state using aqueous solutions of inorganic electrolytes. The absorption of CO_2 into carbonate/bicarbonate proceeds in three steps[60]:

1. $CO_2\ (g) \xrightarrow{k_1} CO_2\ (\ell)$

2. $CO_2 + H_2O \xrightarrow{k_2} HCO_3^- + H^+$ and $H^+OH^- \xrightarrow{v.fast} H_2O$

3. $CO_2 + OH^- \xrightarrow{k_3} HCO_3^-$

The first step is described by the mass transfer coefficient for CO_2, the second is first order w.r.t CO_2 whilst the third is irreversible second order. The experimental conditions for excluding physical mass transfer are not easy to achieve[60] and the reaction kinetics should be known beforehand[73]. When using the method the ratio CO_3^{2-}/HCO_3^- should be kept around 4 and the total ionic strength roughly 2 M ℓ^{-1} [62] to ensure slow enough reaction of CO_2 for the rate to be determined by k_La. The concentration of ions will therefore effect coalescence and hence a, as well as possible influence on k_L due to changes in diffusivity and solubility of the transferring species[55].

Oxygen uptake may be measured by the oxidation of glucose by the enzyme glucose oxidase[60] and its subsequent conversion to gluconic acid. The reaction steps are:

1. Glucose + 1/2 O_2 $\xrightarrow[(FAD,\ catalase)]{Glucose\ Oxidase}$ Glucono-lactone + H_2O

2. Glucono-lactone + H_2O $\xrightarrow{lactonase}$ Gluconic acid

The hydrolysis of lactone must proceed at a very high rate in order to avoid glucano-lactone accumulation, this can be achieved by a sufficiently high lactonase activity ensuring the process is governed by step 1. Glucose oxidase concentrations of at least 1.5 g/ℓ are required for the system oxygen uptake capacity to exceed the intrinsic rate of absorption. An acidometric titration can be used to determine oxygen transfer rate when the system reaches steady-state after a short start up period. Drawbacks of this method appear to be the high levels of enzymes required to ensure no inhibitory glucano-lactone build up and to ensure conversion of all absorbed oxygen.

The hydrazine method was used by Zlokarnik[77] to measure k_La. This is a steady state method in which the concentration of oxygen in the liquid

phase is not reduced to zero i.e. C_L = constant ≠ 0. The salt concentration required is < 1 g/ℓ. The technique involves the reaction between hydrazine and oxygen according to:

$$N_2H_4 + O_2 \longrightarrow N_2 + 2H_2O$$

The reaction products do not alter the liquid properties and the oxygen concentration in the liquid phase is measured using a dissolved oxygen probe. The optimum reaction conditions are at pH = 11-12, achieved by sodium hydroxide addition and a $CuSO_4$ concentration of 0.01 M. Hydrazine is continually added to the system, where (under steady state conditions) the absorption rate equals the reaction rate and the amount of hydrazine added equals the amount of oxygen absorbed per unit time.

Judat[78] compared results obtained using the hydrazine technique with those obtained using dynamic gassing out (see later) and showed an affect of $CuSO_4$ catalyst concentration on k_La. The processes which occur when this method is used are not fully understood and it is therefore necessary to apply the hydrazine method with a certain amount of caution.

Hickman[79] published details of a steady-state chemical technique known as 'NEL/Hickman'. It utilizes the decomposition of hydrogen peroxide in the presence of the enzyme catalase.

$$2\ H_2O_2 \xrightarrow{\text{Catalase}} 2\ H_2O + O_2$$

The technique is claimed to be simple, cost-effective, reliable and independent of complex models of gas-phase mixing. The reaction products (water and oxygen) do not affect the system apart from a slight increase in volume. Hickman[79] used the technique in water and CMC solutions. Further details are given in Chapt.3 and Appendices II and III.

2.8.4 Dynamic Methods.

The most commonly used technique for k_La measurement is the dynamic gassing-out method[73]. Typically the liquid of interest is deoxygenated by passing nitrogen through it, the air flow is resumed and the dissolved oxygen profile measured using a dissolved oxygen probe (usually polarographic). A semi-logarithmic plot of $(C^* - C_L)$ against time results in a straight line with the slope representing the k_La value, from:

$$\frac{d\,C_L}{dt} = k_La\,(C^* - C_L) \qquad (2.36)$$

Two types of dynamic technique are employed.

a) SEMI-BATCH: There is an instantaneous interchange of inlet gasses with different oxygen concentrations. Q_G and N remain unchanged. The commonest interchanges are N_2 to O_2 and N_2 to air.

b) BATCH: Saturate liquid with a gas, then interrupt agitation and gassing to allow bubbles to escape. Next, recommence agitation and introduce a gas with a different oxygen concentration. Alternatively the liquid phase may be deoxygenated by either vacuum desorption or reaction with sulphite ions prior to gas flow start-up.

A large number of publications have dealt with restrictions on the applicability of dynamic methods. They are concerned with the liquid, gas, diffusion film and electrode dynamic effects, which if overlooked can result in considerable error. The probe response time, τ_p (time needed to record a 63% stepchange) should be much smaller than $1/k_La$ for accurate measurement[80]. In practice this is seldom the case and various models have been developed to calculate k_La from probe responses. Heineken[81] and Linek[82] considered the diffusional resistance of the probe membrane to account for response lag where the probe output is not directly related to the instantaneous value of dissolved O_2. However van't Riet[73] demonstrated that these models imply an error in $k_La < 3\%$ for $\tau_p \leq 1/5$

$k_L a$. Therefore when using electrodes with τ_p = 2 or 3 s values of $k_L a$ up to 0.1 s^{-1} may be measured without use of complex models. Evaluation of electrode time constants is therefore necessary before using dynamic techniques.

A response lag of the electrode also occurs due to a mass transfer boundary layer between the bulk fluid and electrode membrane. Dang et.al.[83] showed that in viscous systems the film diffusion influence cannot be neglected, but in water the film time constant is < 15% of τ_p. Further information on liquid film diffusion effects and their modelling are given by Linek et.al.[84] and Ruchti et.al.[80]. The latter note that modelling probe response by first order relaxation (membrane diffusion) and an additional second order relaxation time (film effect) is insufficient due to side diffusion of oxygen towards the cathode. The mass transfer boundary layer thickness is influenced by liquid properties, probe position, agitation intensity and agitator geometry.

The effect of gas bubbles contacting or adhering to the electrode membrane has been discussed by Linek et.al.[85] and Votruba et.al.[86]. Bubble-probe contact causes chaotic probe signals which can be higher or lower than the bulk liquid concentration depending on direction of O_2 transfer. Attempts to quantify bubble-probe interaction in terms of local gas hold up have been unsuccessful due to dependence on bubble size distribution, flow field, membrane properties etc.. A variety of probe positioning and protective measures to eliminate direct bubble probe contact have been suggested[85].

Gas phase dynamic effects can cause considerable errors when using these dynamic techniques. Dunn and Einsele[87] reported an analysis with correction graphs and Dang et.al.[83] provided a more elaborate model. The latter indicated that for high gas phase residence times considerable correction was needed, reducing the accuracy of measurements.

Chapman et.al.[88] developed a technique for measuring both liquid and

gas phase dynamic responses following an inlet [O_2] stepchange. This enabled k_La evaluation to be independent of gas residence time distribution. They compared results of this 'Two-probe technique' with single probe no depletion, perfect mixing and plug flow gas phase O_2 concentration models. There was considerable variation in the resultant data.

When switching gas streams using the semi-batch dynamic technique the original N_2 hold-up mixes with newly introduced air or oxygen. This start-up effect can be modelled[85] as can the initial increase in hold-up that occurs using batch dynamic techniques[85].

Further problems arise when attempting to use dynamic techniques in viscous gas-liquid systems containing a fraction of tiny bubbles (<< 1 mm)[89]. As the rise velocity of these tiny bubbles is very low their residence time is much greater than the time for neutralization of the O_2 gradient between tiny bubble and liquid. As the concentration of O_2 in air is roughly 30 times that in water (25°C), the solubility in the 'homogeneous- phase' liquid with very small bubbles increases sharply with increasing small bubble hold-up. Heijnen et.al.[89] showed that although steady state method results are not influenced by small bubbles, dynamic technique results are.

In summary transient techniques require accurate knowledge of the complete system dynamics in order to measure k_La. Recent reviews of the use of the dynamic technique are given by Spriet et.al.[90] and Linek et.al.[85].

2.8.5 Steady-State Methods.

This category of technique involves a constant dissolved oxygen concentration e.g.

$$\frac{dC_L}{dt} = 0$$

They generally involve the transfer of oxygen from:

(a) Continuously flowing gas phase to the liquid phase.

(b) Liquid phase (O_2 continually generated) to the flowing gas phase.

In order to achieve steady state in case (a) oxygen must be removed from the liquid continuously. This can be achieved by chemical or biochemical reaction or by physical means. Examples of chemical methods used are sulphite oxidation and hydrazine[77] Biochemical reactions used in model fluids include yeast respiration[20] and glucose oxidation[60]. The liquid phase may be continually replaced with deoxygenated liquid e.g. two vessels with one stripping and the other adding O_2. An example of case (b) is the NEL/Hickman[79] technique where O_2 is continually produced in the liquid phase by chemical reaction.

2.9 CHOICE OF $k_L a$ MEASUREMENT TECHNIQUE

From the foregoing section it is apparent that there is a wide choice of techniques for $k_L a$ determination in agitated aerated vessels. All techniques suffer from potential sources of error. A good understanding of the system under study and the technique used is therefore a prerequisite for accurate $k_L a$ measurement. Table 2.1 summarises the potential sources of error applicable to dynamic and steady state techniques.

All techniques require the assumption of a well mixed liquid phase. This becomes tenuous in viscous yield stress and/or shear-thinning fluids on a large scale.

In this work, a steady-state technique was selected in order to avoid transient effects and the influence of tiny bubbles in viscous liquids. The NEL/Hickman method[89] was chosen because of claimed simplicity and low level of chemical addition.

POTENTIAL SOURCES OF ERROR	DYNAMIC	STEADY STATE
Liquid Phase Dynamics	Yes	Yes
Gas Phase Dynamics	Greater	Lesser
Bubbles Clinging to Probe Tip	Yes	Yes
Probe Response Lag (Membrane Diffusion)	Yes	No
Probe Response Lag (Stagnant Liquid Film)	Yes	No
Start-Up Effects	Yes	No
Effect of Tiny Bubbles	Yes	No
Chemical Addition	No	Yes
Complex Reaction Kinetics	No	Yes
Fast Chemical Reaction Enhancement	No	Yes
Small Error in C_L Measurement Leads to Large k_La Error when ΔC Low	No	Yes

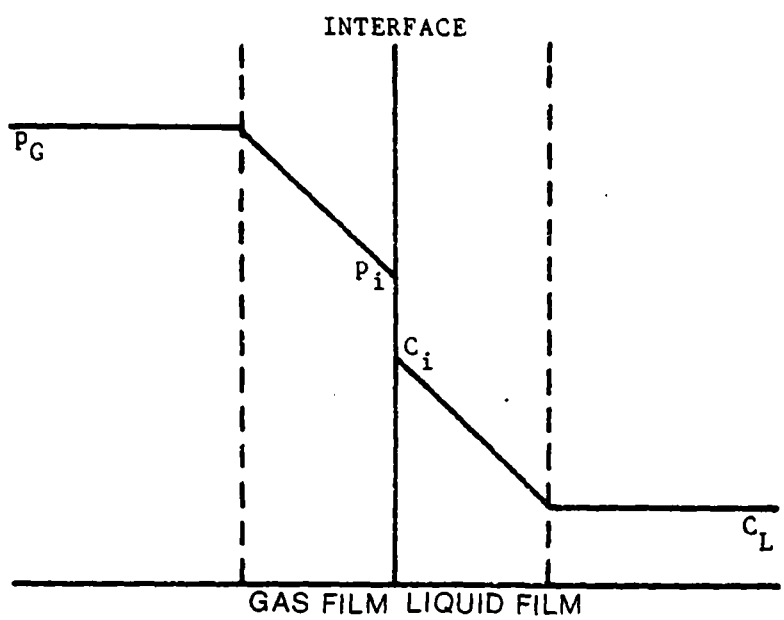

Figure 2.11 Representation of Concentration Profile in Two-Film Theory.

3. EXPERIMENTAL EQUIPMENT AND TECHNIQUES.

3.1 INTRODUCTION

This Chapter is divided into sections, each describing an aspect of the experimental equipment and measurement techniques used. The first section covers mixing vessels, ancillary equipment and agitators and is followed by sections detailing power measurement, bulk and local impeller flow observations and gassed hold-up measurements. Sources of error are discussed in each section. The NEL/Hickman k_La technique is described in Section 3.7. Theory, equipment and chemicals used in the basic technique are covered aswell as the experimental procedure and checks for reproducibility. Further information concerning the solution of development problems, reproducibility, k_La calculations and an assessment of errors are given in Appendix III. The final section of the chapter describes the model fluids used and the equipment/techniques associated with their preparation and rheological measurement. Rheological properties of the test fluids are detailed.

3.2 MIXING VESSELS AND ANCILLARY EQUIPMENT

3.2.1 Mixing Vessels.

Two clear cylindrical Perspex mixing vessels with diameters (T) of 0.45m and 0.72m respectively, were used in this study. These vessels are referred to as T45 and T72, details of both are given in Table 3.1 and T72 is depicted in Fig. 3.1. The design of the pilot-scale mixing vessel, T72, is described by Cronin[13]. To the authors knowledge, T72 is the largest operational Perspex mixing vessel in existence and provides a useful link between model fluid mixing studies and pilot scale fermentations. Previous model mixing and mass transfer studies have been

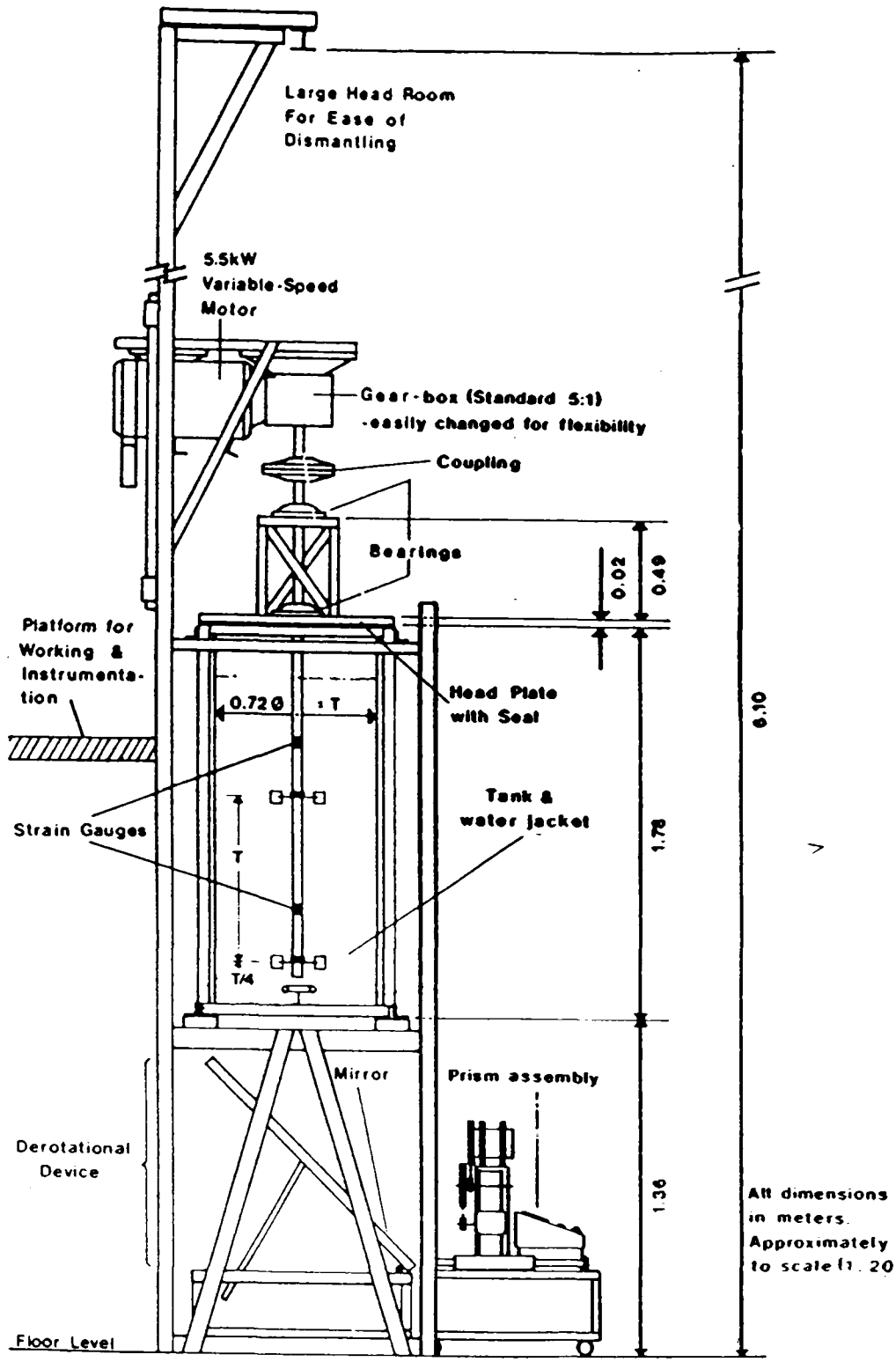

Figure 3.1 Vessel T72.

conducted at laboratory scale in Perspex vessels or at pilot scale in non-transparent vessels which limit the observation of bulk flow and local impeller hydrodynamics.

TABLE 3.1

	T45	T72	
Aspect Ratio, H/T	1	1	2
Diameter, T [m]	0.45	0.72	0.72
Liquid Height, H [m]	0.45	0.72	1.44
Volume, V [m^3]	0.0716	0.293	0.586
Baffle Number	4	4	4
Baffle Width (%)	10	10	10
Motor Power (kW)	1.5	5.5	5.5
Speed Range [rpm]	0-440	0-410	0-410

3.2.2 Air Supply and Measurement.

Air, saturated with water vapour, was introduced via a sparger located centrally beneath the impeller. Air was supplied at a constant pressure of 10 psig and the flowrate controlled using a series of calibrated rotameters. Calibration was carried out regularly using gas meters. Visual checks of rotameter settings were made periodically during experimental runs to ensure that no flowrate drift took place. In the following chapters gassing rates are referred to in terms of both superficial gas velocity, v_s (m/s) and Q_G (volume gas/volume liquid/minute). Table 3.2 shows the conversion between the two for the T72 aspect ratios and gassing rates used.

TABLE 3.2

v_s [m/s]	Q_G [vvm] H/T=1	Q_G [vvm] H/T=2
0.006	0.5	0.25
0.012	1	0.5
0.018	1.5	0.75

Sparger geometries used with each impeller type are given in Tables 4.3 and 5.2.

3.2.3 Temperature and Pressure Control and Measurement.

Temperature control in T45 was achieved by passing water from a thermostatically controlled bath through the Perspex vessel outer jacket. Temperature was controlled at 24°C ± 1°C. In T72, temperature control involved passing heating or cooling water through four U-tubes integral to the stainless steel baffles[13]. Typically the vessel contents were heated to 25°C prior to experimentation and the temperature controlled to 24°C ± 1°C during experimental runs by varying the cooling water flowrate through the baffle tubes. Temperature measurement was by thermocouples mounted independently or within the dissolved oxygen probes. Temperature was recorded regularly during all experimental runs. Accuracy of measurement and variation from position to position was ± 0.1°C.

During normal operation in T45 and T72 headspace pressure was equal to atmospheric pressure. However when operating T72 in conjunction with exit oxygen analysis (see Appendix III), the vessel was sealed and head pressure controlled manually using an exit air line choke valve[13]. The pressure was measured using a mercury manometer and typically maintained

at 10 to 15 [mmHg] depending on aeration rate. Pressure was held constant during each run and values recorded. The effect of enhanced pressure was accounted for in the k_La calculation procedure (A.III), but only needed to be applied to those reproducibility tests in which exit O_2 measurement was used.

3.2.4 Impellers.

The impellers tested are listed below with the abbreviations used.

1)	Rushton disc turbine	6DT
2)	Pipe section disc turbine	6PSDT
3)	Mixed flow impeller - general	6MF
	- pumping down	6MFD
	- pumping up	6MFU
4)	Lightnin A315	A315
5)	Ekato InterMIG (al ways used in pairs)	IM

Only the IM was used in both T45 and T72, all other types being used in T72 only. Details of IM dimensions and geometries are given in Section 4.1 whilst those of the other agitators used are given in Section 5.1.

Values of the Metzner and Otto constant, k_s, used for shear rate and Re determination in non-Newtonian fluids (Eqn. 2.9), are given in Table 3.3 with their literature source.

TABLE 3.3

Impeller	k_s	Ref
6DT	11.5±1.4	5
6PSDT	11.5±1.4	5
6MF	13±2	5
A315	13±2	5
IM	16	91

3.2.5 Vibration Measurement.

Under certain conditions, vessel T45 was seen to vibrate severely with IM. In order to quantify this effect, a dial gauge was mounted independently at a point on the vessel jacket midway between the base and liquid surface. The mounting consisted of a heavy photographic tripod with adjustable legs. Measurements were taken by observing the oscillation amplitude of the gauge needle. These measurements were quite subjective but revealed trends clearly.

3.3 POWER MEASUREMENT

In both T45 and T72, the torque on the shaft was measured using two pairs of strain gauges (Fig. 3.1) and telemetry equipment. Details of the equipment and technique have been previously published[13,14,27,92] and will not be recounted here. Torque signals were logged using a twin pen BBC Goerz Metrawatt SE120 chart recorder. Time averaged torque readings were obtained over periods of 3-6 minutes and the equipment zeroed between readings. Zero drift was typically less than 0.5% f.s.d. and was accounted for during torque calculation by assuming a linear variation with time. Torque measurement accuracy was estimated at ± 3%[14]. Shaft speed was measured using a 60 hole disc attached to the shaft through which a light beam passed. The resulting intermittent beam was detected by an infra-red optical switch and the pulses counted electronicly and displayed on a digital read out. At maximum speed the accuracy of measurement was better than ± 1%.

Calibration of strain gauges was conducted at approximately 3 monthly intervals by removing the shaft, clamping it in a vertical (T72) or horizontal (T45) position[13,14] and suspending a series of weights from a lever arm attached to the shaft tip. In this manner, linear torque against mV calibration plots were produced for both clockwise and anti-clockwise rotation directions for each gauge. Tachometers were

calibrated using a stroboscope and a reflective strip attached to the shaft.

The minimum torque below which it was considered reproducible measurements could not be made was roughly 2 Nm for T72. This minimum torque was arrived at by considering a maximum allowable error of 1% at full scale deflection on the lowest voltage range used for measurement (500 mV). The output voltage for which this constituted a 10% error (e.g. 50 mV) was taken as a minimum for measurement purposes; this corresponded to a torque of 2 Nm. Table 3.4 gives minimum impeller speeds for unaerated water at which 2 Nm was developed. For T45, the lowest output voltage range used was 0-200 mV giving a minimum torque of 0.06 Nm using the same procedure.

As power is proportional to N^3D^5, it is critical that D is measured accurately. In this work diameters were measured by mounting the impeller in a lathe and rotating it to find a swept diameter. This is particularly important for the A315, where flat to flat diameter is significantly less than the swept diameter.

3.4 BULK FLOW AND LOCAL IMPELLER FLUID DYNAMICS

3.4.1 Unaerated Flow Patterns.

The fluid motion within the vessel was observed in the following manner. A thin sheet of light was used to illuminate a vertical section of the fluid into which a number of almost neutral density, plastic particles had been added. The particles follow the liquid flow closely enough to enable the characteristics of the unaerated flow pattern to be identified. The collimated light allows the flow to be viewed two-dimensionally. Distortion free viewing was facilitated by the rectangular Perspex water jacket surrounding the cylindrical vessel.

TABLE 3.4

Minimum Speed for Torque Measurement

VESSEL	IMPELLER	N [rpm]
T45	2 IM	40
T72	2 IM	110
T72	1 6DT	50
T72	1 6PSDT	95
T72	1 6MF	80
T72	1 A315	150

3.4.2 Gassed Bulk Flow and Cavity Observation.

Observation of gassed bulk flow phenomena such as the flooding/loading transition and complete dispersion were made under normal lighting conditions. Problems encountered in making objective assessment of N_F and N_{CD} in CMC and water with agitators other than the 6DT are described in the relevant sections of Chapters 4 and 5.

Gas cavity structure behind agitator blades was viewed in T72 by means of a de-rotational prism apparatus. This equipment has been described fully by Kuboi et al.[27] and enables a stationary image of the lower agitator to be observed via the flat, transparent vessel base. Fig. 3.1 shows the equipment in place below T72. The de-rotational prism was used in conjunction with a JVC GX-N7E video camera in order to record the images.

Difficulties associated with this method were that complete dispersion of gas in water or tiny bubble entrainment in CMC obscured the lower agitator from view. Lighting was also critical in obtaining a satisfactory picture of the lower agitator, the best results being

obtained when it was silhouetted against a well illuminated vessel upper section in an otherwise darkened laboratory.

3.4.3 Concurrent Cavity Observation and Torque Measurement.

In order to link the variation of gassed cavity size with fluctuations of torque in T72, a technique was evolved utilising two video cameras and monitors. The first camera was used to film the impeller and cavities via the de-rotational prism whilst the second was used to film the chart recorder logging torque measurements. Digital timers were superimposed on each recording so that if the timers were started simultaneously the exact effect of cavity size/structure on torque fluctuations could be monitored. This was achieved by playing back the recordings in a synchronized fashion on two video monitors. The only problem associated with the technique was maintaining sufficient light for the recording of the torque trace whilst ensuring the de-rotational prism camera operated at low enough light levels to clearly distinguish the cavities.

3.5 GASSED HOLD-UP

Gassed hold-up was measured using an ultrasonic unit in T45 and visually in T72. This was made necessary because the latter vessels stainless steel head-plate made fitting the ultrasonic unit impossible. The methods used in the two vessels will be described in turn.

3.5.1 T45

An ultrasonic ECHO unit, NIVOSONIC FMU2780 connected to SENSOR DU213 allowed continuous non-contact level measurement of single or two phase mixtures. Surface wave formation or a thin foam layer does not affect measurement. Ultrasonic pulses at approximately 46 kHz are emitted from FMU2780, reflected from the liquid surface and received by DU213, the

round trip time being measured electronically and appearing as an output signal (0-5VDC) directly proportional to liquid level. The output was logged using a chart recorder. The instrument was calibrated by changing the liquid level within the measuring span and producing a calibration curve. Measurement accuracy was ± 2mm of the liquid level. The sensor was positioned in the centre of the quadrant formed by the shaft and a pair of baffles, in order to obtain representative measurements.

3.5.2 T72

The ultrasonic probe could not be used in T72 due to the stainless steel headplate. Visual observations of the liquid level under gassed and ungassed conditions were therefore used to evaluate hold-up. This was facilitated by use of a stepladder in order to view the liquid level horizontally and a vertical tape (graduated in mm) attached to the clear Perspex vessel wall. Observations were made at a point midway between baffles for a duration of roughly two minutes. This reduced errors due to uneven distribution of hold-up. Measurement accuracy was estimated as ± 5mm. Measurements made during k_La experiments were timed to coincide with full steady-state conditions ensuring a stable hold-up value.

3.6 k_La MEASUREMENT : THE NEL/HICKMAN TECHNIQUE.

In this section the basic equipment, chemicals and technique are described. Further information concerning technique reproducibility, calculations and errors are given in Appendices II and III.

3.6.1 Theory.

Hydrogen peroxide is broken down by the enzyme catalase according to:

$$2H_2O_2 \longrightarrow 2H_2O + O_2 \qquad (3.2)$$

Where:

$$r = k\ [H_2O_2]^A\ [cat]^B \qquad (3.3)$$

The reaction rate (r) is first order with respect to hydrogen peroxide (i.e. A=1) and independent of catalase concentration over a wide range (i.e. B=0).

Typically a set amount of catalase is introduced into the reactor at the start of the experiment and hydrogen peroxide is then added continuously. Thus ,oxygen is continuously produced in the liquid phase. This oxygen is stripped from the liquid by a continuous flow of air through the vessel. Initially hydrogen peroxide and oxygen accumulate in the liquid until steady-state is reached. At steady-state the reaction rate is balanced by the peroxide addition rate and the rate of oxygen production is equal to the rate of oxygen transfer from the liquid to the gas phase.

$$r = Q_{H_2O_2}\ [H_2O_2]_{IN} \ / \ V \qquad (3.4)$$

and

$$r/2 = OTR = k_L a\ \Delta C \qquad (3.5)$$

The oxygen concentration driving force (ΔC) is determined from the dissolved oxygen concentration in the bulk liquid, C_L, the gas phase oxygen concentration, C_G and the solubility, H . The value of C_G may be determined by using either a fully back-mixed gas phase or plug flow gas phase mixing model (see Appendix III). For the calculation of $k_L a$, the only parameters required are:

- Concentration and feed rate of hydrogen peroxide.
- Dissolved oxygen concentration at steady-state.
- Gas flow rate and pressure.
- Liquid volume.

- Temperature.
- Henry's law constant.

Hickman[79] stated that the $k_L a$ values obtained from this method were independent of peroxide feed rate and catalase concentration over a wide range of test conditions. This is discussed further in Appendix III.

3.6.2 Hydrogen Peroxide.

Hydrogen peroxide (B.D.H. Ltd. G.P.R., 30% w/v concentration) was pumped into the vessel using a Watson-Marlow peristaltic pump via 4mm i/d silicon rubber tubing. The silicone tubing was attached to a thin bore stainless steel tube, fixed to one baffle and discharging beneath the liquid surface into a well mixed zone. The addition rate was monitored by placing the peroxide reservoir (3ℓ glass aspirator) on an Oertling digital balance (accurate to 0.01g) and recording weight loss with time.

The peroxide concentration in each bottle was checked by titration using potassium permanganate[93]. The average concentration was found to be 8.34 mol ℓ^{-1} e.g. some 5% below the concentration stated by the manufacturers (8.82 mol ℓ^{-1}), indicating the importance of checking concentration by titration. Periodically titrations were performed twice on the same peroxide sample, they showed a maximum variation of ± 2% of resultant peroxide concentration. Peroxide concentrations obtained in this way were incorporated in the $k_L a$ calculation procedure (Appendix III). Peroxide was stored in a cold room at 4^{o}C before being placed in the laboratory refrigerator.

The peroxide addition rate was manipulated to achieve a peroxide induced steady-state of between 130% and 300% of the pre-peroxide steady state dissolved oxygen value[94]. Steady-state levels of less than 130% saturation provide a low concentration driving force and are hence prone to increased errors (Appendix III). Levels of greater than 300%

saturation may allow spontaneous bubble formation which causes transfer to occur by a mechanism outside that normally found in the systems of interest. The above conditions were typically satisfied by molar addition rates of from 2×10^{-3}[mol/m^3/s] in 0.8% CMC to 2×10^{-2}[mol/m^3/s] in water.

3.6.3 Catalase.

Catalase solution (B.D.H. Ltd., bovine liver extract, 2×10^5 enzyme units per ml) was used to catalyse the degradation of hydrogen peroxide. The catalase was supplied in a solution containing 30% v/v glycerol and 10% v/v ethanol. Catalase addition was achieved by injecting a quantity of the enzyme (using a syringe) into a stainless steel tube which discharged beneath the liquid surface into a well mixed zone. When it was desired to add catalase continuously (see Appendix III) an aqueous solution was made up in a 1ℓ reservoir and pumped into the vessel. Catalase was stored in a cold room at 4°C and kept in ice immediately prior to addition.

There has to be a minimum concentration of active catalase in the vessel for the assumption of first order reaction rate, with respect to hydrogen peroxide, to hold. Insufficient active catalase will prevent steady state from being achieved or produce a pseudo steady-state. This problem can manifest itself either through insufficient initial active catalase or through catalase activity loss with time. On the other hand, high catalase addition levels (>0. 1 ml/l) may affect the system coalescence characteristics (due to presence of glycerol, ethanol and catalase). The concentration of catalase used is therefore important in determining the experimental accuracy and reproducibility. As both reaction rate and coalescence properties are system dependent, careful attention was paid to determining the correct concentration. The problems encountered due to catalase activity and their solutions are discussed in Appendices II and III. Recommendations for catalase concentration are

given.

3.6.4 Dissolved Oxygen Electrodes.

The dissolved oxygen concentration was measured using polarographic O_2 electrodes manufactured by Schott Gerät (model no. CG867) and supplied by Camlab Ltd.. Membranes used were 25μm P.T.F.E.. Three probes at 2:1 aspect ratio and 2 probes at 1:1 aspect ratio were mounted vertically in water tight tubes with just the probe tips showing. The probe positions within the vessel are shown in Fig.3.2. The deepest (no.1) probe was always mounted in the impeller discharge stream. The no.2 probe was in the upper IM discharge stream at H/T=1. Comments on multiple electrode readings are given in Appendix III.

Probes were mounted vertically in order to allow removal without draining the vessel contents. Although vertical probe mounting may increase bubble contact with the membranes (as opposed to horizontal, angled or membrane up orientation), the membrane surfaces were generally well swept by liquid. The Schott Gerät electrodes were used in conjunction with digital meters giving a visual readout and incorporating both temperature measurement and compensation. The dO_2 meters were connected to a chart recorder for data logging.

Probe maintenance consisted of daily replacement of membranes, 'O'-rings and electrolyte. Particular care was taken to ensure that no creases were present in the membranes, no air bubbles present in the electrolyte and a good membrane-probe seal obtained. Probes were zeroed in sodium sulphite prior to insertion into the vessel and spanned in the agitated-aerated vessel (i.e. at 100% saturation) prior to catalase/peroxide addition.

3.6.5 Typical Experimental Sequence.

Preliminary steps included filling the vessel with deionised water,

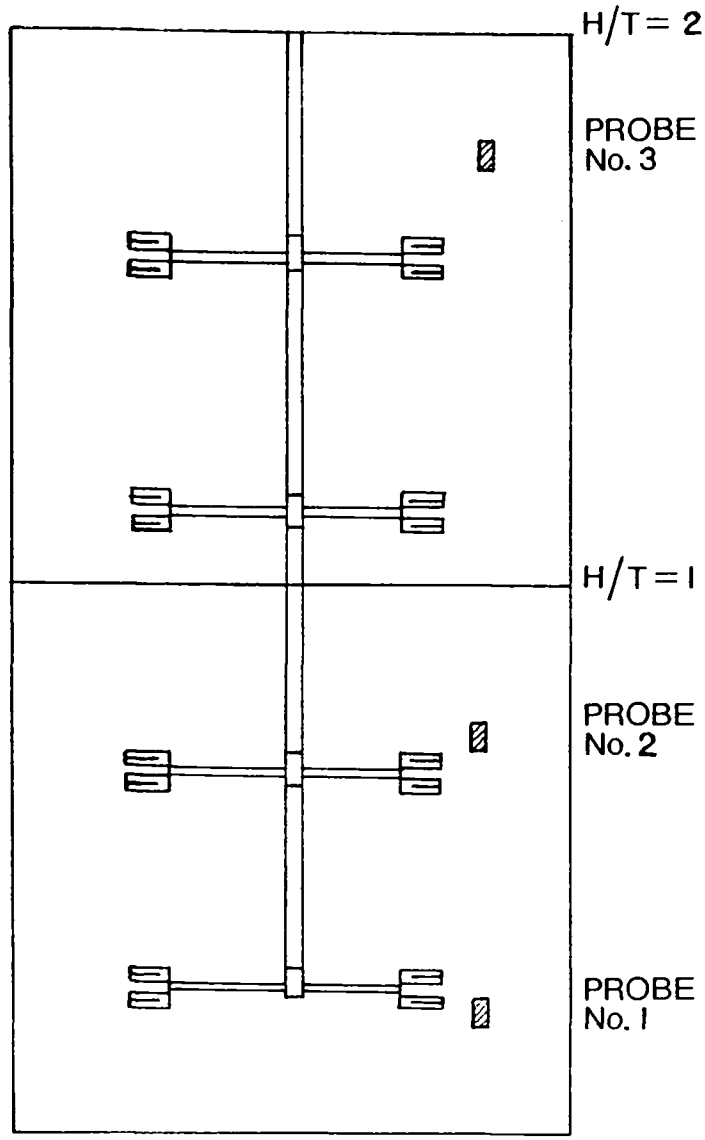

Figure 3.2 Schematic of Dissolved Oxygen Probe Positions.

adding and preparing any viscosity enhancing agent (Section 3.7.2), attaining vessel operating temperature, zeroing probes (with new membranes/electrolyte), mounting probes in the vessel and filling the H_2O_2 aspirator. Fig.3.3 shows a stylized dO_2 trace corresponding to the following numbered steps:

1. Aerate and agitate vessel, allow dO_2 to attain equilibrium, span probes (100%) for 5 mins.
2. Pump peroxide for up to 5 minutes to prime pump and tubing and to check for response of probes to peroxide. This will indicate a faulty probe-membrane seal. Cease pumping.
3. Add a pre-determined amount of catalase, dO_2 rises sharply as peroxide broken down. Allow dO_2 to return to equilibrium (100%).
4. Start timer and peroxide pump. dO_2 rises to peroxide induced equilibrium. Time for this was from 5 mins (water) to 30 mins (0.8% CMC). Allow at least 5 minutes at equilibrium.
5. Cease pumping; note aspirator weight and time, adjust N, Q_G and/or pump speed.
6. Commence pumping; allow dO_2 to attain new peroxide induced equilibrium value.

Various speeds, gassing rates and peroxide flowrates can now be investigated. Periodic checks should be made. The calibration of the dO_2 meters is checked by allowing the dO_2 level to fall to its equilibrium value. Repeat measurements are made under the same conditions (N, Q_G) to ensure no loss of catalase activity (Appendix III), change in liquid properties or equipment malfunction. At peroxide induced equilibrium the standing concentration of peroxide and catalase activity may be checked by adding a small quantity of catalase. The dO_2 level will rapidly increase and should then return to the original peroxide induced equilibrium level (unless insufficient catalase is present). If the resulting peak is very

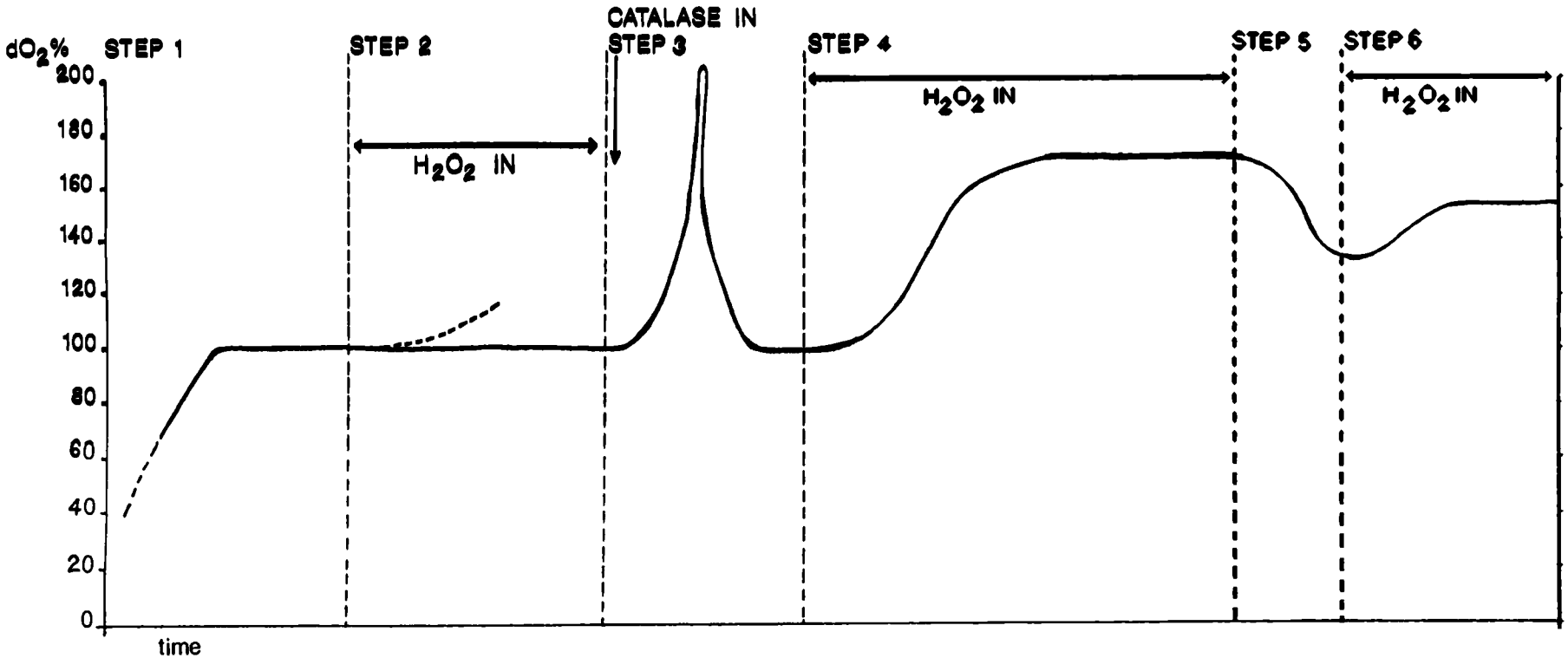

Figure 3.3 Stylized Dissolved Oxygen Trace for Typical Experimental Sequence.

large the standing concentration of peroxide is too high (see Appendix II).

3.7 TEST FLUIDS

The principal model fluids used in this study were deionised water and various concentrations of sodium carboxymethylcellulose (CMC). CMC is a clear, shear thinning, water soluble polymer which exhibits no yield stress. CMC, a cellulose ether, is produced by reacting cellulose with sodium monochloroacetate. It has a variety of commercial applications, acting as a thickening, binding and stabilising agent in the food and pharmaceutical industries. At high concentrations CMC exhibits viscoelastic effects[17,20]. Polymer solutions such as CMC have been used to model fermentation broths whose rheological properties arise from the presence of high molecular weight extracellular polymers e.g. Xanthan and Dextran , for example. Polymers may also be used to model mycelial fermentations whose rheological properties arise from the morphology and concentration of the micro-organism.

3.7.1 Deionised Water.

The vessel was always filled with water passed through a Houseman model deioniser which provided water of conductivity less than 22 mOhm/cm. This prevented variation in coalescance properties due to fluctuating trace chemicals and dissolved solids in the tap water supply. The use of deionised water allows accurate comparison with results of other workers assuming they also used deionised water. This avoids problems associated with regional variation in tap water quality.

3.7.2 CMC Preparation and Use.

A standard procedure was followed when preparing CMC in order to reduce inter-batch variation in rheological properties. Concentrations of

0.07% w/w, 0.4% w/w and 0.8% w/w were used. The CMC type was 7H4 (Hercules Ltd, London, UK). The moisture content of each bag of CMC was evaluated by weighing a sample before and after drying in an oven. Subsequently the CMC was stored in an air-tight container to prevent further change in moisture content. After weighing the required amount of CMC (accounting for water content), the powder was slowly added to the agitated vessel containing deionised water. Slow addition reduced lump formation. A tube inserted through the vessel headplate and ending just above the liquid level prevented powder from adhering to the vessel walls. The solution was agitated overnight at a speed below that at which surface aeration occurred in order to fully hydrate the polymer.

CMC prepared in this way was used for experiments during the following day only, in order to avoid degradation of the polymer due to microbial action, repeated shearing or changes in volume. Samples were taken for rheological analysis both before and after the experiments conducted using a particular batch of CMC.

3.7.3 Rheological Measurement.

The rheological properties of CMC were measured using a concentric cylinder Contraves Rheomat 30 (Contraves Industrial Products Ltd, Ruislip, Middlesex, UK). The operating principles of this class of rheometer are described by Barnes et al.[1]. The fluid under test was subjected to a reversible speed cycle giving a range of shear rates dependent upon the measuring system used. The torque and speed data were processed to provide shear stress values. Measuring systems A and B were used giving maximum shear rates of 660 s^{-1} and 157 s^{-1} respectively. Readings were taken during the increasing shear rate phase of the cycle over the range 57 s^{-1} to 660 s^{-1} (A) and 14 s^{-1} to 157 s^{-1} (B). These shear rates correspond to the average vessel shear rate range calculated according to Equation 2.6 of 25 s^{-1} to 110 s^{-1}.

The temperature of the measuring head was controlled by placing it in a water bath. Sample temperature was chosen to correspond with the particular experimental mean temperature in the range 24°C ± 1°C. In this way rheological measurements were matched as closely as possible to the conditions in the vessel.

The shear stress-shear rate characteristics of a sample were determined by fitting the data to the power law model (Equation 2.3) using linear regression, which gave an excellent fit. This provided values of K (consistency index) and n (flow behaviour index).

3.7.4 Rheological and Physical Properties of Test Fluids.

Figure 3.4 shows the power law parameters n versus K for the three concentrations of CMC used. Both pre-experimental and post-experimental data are shown. The scatter of pre-experimental data indicates that it is not possible to reproduce these parameters exactly when preparing CMC solutions. Post-experimental samples showed a similar degree of scatter to that seen when preparing CMC. The post-experimental K values tended to be marginally lower than the pre-experimental ones. This was probably because of the slight dilution due to water production in the NEL/Hickman technique and/or continued shearing. Values of K and n for each run were obtained by linear interpolation between pre and post-experimental measured values.

The density and surface tension of CMC solutions used was taken as that of water. This has been shown to be satisfactory by a number of authors[2,95,96] for CMC concentrations of less than 1%.

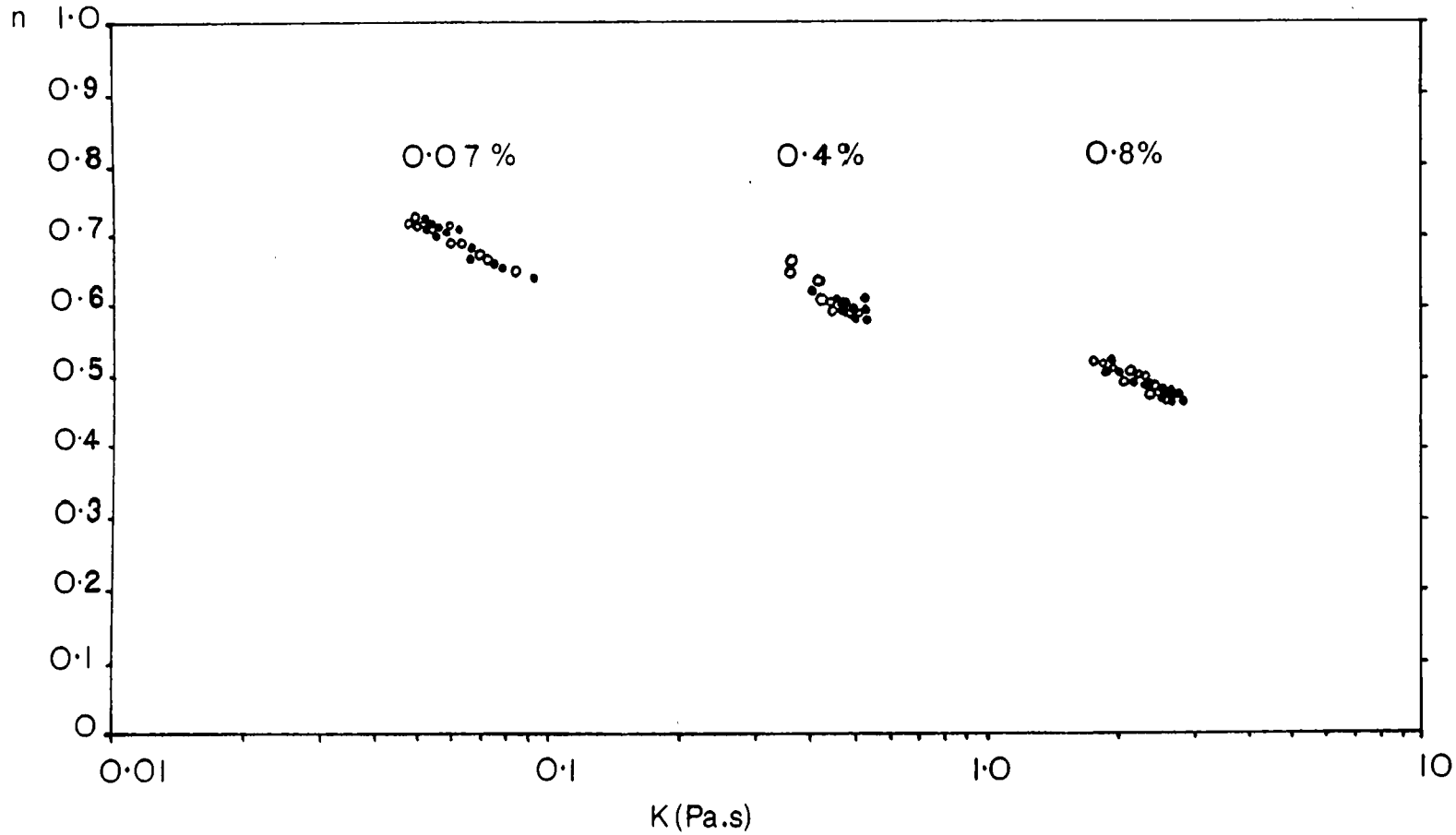

Figure 3.4 Variation of Power Law parameters, K and n in CMC Solutions.

Pre-Experimental: • Post-Experimental: o

4.1 INTRODUCTION

This chapter is concerned with investigation of the fluid dynamics and power demand of InterMIG^{R} (IM) agitators in the 0.45m and 0.72m diameter vessels (see Section 3.2). A detailed literature survey of the information pertaining to these agitators is given in Appendix I.

The IM impellers used in conjunction with T45 and T72 were of the bifurcated variety and had the dimensions given in Table 4.1 and Fig.4.1. Both sets of impellers were manufactured by Ekato Gmbh to vessel specifications supplied to them by Birmingham University. As Table 4.1 shows, the D/T ratios were not identical for the IM used in the two vessels. This resulted in a situation where the effect of scale-up on the impeller power characteristics could not be precisely identified due to geometric dissimilarity. However, the inner and outer blade diameter to overall impeller diameter ratios of the two sets of IM corresponded.

The agitator shaft in T45 was solid whereas that in T72 was hollow, causing their shaft to vessel diameter ratios and IM hub dimensions to differ (Table 4.1). The T72 IMs had a much larger hub to vessel diameter ratio. The blade angles were the same for the two sets of impellers (Fig.4.1).

The separation (S/T) of IM impeller stages and the clearance of the lower IM from the tank base (C/T) are given in Table 4.2 for the two vessels. The recommended separation of stages given by Ekato[97] is S/T = 0.5, however, in T45 and T72, S/T values were 10% and 6% lower respectively. These separations were necessitated by a requirement to reproduce conditions used by Perfect[98] in the T45 case and to avoid the positioning of impellers directly over strain gauge mounting points in the

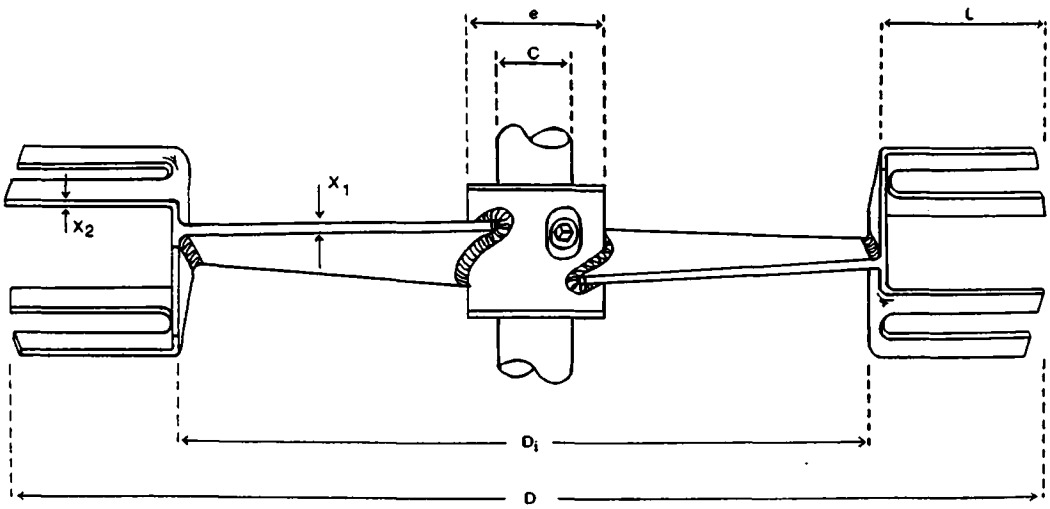

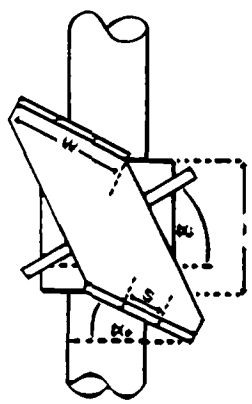

Figure 4.1 InterMIG Impeller.

TABLE 4.1

SPECIFICATION OF INTERMIG^{R} IMPELLERS

Dimension	T45	T72
D(m)	0.267	0.396
D/T	0.593	0.55
D_i/D	0.68	0.68
L/D	0.16	0.158
W/D	0.11	0.11
s/D	0.037	0.044
e/D	0.13	0.22
c/D	0.07	0.157
I/D	0.13	0.215
x_1/D	0.009	0.0101
x_2/D	0.006	0.0063
α inner	25°	25°
α outer	30°	30°

TABLE 4.2

STANDARD GEOMETRIES FOR INTERMIGS IN T45 AND T72

Dimension	T45	T72
D/T	0.593	0.55
C/T	0.3	0.24
S/T	0.45	0.47
H/T	1	1 or 2

TABLE 4.3

SPARGERS USED WITH INTERMIG IMPELLERS

Units [m]

Vessel	Sparger Name	D_s/D	D_s/T	C_s/C	d_h	n	d_z
T45	Medium Ring	0.71	0.42	0.32	0.003	12	0.01
T72	Point	-	-	0.64	0.01	1	0.0125
T72	Small Ring	0.43	0.24	0.35	0.002	32	0.0125
T72	Medium Ring	0.86	0.47	0.35	0.002	65	0.0125
T72	Large Ring	1.22	0.67	0.35	0.002	91	0.0125

case of T72. Ekato[97] recommended lower impeller clearances of C/T = 0.22 for IM. Again constraints due to reproducing the conditions of Perfect[98] in the T45 case and distance between shaft tip and base in the T72 case led to the use of higher clearances of C/T=0.3 and 0.24 respectively. In vessel T72, a lower clearance would have caused the bottom impeller hub to project beyond the shaft tip to an unacceptable extent.

Each IM stage is mounted at 90° to the preceding stage and the impellers are always used in at least pairs for each H/T=1. Therefore, in T45, 2 IM 06 were used and in T72 either 2 or 4 IM 055 at H/T = 1 or 2. The usual rotation direction for IM is such that the outer blades pump downwards whilst the inner pump upwards, and is referred to as the U.P.M. (Upward Pumping Mode), describing the inner blade action.

Gas spargers used in conjunction with IM impellers are detailed in Table 4.3 and are stipulated when results are presented. The sparger positions relative to the vessel base and lower impeller are also given in Table 4.3 although in the case of the D_S/D = 1.22 ring sparger considerable sparger oscillation occurred due to fluid dynamic forces at high gas rates and stirrer speeds.

A variety of spargers were tested with IM in T72 in order to assess the influence of sparger type on individual impeller and total torque, gas dispersion, gas hold-up and k_La. Appendix I delineates references to tests on different sparger types used with IM[7,20]. The ring sparger being the most common although usually of unspecified dimensions. Generally, centrally located spargers have been found to perform slightly worse (k_La, gas dispersion) due to gas preferentially rising in the shaft region, avoiding the impeller tip regions in the U.P.M.. No affect on gassed power draw or hold-up has been commented upon.

4.2 FLOW PATTERNS AND SURFACE AERATION

4.2.1 Introduction

During agitation, impellers create fluid flow within a vessel, the characteristics of which are dependent upon agitator type, agitator dimensions, vessels geometry, fluid type(s) and impeller rotation direction and speed. Observations of flow patterns are therefore useful in determining the ability of an agitation system to blend fluids, contact phases, suspend solids and provide adequate heat transfer. The relationship between flow pattern generated at different impeller spacings and clearances and the power drawn may also be useful for achieving optimum agitator configuration. Both bulk flow and local turbulence are required for a good mixing performance, the former in order to homogenize vessel contents rapidly and the latter to provide a high degree of shear for bubble breakup, mass transfer, heat transfer and micromixing. Stagnant zones where little or no motion is imparted on the fluid should be avoided to prevent temperature or concentration gradients which may adversely effect mixing vessel performance. For more exact analysis of flow behaviour the measurement of fluid velocity fields may be achieved using Hot-wire Anemometry or Laser-Doppler Anemometry, these techniques may also provide details of the distribution of energy dissipation or shear stress. Appendix I details studies of IM velocity fields using L.D.A.

4.2.2 Flow Patterns

In this work a qualitative picture of IM flow patterns was achieved by adding neutral buoyancy tracer particles to the fluid under agitation (water) and observing the resultant tracer movement in the clear Perspex vessels. Figures 4.2 and 4.3 show generalised flow patterns for 2 IM at 1:1 aspect ratio, the former in the U.P.M. and the latter in the D.P.M., both are under unaerated conditions. It should be noted that although the

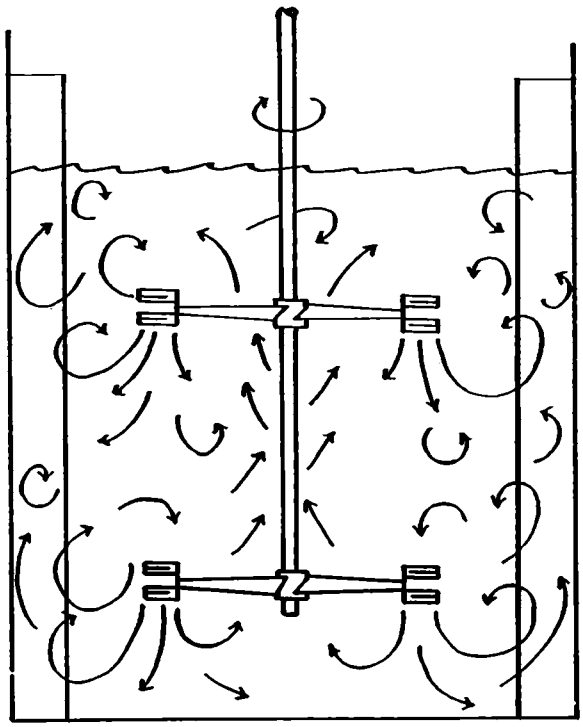

Figure 4.2 InterMIG Flowpattern (UPM).

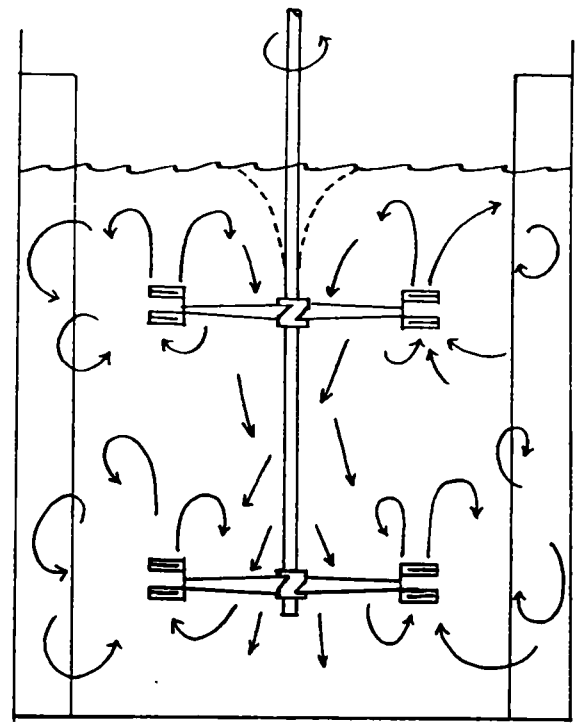

Figure 4.3 InterMIG Flowpattern (DPM).

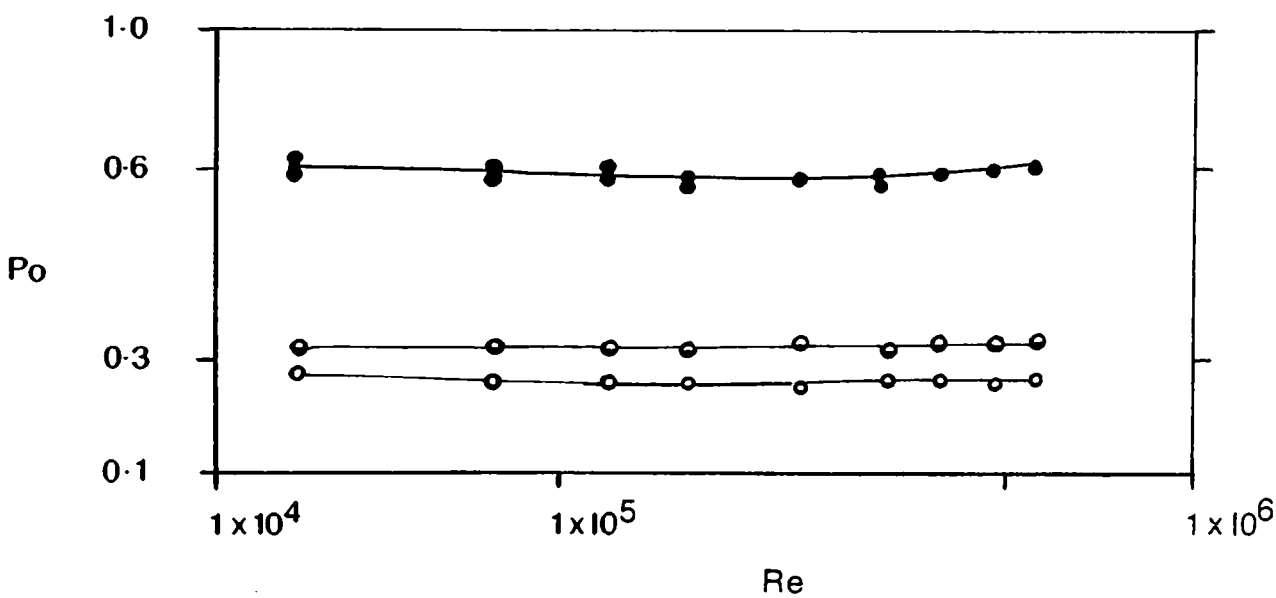

Figure 4.4 T45 InterMIG Powercurve, H/T=1, Water.

Both IM: • Upper IM: ⊖ Lower IM: ○

IM impellers in Figs.4.2 and 4.3 are depicted as being in the same vertical plane this is for pictorial convenience and the impellers were in fact mounted at 90° to each other.

The unaerated IM flowpattern in the U.P.M. is characterized by strong downward flow in the region of the impeller outer blades and less strong upward flow around the shaft associated with the impeller inner blades. Large eddies are formed in the outer blade region from which small eddies break-off and scour the vessel wall and base. Hence, IMs provide primarily axial flow with a strong radial component imparted by the outer blades. Observation from underneath the vessel also shows fluid movement in a tangential direction corresponding to the impeller rotation direction.

It is apparent that due both to the counter-current nature of the induced flow and the multiple IM stages, the flow pattern produced is highly chaotic and not as easy to define as that of the Rushton turbine. Stagnant zones are likely to occur at most speeds in the region where the agitator shaft enters the liquid. This phenomenon indicates the shortcomings of surface additions to the mixing vessel, as blending times may be considerably increased[13]. At low impeller speeds the periphery of the vessel base is also poorly mixed with unsuspended particles congregating in front of the baffles[99].

Reversing the impeller rotation direction leads to changes in the flowpattern depicted in Fig.4.3. The inner blades produce a downward flow which creates a vortex around the shaft. This leads to surface aeration at lower speeds than when operating in the U.P.M. As the vortex approaches the upper impeller air is dispersed into the surrounding liquid. This configuration may be advantageous for ingesting floating solids.

4.2.3 Surface Aeration

The shaft speed (N_{SA}) at which gas bubbles were entrained from the free liquid surface and dispersed within the vessel was recorded for various fluids and geometries using IM impellers. These results are shown together in Table 4.4 and are also shown on each power curve in Sections 4.3.1 and 4.3.2. The criterion for the onset of surface aeration was taken as the observation of entrained bubbles to the depth of the bottom agitator (H/T = 1 and H/T = 2).

Doubling H/T increased N_{SA} in water and 0.07% CMC. The increase in N_{SA} at H/T = 2 was due to a greater upper impeller depth (C_2/T) and a greater depth to which the bubbles had to be entrained (lower impeller). N_{SA} was also raised by increased liquid viscosity, no surface aeration being seen at any speed in 0.8% CMC. N_{SA} was reduced in the D.P.M. due to a vortex around the shaft drawing air down to the upper InterMIG.

4.3 UNAERATED POWER CHARACTERISTICS

4.3.1 Standard Geometry, U.P.M.

In this section unaerated Power numbers found using IMs in T45 at H/T = 1 and T72 at H/T = 1 and H/T = 2 are presented in the form of power curves.

Figure 4.4 shows the combined and individual IM Po obtained in vessel T45. Over the range Re = 4×10^4 to 5.8×10^5 (turbulent), $\bar{P}o = 0.6$. The lower IM stage was found to draw slightly less power than the upper stage so that $\bar{P}o$ (lower) = 0.28 and $\bar{P}o$ (upper) = 0.32.

Comparison with the results of Bujalski[12] who obtained $\bar{P}o = 0.65$ in T45 with S/T of 0.5 as opposed to 0.45, suggests that increased separation increased Po slightly[7] (see Section 4.3.2). The power data obtained by Perfect[98] is very different from that found here and by Bujalski[12], inspection of the raw data reveals gross inconsistencies which make it unusable. Surface aeration did not influence $\bar{P}o$ in the U.P.M..

TABLE 4.4

N_{SA}; INTERMIG IMPELLERS

Vessel	H/T	Test Fluid	Pumping Mode	C_2/T	N_{SA} [rpm]
T45	1	Water	UPM	0.25	240
	1	"	DPM	"	200
T72	1	"	UPM	0.29	225
	1	"	DPM	"	180
	2	"	UPM	0.35	250
	1	0.07% CMC	UPM	0.29	260
	1	"	DPM	"	210
	2	"	UPM	0.35	280
	1	0.4% CMC	UPM	0.29	325

The IM power curve for T72 at H/T = 1 is shown in Fig.4.5. Data for 3 concentrations of CMC and water is shown. The total unaerated $\bar{P}o$ fell from 0.89 at Re = 5 x 10^2 to 0.65 at Re = 4 x 10^3 in 0.8% CMC and from 0.65 at Re = 1.75 x 10^3 to 0.6 at Re = 1.2 x 10^4 in 0.4% CMC, the two concentrations overlapping between Re = 1.75 x 10^3 and 4 x 10^3. For Re > 7 x 10^3 the $\bar{P}o$ had a constant value of 0.6 (0.4%, 0.07% CMC and water). Values of Re at which entrained gas was dispersed to the bottom agitator are shown for each fluid, but no reduction of $\bar{P}o$ was apparent. The individual Po are also shown in Fig.4.5. As was found in T45 the lower impeller drew less power ($\bar{P}o$ = 0.28; Re > 7 x 10^3) than the upper ($\bar{P}o$ = 0.32 for Re > 7 x 10^3). The $\bar{P}o$ in T45 and T72 were very similar in the turbulent regime in spite of the previously mentioned geometrical differences of D/T, S/T and hub size.

Comparison with unaerated power data from literature sources (Appendix I) generally shows good agreement[20,91,99]. The literature indicates higher power draw for the upper stage in the U.P.M. No minima were apparent in the power curve, as has been commented on previously[20]. The shape of the power curve obtained here can be compared with Fig.A.I.3 and the close similarity seen. The only other workers who reported data in CMC[20,91] operated at Re < 1.5 x 10^3. However, Hickman[20] showed Po falling from 1.0 to 0.8 between Re = 5 x 10^2 and 1.5 x 10^3 whereas here Po fell from 0.9 to 0.66 over the same range. Allsford[91] on the other hand gave Po = 0.65 and Po = 0.5 for CMC and Carbopol respectively at Re = 1 x 10^3 which is slightly lower than this work. Himmelsbach[100] obtained $\bar{P}o$ = 0.7 to 0.8 in Xanthan (Re = 1000) which agrees well with the findings here. Power curves obtained by Ibrahim[99] and Bujalski[12] in glucose show good agreement with the shape of the power curves obtained using CMC in this work.

The power curve obtained using 4 IM 055 at H/T = 2 is shown in Fig.4.6. The shape of the curve was identical to that found at H/T = 1, the total

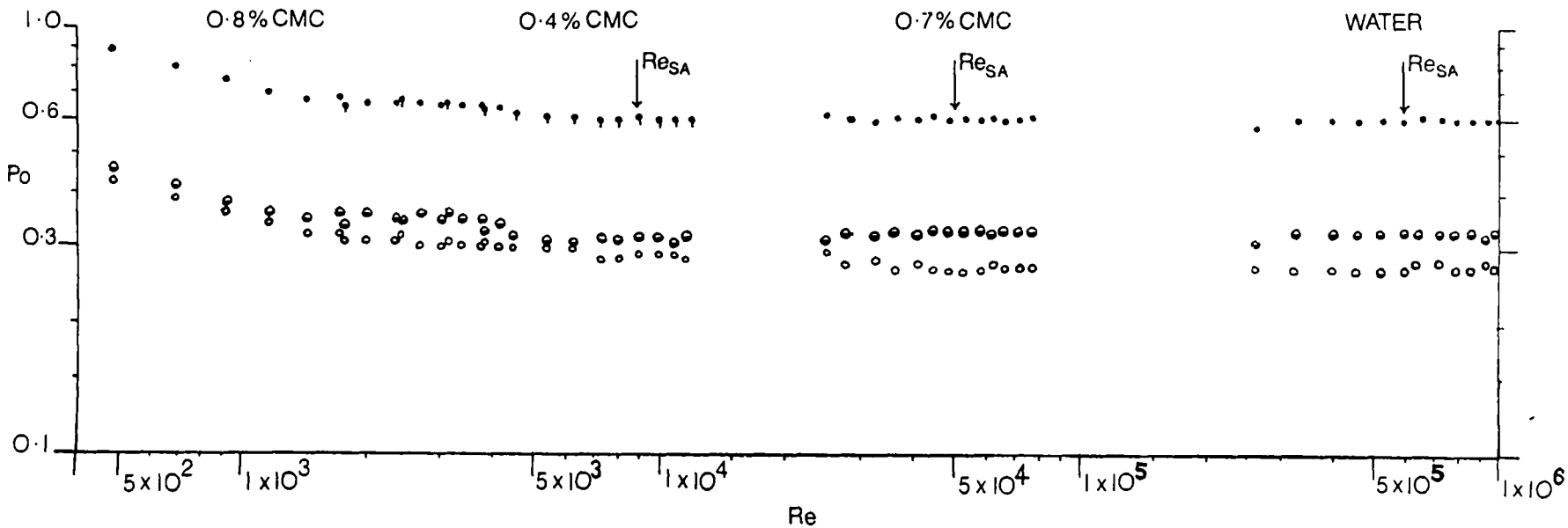

Figure 4.5 T72 InterMIG Powercurve, H/T=1.

Both IM: • Upper IM: ● Lower IM: o

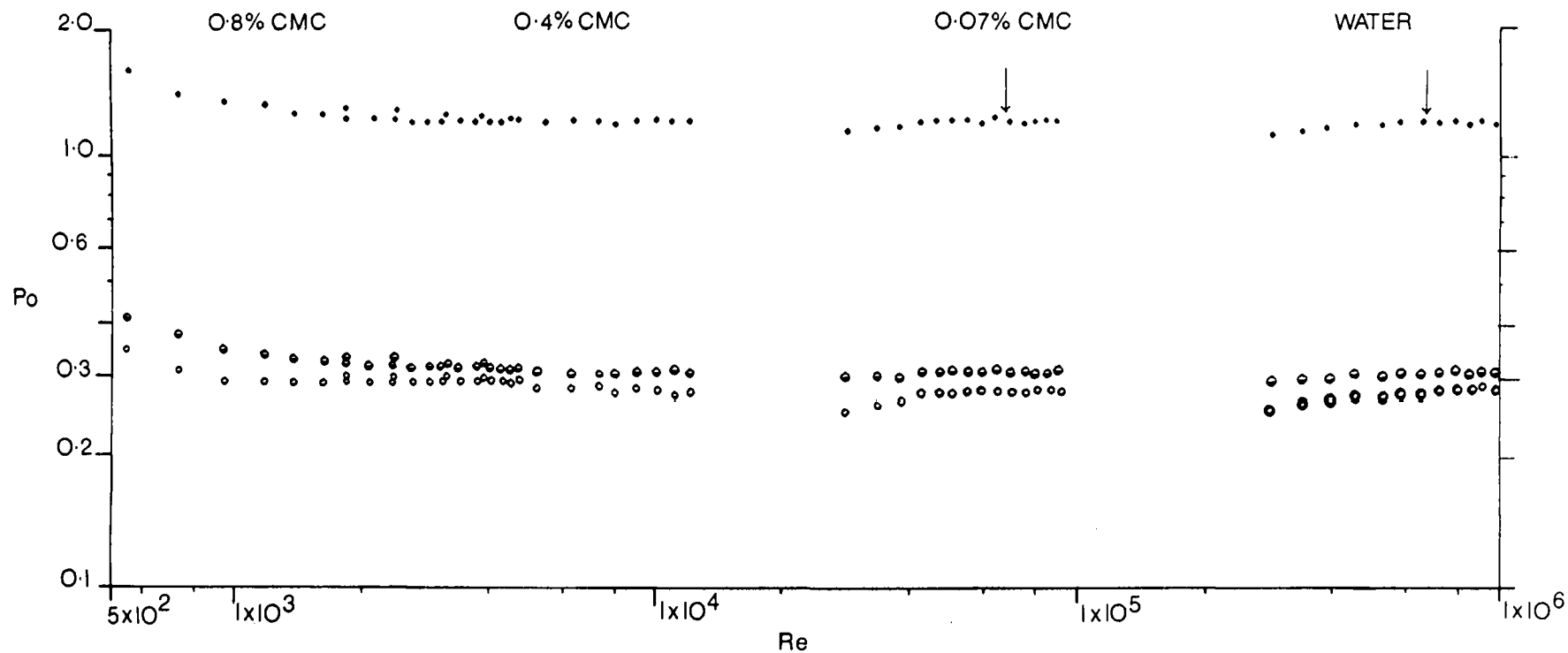

Figure 4.6 T72 InterMIG Powercurve, H/T=2.

4 IM: • Each upper IM: ⊙ Lower IM: ⊙

$\bar{P}o$ being doubled due to the 2 additional agitators. The torque developed by the bottom impeller and total torque were measured enabling the torque developed by the upper three impellers to be found by subtraction. This torque was divided by three to give an approximate torque value for each upper impeller shown in Fig.4.6. In the turbulent flow regime the lower impeller $\bar{P}o$ = 0.275 and each upper $\bar{P}o$ = 0.315. The results demonstrate that the Po in vessels of H/T > 1 may be predicted by treating each additional agitator as the upper agitator in H/T = 1 configurations (adjusting for S/T see Section 4.3.2 below). No literature data are available for comparision at H/T > 1.

The constant value of the Po at Re > 5 x 10^3, when compared with that of the 6DT and 6PSDT (see Section 5.2) suggests easier mixer design for bioreactors where viscosity increase causes Re to fall over the duration of a fermentation.

4.3.2 D.P.M. and S/T Variation

In this section, the effects of changes from the standard IM geometry and pumping mode on the unaerated Po are considered. Fig.4.7 compares Po for the U.P.M. and D.P.M. in T72 using water. The two pumping modes provided very similar Power numbers at low and intermediate speeds but the D.P.M. Po fell below that of the U.P.M. at Re > 8 x 10^5. This behaviour was due to the intensity of surface aeration caused by the vortex formed by the inner blade pumping action in the D.P.M.

In the U.P.M., air was entrained from the surface in the Re range over which the D.P.M. Po reduction was seen, but the extent of surface aeration was not sufficient to reduce Po. The volume of gas entrained by the D.P.M. was sufficient for gas filled cavities to form and enlarge to the point at which torque was reduced, even on the lower impeller.

The absence of effect of rotational direction on Po for IM has been found by other workers[20,91] at different scales. Allsford[91] also found a

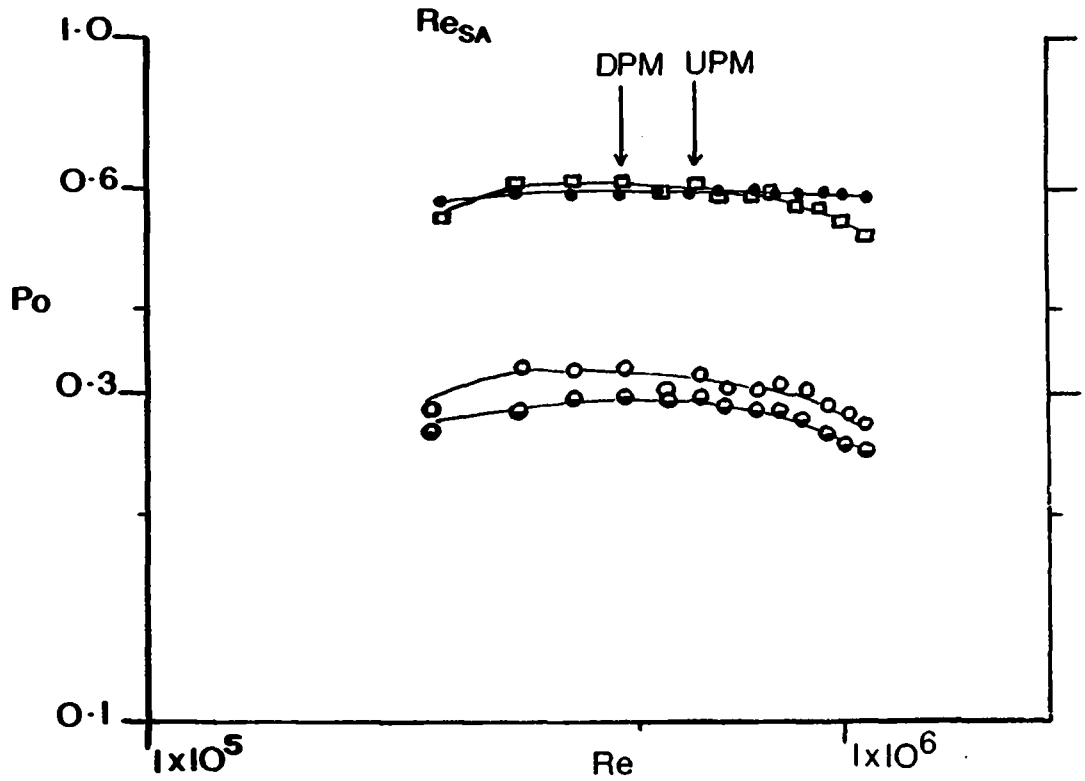

Figure 4.7 T72 InterMIG Powercurve, Water.

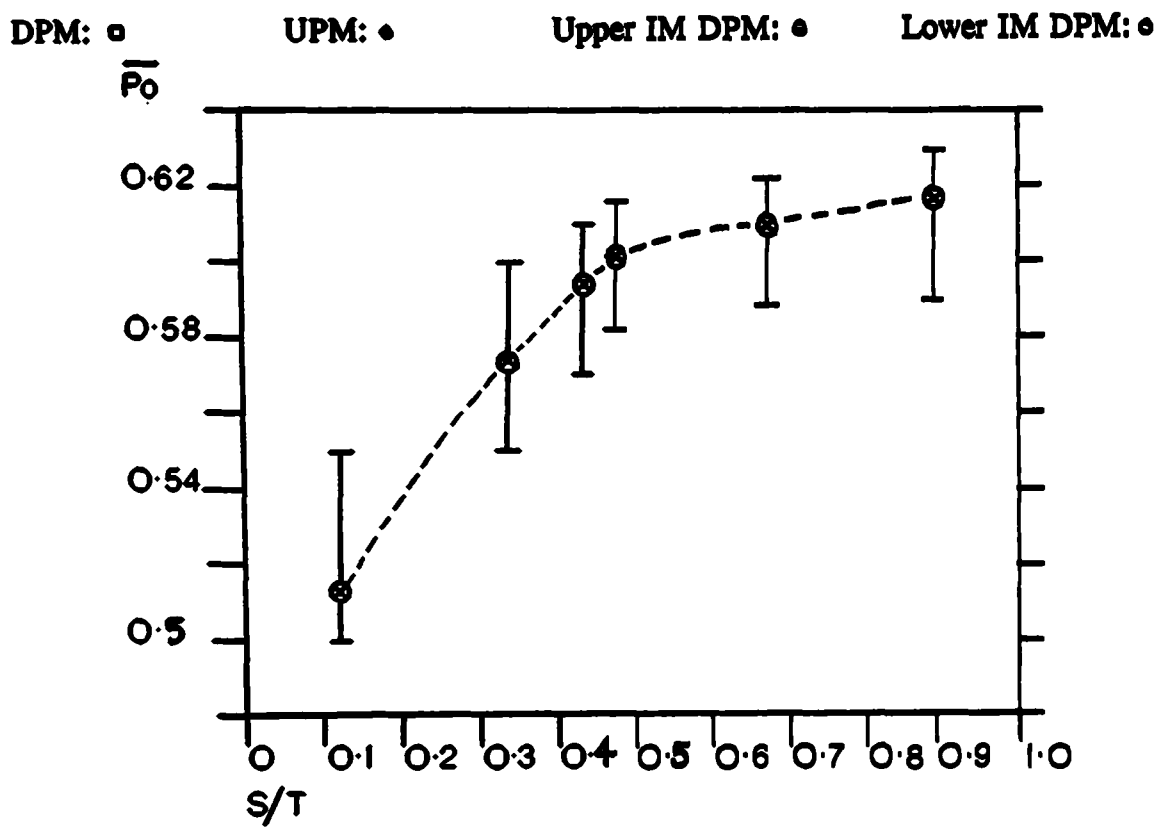

Figure 4.8 Effect of InterMIG Separation, Water.

reversal of the relative power draw of the upper and lower IMs when the D.P.M. was used, as was observed in this work.

The effect of mounting the two IM stages in a planar fashion as opposed to the usual 90° orientation was found to have a negligible effect on Po in water.

A series of experiments were conducted in order to quantify any effect of inter-impeller spacing (S/T) on power draw in water. In order to accomplish this the upper IM was moved whilst the lower was held stationary at C/T = 0.24. For this set of experiments, 2 IM 055 were used with the vessel filled to H/T = 2 to avoid surface aeration. Fig.4.8 shows the average unaerated Po vs S/T and includes the Po range from which the average was obtained. As can be seen from this figure, reducing S/T from 0.5 to 0.12 (impeller hubs touching) reduces $\bar{P}o$ by roughly 15% whereas increasing S/T from 0.5 to 0.89 increased $\bar{P}o$ by only about 3%.

These results can be explained by the interference effect of the flow produced by the lower agitator on that of the upper. At low S/T the interference between stages was magnified and reduced Po quite strongly. As S/T increased, the interference between flow patterns was reduced until at S/T $\simeq$ 0.5, the induced flows barely effected each other. At S/T > 0.5, the stages acted almost independently so that $\bar{P}o$ only increased marginally.

These findings indicate an optimum inter-impeller spacing of approximately 0.5T as recommended by the manufacturer[97]. The reduction in power drawn by a stage due to the inability of the flow pattern to properly develop explains the slightly lower $\bar{P}o$ found for the bottom impeller in the U.P.M. where the vessel base interferes with the flow produced by the outer blades. In the D.P.M., the most intense flow (from the outer blades) is in the upward direction enabling full flowpattern development and consequentially a higher Po for that stage. As previously mentioned (Section 4.2.2), the IM flow pattern is very chaotic and not

easy to define. It is therefore interesting to note that the development of this 'flow pattern' effects the power drawn.

The effect of inter-impeller spacing on Po has been studied using 6DT agitators of D/T = 0.5[13], 0.33[15] and 0.4[16]. Combined Po was found to be reduced by 35% when impeller hubs were touching. Full power (twice the single agitator power) was achieved at S/T = 0.5 (D/T = 0.33), S/T = 0.7 (D/T = 0.4) and S/T = 1.0 (D/T = 0.5). Increasing diameter ratio clearly increases the separation required before full power is drawn, due to the size of the circulation loops. The power reduction observed with IM was considerably less than that reported for the 6DT. This may be due to the 90° stage orientation or less defined flow pattern enabling more complete flow development at low S/T. These findings confirm the multi-stage principle inherent in IM design which achieves high D/T impellers operated at low S/T with no loss of potential energy dissipation.

4.4 AERATED POWER CHARACTERISTICS IN WATER.

4.4.1 Bulk Flow Regimes

A number of bulk (or bubbling) flow regimes have been defined for the 6DT and other impellers (see Chapt. 2) which describe the stages of gas dispersion within a vessel. The criteria for defining the changes from one regime to the next have been applied for the IM as shown in Fig.4.9 (for spargers of Ds/D < 1). When increasing N from zero at constant Q_G, the 2-phase flow is initially gas dominated (4.9a), i.e., flooded. The transition from flooding to loading is not as easy to define as with the 6DT. The IM becomes partially loaded, (4.9b), as the outer vanes intermittently disperse gas radially and downwards, the main gas flow still rises via the vessel shaft. As N was increased further, a greater proportion of the influent gas was dispersed by the outer vanes and the central flow reduced (4.9c). The observation of N_F was taken as continual dispersion of gas by the outer vanes and reduced centrally rising gas

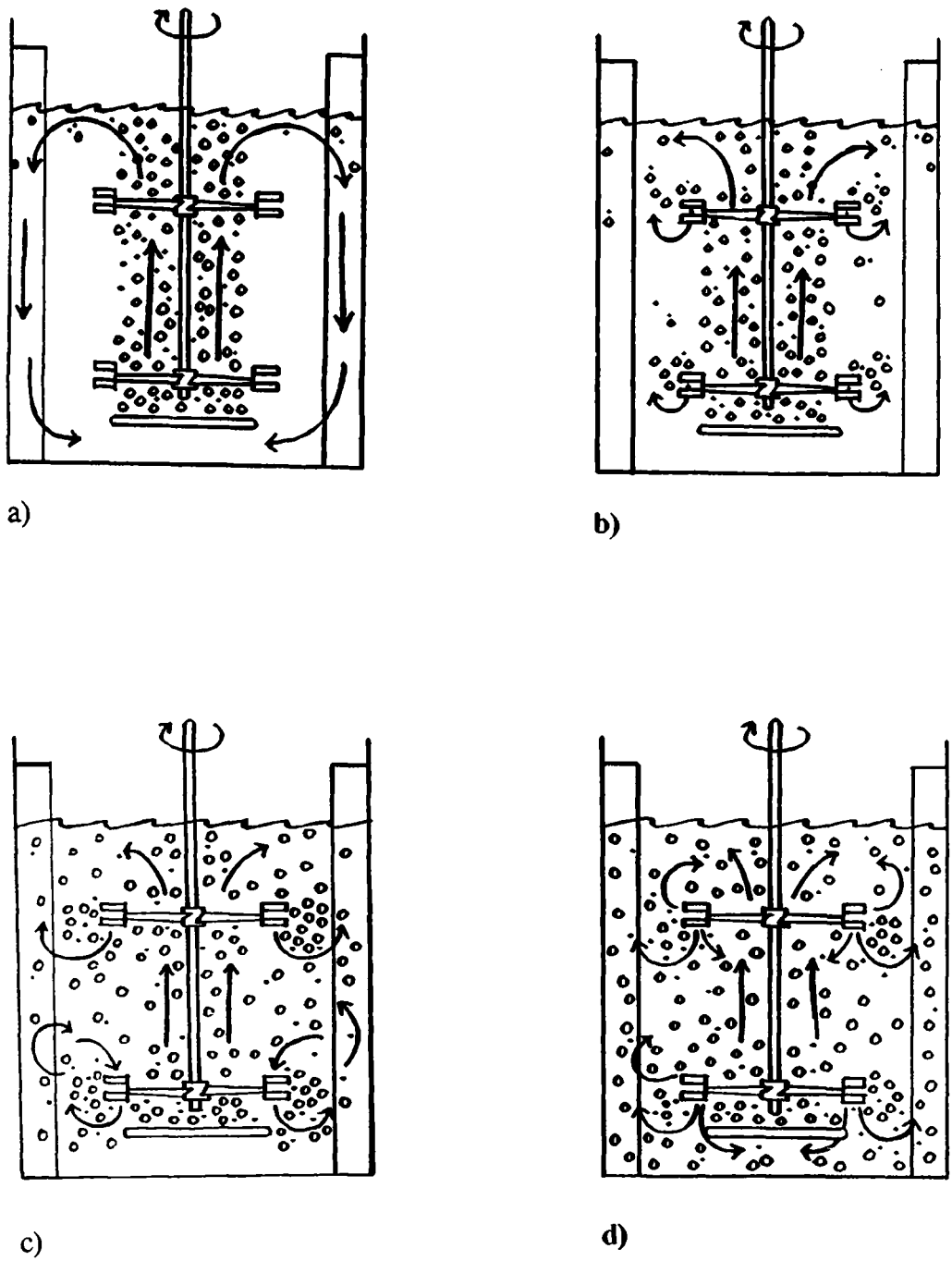

Figure 4.9 **InterMIG Gas-Liquid Bulk Flow.**

flow. This judgement was however highly subjective.

Further N increase caused the gas to be dispersed downwards to the vessel base. This condition is known as complete dispersion (Fig.4.9d), the criterion for this transition being regular contact between bubble swarms and the vessel base. The speed at which complete dispersion occured, N_{CD}, was not easy to define as the transition was gradual with occasional bubble/base contact becoming increasingly frequent with N increase. Some influent gas still passed up the agitator shaft even after the onset of complete dispersion. This bypassing was especially noticeable when using spargers which introduce gas into the inner as opposed to outer blade region.

Values of N and P/V for the flooding/loading transition and complete dispersion are summarised in Table 4.5 for water. Correlations relating the specific power input required for the flooding/loading transition and complete dispersion are detailed in Tables 4.6 and 4.7 respectively.

Flooding was strongly affected by sparger type. The highest P/V was required when using the point sparger or small ring sparger (SRS). Both of these spargers introduce air into the inner blades which produce non-intense upward flow. The gas stream must therefore travel radially before encountering the more intense downward flow from the outer vanes, higher speeds being required for this.

The medium ring sparger (MRS) discharged gas into the outer vanes, lower speeds and power being needed to overcome the buoyancy of the gas stream because of the more intense flow from this part of the impeller.

The large ring sparger (LRS) required the lowest P/V for loading, air was dispersed radially at $N \leq 50$ [rpm] which was too low for accurate torque measurement. The LRS gas stream was introduced into the strong axial/radial flow generated by the outer vanes, but did not enter the impeller directly. The lower IM therefore had a greater pumping capacity

TABLE 4.5

FLOODING/LOADING AND COMPLETE DISPERSION IN WATER

Vessel	Impeller	Sparger	Q_G (1:1) [vvm]	N_F [rpm]	N_{CD} [rpm]	P/V_F [kWm^{-3}]	P/V_{CD} [kWm^{-3}]
T72	InterMIG 055	Point	0.5	140	220	0.15	0.6
			1	180	260	0.29	0.8
			1.5	200	280	0.36	0.95
T72	InterMIG 055	Ds/D=0.43 (SRS)	0.5	140	220	0.15	0.6
			1	180	240	0.29	0.64
			1.5	180	280	0.28	0.95
T72	InterMIG 055	Ds/D=0.86 (MRS)	0.5	90	200	0.03	0.47
			1	130	220	0.11	0.5
			1.5	130	260	0.1	0.8
T72	InterMIG 055	Ds/D=1.22 (LRS)	0.5	-	110	-	0.07
			1	-	125	-	0.11
			1.5	-	125	-	0.1
T45	InterMIG 06	Ds/D=0.71 (MRS)	0.46	60	185	0.02	0.36
			0.93	85	200	0.04	0.45
			1.15	85	215	0.04	0.55

TABLE 4.6

FLOODING/LOADING IN WATER

$(P/V)_F = A\ (Q_G)^{\beta}$; [$kWm^{-3}$], [vvm]

Vessel	Sparger	A	β	R^2
T72	P.S.	0.27	0.81	0.98
T72	S.R.S. Ds/D=0.43	0.244	0.61	0.83
T72	M.R.S. Ds/D=0.86	0.077	1.18	0.82
T45	M.R.S. Ds/D=0.71	0.039	0.81	0.95

TABLE 4.7

COMPLETE DISPERSION IN WATER

$(P/V)_{CD} = A(Q_G)^{\beta}$; [$kWm^{-3}$], [vvm]

Vessel	Sparger	A	β	R^2
T72	P.S.	0.801	0.42	0.99
T72	S.R.S. Ds/D=0.43	0.741	0.38	0.73
T72	M.R.S. Ds/D=0.86	0.598	0.44	0.71
T72	L.R.S. Ds/D=1.22	0.095	0.36	0.70
T45	M.R.S. Ds/D=0.71	0.494	0.43	0.93

when using the LRS as opposed to the MRS. Comparison of $(P/V)_F$ from the two scales shows a reduction in specific power required at the smaller scale.

$(P/V)_{CD}$ followed a similar trend to that found for the flooding/loading transition using differing spargers. A reduction in specific power was seen with increasing sparger diameter. The reasons for this phenomenon are the same as those detailed for flooding. For scale-up at constant Q_G, [vvm], a higher specific power input was required for complete dispersion at the larger scale. Similar increases have been noted for 6DT[22], 6MF[34] and Prochem Maxflo T hydrofoil impellers[36]. The exponents, β, found for IM were lower than those reported for the 6DT[12,22,36], Prochem pumping down[36], A315[36], 4MFD[34] and 6MFD[12] but similar to those of the 4MFU[34], 6MFU[12] and Prochem pumping up[36].

This indicates an insensitivity of IM $(P/V)_{CD}$ to Q_G increase and may be due to an increasing proportion of the influent gas passing up the vessel via the inner blades, bypassing the outer vanes.

4.4.2 Gas Cavities in Water

The formation of gas-filled cavities is caused by gas being sucked into low pressure regions behind the agitator blades. This generally results in a reduction in power drawn due to streamlining and reduced pumping capacity. In this work cavities were observed using a de-rotational prism (see Chapt.3) from underneath the agitator and using a stroboscope from the side. The cavities described here can be seen on video by application to the School of Chemical Engineering, The University of Birmingham. The sequence of cavities is described with increasing N using a point sparger.

In order to investigate the influence of changing cavity size and shape on the torque developed by the observed agitator, the lower impeller strain gauge output was filmed concurrently (Section 3.4.3).

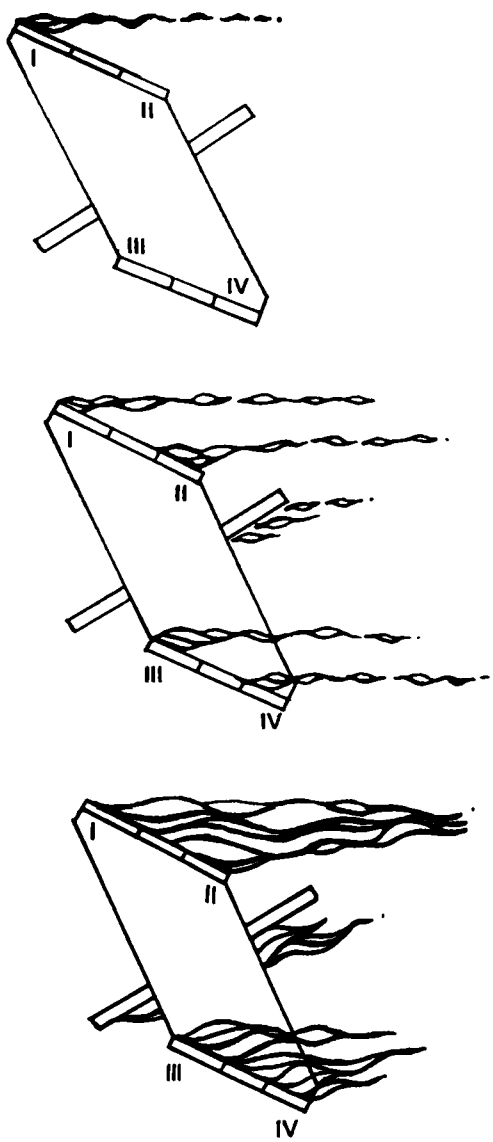

Figure 4.10 InterMIG Cavities (Side View).

When viewed from the vessel side the first cavities appeared on the upper leading vane (vane I) of the IM outer blades (Fig.4.10a) and at N ≃ 60 [rpm], they were transient in nature. With increased speed cavities appeared on vane II. At about 90 rpm, cavities appeared behind vanes III and IV in a transient fashion whilst those attached to vanes I and II became more permanent (Fig.4.10b), with occasional bubbles breaking from the rear of the cavities. At this stage, all 4 split vanes had separate cavities attached and occasional gas was seen in the region of the inner blade where it connects to the outer vanes.

When viewed via the vessel base at 100 rpm (Fig.4.11a), the cavities were still transient, disappearing and reappearing regularly. Cavities were seen on the top vane pair, both vane pairs or neither. When viewed from the side at 120 rpm, (Fig.4.10c) the cavities attached to each vane appeared to have connected with the other vane of the pair, forming two cavities instead of four. The upper vane pair produced the longer cavity. These cavities behind each vane pair were the ones seen clearly at 100 rpm (Fig.4.11a especially at 1.5 vvm) from the base. Those attached to each vane (Figs.4.10a and 4.10b) were not visible properly from the base as they were much shorter.

In the U.P.M., it was apparent that the pressure drop over the upper vanes was greater than that over the lower, so that cavities were never seen on the lower vane pair alone. This phenomenon was due to the interference effect of the upper vane pair on the lower from which the InterMIG derives it's name (see Appendix I). Fig.4.11a also indicates that gas collected behind the inner blade outer edge occasionally feeds into the outer vane cavities. This gas may also be associated with the vertical plate connecting the inner blades and outer vanes. The lower IM torque was seen to double when both cavities disappeared, approximately equating with the unaerated torque. These fluctuations occurred regularly but were of short duration.

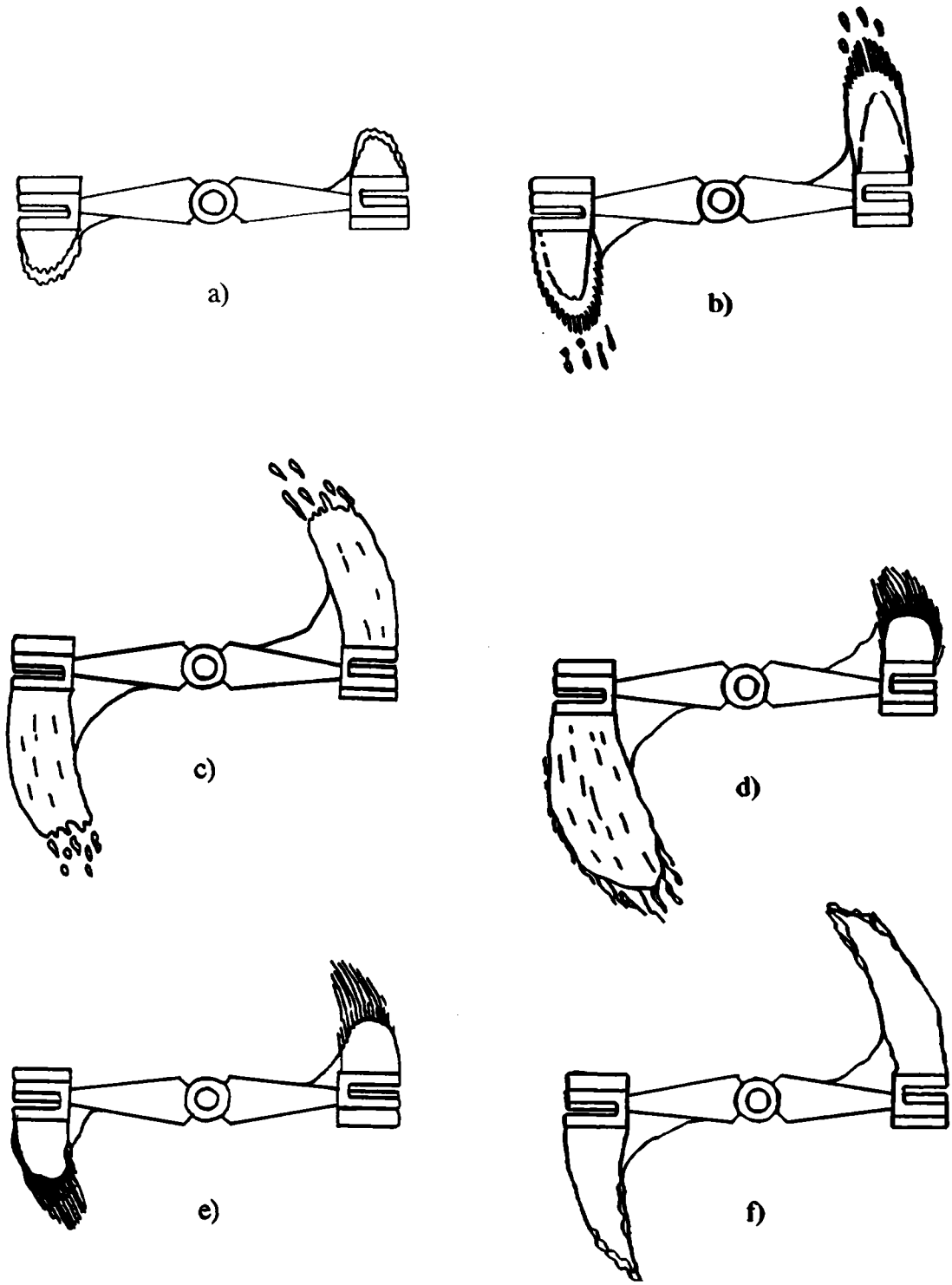

Figure 4.11 InterMIG Cavities (Viewed from beneath).

By 150 rpm (Fig.4.11b) the cavities had enlarged and gas was often entering via the inner blades. A pronounced wake was visible as clouds of bubbles broke from the cavity. The cavities only disappeared occasionally and appeared to fluctuate in size at the same rate on both outer sets of vanes. Disappearance of one cavity led to a torque increase of up to 45% whereas the occasional disappearance of both increased torque by 80% - 90% (spike). It was not clear whether the cavities which could be seen originated from the upper two vanes only or from the upper and lower vane pairs superimposed on each other.

As N increased the cavities enlarged and no longer disappeared whilst gas permanently fed in from the centre blades (Fig.4.11c). The cavities appeared much more stable at 200 rpm. Concurrent torque observation indicated fluctuation of 10% - 15% of total impeller torque with cavity growth/shrinkage.

With further N increase to 250 rpm, a significant change took place. At 0.5 vvm the previously observed cavities (by now becoming obscured by dispersed gas between base and agitator) grew still further but were occasionally replaced by much smaller clear cavities. At 250 rpm and 1 vvm, the interchange between small clear and large opaque cavities occurred more frequently and at 1.5 vvm, small clear cavities were present most of the time (Fig.4.11e). Occasionally one end of the agitator exhibited small clear cavities whilst the other showed large opaque (Fig. 4.11d).

The appearance of the clear cavities may have been due to either cavity bridging between upper and lower vane pairs or the appearance of a cavity beneath the lower vane pair (assuming none existed previously). The latter would seem unlikely as cavities were seen from the side at 120 rpm attached to the lower vane pair and the appearance of a clear cavity was always accompanied by a reduction in size. It therefore seems likely that one clear cavity was formed enveloping each set of four outer vanes.

The opacity of the larger cavities may therefore have been due to the superimposition of cavities originating from the upper and lower vane pairs.

Concurrent torque observation showed a drop in lower impeller torque of 20% to 40% on small clear cavity formation (both blades). Similarly at 250 rpm and 1.5 vvm, change from small clear to large opaque cavities increased torque by roughly 25%. Increasing N to 300 rpm increased the size of the clear cavities and increased their stability (Fig. 4.11f).

To summarise, with increasing N, cavities appear firstly behind one of the outer vanes followed by one on each of the upper two vanes and then one on each of the 4 vanes. These cavities were similar to vortex cavities seen with other agitators[12,23]. Further N increase leads to much larger cavities behind the upper (and lower) vane pairs. These increase in size until replaced by a clear cavity encompassing all 4 vanes. The transition is marked by a reduction in size and increased transparency. These cavities continue to grow in size with speed increase.

Within the N and Q_G range in which cavities disappear completely and reappear (up to 150 rpm and 1 vvm), large torque spikes were seen (up to 90% increase). These spikes were measured on one (bottom) agitator, so that overall torque (2 agitators) was much less influenced by the cavity disappearance, which did not occur simultaneously on both agitators.

Once the speed and gassing rate were sufficiently high to prevent cavity disappearance, torque fluctuation was cut significantly. The appearance of small clear cavities reduced torque on the agitator by 20% to 40%. Operation at the transition between long opaque and small clear cavities produced larger torque fluctuations than at slightly lower speeds. Once small clear cavities were more permanent, fluctuation was reduced to $< \pm$ 10% of impeller torque.

4.4.3 Torque Instability

During gassed power measurement in T45, considerable fluctuation in measured torque was noted at N = 380 rpm, Q_G = 0.39 vvm and Fl_G = 0.004. Two distinct torque values interchanged at roughly one minute intervals (Fig.4.12). The two torque values gave overall Pog/Po = 0.85 and 0.62 respectively and occurred in the region of sharply falling Pog/Po in Fig.4.16. Individual stage power measurement demonstrated that this torque fluctuation was entirely due to the lower impeller. Lower impeller torque fluctuated between 1.4 and 2.0 [Nm]. Although this fluctuation was reproducible in T45 equivalent fluctuation of similar magnitude were not observed in T72 at high speeds and low gassing rates. Torque fluctuations of a similar proportion of the total lower impeller torque were seen in T72 at 100 to 150 rpm and 0.5 to 1 vvm, but took the form of spikes and were of shorter duration . The cause of the instability was the appearance and disappearance of cavities of the type shown in Fig.4.11a. The severity of torque fluctuation found suggests that it would be unwise to design an agitation system with IM that operates in the region of sharply falling Pog/Po shown in Figs.4.16 and 4.17.

4.4.4 Pog/Po v Fl_G at Constant Gassing Rate

The gassed to ungassed power number ratio has been plotted against Fl_G as the ungassed power number was found to be constant over the speed range covered. Fig.4.13 shows Pog/Po for three gassing rates in T45. In the case of the lowest Q_G (0.47 vvm), Pog falls from a maximum at Pog/Po = 0.78 to a minimum at Pog/Po = 0.62 after which Pog rises slightly. The two higher gassing rates (0.95 vvm and 1.13 vvm) both show a steady fall of Pog with increasing N, eventually reaching Pog/Po = 0.51 in both cases.

At high N (low Fl_G), the results show an effect of Q_G on Pog for

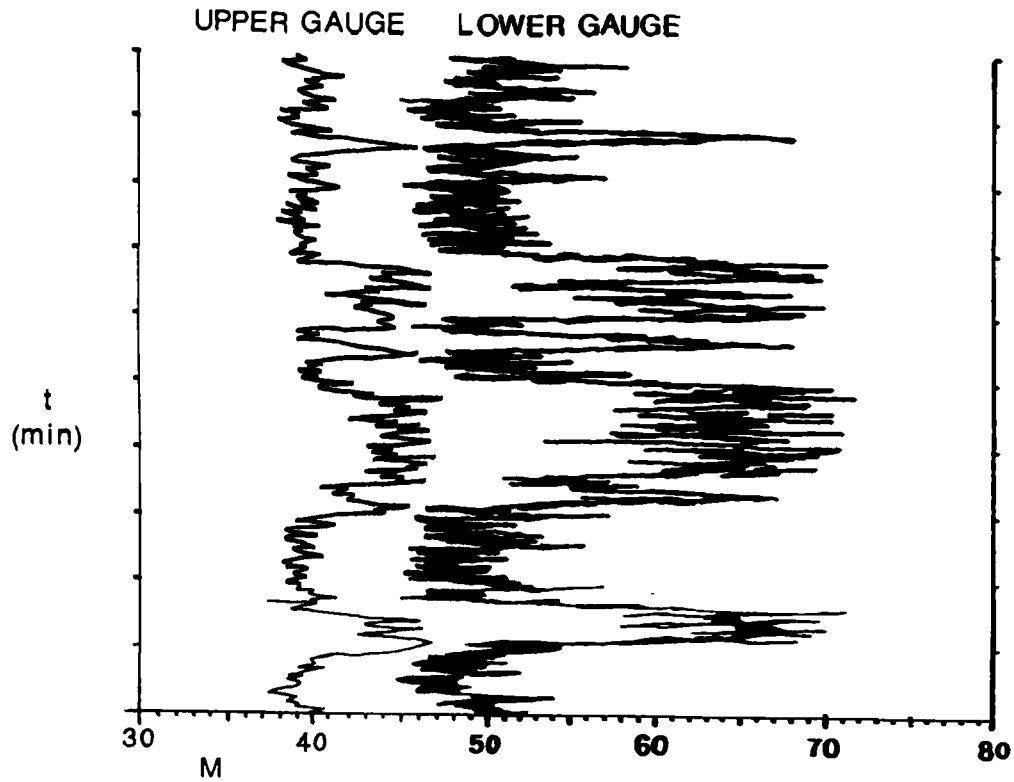

Figuer 4.12 InterMIG Torque Instability.

Lower Gauge, 10 Units= **0.3 [Nm]**

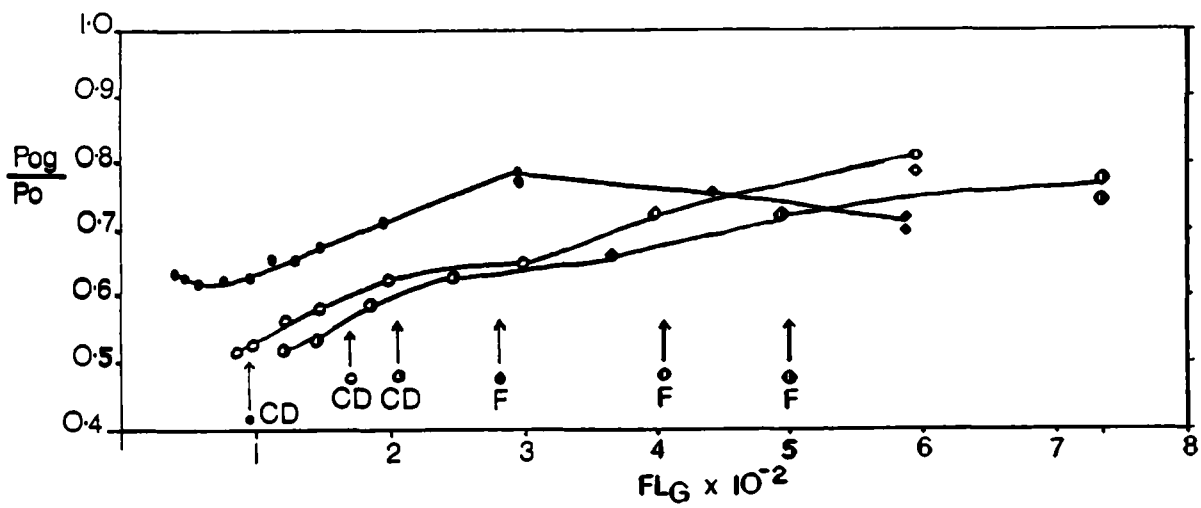

Figure 4.13 Pog/Po v Fl_G, InterMIG, T45, Water.

Constant Q_G = 0.47 vvm:• ,0.95 vvm:◦ ,1.13 vvm:• .

IM in water. For the two higher gassing rates no minima were found (unlike 6DT) and no change in the shape of the curves could be associated with the flooding/loading transition or complete dispersion. However, in the 0.47 vvm case, the maximum was close to the flooding/loading transition and the minimum close to the complete dispersion point.

The increase to maxima at low gas flowrates appears analogous with that seen for the 6MFU impeller[12]. It occurs in this case prior to loading and stable cavity formation. It may be due to increasing pumping capacity of the impeller and comparatively lesser effect of the upward flow of sparged gas (although the flow was still gas dominated). The effect was not seen by Bujalski[12] for 6MFD impellers and therefore maybe associated with the inner blade upward pumping action.

The steady fall of Pog from the maximum is a result of increasing cavity size (Section 4.4.2) reducing drag for a given speed. No particular discontinuity on the curve could be linked to change to 'clear' cavities.

Fig.4.14 shows Pog/Po v Fl_G for 3 gassing rates and 4 sparger types tested with IM in T72. Dimensions of spargers are given in Table 4.3. Each sparger type will be discussed in turn.

L.R.S. (Ds/D = 1.22)

At the lowest gassing rate, Pog was higher than with any other sparger tested due to relatively greater power draw of the bottom impeller. The bottom impeller was not directly gassed and hence drew more power and had a greater pumping capacity, dispersing gas throughout the vessel at very low speed (N_{CD} = 110 rpm).

At 1 vvm, no maximum was apparent with this sparger, Pog fell slightly subsequent to complete dispersion and then remained roughly constant at Pog/Po = 0.58 until falling quite sharply to Pog/Po = 0.52. This latter fall may be due to increased recirculation of gas into the

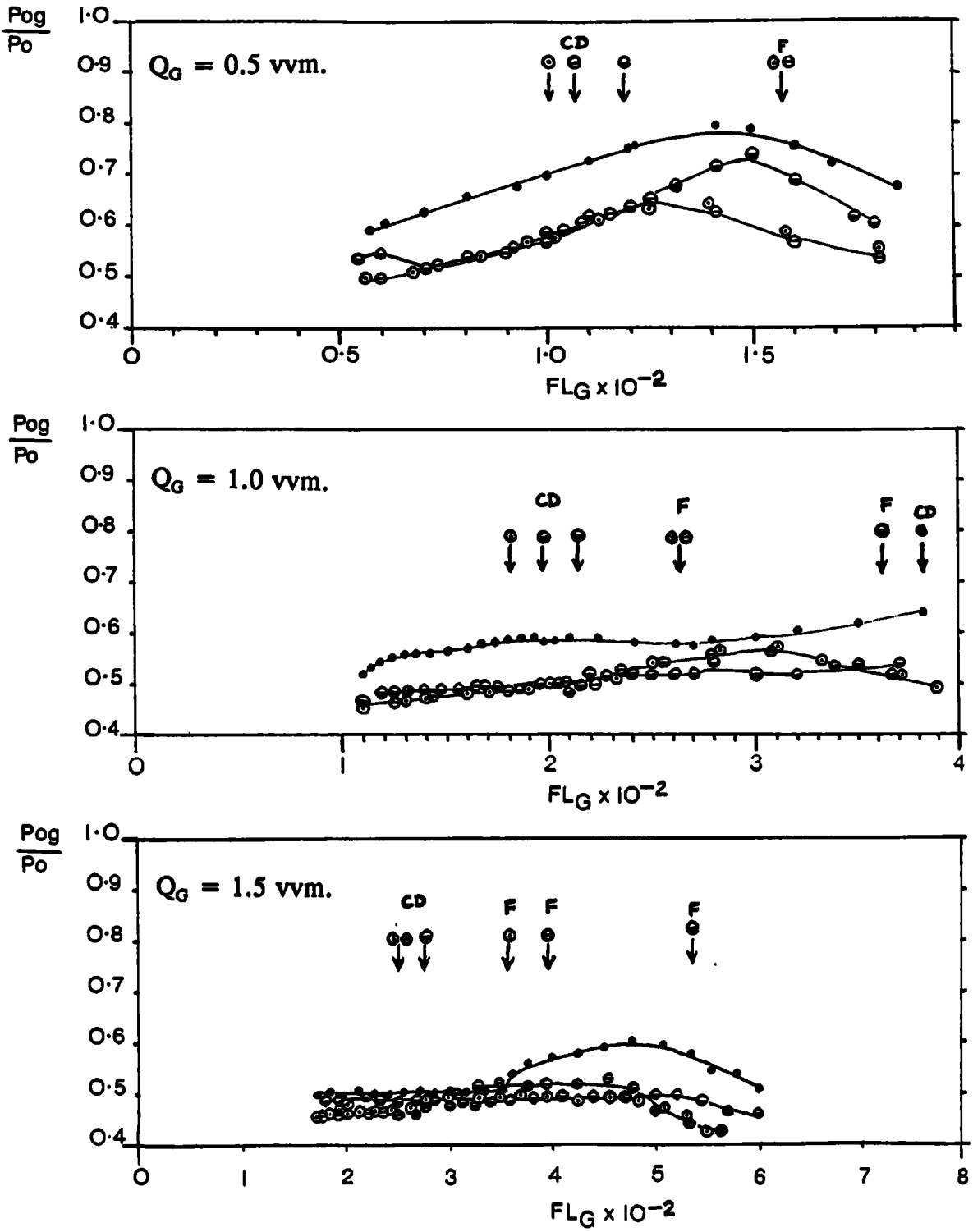

Figure 4.14 Pog/Po v Fl_G, InterMIG, T72, Water, Constant Q_G.

LRS:• MRS:• ,SRS:• ,PS:• .

lower agitator or formation of 'clear' cavities. As before, Pog with the LRS was higher than with the other sparger types.

At the highest gassing rate, Pog rose to a maximum Pog/Po = 0.6, fell to Pog/Po = 0.5 and remained constant at this value. Again Pog was somewhat higher than with the other spargers. With this sparger, increases in Q_G lowered Pog at all speeds.

M.R.S. (Ds/D = 0.86)

This diameter sparge ring introduced gas into the IM outer vanes. At Q_G = 0.5 vvm, Pog rose to a maximum at a lower N than P.S.and S.R.S. as the flow became impeller dominated at lower speed. Prior to and immediately subsequent to the maximum, Pog was between that found for the L.R.S. and P.S./S.R.S., due to lack of gas flow through the inner blades. Subsequent to the maximum Pog fell due to increase in cavity size and coincided with that found for P.S. and S.R.S. A rise in Pog was observed at high speed with the M.R.S. at the lowest gassing rate, as was the case in T45.

At Q_G = 1 vvm, Pog/Po fell gradually from a maximum of 0.54 to 0.48 with no discontinuity associated with loading or complete dispersion. Subsequent to complete dispersion little difference between Pog for M.R.S., S.R.S. and P.S. could be detected.

At the highest gassing rate Pog rose slightly and then remained constant at Pog/Po = 0.49. Power numbers for the two highest gassing rates were very similar with this sparger subsequent to loading.

S.R.S. (Ds/D = 0.43) and Point Sparger

These two sparger types exhibited very similar aerated power characteristics to each other and will therefore be discussed together. Cavities described in Section 4.4.2 for the point sparger may be related to these curves. Both spargers introduced gas into the agitator inner

blades.

At the lowest gassing rate, Pog increased to a maximum at approximately N = 3 rps, this rise continued after the loading point was passed and occurred despite cavity formation of the type seen in Fig.4.11a. As previously mentioned this effect was probably due to the volume of gas passing through the inner blades which was substantial even after the outer vanes continually dispersed gas radially (loaded). As speed increased the pumping capacity of the inner blades increased whilst the centrally rising gas contributed a constant or decreasing (due to outer vane dispersion) upward flow. Once the maximum Pog was passed sufficient power reduction (due to outer vane cavities growing) counteracted the declining influence of the centrally rising gas. Po_g steadily fell with growing cavity size and no change in slope was seen at the point where clear cavities were formed. Pog/Po fell to 0.5 and was very similar to that found for the M.R.S. subsequent to the maximum.

For Q_G = 1 vvm the maximum was not pronounced and Pog/Po fell gradually to 0.46 with no obvious discontinuity at the loading point or complete dispersion. For the highest gassing rate, the maximum was again reduced and Pog fell gradually although in this case a small drop occurred at roughly the point at which 'clear' cavities were first observed. At the two highest gas flowrates little effect of Q_G on Po_g was evident subsequent to loading.

Comparison of Pog/Po for 6DT $(T/2)^{13}$ and IM 055 (MRS and LRS) in T72 is made in Fig.4.15. N has been used instead of Fl_G in order to simplify the comparison of agitators of differing diameter. Reduction of power draw on gassing for $N \geq N_{CD}$ was greater for IM at Q_G = 0.5vvm. At Q_G = 1 and 1.5 vvm, Pog/Po values for 6DT and IM (MRS) were approximately equal for $N \geq N_{CD}$.

The use of a ring sparger of greater diameter than the impeller (LRS) minimises the power reduction on gassing as the lower IM is loaded

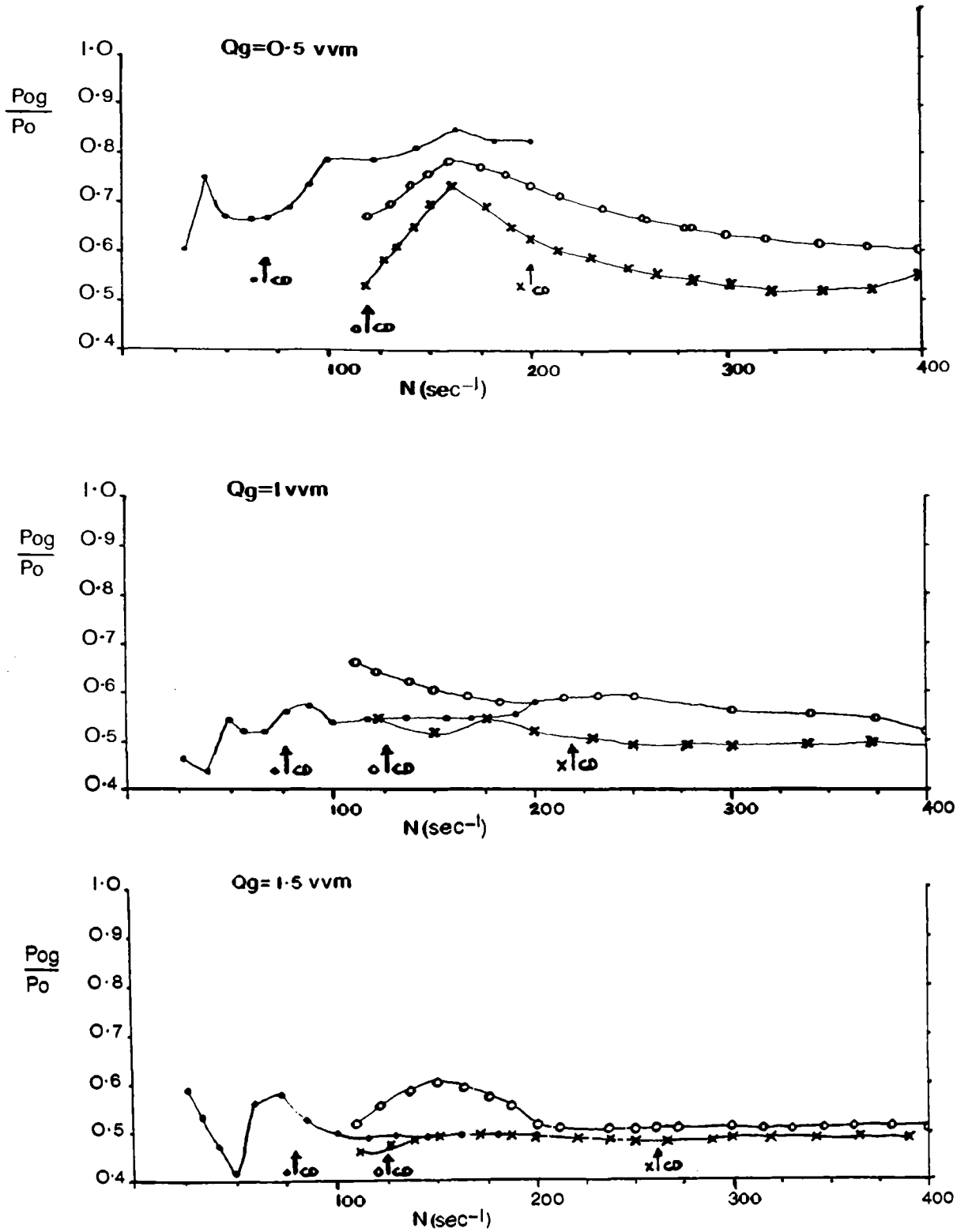

Figure 4.15 Pog/Po v N, T72, Water, Constant Q_G.

InterMIG (MRS): × , InterMIG (LRS): ○ , 6DT(T/2): • .

indirectly. This sparger therefore appears advantageous for gas dispersion applications over the speed range used and for $Q_G \leq 1$ [vvm]. At higher gassing rates no difference between MRS and LRS was evident.

4.4.5 Pog/Po v Fl_G at Constant Speed

This type of plot indicates the effect of increasing Q_G from zero to the maximum attainable at constant N. Fig.4.16 shows the results obtained at four speeds in T45 and Fig.4.17 shows three speeds in T72. The two figures show a marked similarity for equivalent Froude numbers. Gassed power initially fell rapidly as Q_G was increased, the curves then flattened out until a roughly constant Pog was attained at which point further Q_G increases had no effect on Pog.

The explanation of the curves with respect to cavity formation is as follows. The initial slight drop in Pog/Po from 1.0 to 0.95 (Fig.4.16 only) was due to the formation of 'vortex' type cavities attached to one or more of the split vanes. The appearance of cavities of the type shown in Figs.4.11a and 4.11b caused a steep decrease in Pog. Torque signals oscillated strongly over the Fl_G range of this decline as cavities formed and disappeared. The instability of the torque signal was greatest at Fr = 1.103, Fl_G = 0.004 in T45 (see 4.4.3).

The cavities enlarged at constant N and increasing Q_G until they approached their maximum size and became more stable, after which Pog fell only gradually. The appearance of 'clear' cavities around all 4 IM outer vanes can be associated with the lower Pog for $Fl_G > 1.5 \times 10^{-2}$ and for N > 4 rps. The stirrer speed determines at what Q_G and hence Fl_G stable cavities are formed, higher N values requiring lower Q_G for the formation of stable cavities, hence the differences in slope.

After stable cavity formation Pog/Po values of 0.5 to 0.53 were found in T45 and 0.48 to 0.51 in T72 for $0.54 < Fr < 1.15$. The lower values at higher Fr possibly due to stable 'clear' cavity formation. The lack of

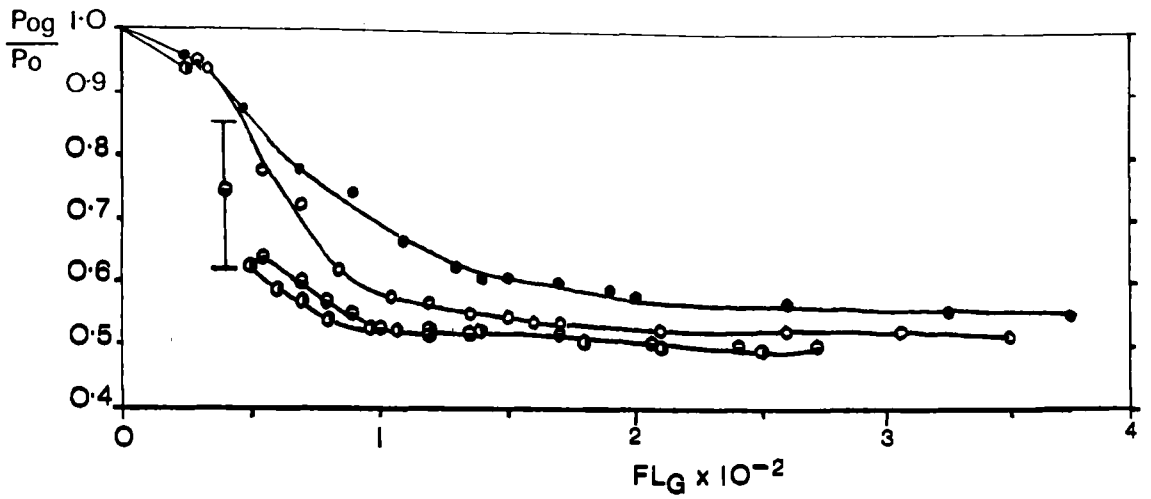

Figure 4.16 Pog/Po v Fl_G, T45, Water, InterMIG (MRS).

Constant N = 3.55 rps: • , 4.43 rps: o , 5.55 rps: ⊖ ,6.33 rps: ⊙ .

Fr = 0.34, 0.53, 0.84, 1.09.

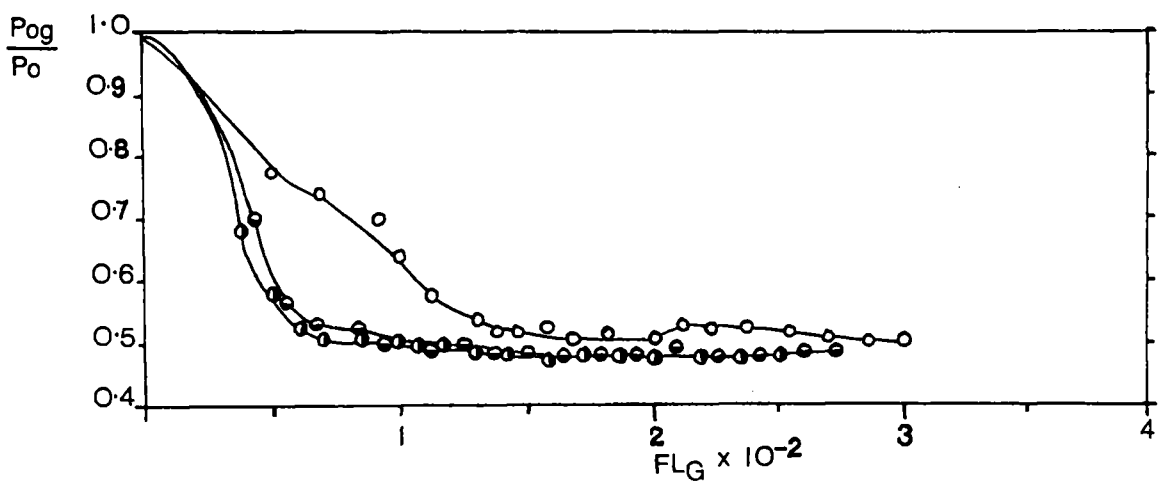

Figure 4.17 Pog/Po v Fl_G, T72, Water, InterMIG (MRS).

Constant N = 3.75 rps: o , 4.67 rps: ⊖ , 5.33 rps: ⊙ .

Fr = 0.57, 0.88, 1.15.

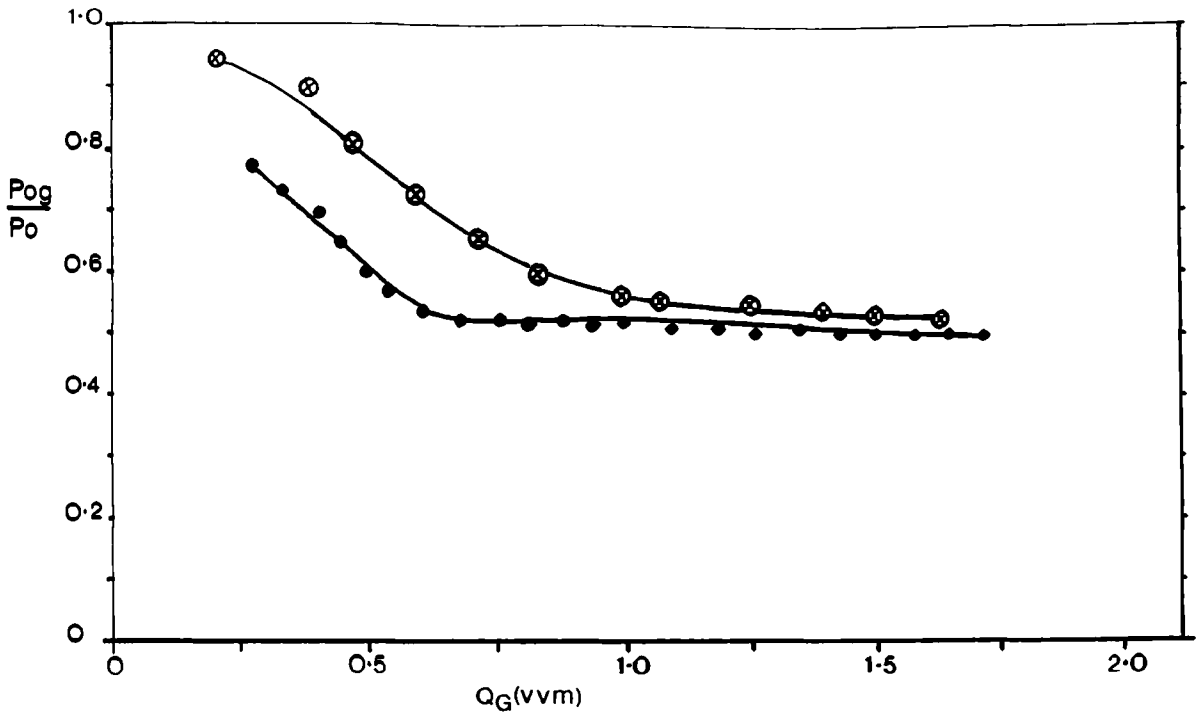

Figure 4.18 Pog/Po v Q_G, T72, Water, at a speed giving 1 [kWm^{-3}] unaerated.

InterMIG (MRS): ● , 6DT (T/2): ⊛ .

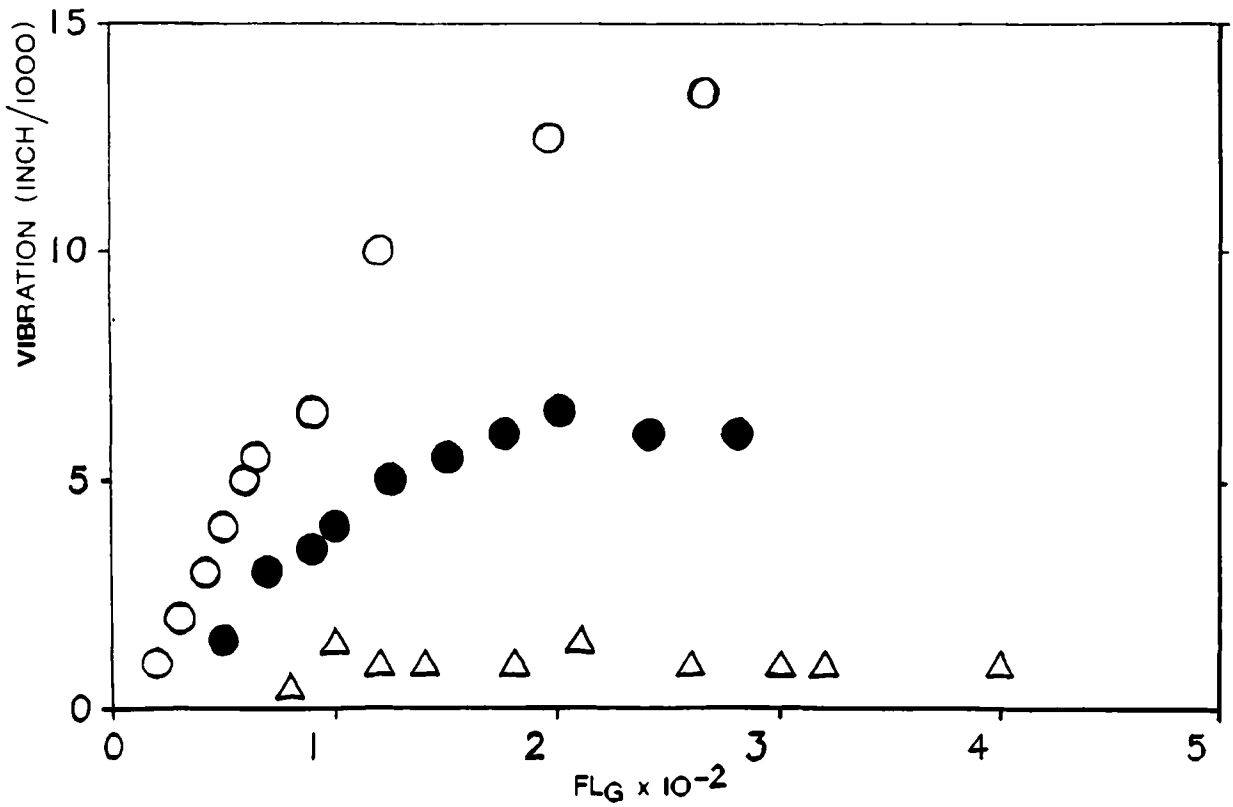

Figure 4.23 Vessel Vibration v Fl_G.

Constant N = 6.33 rps: o , 5.55 rps: ● , 4.43 rps: Δ .

decrease in Pog after stable cavity formation indicated the insensitivity of IM to Q_G changes in this range. The flooding point was not reached for any of the speeds tested.

Comparison of the Pog/Po for 6DT (T/2) and IM 055 (MRS) in water at H/T = 1, for various Q_G at representative speeds equivalent to an unaerated power input of 1 kWm^{-3} is shown in Fig.4.18. The reduction in specific power on aeration was greater for InterMIG at Q_G < 1 [vvm]. For Q_G > 1 [vvm] the reduction in specific power on aeration was approximately equal for the two agitator types. Retrofitting IM for 6DT (T/2) at equal unaerated power input will not therefore increase aerated power input.

4.5 AERATED POWER CHARACTERISTICS IN CMC.

4.5.1 Bulk Flow in CMC (T72)

Observations were made of the bulk flow regimes present when agitating CMC solutions with IM. The criteria described in Section 4.4.1 were used when attempting to determine N_F and N_{CD}. Values obtained for these transitions were more subjective than in water due to the presence of many tiny bubbles entrained in the CMC obscuring vision of the agitators. The determination of N_{CD} was complicated by the recirculation of these tiny bubbles which brushed the base at relatively lower speeds than the occurrence of N_{CD} in water.

Table 4.8 details values of N_{CD} and N_F found in CMC. Comparison of Tables 4.5 and 4.8 indicates that in 0.07% CMC N_{CD} and N_F were less than or equal to those found in water. As CMC concentration was increased so too did N_{CD} and N_F. The relatively low values of N_{CD} in CMC when compared with water were due to the wider bubble size distribution in CMC, tiny bubbles brushing the base whilst large slugs rose straight to the liquid surface. The values of N_F and N_{CD} were less meaningful for reasons mentioned 4.4.1 (partial loading) and also highly subjective in CMC , so that no attempt to correlate the data was made.

TABLE 4.8

FLOODING/LOADING AND COMPLETE DISPERSION IN CMC T72

CMC Concentration	Sparger	Q_G [vvm]	N_F [rpm]	N_{CD} [rpm]	P/V_F [kWm^{-3}]	P/V_{CD} [kWm^{-3}]
0.07%	Point	0.5	140	180	0.13	0.27
		1	140	220	0.13	0.5
		1.5	180	250	0.24	0.65
0.07%	Ds/D=0.86 (MRS)	0.5	90	160	0.04	0.2
		1	120	200	0.075	0.37
		1.5	140	230	0.13	0.5
0.4%	Ds/D=0.86 (MRS)	0.5	140	220	0.13	0.5
		1	160	240	0.2	0.65
		1.5	180	265	0.29	0.89
0.8%	Point	0.5	160	240	0.2	0.68
		1	180	275	0.3	1.08
		1.5	195	300	0.4	1.35
0.8%	Ds/D=0.86 (MRS)	0.5	150	240	0.2	0.64
		1	160	260	0.27	1.03
		1.5	180	285	0.32	1.25

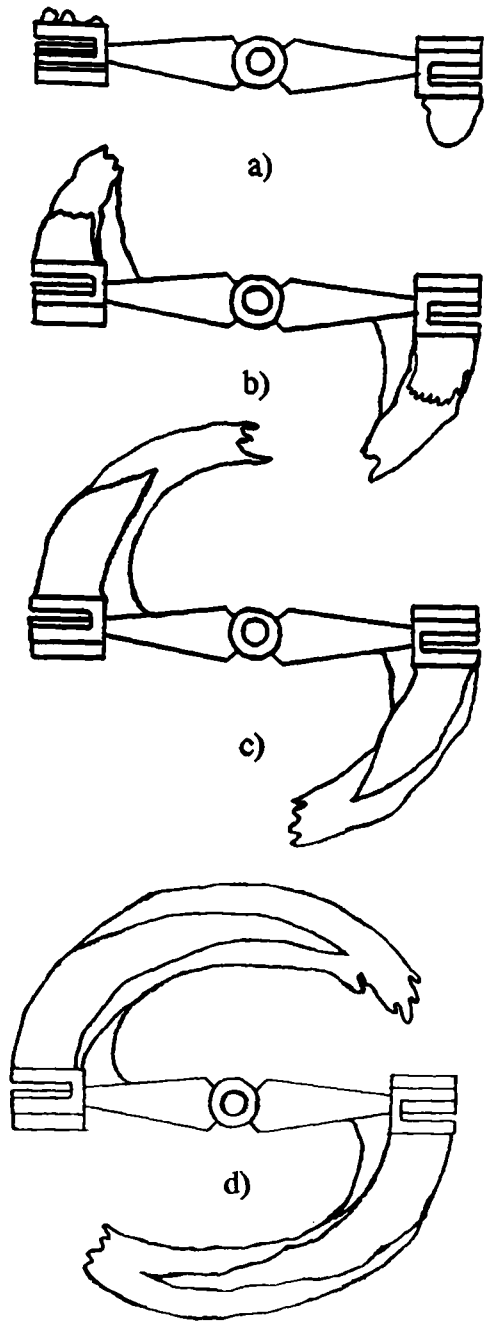

Figure 4.19 InterMIG Cavities in CMC.

4.5.2 Gas Cavities in CMC

Gas cavities observed in CMC solutions with increasing N were similar to those found in water, but more stable. Initially small ragged cavities were seen on each IM outer vane. These were replaced by cavities encompassing each upper (and lower) vane pair by 120 rpm (Fig.4.19a). Increase in speed to 180 rpm (Fig.4.19b) led to longer upper vane pair cavities and shorter lower vane pair cavities. Cavitation behind the inner blade fed gas into the outer vane cavities. The cavity sizes increased further with speed until at 300 rpm they stretched almost to the following blade (Fig.4.19d). The increased viscosity enabled longer cavities to form than in water due to their greater stability.

These observations suggest that the lack of effect of Q_G on Pog seen with IM in CMC was due to the formation of long, stable cavities at relatively low N. Altering Q_G effected the cavity length but once long cavities were formed further increase in length did not reduce drag appreciably and hence Pog remained constant.

4.5.3 Aerated Power in CMC

Fig. 4.20 shows Pog/Po v Fl_G at constant Q_G in 0.07% CMC (point sparger). The shape of the curves were very similar to those found in water. At Q_G = 0.5 vvm the maximum occurred at higher Fl_G as the agitator required higher N than in water to overcome the upward gas flow. Pog/Po then fell gradually to 0.5. Gassed power numbers were also very similar for Q_G = 1 and 1.5 vvm, where Pog/Po gradually fell to between 0.48 and 0.46. Pog showed only a small variation with Q_G at high N in 0.07% CMC.

Figure 4.21 and 4.22 show Pog v Re in T72 at H/T = 1 and H/T = 2 respectively. Pog values for 0.8% and 0.4% CMC were not affected by Q_G changes to any significant extent. In 0.07% CMC a slight decrease in Pog with increased Q_G was seen. As with the unaerated power curve there was no minima in the IM aerated power curve. Pog values fell until Re = 1 x

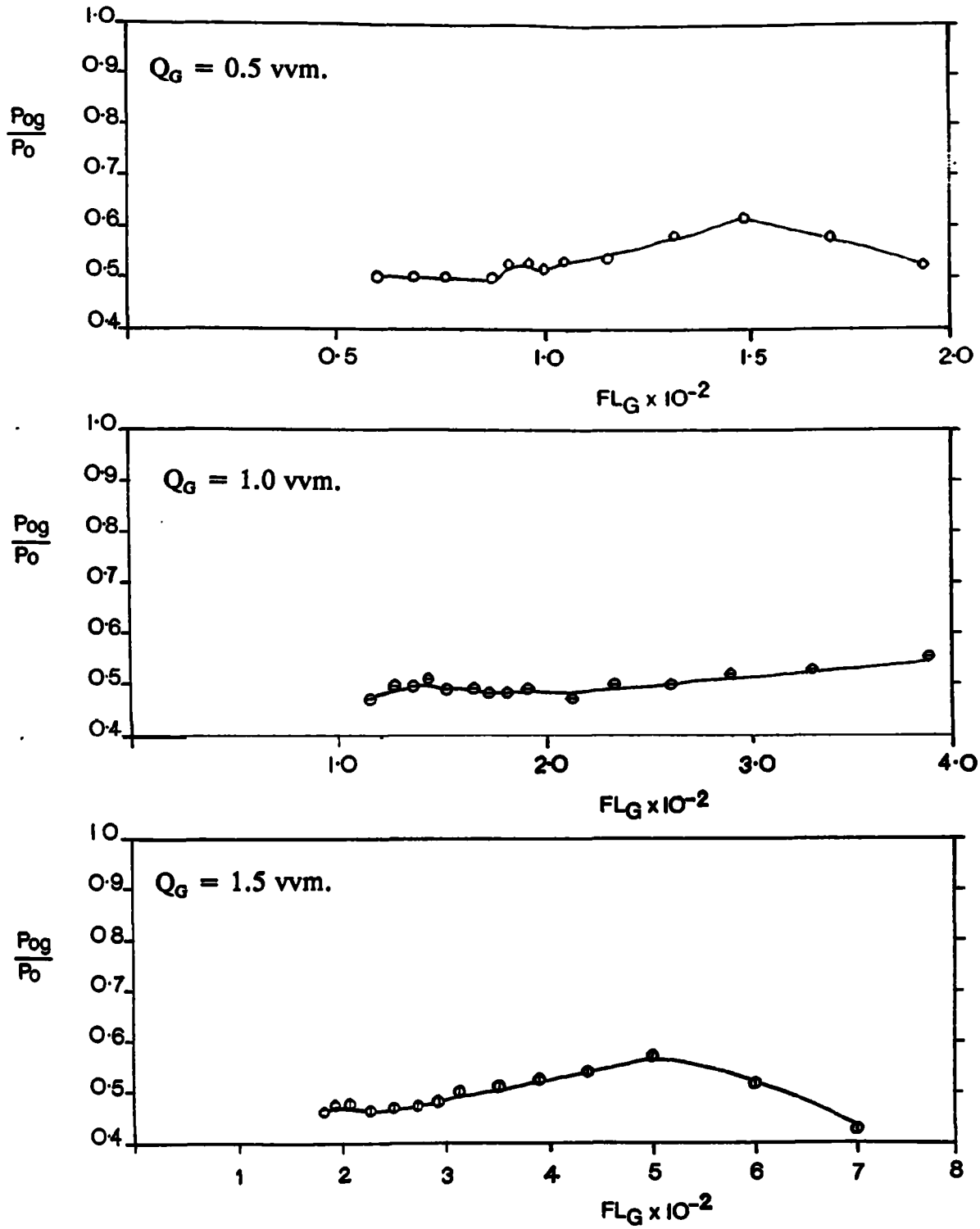

Figure 4.20 Pog/Po v Fl_G ,T72, InterMIG, 0.07% CMC, Constant Q_G.

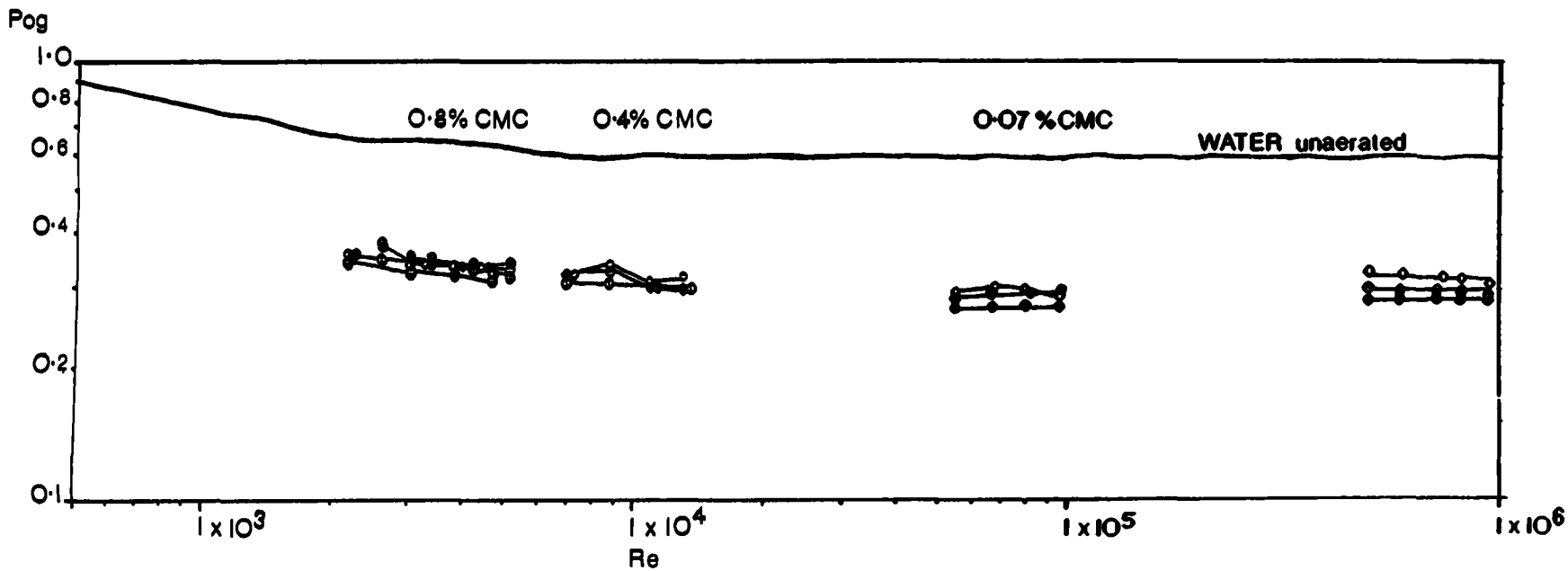

Figure 4.21 Pog v Re, T72, InterMIG (MRS): ● , (PS): ○ .

Q_G = 0.5 vvm: ○● , 1.0 vvm: ●● , 1.5 vvm: ●○ .

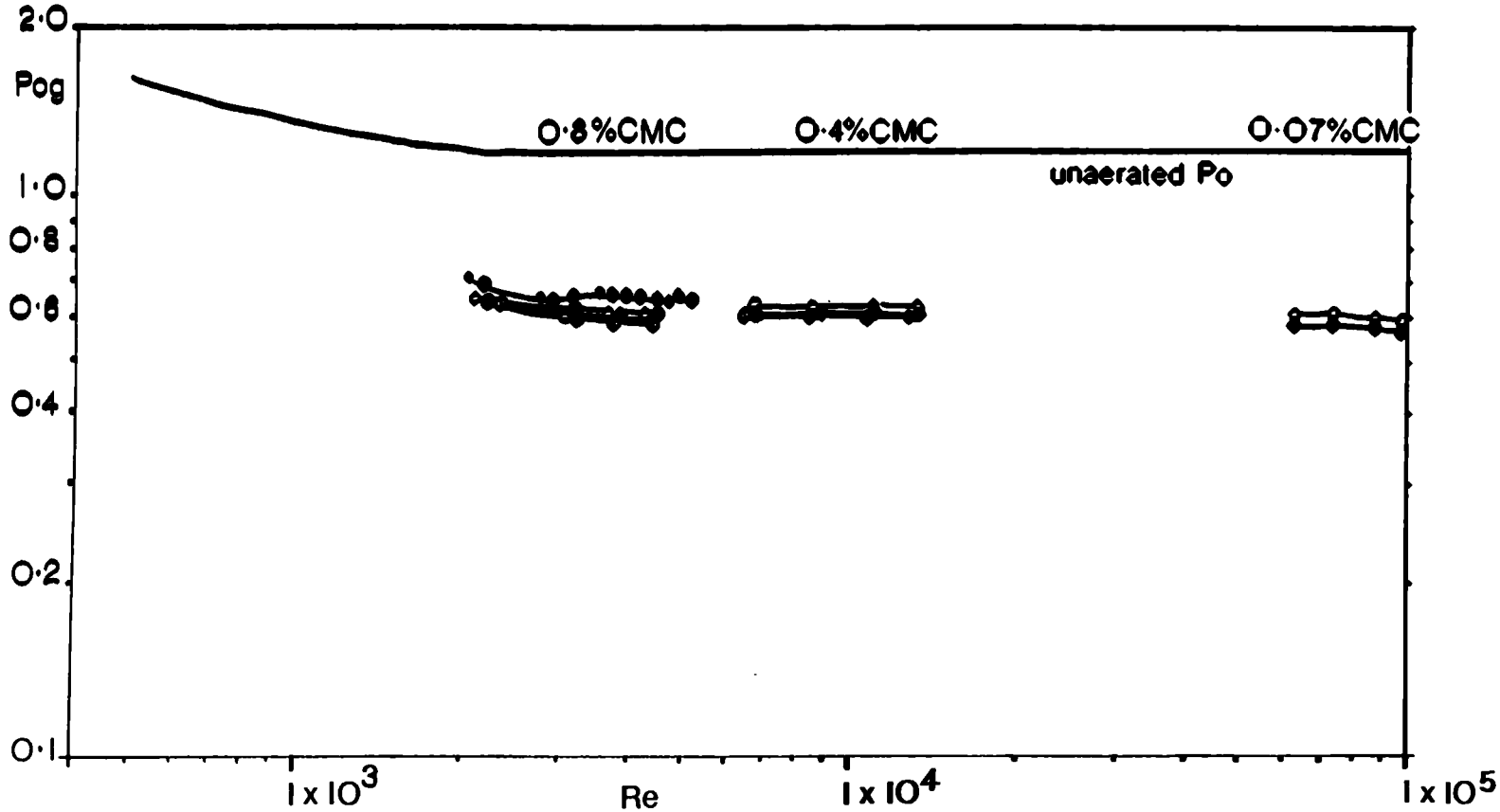

Figure 4.22 Pog v Re, T72, InterMIG, H/T = 2.

MRS: ● , PS: ○ .

Q_G = 0.25 vvm: ○● , 0.5 vvm: ●● , 0.75 vvm: ●●.

10^4 after which they remained constant.

At H/T = 1 in 0.8% CMC, the point sparger Pog values were slightly higher than those found for the Ds/D = 0.86 ring sparger. Aspect ratio had no effect on the Pog/Po values found. Comparison with literature[7] aerated power data for MIG in CMC[7] indicates good agreement in terms of variation of Pog with Q_G at differing μ_a and general curve shape. Details of Höckers[7] data is given in Appendix I, Fig.A.3.. He found a decrease in the effect of Q_G on Pog with increasing viscosity, speed and Q_G. Pog increased at high μ_a following the unaerated power curve and no minima were found in the transitional flow regime. The aerated power data for IM in this work is therefore consistent with that found for MIG.

4.6 VESSEL VIBRATION

A number of reports in the literature (Appendix I) have described vessel vibration occurring with IM [20,101-103]. In this work, measurements were made in T45 using equipment described in Chapt.3 in order to relate the vessel vibration to agitation and aeration rate. The presence and degree of vessel vibration clearly depends upon the characteristics of the vessel and shaft used. Fig.4.23 shows the effect of increasing N and Q_G on vessel vibration measured in [inches/1000].

In T45, vibration was minimal at speeds of less than 5 [rps] in water, irrespective of Q_G. Increasing N above 5 [rps] led to increased vibration although at high N and low Q_G, vibration was minimal. The tendency of IM agitators to cause vessel vibration was therefore largely due to the effect of aeration.

The two bladed, large D/T IM configuration may exacerbate torque fluctuations. These are caused by changing cavity size and shape and interactions due to the proximity of the baffles. The two phase mixture in the vessel may then 'amplify' the shaft unbalanced forces to promote large oscillations of force on the baffles and hence vessel.

4.7 CONCLUSIONS

The following section draws conclusion concerning data reported in this chapter. Wider conclusions concerning comparative impeller power draw and fluid dynamics (including IM) are discussed in Section 5.5.

4.7.1 Flowpatterns and Surface Aeration

Observed flow patterns agreed well with previous reports (Appendix I), they were highly chaotic and tended to support the claims of uniform energy dissipation[104,105]. Surface aeration occurred at lower speed in the D.P.M. In the U.P.M., surface aeration did not effect unaerated power draw under any conditions. Po reduction was however seen in the D.P.M..

4.7.2 Unaerated Power Characteristics

The data from this work agrees well with the literature where available (Appendix I). No effect of vessel scale was found. No effect of rotation direction was observed until $N > N_{SA}$ for the D.P.M. $\bar{P}o$ fell with increasing Re until $Re > 7 \times 10^3$ after which $\bar{P}o = 0.6$ (2 IM 055). No minima were apparent in the power curve. The lower impeller drew slightly less power than the upper impeller(s). $\bar{P}o$ for 4 IM 055 at H/T = 2 was double that for H/T = 1. Mounting IM stages in a planar fashion did not effect $\bar{P}o$. The optimum S/T was found to be approximately 0.5, supporting Ekato claims. Reduction of S/T (impeller hubs touching) reduced $\bar{P}o$ by a maximum of 15%, considerably less than the reduction seen with 2 6DT at equivalent S/T.

4.7.3 Bulk Flow Regimes

The IM was found to flood at low N and high Q_G in water contradicting the claims of Hocker[7] and Kipke[41] and supporting those of other authors[20,91,98,106]. However definition of a loading point with IM

was highly subjective. Gas bypassed the outer vanes via the inner blades at $N > N_F$ and even $N > N_{CD}$. The degree of bypassing was strongly influenced by sparger type, increased sparger diameter reduced bypassing. The optimum sparger geometry for gas dispersion (loading and complete dispersion) was a Ds/D = 1.22 ring. For scale up at constant Q_G higher P/V was required for both loading and complete dispersion at the larger scale. P/V_{CD} was found to be influenced to a relatively smaller degree by $Q_G$increases than the 6DT, possibly due to gas bypassing.

4.7.4 Gas Cavities and Torque Fluctuation

A range of cavity sizes and types were recorded in water and CMC. Torque fluctuation was directly linked to intermittent cavity disappearance (largest fluctuations) and cavity size variation (smaller fluctuations). Torque fluctuation of up to 20%-40% of lower impeller mean torque were recorded. These fluctuations occurred mainly in the narrow region of rapidly falling gassed power (Pog/Po v Q_G const. N). Mixer design with IM should avoid this region. Torque fluctuation was reduced with viscosity increase due to the formation of more stable cavities.

4.7.5 Aerated Power Characteristics

Sparging air caused a sharp decrease in power drawn, to values less than or equal to those for 6DT (D = 0.5T) at equivalent unaerated P/V and Q_G in both water and CMC. Pog was influenced by variation of Q_G in water but the effect of Q_G was reduced with increased viscosity. In 0.4% and 0.8% CMC little or no change of Pog was seen with Q_G variation due to stable cavity formation. These findings agree with those reported in the literature[7,41,100].

The gassed power curve was the same shape as the ungassed curve, Pog rising gradually with μ increase in the transitional regime. These phenomena may be useful during fermentations where the rheological

properties of the broth change and/or the air flow is altered as IM impellers would continue to draw the same power. Sparger type had little effect on Pog once $N > N_{CD}$ (except for the case of the L.R.S., the use of which resulted in higher power drawn by the lower agitator).

4.7.6 Vessel Vibration

Vessel vibration became severe under certain conditions in T45 but was not as evident in T72 due to differing vessel natural frequencies. In T45 the highest amplitude vibrations occurred at the highest aeration rates and stirrer speeds. Vibration was negligible under unaerated conditions and increased with gassing rate if $N > 5$ rps. Vessel vibration may be a serious drawback when using IM but does not invariably occur and may be minimised by the use of low Q_G.

5. THE POWER AND FLUID DYNAMICS OF OTHER IMPELLERS STUDIED.

5.1 INTRODUCTION

In this chapter the unaerated and aerated power characteristics, local impeller hydrodynamics and bulk flow phenomena of four types of agitator (with the 6MF in both pumping modes) are discussed. A greater understanding of the reasons for the variation in k_La and hold-up (Chapts.6 and 7) may be obtained by studying the way in which power consumption and two-phase mixing are affected by impeller type, speed, gassing rate and rheological properties. In this work the agitator of primary interest was the InterMIG (Chapt.4), the characteristics of the agitators discussed in this chapter were not studied in as great detail. Literature sources (Chapt.2) will therefore be used to provide a more intimate understanding of the local impeller hydrodynamics and their relationship with measured aerated power draw.

The impeller dimensions, vessel and sparger geometries used in this and subsequent chapters are detailed first. The flowpatterns observed when using the various impellers are then compared and discussed. Unaerated power curves are shown for CMC solutions and water for each agitator in turn. The aerated power data is presented with reference to bulk flow and cavity formation. Finally results from Chapters 4 and 5 are discussed and compared.

5.1.1 Impeller Dimensions, Vessel Geometries

The agitators described are the T/2 6DT (Rushton turbine), T/2 6MFU/D (Six bladed mixed flow), 0.4T 6PSDT (Pipe-section disc turbine) and the Lightnin' A315 hydrofoil. The agitators are depicted in Fig.5.1 to Fig.5.4 and their dimensions detailed in Table 5.1. The vessel geometries, impeller clearances and sparger geometries are given in Table 5.2.

TABLE 5.1 IMPELLER DIMENSIONS USED IN VESSEL T72

Dimensions	6DT	6PSDT	6MF	Lightnin A315
D [m]	0.36	0.288	0.36	0.3
D/T [-]	0.5	0.4	0.5	0.417
L/D [-]	0.249	0.25	0.383	0.365
W/D [-]	0.199	0.2	0.2	0.303
c/D [-]	0.174	0.215	0.174	0.207
e/D [-]	0.233	0.29	0.233	0.275
I/D [-]	0.219	0.208	0.201	0.19
x_1/D [-]	0.0167	0.0139	-	-
x_2/D [-]	0.0139	0.0069	0.0167	0.0083
D_D/D [-]	0.744	0.75	-	-
α [Degrees]	-	-	45	35

TABLE 5.2 IMPELLER, VESSEL AND SPARGER GEOMETRIES; T72

DIMENSIONS	6DT	6PSDT	6MF	Lightnin A315
D/T	0.5	0.4	0.5	0.417
H/T	1 or 2	1	1	1
C/T	0.25	0.25	0.25	0.33
S/T	1	-	-	-
Sparger	Point	Point	Ring	Ring
D_s/D			0.94	0.58
C_s/C	-	-	0.5	0.71

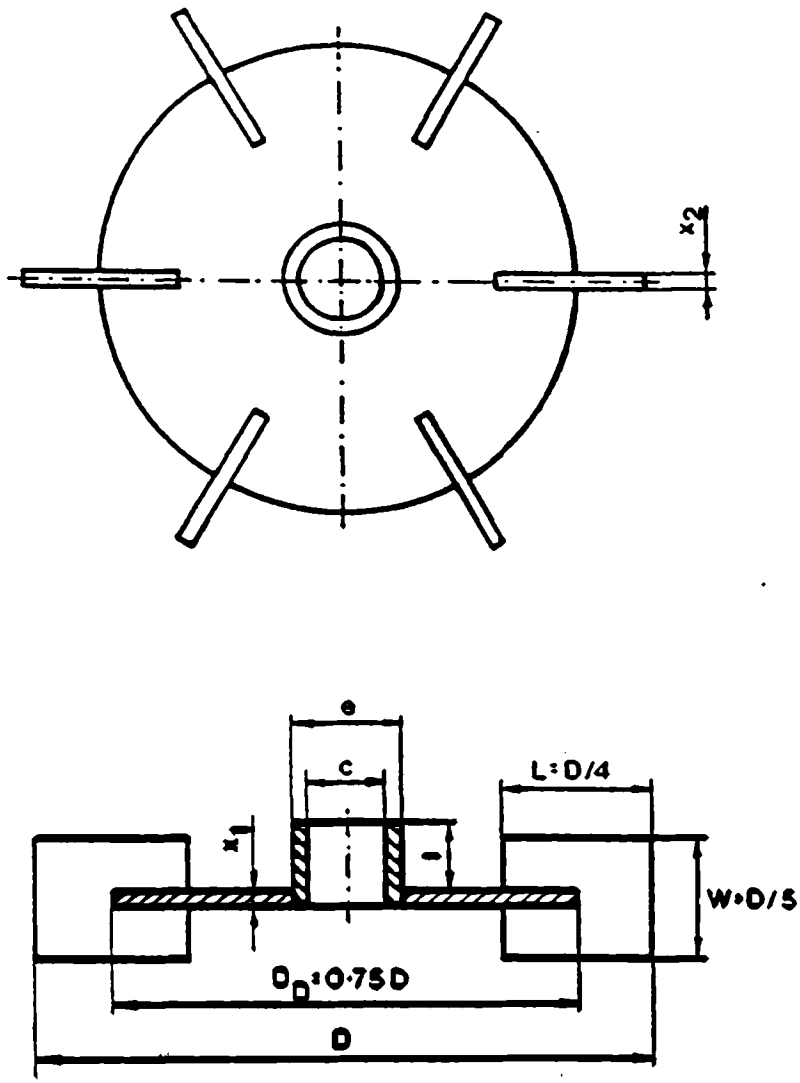

Figure 5.1 6DT.

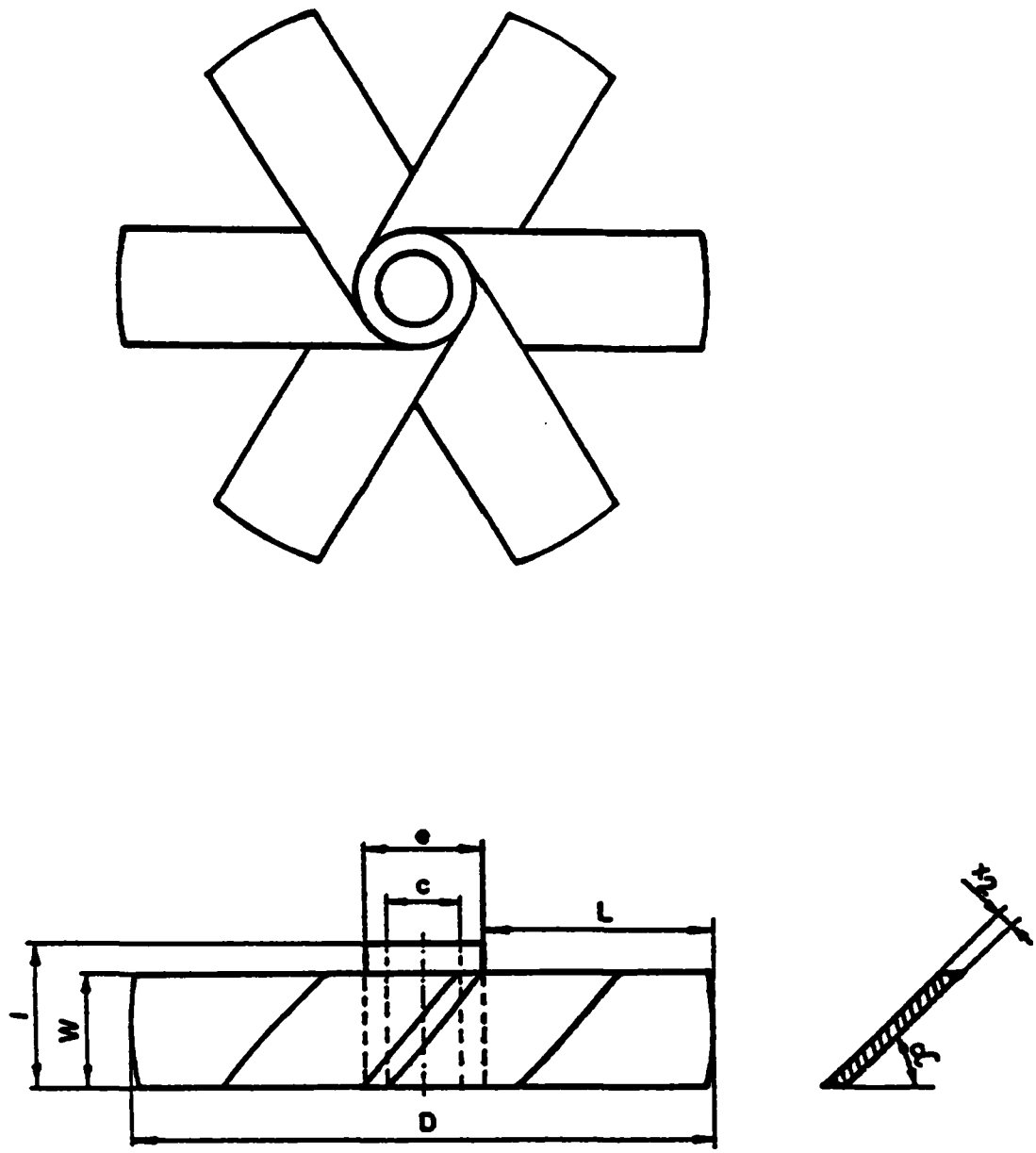

Figure 5.2 6MF.

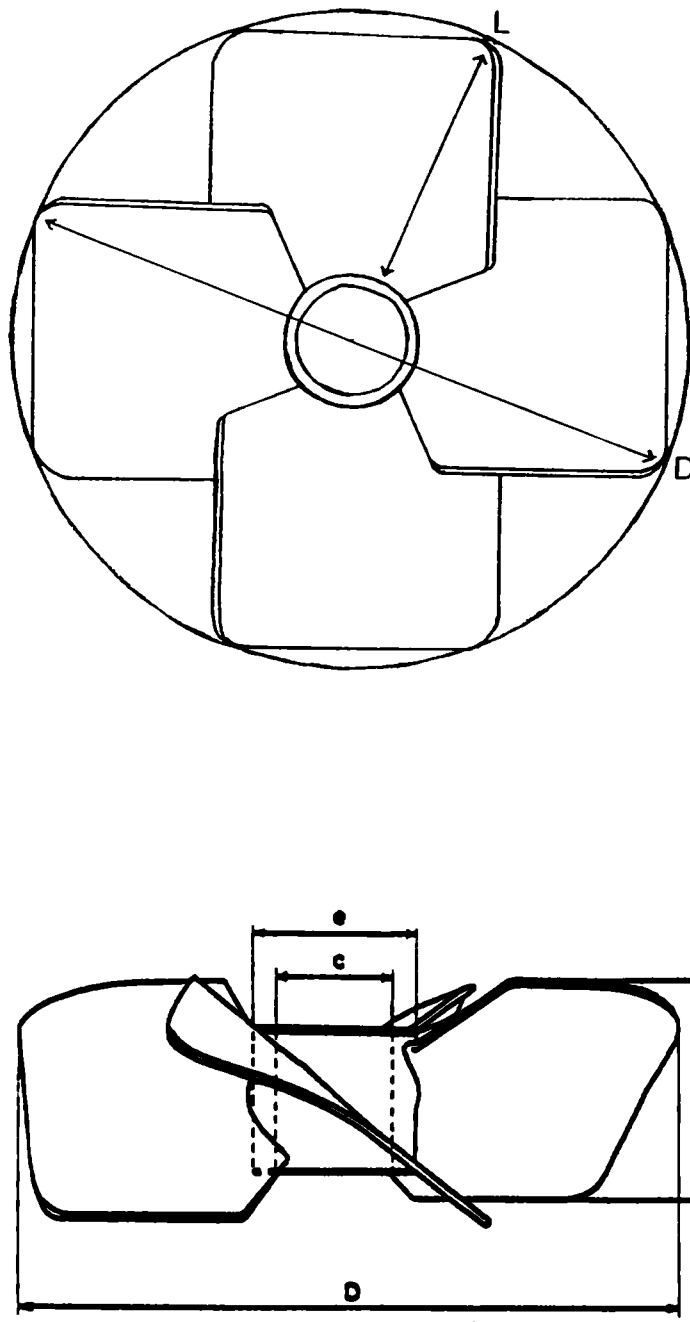

Figure 5.3 A315 Hydrofoil.

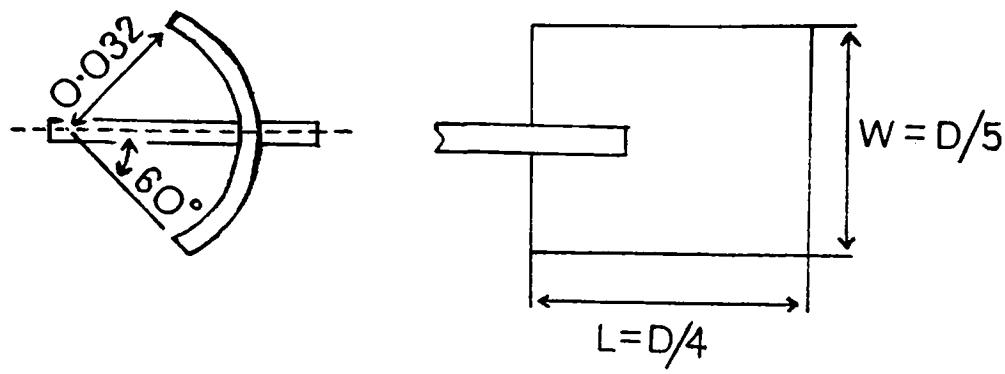

Figure 5.4 6PSDT Blade Detail.

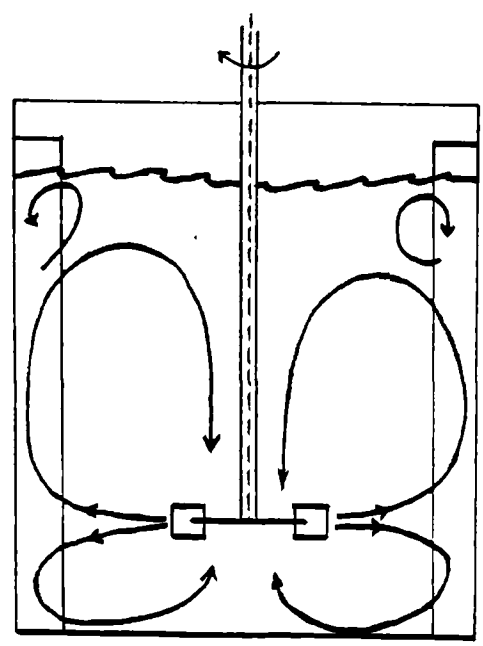

Figure 5.5 6DT Flowpattern.

The 6DT agitator D/T of T/2 was selected because of reduced power required for loading and complete dispersion when compared with T/3 6DT[25]. A C/T value of 0.25 was used as improved gas dispersion can be achieved when compared with higher clearances[22]. It also enables comparison with many recent works such as Cronin[13], Allsford[91], Bujalski[12], Hickman[20], etc.

The 6MF agitator D/T was chosen as 0.5 in order to reduce torque instabilities in the D.P.M.[33,34]. The large ring sparger was used as it has been reported that P/V required for complete dispersion and loading is reduced[12] and that direct-indirect loading instabilities are lessened by its use in the D.P.M.[34].

The four bladed Lightnin' A315 (a patented design of the Mixing Equipment Co. Inc. U.S.A.) was supplied to vessel specification provided by Birmingham University. A D/T ratio of 0.4 is typical[35,36]. A C/T of 0.33 was used as it corresponds to the intermediate value of C/T (0.25, 0.33 and 0.45) used by McFarlane[36]. The sparger type and clearance were selected in order to correspond with those recommended by the Bakker[35] and McFarlane[36].

The 6PSDT D/T of 0.4 was chosen to enable comparison with Warmoeskerken et al[29]. The clearance provided optimum gas dispersion and corresponded with that used for 6DT[22]. The 6PSDT similarity to the commercially available Scaba SRGT and Chemineer CD6 make it an interesting impeller.

5.2 FLOWPATTERNS

5.2.1 6DT and 6PSDT

The 6DT produces a flow pattern which is predominantly radial (Fig.5.5). In the impeller discharge stream (primary flow) the radial and tangential velocities are approximately equal at the blade tip. As the distance from the tip increases the tangential velocity decreases more

rapidly than the radial velocity in a fully baffled vessel[107]. Secondary flows caused by interaction with the vessel wall and base, entrainment of fluid etc. provide axial circulation of the liquid. The slow rate of axial circulation can cause pronounced zoning of flows or compartmentalisation[108]. The 6PSDT impeller produces a flowpattern indistinguishable from that of the 6DT, although lower energy dissipation through trailing vortices has been suggested[29].

5.2.2 6MFD and 6MFU

The mixed flow impeller produces both axial and radial flow components (Fig.5.6 and Fig.5.7)[21]. The primary flow pattern is helical, comprising of an axial component superimposed on a tangential flow. Axial circulation loops result from the interaction between the primary flow pattern and the baffles/wall. Velocity studies[109] on 45° pitched blades showed approximately equal radial and tangential velocities but axial velocities of double their magnitude.

A region of upward flow has been identified in the DPM below the centre of the impeller[110]. This has been noted a poor area for gas sparging as the gas/liquid flow would be concurrent[12] in the D.P.M.. Flow generated has been shown to be dependent on impeller and system geometry, large D/T (D/T > 0.5) or small C/T resulting in an enhanced radial flow component[12,111]. Tatterson[111] also commented on unaerated flow instabilities in the D.P.M..

5.2.3 A315

It has been suggested that hydrofoil impellers provide more uniform axial flow than mixed flow impellers, with a smaller radial component[35]. As with mixed flow impellers, the axial flow component is likely to reduce compartmentalisation between multiple impellers but does not eliminate it entirely. The flowpatterns generated with increasing N are shown in

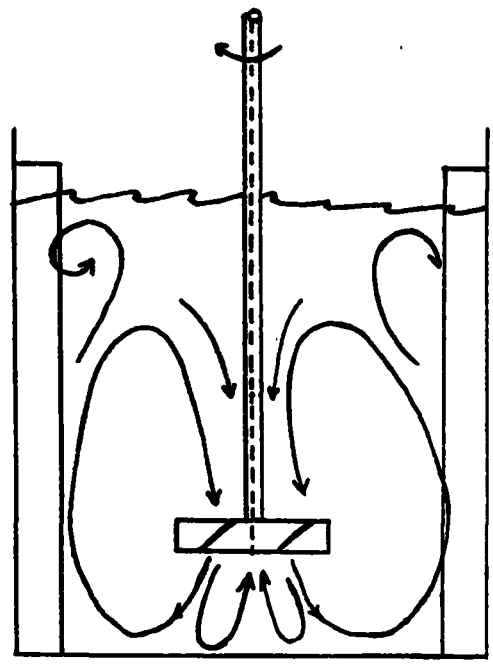

Figure 5.6 6MFD Flowpattern.

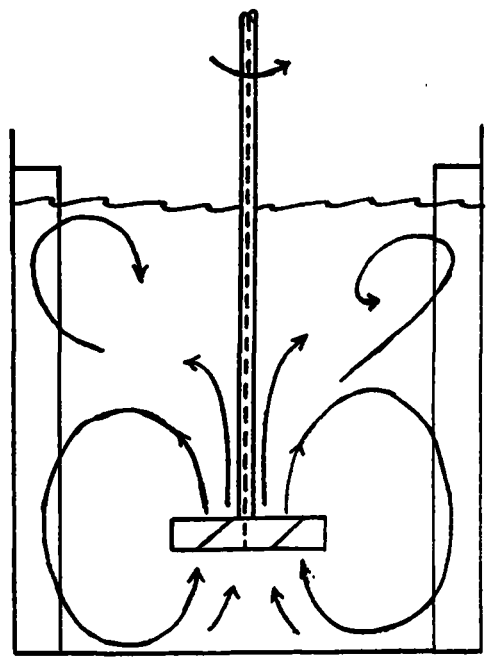

Figure 5.7 6MFU Flowpattern.

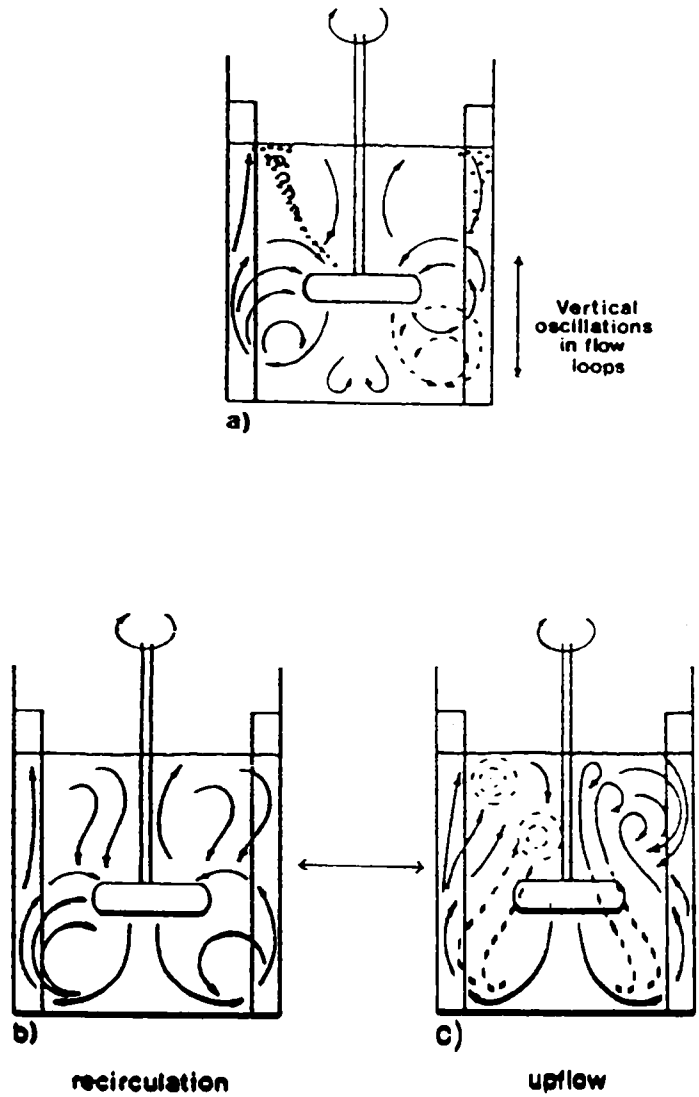

Figure 5.8 A315 (DPM) Flowpattern[34].

Fig.5.8. Vertical oscillations of flow pattern have been observed[36] with recirculation into the impeller alternating with strong vertical liquid upflow (5.8 b to c). A small region of upward flow close to the axis of the shaft occurs with the A315 (as with the 6MFD).

5.3 UNAERATED POWER DRAW

5.3.1 6DT

The unaerated power curve obtained using a single 6DT (T/2) in T72 (H/T = 1) is shown in Fig.5.9. The Re range covered using three CMC concentration and water was $2.2 \times 10^2 < Re < 5.6 \times 10^5$. The value of Re at which gas entrained from the surface was dispersed throughout the vessel is shown for each liquid. At low Re in 0.8% CMC (transitional regime), Po rose steadily from Po = 3.3 to Po = 4.75 ($Re = 2.4 \times 10^2$ to 1.6×10^3). The data from 0.4% CMC overlaps that of 0.8% CMC and shows good agreement in that region. At approximately $Re = 2 \times 10^3$ (0.4% CMC), the rate of increase of Po with Re slowed and Po reached a maximum at approximately $Re = 2 \times 10^4$ (0.07% CMC). However, due to clinging cavity formation[12], caused by surface entrained gas in 0.07% CMC, Po was reduced with increased Re. When using higher concentration CMC solutions (0.8% and 0.4%), surface aeration occurred but appeared not to effect Po. Typically Po reduction has been reported at 1.5 to 2 Re_{SA}[12], indicating that if higher N had been attainable in these solutions, Po reduction would have been seen.

In water ($1.1 \times 10^5 < Re < 5.6 \times 10^5$), Po rose gently to a maximum (Po_{max} = 5.35) before falling due to surface aeration. Cronin[13] found Po of 5.0 to 5.4 under identical conditions in water, the range given being due to the curvature mentioned. The Po variation due to curvature in water was > 7% of Po_{max}. This curvature has been reported previously[18,22].

In the transitional flow regime the 6DT power curve typically

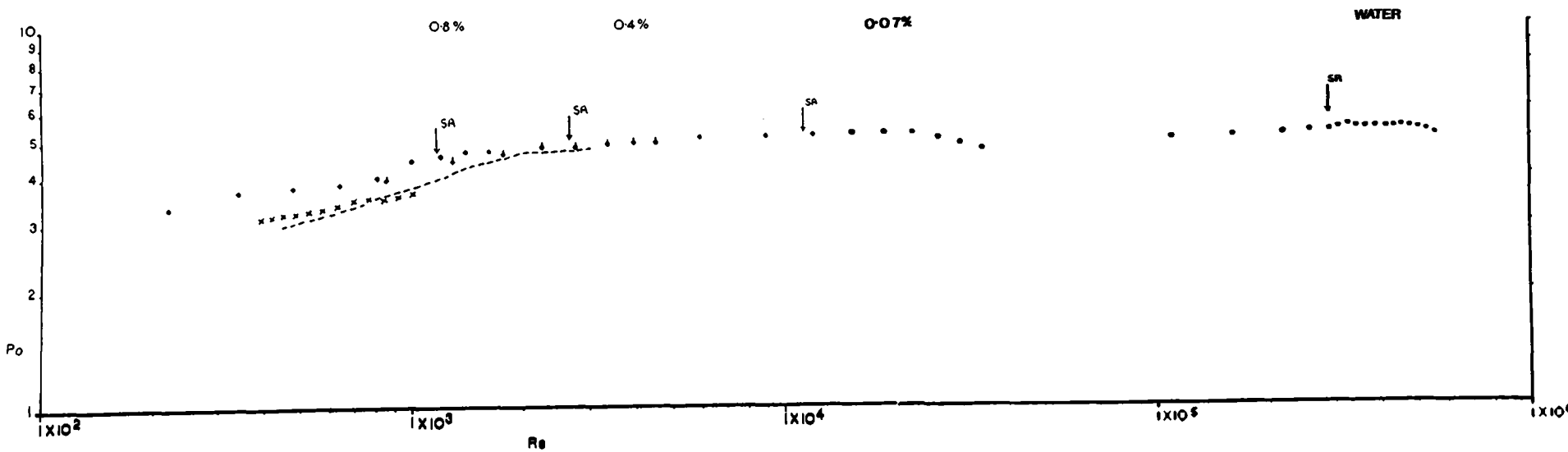

Figure 5.9 T72 Powercurve, 6DT, H/T = 1.

Ref.20 ×××× , Ref.13 ----.

exhibits a minimum in all but highly viscoelastic solutions[7]. The Re value at which the minimum occurs is dependent on fluid rheological properties[18,20] and impeller dimensions[17]. In this work the minimum Po was not discernible at Re > 2.2×10^2 and therefore was assumed to occur at lower Re. The Po in the transitional regime is compared in Fig.5.9 with that obtained by Cronin[13] under identical conditions. A slightly higher Po was obtained here for Re < 1.5×10^3. Comparison with Hickman[20] for 2×10^2 < Re < 1×10^3 in T40 also shows a lower Po than in this work. Hickman[20] found the minimum at Re ≃ 200 in CMC solutions.

Po results in 0.07% CMC (6×10^3 < Re < 3.4×10^4) were very close to those found in water (1.1×10^5 < Re < 5.6×10^5) indicating that Po attains a constant value (ignoring surface aeration) at Re ≃ 5×10^3. Comparison of the power curve with those obtained for Newtonian fluids indicates a slightly steeper increase of Po for 2×10^2 < Re < 2×10^3 but stabilisation of Po at similar Re. The inelastic non-Newtonian power curve and Newtonian power curve therefore appear to be in moderately good agreement over the Re range covered.

Bujalski[12] provided a correlation for predicting Po in the range $2 \times 10^4 \leq Re \leq 2\ Re_{SA}$ for 6DT agitators:

$$\bar{Po} = 2.5\ (x_1/D)^{-0.2}\ (T)^{0.065}$$

where : x_1 = disc thickness [m] D = impeller diameter [m]

T = tank diameter [m]

Applying this correlation to T72 predicts $\bar{Po} = 5.55$ for water agitated by one T/2 6DT, a value less than 5% greater than $\bar{Po} = 5.3$ found here.

Power data obtained when using 2 6DT at H/T = 2 with $\Delta C/D = 2.0$ is shown in Fig.5.10. The shape of the power curve is identical to that found for 1 6DT at H/T = 1 except that the influence of surface aeration is less. The reason for this is that only the upper agitator is affected over the speed range used[13]. The Po for both agitators combined is approximately double that found for one agitator at H/T = 1. This

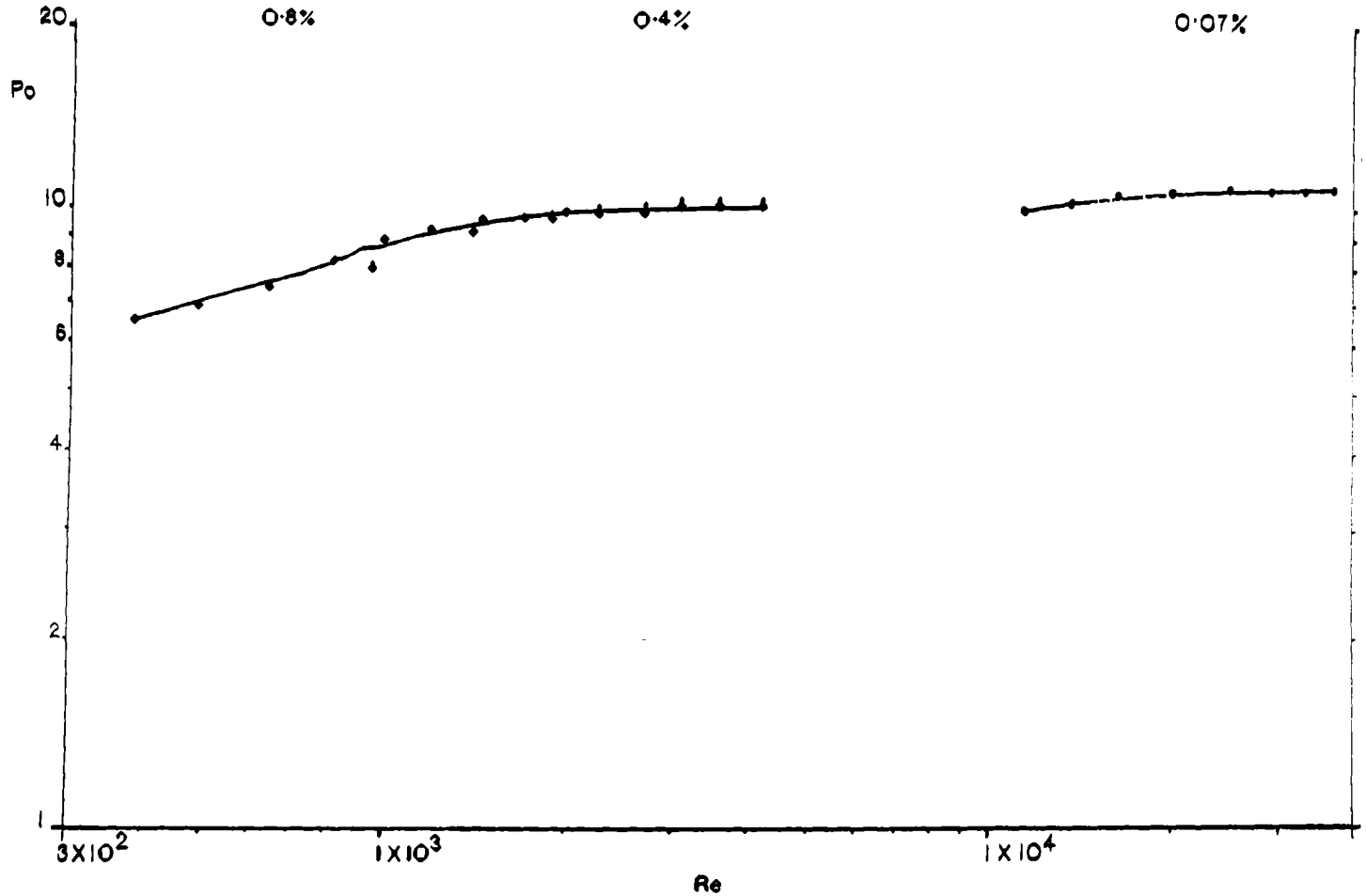

Figure 5.10 T72 Powercurve, 6DT, H/T = 2.

confirms the findings of Cronin[13] and extends them to lower Re. The $\Delta C/D$ used was the optimum found for T/2 6DT and corresponds to a situation where the circulation loops of the impellers do not interfere[13].

5.3.2 6PSDT

The power curve obtained with a single 6PSDT agitator (concave rotation direction) in T72 at H/T = 1 is shown in Fig.5.11. Po increased from 2.05 to 4.0 over the range $2.25 \times 10^2 < Re < 2 \times 10^4$. The shape of the curve in the transitional flow regime is very similar to that found using the 6DT. The Re range where 0.4% and 0.8% CMC data overlapped showed excellent agreement of Po. For $Re > 2 \times 10^4$, $\bar{P}o$ had a constant value of 4.0, somewhat lower than $\bar{P}o = 5.3$ found in the turbulent regime for 6DT. In the opposite rotation direction (convex) Otomo[112] reported $\bar{P}o = 4.4$ in the turbulent regime. Warmoeskerken et al[29] found Po for the 6PSDT lower than for 6DT of equivalent blade projected area, they postulated that this was due to modified flow over and under the blade edges. They found Po = 3.8 (concave rotation) and Po = 4.3 (convex rotation) in a T=0.44m vessel with C/T = 0.4.

5.3.3 6MFD and 6MFU

The unaerated power curves of the 6MF agitator in the U.P.M and D.P.M. are shown in Fig.5.12. The 6MFD Po decreased from Po = 1.95 at $Re = 3.6 \times 10^2$ to Po = 1.7 at $Re \simeq 2.5 \times 10^3$. The Po remained constant at $\bar{P}o = 1.7$ for $Re > 3 \times 10^3$. The 6MFU power curve followed that of the 6MFD closely. In the turbulent regime $\bar{P}o = 1.7$ for the 6MFU. Values of Re_{SA} are shown in Fig.5.12 for each test fluid except in 0.8% CMC where surface aeration did not occur.

Po was not influenced by surface aeration, except in 0.07% CMC at $Re = 4.5 \times 10^5$ (approx. 2.5 Re_{SA}) for both pumping modes. Re_{SA} for the D.P.M. was consistently lower than for the U.P.M.. Bujalski[12] reported a decline

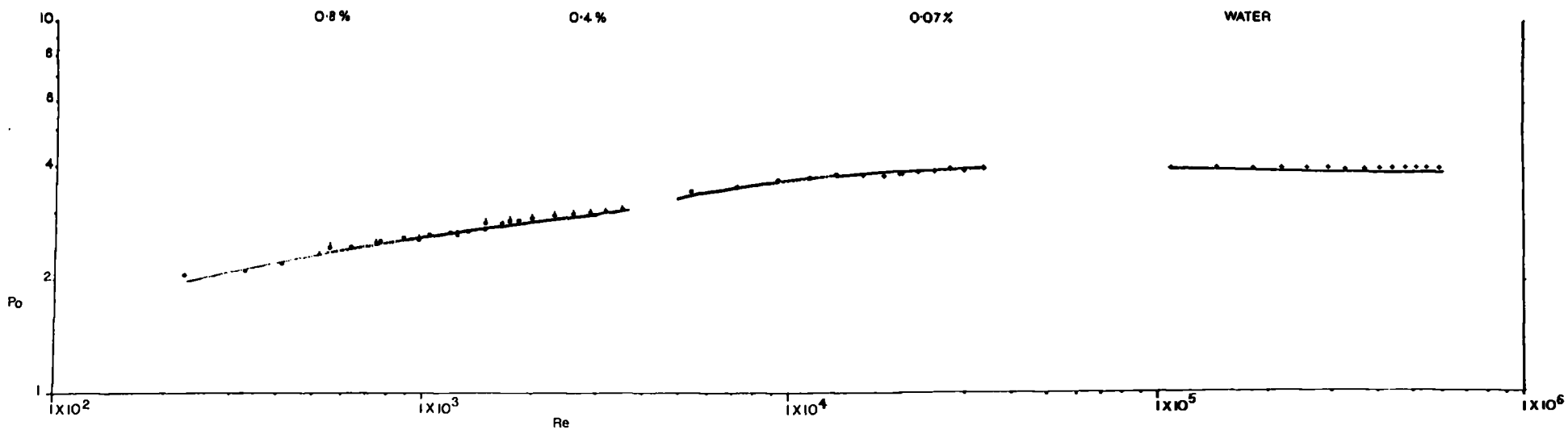

Figure 5.11 T72 Powercurve, 6PSDT, H/T = 1.

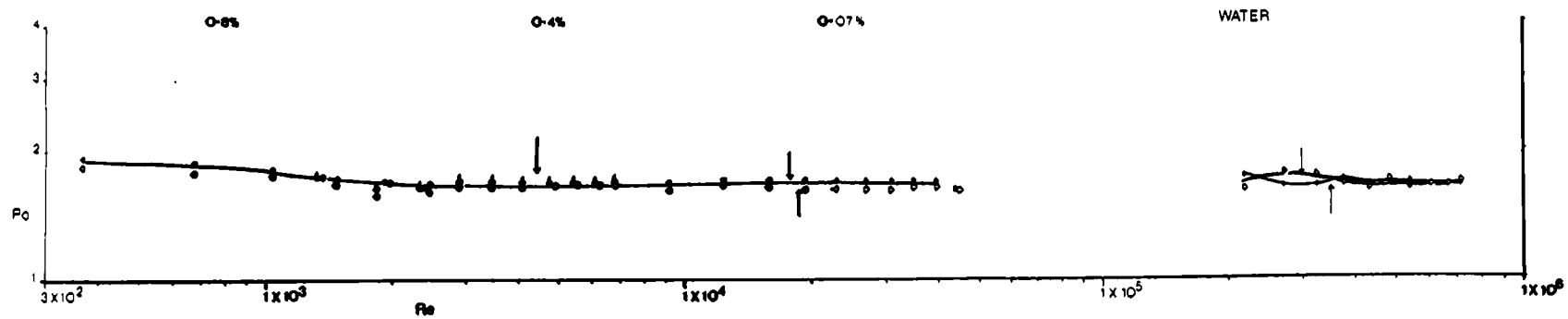

Figure 5.12 T72 Powercurve, 6MFD/U, H/T = 1.

6MFD: ◆ , 6MFU: ◇ .

in Po at $3Re_{SA}$ in small vessels where sufficiently high N could be attained. He also stated that $\bar{P}o$ values for the two pumping modes were very similar for $D/T \leq 0.5$. Bujalski[12] provided two correlations for predicting $\bar{P}o$ using D/T and either T or x_2/D as independent variables. These correlations are as follows :

$$\bar{P}o = 1.54\ (D/T)^{-0.127}\ T^{0.078} \qquad (5.2)$$

$$\bar{P}o = 0.775\ (D/T)^{-0.171}\ (x_2/D)^{-0.143} \qquad (5.3)$$

Predicted $\bar{P}o$ for T72 were 1.64 (Eqn.5.2) and 1.57 (Eqn.5.3). The average values (1.7) found in this work being 4% greater than Eqn.5.2 and 8% greater than Eqn.5.3, indicating good agreement

Bujalski[12] also showed power curves for 6MFD(U) in Newtonian glucose solution. Po fell from 1.9 at $Re = 4 \times 10^2$ to a constant value at $Re = 2 \times 10^3$. This shows close agreement with the findings here for non-Newtonian CMC. Unlike 6DT and 6PSDT no minima in the power curve are reported in the literature[9,12] for 6MFD(U). This work supports these findings.

5.3.4 Lightnin' A315

The A315 unaerated power curve is shown in Fig.5.13. As was found for the 6MFD(U) and IM, Po fell in the transitional regime reaching a constant value at the onset of fully turbulent flow ($Re \simeq 1 \times 10^4$ for A315). The A315 gave $\bar{P}o = 0.84$ at $C/T = 1/3$ for $Re > 1 \times 10^4$.

In the transitional regime Po fell from 1.75 to 0.84 over the range $2.35 \times 10^2 < Re < 1 \times 10^4$. Different CMC solutions showed excellent agreement of Po over the Re ranges where they overlapped. Comparison with the findings of McFarlane[36] and Bakker et al[35] indicated moderately good agreement of $\bar{P}o$ in the turbulent regime. For $C/T = 0.33$ McFarlane found $\bar{P}o = 0.77$ for $D/T = 0.4$ whilst Bakker et al[35] found $\bar{P}o = 0.76$ ($D/T = 0.4$, $C/T = 0.4$). A reduction in Po from 1.0 to 0.78 over the range $1.8 \times 10^3 < Re < 1 \times 10^4$ was reported[36]. The slightly greater D/T

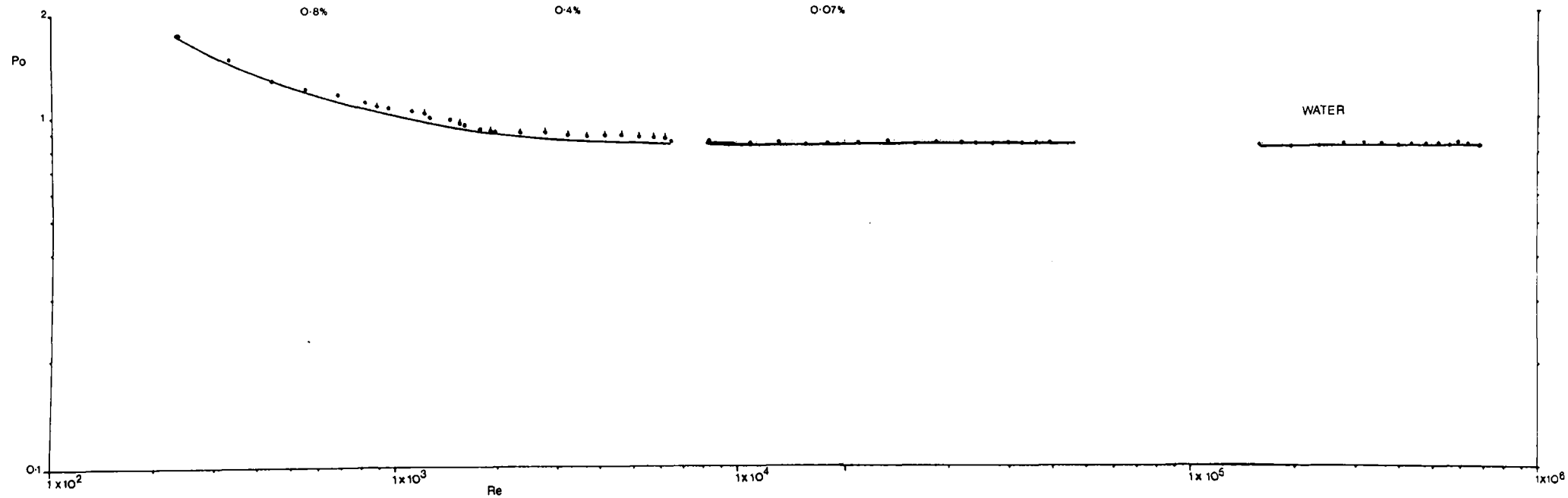

Figure 5.13 T72 Powercurve, A315, H/T = 1.

in this work may have caused the 9% greater $\bar{P}o$ in the turbulent regime. Surface aeration was not sufficiently intense to reduce Po in 0.07% CMC or water and did not occur at all in 0.4% or 0.8% CMC.

5.4 AERATED POWER AND BULK FLOW CHARACTERISTICS

This section opens by detailing the speeds and aerated power input required to completely disperse the gas phase using different agitators in water. There follows sub-sections describing aerated power data for each agitator in turn using water and CMC. Aerated power characteristics are linked to cavity observations made by other workers. Details of the cavity types discussed are given in Chapt.2. Power data in CMC was obtained during k_La measurement experiments and is therefore of relatively limited N range in each concentration.

5.4.1 Complete Dispersion in Water (T72)

N_{CD} and P/V_{CD} for each impeller type are given in Table 5.3. P/V_{CD} was correlated with Q_G and the resultant constants and exponent presented in Table 5.4. The agitator type obviously influenced the power required to completely disperse the gas phase. The 6MFU showed the best performance in this respect with only modest P/V increase needed to overcome increasing Q_G (β = 0.2). The improved gas dispersion capability

TABLE 5.3

COMPLETE DISPERSION IN WATER VESSEL T72, H/T = 1

Impeller	Q_G (vvm)	N_{CD} [rpm]	P/V_{CD} [kWm^{-3}]
6DT	0.5	65	0.09
	1	80	0.137
	1.5	90	0.2
6PSDT	0.5	150	0.39
	1	200	0.68
	1.5	200	0.625
6MFD	0.5	130	0.29
	1	180	0.45
	1.5	210	0.62
6MFU	0.5	75	0.08
	1	80	0.09
	1.5	85	0.1
A315	0.5	175	0.2
	1	250	0.4
	1.5	325	0.55

TABLE 5.4

COMPLETE DISPERSION IN WATER

$(P/V)_{CD} = A\ (Q_G)^{\beta}$; [$kWm^{-3}$], [vvm]

Impeller	A	β	R^2
6DT	0.14	0.71	0.98
6PSDT	0.57	0.47	0.76
6MFD	0.46	0.69	0.99
6MFU	0.09	0.2	0.99
A315	0.39	0.93	0.99

of the mixed flow impeller in the UPM has been commented on by Bujalski[12] who found $(P/V)_{CD} \propto Q_G^{0.7}$ and $(P/V)_{CD} \propto Q_G^{0.27}$ for the 6MFD and 6MFU respectively. The 6DT required higher P/V at high Q_G ($\beta = 0.71$). The 6MFD (D/T = 0.5) and A315 (D/T = 0.417) showed similar dispersion performances inspite of their differing diameters, suggesting an advantage of the hydrofoil design, this supports the findings of Bakker et al[35]. McFarlane[36] found $(P/V)_{CD} \propto Q_G^{1.1}$ for A315 at C = 0.45T which is close to the results of this work. The 6PSDT (D/T = 0.4) exhibited the highest P/V for gas dispersion at any gassing rate (excluding IM), this may be due to smaller D/T when compared with the 6DT (D/T = 0.5). Figure 5.14 presents the P/V_{CD} data graphically and includes IM results from Chapt.4.

5.4.2 6DT

Fig.5.15 shows Pog v Re for 0.8%, 0.4% and 0.07% CMC and water at three v_s, the unaerated power curve is shown for comparison. In 0.8% and 0.4% CMC Pog rose with increasing Re for all gassing rates. Previous studies[18,20,41] using 6DT in the transitional regime at constant Q_G with increasing N have shown Pog falling to a minimum and subsequently rising. The fall in Pog has been associated with increased cavity size causing reduced drag (streamlining) and reduced pumping capacity. The gas cavities increase in size until gas dispersion occurrs. Subsequently the size of cavities decreases with increasing N, more tiny bubbles are formed and Pog increases as does pumping capacity.

The value of Pog(min) is likely[18] to depend on the cavity size, the amount of gas in the impeller region and the impeller pumping capacity. The reduction in cavity size at high N may be due to increased liquid flow in the impeller region sweeping the gas away from the blades and increased shear rate leading to a reduction in μa (shear thinning fluids). Hickman[20] reported Re values for Pog(min) in 0.8% and 0.4% CMC of Re = 532 and 888 at 1 vvm and Re = 590 and 827 at 0.5 vvm. The increase in Pog

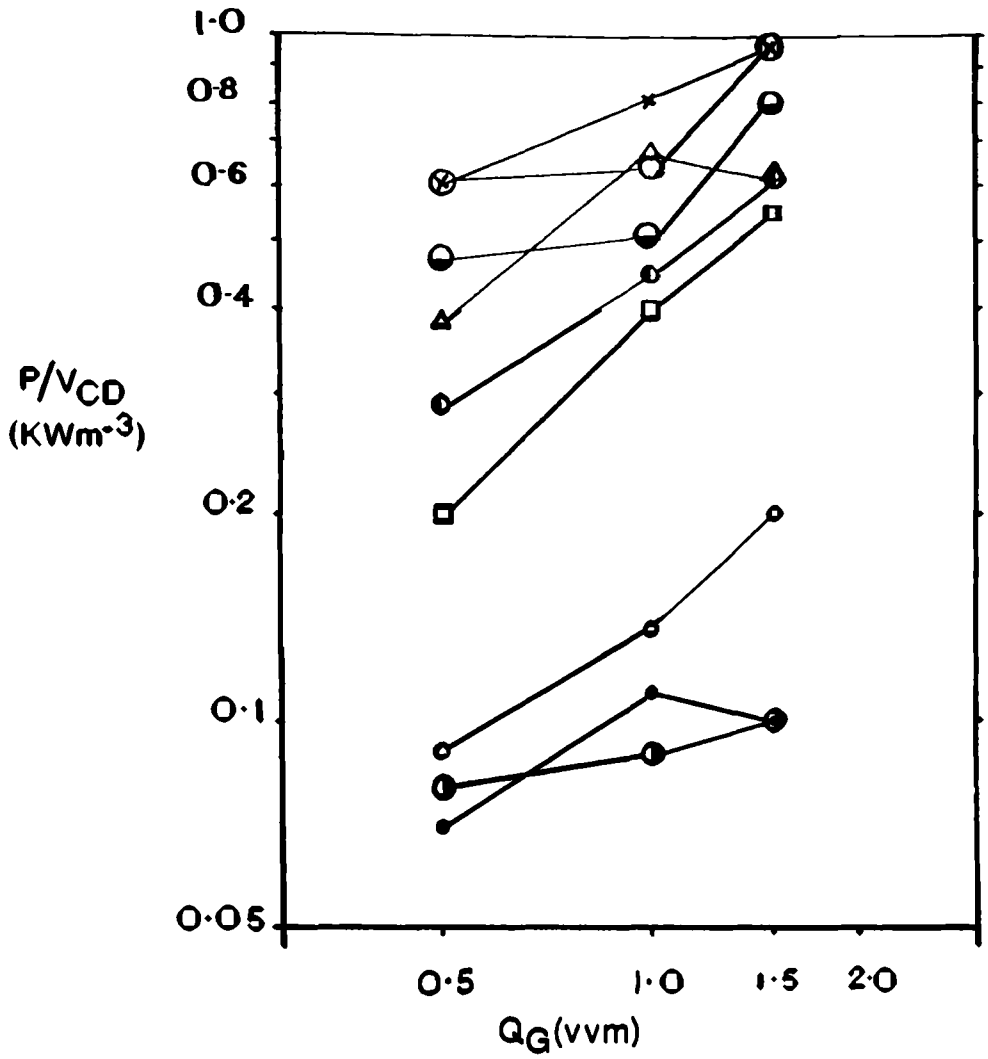

Figure 5.14 T72 P/V_{CD} v Q_G.

IM (PS): × , IM (SRS): ○ , IM (MRS): ● , IM (LRS): ◆ , 6DT: ⊙ ,

6PSDT: △ , 6MFU: ◑ , 6MFD: ◐ , A315: ◘ .

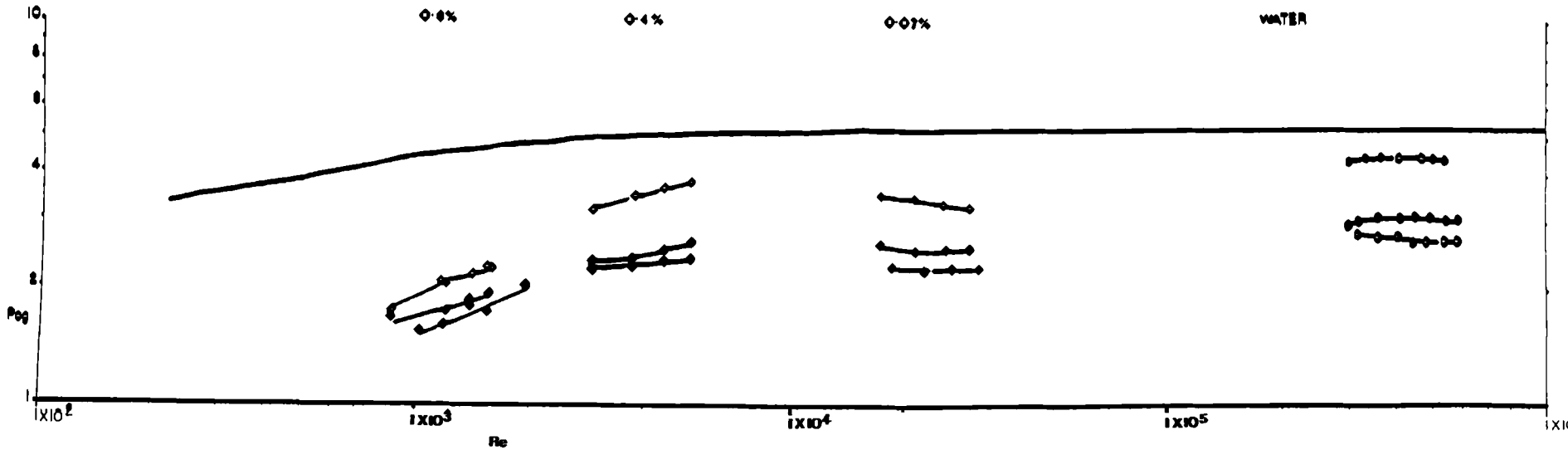

Figure 5.15 Pog v Re, T72, 6DT, H/T = 1.

Q_G = 0.5 vvm: o , 1.0 vvm: ⊖ , 1.5 vvm: ⊕ .

with Re seen using 0.4% (2900 < Re < 5400) and 0.8% (860 < Re < 1900) CMC in this work can therefore be related to decreasing cavity size subsequent to Pog(min).

Fig.5.15 also indicates a lower effect of Q_G on Pog in 0.8% CMC. Earlier work[3,7,18,20,41] showed a lack of effect of Q_G on Pg/P at low Re. This implies that at constant N, Q_G does not effect cavity size or pumping capacity. It appears that a minimum ratio of inertial to viscous forces is necessary before cavity size and type become critically dependent on gassing rate[18]. Nienow et al[18] found Pog independent of Q_G for 10 < Re < 900 using various fluids as did Kipke[41] for Re < 700 to 1300 using CMC. The 0.8% CMC data from this work corresponds to the Re values (Re > 850) at which Q_G was just beginning to influence Pog. These findings support those of earlier workers[18,41].

For Re > 2 x 10^3 (0.4%, 0.07% and water) the reduction in power on gassing was strongly dependent upon Q_G. At Q_G = 0.5 vvm, Pog/Po fell to between 0.67 and 0.83, dependent upon N and fluid. At Q_G = 1 vvm the power number ratio was 0.49 < Pog/Po < 0.58 and at Q_G = 1.5 vvm, 0.44 < Pog/Po < 0.5. Hence increasing Q_G from 0.5 to 1 vvm reduced Pog significantly more than increasing Q_G from 1 to 1.5 vvm. This can be related to gassed power curves (constant N) in the literature[22], where Q_G = 0.5 vvm in this work corresponds to the region where Pog/Po falls sharply and Q_G = 1 and 1.5 vvm correspond to the region of gradually declining Pog/Po. Gassed power data for water (Fig.5.15) agrees well with that obtained by Cronin[13] under identical conditions in T72.

Fig.5.16 shows Pog v Re for 2 6DT T/2 impellers at H/T = 2 in 0.4% and 0.8% CMC. The Pog values were more than doubled by the addition of the second agitator. This is because the lower agitator acts as a gas distributor, so that the upper impeller receives less air through it and hence draws more power, until a speed sufficient to cause gross recirculation is achieved[13,14,15]. As at H/T = 1, Pog rose with

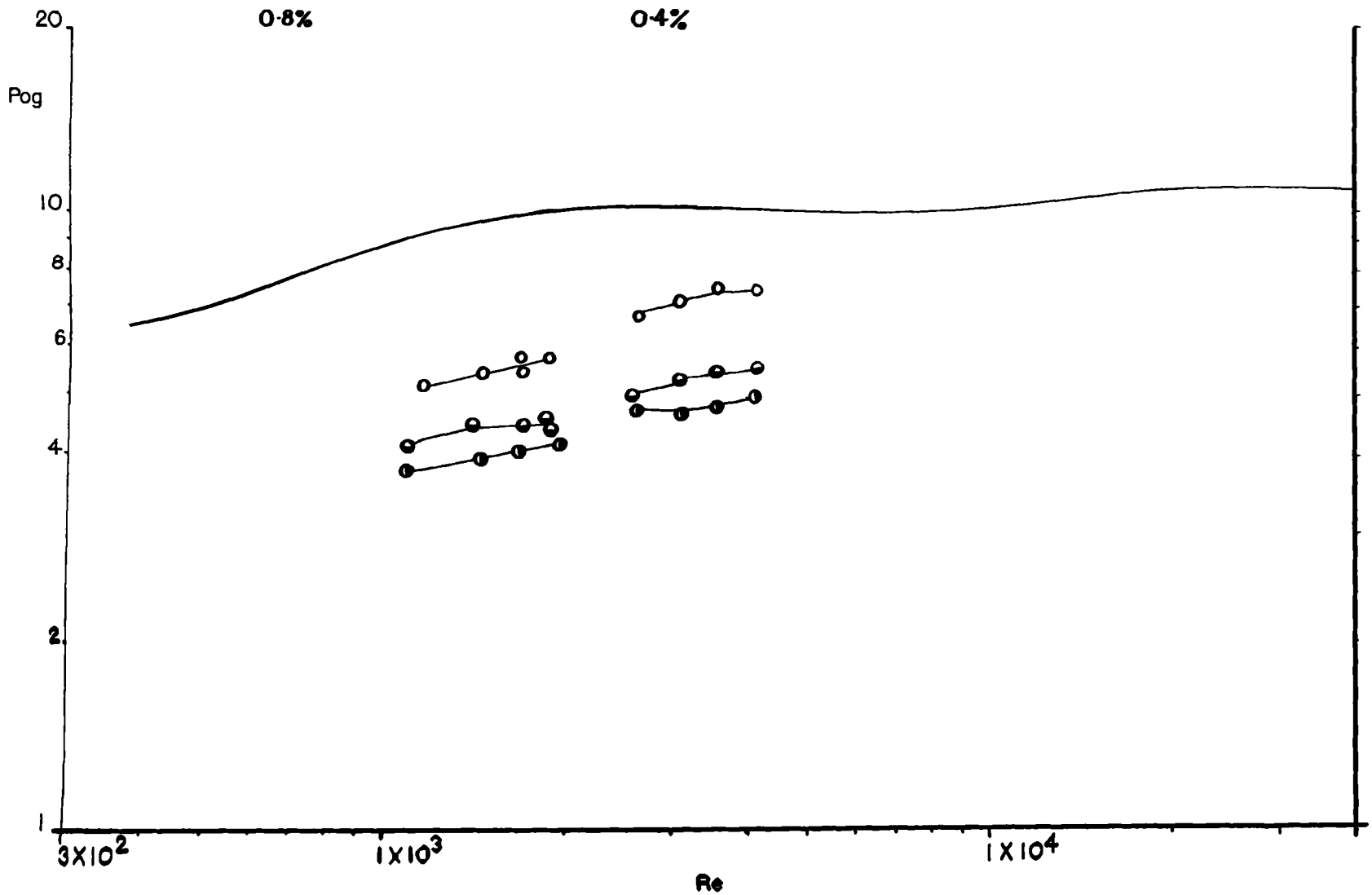

Figure 5.16 Pog v Re, T72, 6DT, H/T = 2.

Q_G = 0.25 vvm: o , 0.5 vvm: ● , 0.75 vvm: ◉ .

increasing Re due to decreasing cavity size and increased pumping capacity. The effect of Q_G on Pog for 0.8% CMC was slightly greater at H/T = 2 than at H/T = 1.

5.4.3 6PSDT

Fig.5.17 shows 6PSDT Pog v N for 3 gassing rates at H/T = 1 with water as a test fluid. The data shown was reported by Otomo[112] who also compared 6PSDT with 6DT and Scaba SRGT impellers[31]. Pog rose subsequent to loading at Q_G = 0.5 vvm attaining a value of Pog/Po = 0.94 for N > 225 rpm. At Q_G = 1.0 and 1.5 vvm Pog fell after N_F had been passed to Pog/Po = 0.7 and 0.625 respectively. Therefore for N > N_F the Pog/Po ratio obtained with 6PSDT was higher than at equivalent gassing rates using the 6DT. This phenomenon was due to the concave shape of the 6PSDT blades which delay the formation of large cavities until higher Q_G[29]. The 6PSDT does not however minimise the fall of power on gassing to the extent achieved when using the Scaba SRGT[31] which has a parabolic blade cross-section. The latter blade shape conforms more closely to cavity shape seen with aerated 6DT. The increase in Pog immediately prior to loading seen in Fig.5.17 was also observed for the 6DT[13].

6PSDT aerated power numbers obtained in CMC are shown in Fig.5.18. As was found with the 6DT, Pog increased with increasing Re in the range $1.45 \times 10^3 < Re < 4 \times 10^3$. With the 6PSDT however, a restricted Re range ($8.8 \times 10^2 < Re < 1.3 \times 10^3$) gave constant Pog. This may correspond to the minimum in the power curve seen in other studies with the 6DT. Also a very low effect of Q_G on Pog was seen for $Re < 1.25 \times 10^3$. At higher Re the gassed power number for Q_G = 0.5 vvm rose above those found for Q_G = 1 and 1.5 vvm. Comments made concerning these phenomena seen using the 6DT are likely to apply equally to the 6PSDT.

The reduction of power on gassing was found to be less with the 6PSDT than 6DT in all concentrations of CMC used. As in water, the blade shape

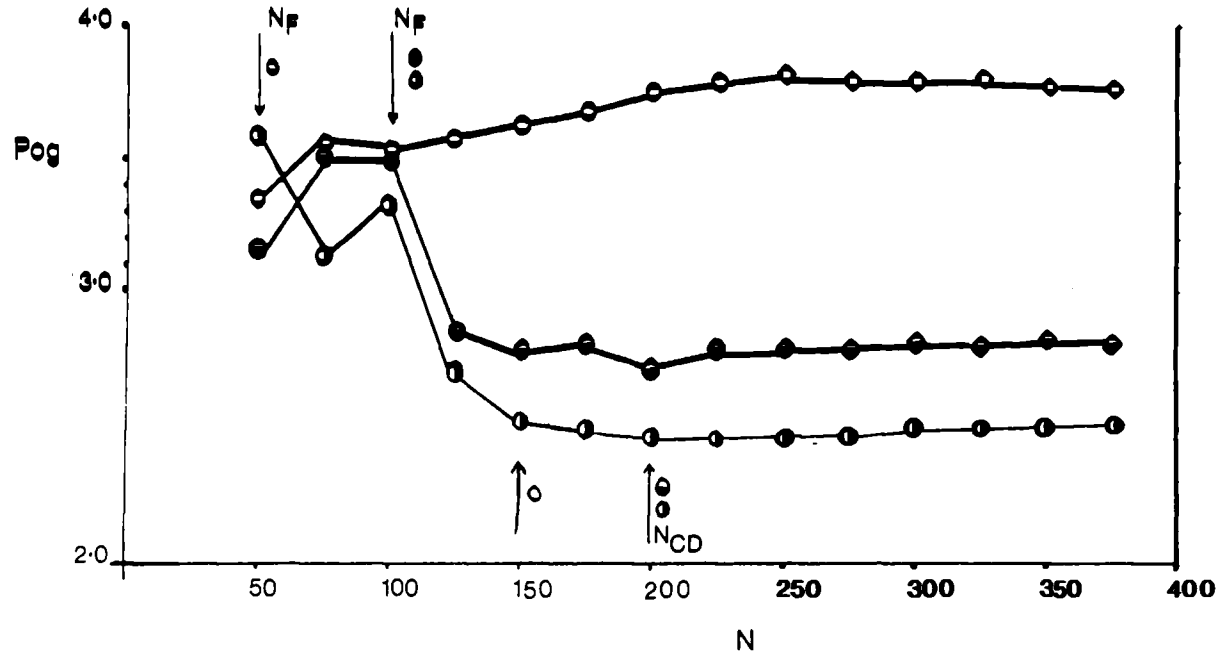

Figure 5.17 Pog v N, T72, 6PSDT, H/T = 1.

Q_g = 0.5 vvm: o , 1.0 vvm: ● , 1.5 vvm: ⊕ .

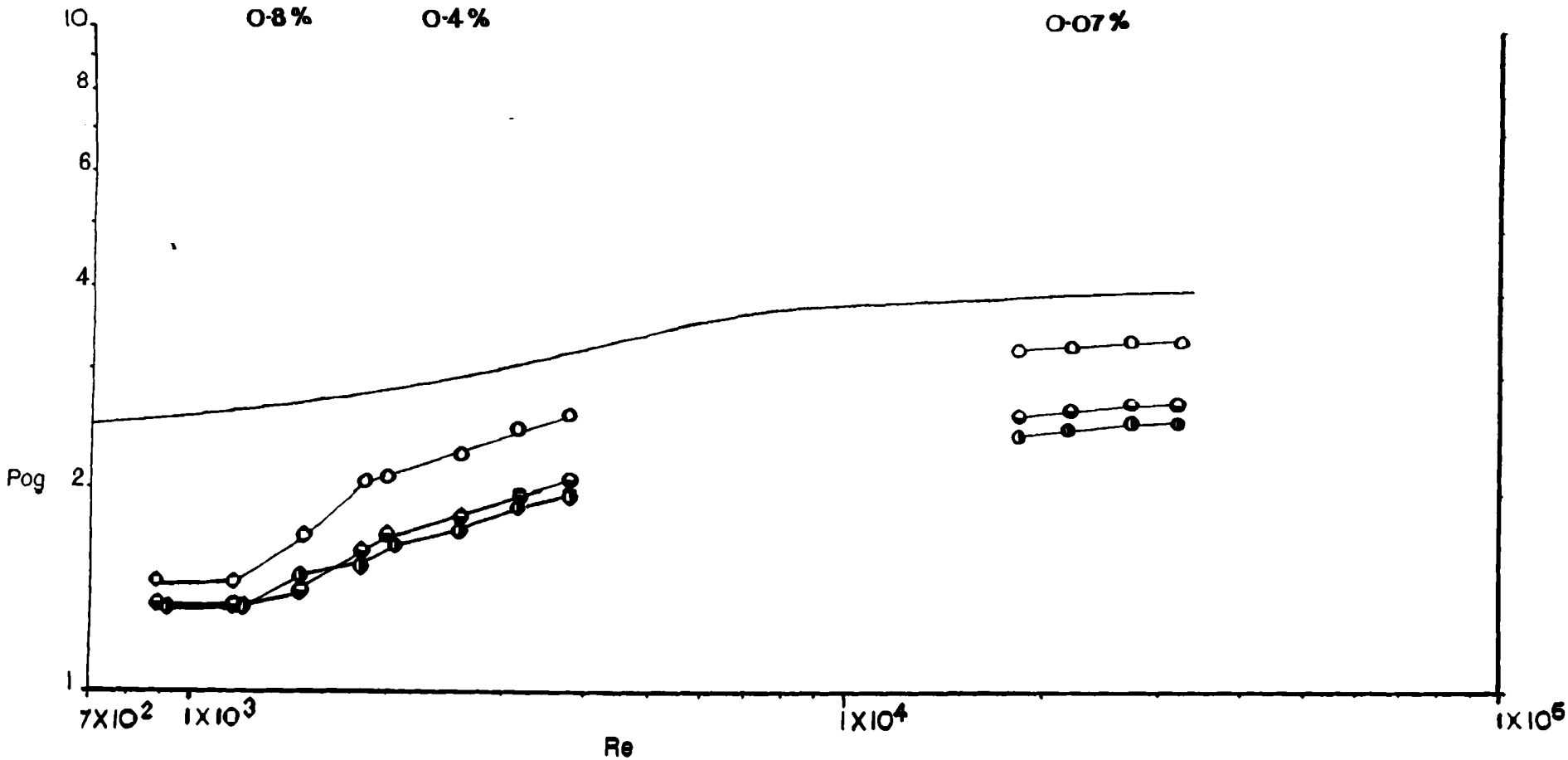

Figure 5.18 Pog v Re, T72, 6PSDT, H/T = 1.

Q_G = 0.5 vvm: o , 1.0 vvm: ● , 1.5 vvm: ◑ .

is likely to delay the formation of large cavities and hence maintain a higher Pg/P with increasing Q_G (see Section 5.5.5).

5.4.4 LIGHTNIN A-315

The aerated power data for the Lightnin A-315 impeller in water is shown in Fig.5.19. In describing the local impeller hydrodynamics and their relation to Pog, the work of McFarlane[36] has been referred to. At low rotational speeds the impeller was flooded. This condition was characterised by the irregular appearance of diffuse cavities bridging successive blades. Pog was found to be greater than Po prior to loading.

At the lowest gassing rate (Q_G = 0.5 vvm), Pog fell to a shallow minimum due to fully developed cavity formation. Subsequently Pog rose, corresponding to the competitive flow regime[36]. The competitive regime approximates to a direct-indirect loading transition with dominant radial flow alternating with dominant axial flow. The transition from radial to axial flow was accompanied by a reduction in cavity size, the maximum (N_{MAX}) corresponding to the establishment of axial flow. Complete dispersion of the gas flow occurred immediately after N_{MAX}.

At Q_G = 1 vvm the transition from radial to axial flow was delayed and the maxima more distinct than at 0.5 vvm. In the region 240 rpm < N < 280 rpm (competitive flow)[36] large (up to 40% of mean) torque fluctuations were recorded. At the highest gassing rate (Q_G = 1.5 vvm) no maxima or minima were discernible, although complete dispersion had occurred by N = 325 [rpm]. The reduction in Pog subsequent to the transition to axial flow at all gassing rates was due to increased gas recirculation and an increase in cavity size with N.

The gassed to ungassed power number ratio was found to be greater than unity for N < 300 rpm at Q_G = 0.5 vvm, reducing to Pog/Po = 0.89 at N = 375 rpm. For Q_G = 1 vvm, Pog/Po fell to 0.66 and for Q_G = 1.5[vvm] Pog/Po = 0.48 at N = 350 [rpm]. The reduction of power draw on gassing

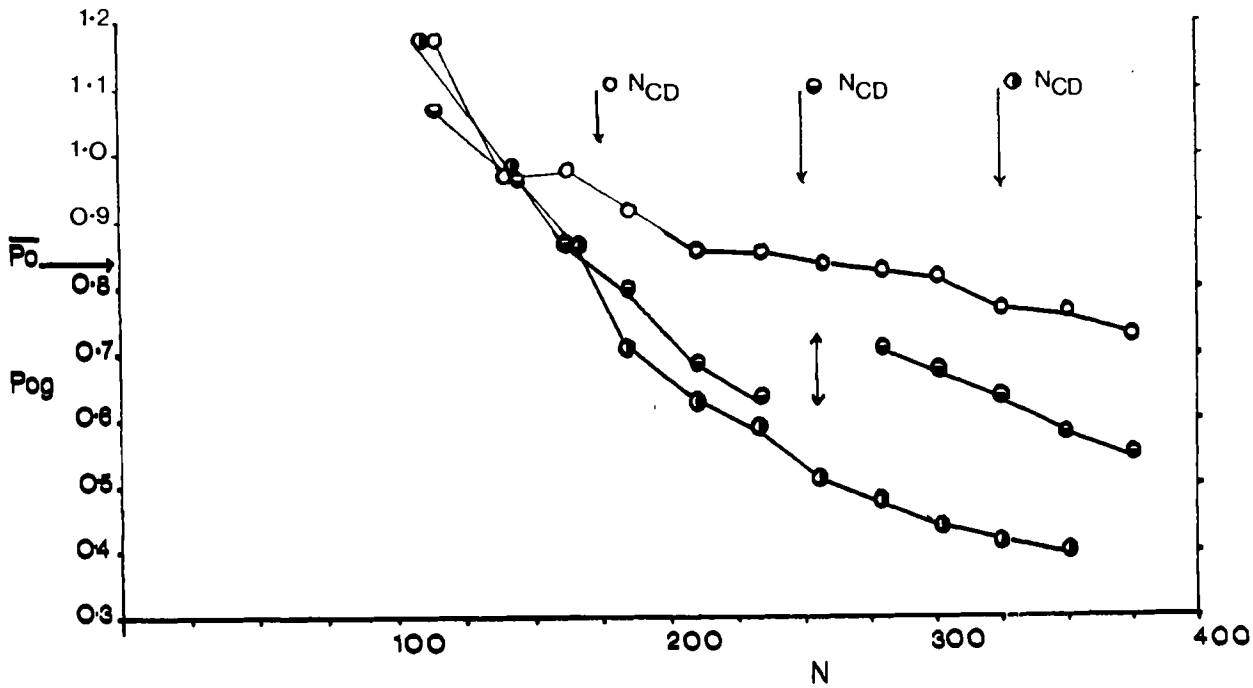

Figure 5.19 Pog v N, T72, A315, H/T = 1.

Q_G = 0.5 vvm: o , 1.0 vvm: ⊖ , 1.5 vvm: ◑ .

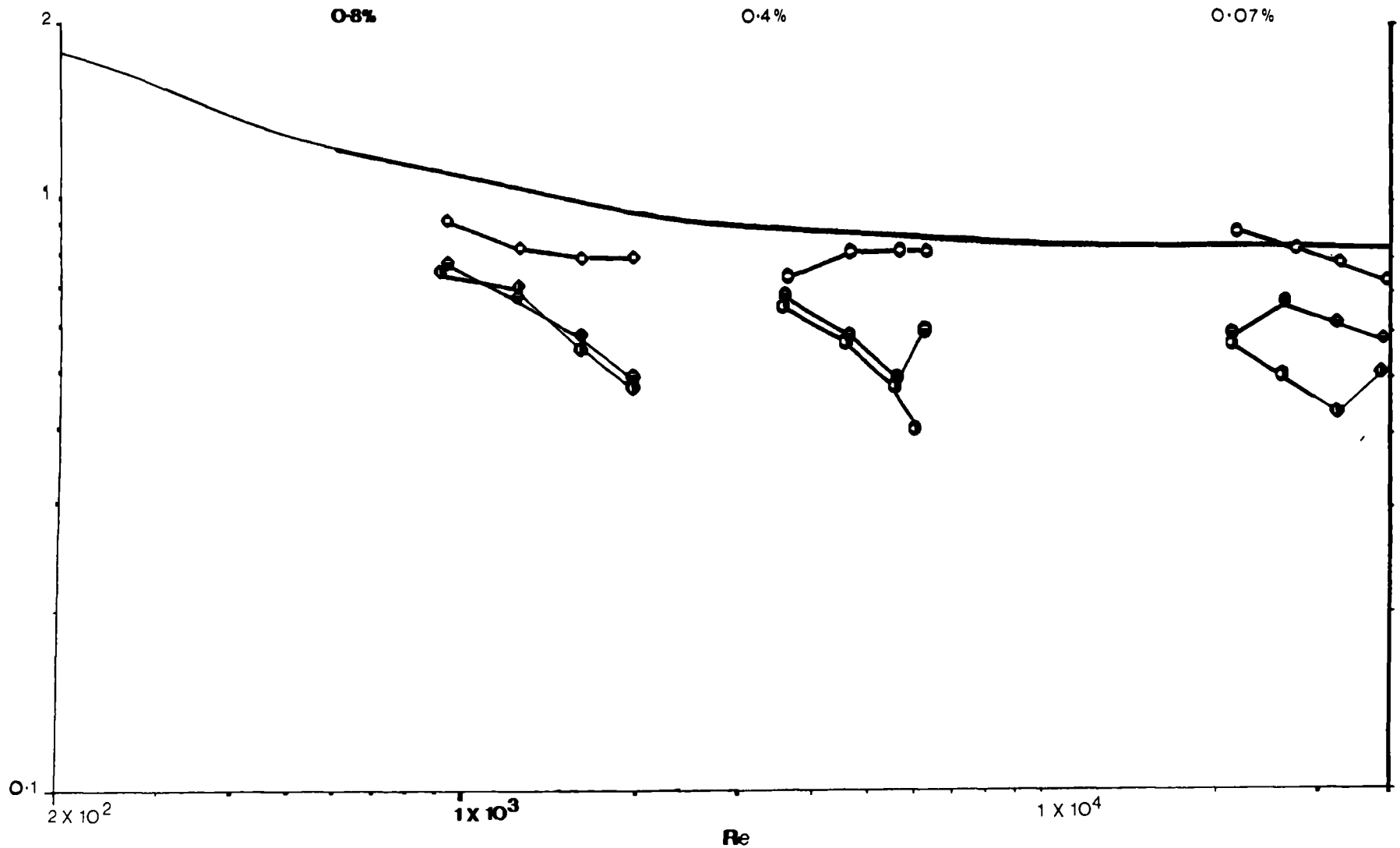

Figure 5.20 Pog v Re, T72, A315, H/T = 1.

Q_G = 0.5 vvm: o , 1.0 vvm: e , 1.5 vvm: o .

was therefore less than that of the 6DT particularly at low Q_G (see Section 5.5.5).

Figure 5.20 shows Pog v Re at three gassing rates for 0.07%, 0.4% and 0.8% CMC. In 0.07% CMC, ($2.15 \times 10^4 < Re < 3.9 \times 10^4$), the gassed power behaviour was found to be very similar to that of water. At Q_G = 0.5 vvm Pog/Po fell from 1.06 to 0.88 with no maxima apparent. At Q_G = 1.0 vvm, Pog rose to a maximum (transition to axial flow) at Re = 2.6×10^4 and then fell to Pog/Po = 0.69. At the highest gassing rate, Pog fell to a minimum (Re = 3.2×10^4, Pog/Po = 0.52) before rising to a maximum. The onset of axial flow was therefore delayed with increased Q_G.

In 0.4% CMC ($3.55 \times 10^3 < Re < 6.2 \times 10^3$), the transition to axial flow occurred at relatively higher N for a given gas flow rate than in water or 0.07% CMC. The gas cavities formed were more streamlined and stable than in water resulting in a greater reduction of power draw under equivalent conditions. At Q_G = 0.5 vvm, Pog rose subsequent to a minimum and remained constant at Pog/Po = 0.91. At Q_G = 1.0 vvm Pog fell to a minimum (Re = 5.6×10^3) prior to increasing whilst at Q_G = 1.5 vvm, Pog fell steadily with no minimum.

In 0.8% CMC the reduction of power draw due to aeration was greater than with lower viscosity fluids. Pog fell gradually at Q_G = 0.5 vvm and more steeply at Q_G = 1.0 and 1.5 vvm. No minima were apparent in the latter cases, although at Q_G = 0.5 vvm, Pog stabilised.

Overall in CMC the onset of axial flow was delayed and Pog/Po lower than in water. The greater stability of cavities formed led to a reduced tendency for torque instabilities.

5.4.5 6MFD

Figure 5.21 shows Pog v Re for the 6MFD (T/2) impeller used in conjunction with a larger ring sparger (Ds/D = 0.94) at three gassing rates in 0.07%, 0.4% and 0.8% CMC.

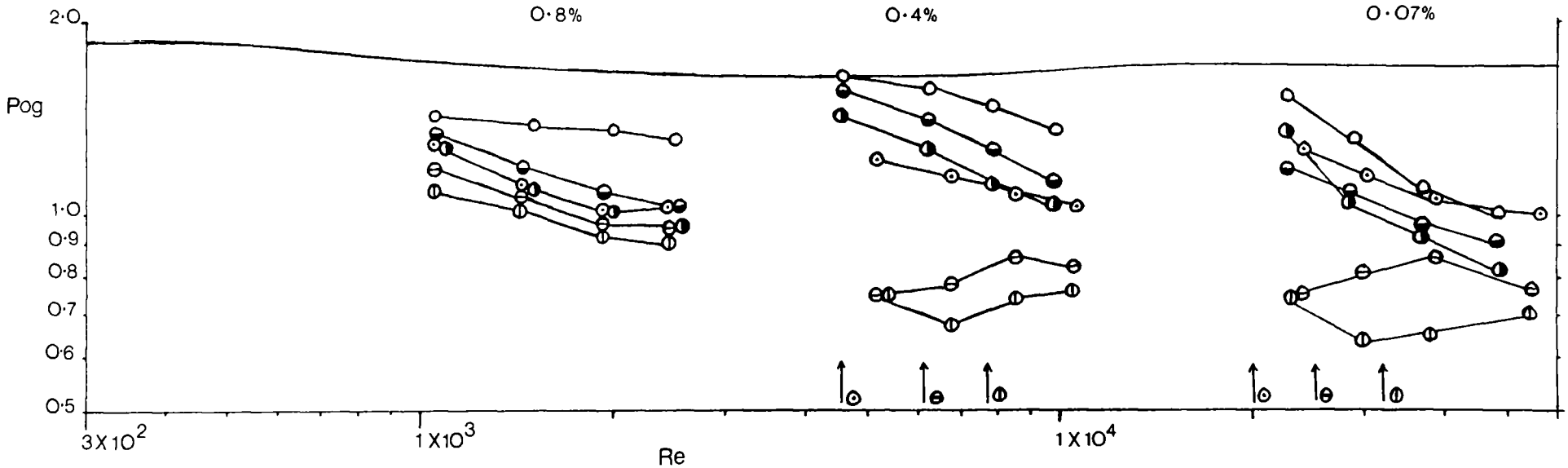

Figure 5.21 Pog v Re, T72, 6MF, H/T = 1.

6MFD: 0.5 vvm: ⊙ , 1.0 vvm: ⊖ , 1.5 vvm: ⊕ .

6MFU: 0.5 vvm: ○, 1.0 vvm: ⊖, 1.5 vvm: ●.

In 0.8% CMC, ($1 \times 10^3 < Re < 2.5 \times 10^3$) Pog fell with increasing N but the rate of fall was reduced at high N. The effect of Q_G upon Pog was small at this CMC concentration, indicating a limited effect of Q_G on cavity size at a given speed. The reduction in Pog with increased N can be associated with increasing 'large' cavity size until 'clinging' cavities are formed. As with the A315, the transition between 'large' and 'clinging' cavities is associated with the direct-indirect loading transition and complete gas dispersion. Fluctuations between direct and indirect loading and changing 'clinging' cavity size caused torque fluctuations. At the highest N and Q_G in 0.8% CMC the maximum torque fluctuation was ± 15% of mean torque. Subsequent to complete dispersion Pog levels off[12].

In 0.4% CMC ($5 \times 10^3 < Re < 1.05 \times 10^4$), the effect of Q_G on Pog was greatly increased. At Q_G = 0.5 vvm Pog fell steadily, the gas being completely dispersed at the lowest speed used. Cavity type was assumed to be 'clinging' with torque fluctuations of ± 17%. For Q_G = 1.0 vvm, Pog rose (from a minimum) to a maximum before falling slightly. The minimum corresponded to the transition from 'large' to 'clinging' cavities and was followed by complete dispersion. The increase in Pog at this point being due to 'clinging' cavity formation. As these cavities grew further and recirculation increased, Pog fell. At the highest gassing rate (Q_G = 1.5 vvm) the speed required for the 'large' to 'clinging' cavity interchange increased. Pog initially fell due to 'large' cavity size increase, the minima corresponded to 'direct'-'indirect' ('large'-'clinging') transition and was followed by an increase in Pog due to 'clinging' cavity formation. Torque fluctuations were ± 17% maximum.

The 6MFD Pog v Re curves in 0.07% CMC were of a similar shape to those described for 0.4% CMC, due to the occurrence of similar physical phenomena. Torque fluctuations were up to ± 30% of mean torque. The increase in maximum torque fluctuations with reduced viscosity being due

to reduced stability of cavities and reduced damping.

Reduction of power on gassing was similar for all CMC concentrations at Q_G = 0.5 vvm (Pog/Po (min) ≃ 0.6). At higher gassing rates, Pog fell to lower minimum values with increasing Re.

5.4.6 6MFU

Fig.5.21 also shows Pog v Re in the three concentrations of CMC using the 6MFU. In 0.8% CMC ($1.05 \times 10^3 < Re < 2.5 \times 10^3$), the influence of Q_G on Pog was greater than with the 6MFD. The gassed power curves for the 6MFU lay above those of the 6MFD, although only marginally so at Q_G = 1 and 1.5 vvm. The reduction in Pog with increasing N can be related to increasing 'clinging' cavity size[12]. Torque fluctuations were ± 8% of mean torque at most.

In 0.4% CMC ($4.5 \times 10^3 < Re < 1 \times 10^4$), Pog gradually fell at all Q_G. No maxima or minima were apparent. The effect of Q_G on Pog was less than with the 6MFD under identical conditions. Reduction of power draw on gassing was considerably less than was found for the D.P.M.. At low Q_G and the lowest N, Pog/Po = 1. Previous research using this agitator[12] indicated that Pog fell from values greater than Po subsequent to complete dispersion as clinging cavities grew in size. The data obtained here therefore corresponds to the region of the gassed power curve were Pog has fallen to ≤ Po. Maximum torque fluctuations were ± 11% in 0.4% CMC.

In 0.07% CMC, the Pog fell in a similar manner to that found in 0.4% CMC. The effect of Q_G on Pog was less than with the 6MFD and Pog values were higher. Maximum torque fluctuations were ± 18%, therefore as with the 6MFD torque fluctuation increased with reduced viscosity.

Comparing the two pumping modes of the mixed flow impeller it can be seen that the D.P.M. is less stable due to the direct-indirect loading transition and hence exhibits larger torque fluctuations and maxima/minima in the gassed power curve. The Pog/Po ratio is lower for the D.P.M.

particularly at high Q_G and low μa.

5.5 DISCUSSION AND CONCLUSIONS

5.5.1 Flowpatterns

Predominantly radial flow is produced by the 6DT and 6PSDT whereas IM, 6MFU and 6MFD provide both axial and radial components and the A315 hydrofoil predominantly axial flow. Compartmentalisation may be reduced and better top to bottom blending achieved by using agitators with a strong axial flow component. The IM flowpattern is the most chaotic and lends credence to the claims (Appendix I) of more uniform energy dissipation.

5.5.2 Surface Aeration

Surface aeration was found to reduce Po in T72 at Re > 1.5 Re_{SA} for the 6DT and at Re > 2.5 Re_{SA} for the 6MFD and 6MFU. Po reduction only occurred with IM in the D.P.M. and was not evident when using 6PSDT, A315 or IM (UPM). Increased viscosity prevented Po reduction due to surface aeration. Surface aeration is undesirable in single phase mixing processes.

5.5.3 Unaerated Power

The unaerated power curves of the 6DT and 6PSDT impellers showed an increase with Re in the transitional flow regime whilst the IM, A315, 6MFD and 6MFU power curves decreased over a similar Re range. Constant Po values were attained at $7.5 \times 10^3 < Re < 2 \times 10^4$ for all impellers except the 6MF for which Po was constant at $Re > 3 \times 10^3$. $\bar{P}o$ values in the turbulent regime were 5.3 (6DT), 4.0 (6PSDT), 1.7 (6MFU and 6MFD), 0.84 (A315) and 0.6 (2IM). The low Po impellers operate at higher N for constant P/V and therefore lower apparent viscosity in shear-thinning liquids (assuming equal D/T), this may be advantageous for mass transfer

(see Chapt.6 and 7).

Replacing high Po 6DT agitators with low Po types at equal P/V and equal D/T requires gearbox changes unless a multi or variable speed motor is used. Alternatively, retrofitting at equal P/V and N requires an increase of the low Po impeller's D/T and/or the use of more stages, (bearing in mind optimum S/T values). IM have been shown to develop full power at lower S/T than equivalent D/T 6DT impellers and therefore are particularly useful for constant P/V and N retrofitting. A315 and 6MF types may require a greater S/T than IM to draw optimum power. Further work is required to ascertain this. Simply fitting axial or mixed flow agitators of equal D/T and number of stages at constant N will result in a considerable loss of power transferred to the fluid.

5.5.4 Gas Dispersion

The power input required for complete gas dispersion (Tables 4.5 and 5.3) at Q_G = 1/2 vvm was lowest for the 6MFU, IM (LRS) and 6DT (T/2). The 6DT however required more power than the latter two at higher gassing rates. The A315 of smaller D/T than the above required the next highest P/V followed by 6MFD, 6PSDT, IM (MRS), (SRS) and (PS). The IM was therefore only competitive in terms of P/V_{CD} if used with a sparger of greater diameter than the impeller. These data are summarised in Fig.5.14.

5.5.5 Aerated Power

A reduction of power draw on aeration was seen for all agitators in all test fluids for $N > N_{CD}$. The agitator type, fluid viscosity, Q_G and N were found to influence the degree of power reduction due to size and type of cavity structure. Figures 5.22 to 5.24 show Pog/Po v Q_G for all the impellers at speeds equivalent to a representative unaerated power input of 5 kWm^{-3} in 0.07%, 0.4% and 0.8% CMC. This method of presentation

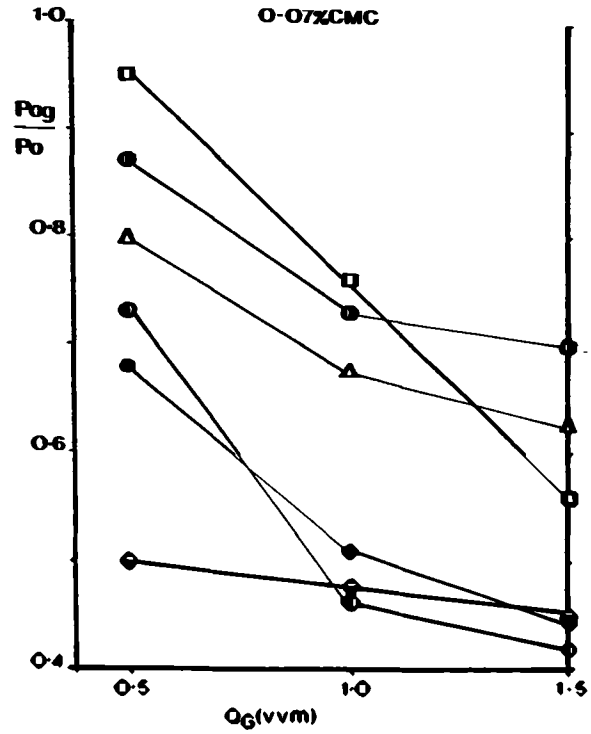

Figure 5.22 Pog/Po v Q_G, CMC Solutions.

6DT: ● , 6PSDT: △ , A315: □ , 6MFU: ◐ , 6MFD: ◆ , IM (MRS): ● .

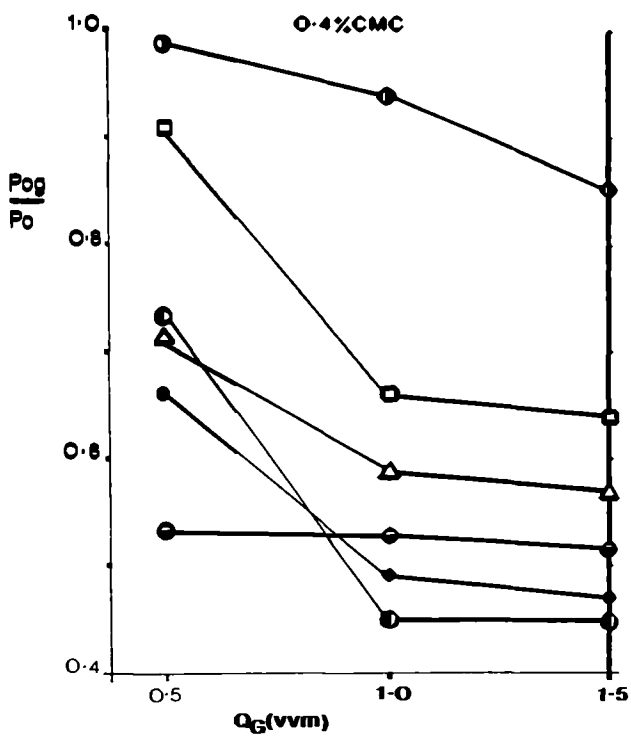

Figure 5.23

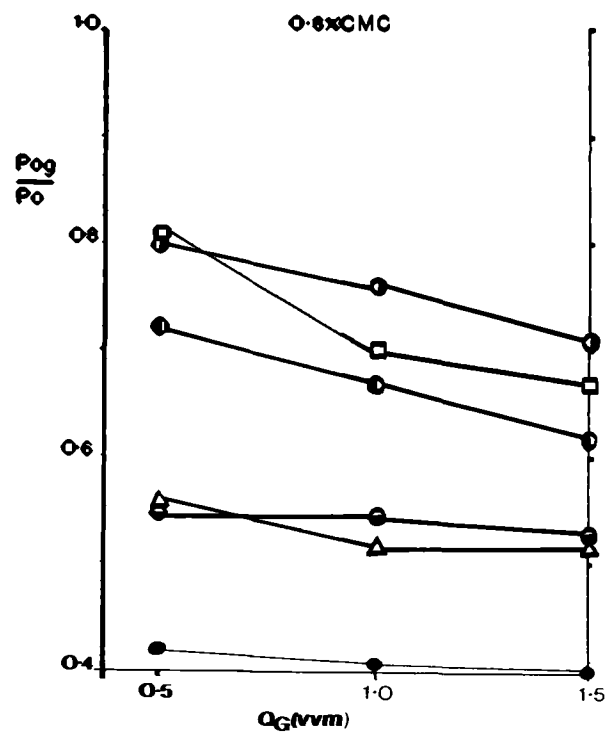

Figure 5.24

indicates the fall of power input on aeration assuming the motor has been designed to cope with the full speed unaerated situation, a common but conservative approach.

With a constant speed motor, different shaft speeds and hence gearbox ratios would be needed to obtain the full power potential of the motor with the various agitators. The smallest reduction of power draw on aeration was obtained with the A315, 6MFU and 6PSDT in 0.07% CMC, although Pog/Po decreased with increasing Q_G. The 6DT, 6MFD and IM (MRS) gave similar lower Pog/Po values at Q_G = 1 and 1.5 vvm. At Q_G = 0.5 vvm, IM (MRS) showed by far the greatest reduction in power draw. In 0.4% CMC, Q_G affected Pog/Po strongly for all but the IM. The 6MFU gave the highest Pog/Po followed by A315, 6PSDT, IM, 6DT and 6MFD.

In 0.8% CMC the influence of Q_G was greatly reduced. The power reduction of the two pumping modes of the mixed flow impeller were closer than in less viscous fluids. The relative loss of power was greatest for 6DT followed by 6PSDT, IM, 6MFD, A315 and 6MFU. The optimum agitator choice to avoid large reduction in power draw on aeration would therefore appear to be 6MFU or A315 over this range of test conditions.

5.5.6 Torque Fluctuation

During the course of aerated agitation, certain impellers exhibited regions of torque fluctuation due to changing cavity structure and/or the direct-indirect loading transition. These fluctuations were most marked for the A315 and 6MFD, their primary impeller flow directly opposes the buoyancy of the rising gas. The amplitude of fluctuation decreased with increasing viscosity. Maximum fluctuations were 6MFD ± 30%, 6MFU ± 18%, A315 ± 40% and IM ± 20% of total mean torque. The 6DT and 6PSDT showed only minor fluctuations.

6. GASSED HOLD-UP

6.1 INTRODUCTION

In this chapter gassed hold-up (ε_G) values found when using a variety of impellers are presented for both deionised water and non-Newtonian CMC solutions. Hold-up can play an important role in the determination of gas-liquid mass transfer rates. The variation of the mass transfer coefficient, k_L, is often small in a given system whereas the variation of the volumetric mass transfer coefficient, k_La, is much greater due to changes in the interfacial area, a. The interfacial area is related to the gas hold-up by bubble size and shape, for a given bubble size distribution increasing hold-up increases a. However, in viscous liquids the bubble diameter, shape and residense time may affect both k_L and a making the relationship between gas hold-up and volumetric mass transfer coefficient very complex. However the hold-up may still be a useful indicator of agitation efficiency in two-phase systems and increased hold-up generally signifies increased interfacial area.

All tests were carried out in vessel T72, except for those with IM impellers in vessel T45, conducted in order to evaluate the effect of scale on hold-up when using this impeller type in water. The IM impellers were more rigorously tested than other types in order to assess the effect of scale, sparger design, aspect ratio and fluid rheology on hold-up. Experiments with IM were conducted at either constant N or constant v_s. The hold-up data obtained for the other impeller types used was collected during oxygen mass transfer experiments (Chapt.7) and therefore at constant v_s.

6.2 HOLD-UP RESULTS IN DEIONISED WATER.

6.2.1 Effect of impeller type.

Four impeller types were tested in water (IM, A315, 6DT and 6PSDT) at H/T=1 in T72. IM was used with the four sparger types described in

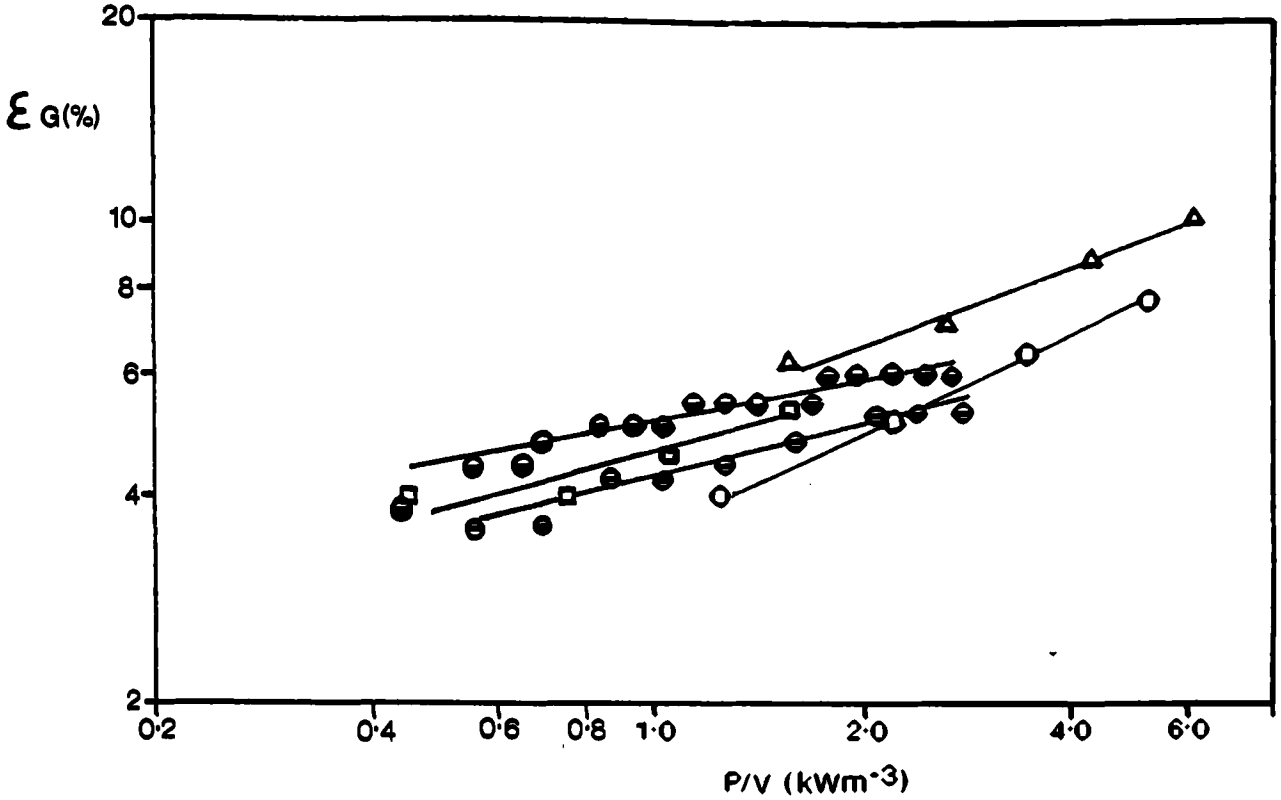

Figure 6.1 T72, ϵ_G v P/V, Water, v_s = 0.006 [m/s].

IM (MRS): ● , IM (PS): ● , 6DT: ○ , 6PSDT: △ , A315: □ .

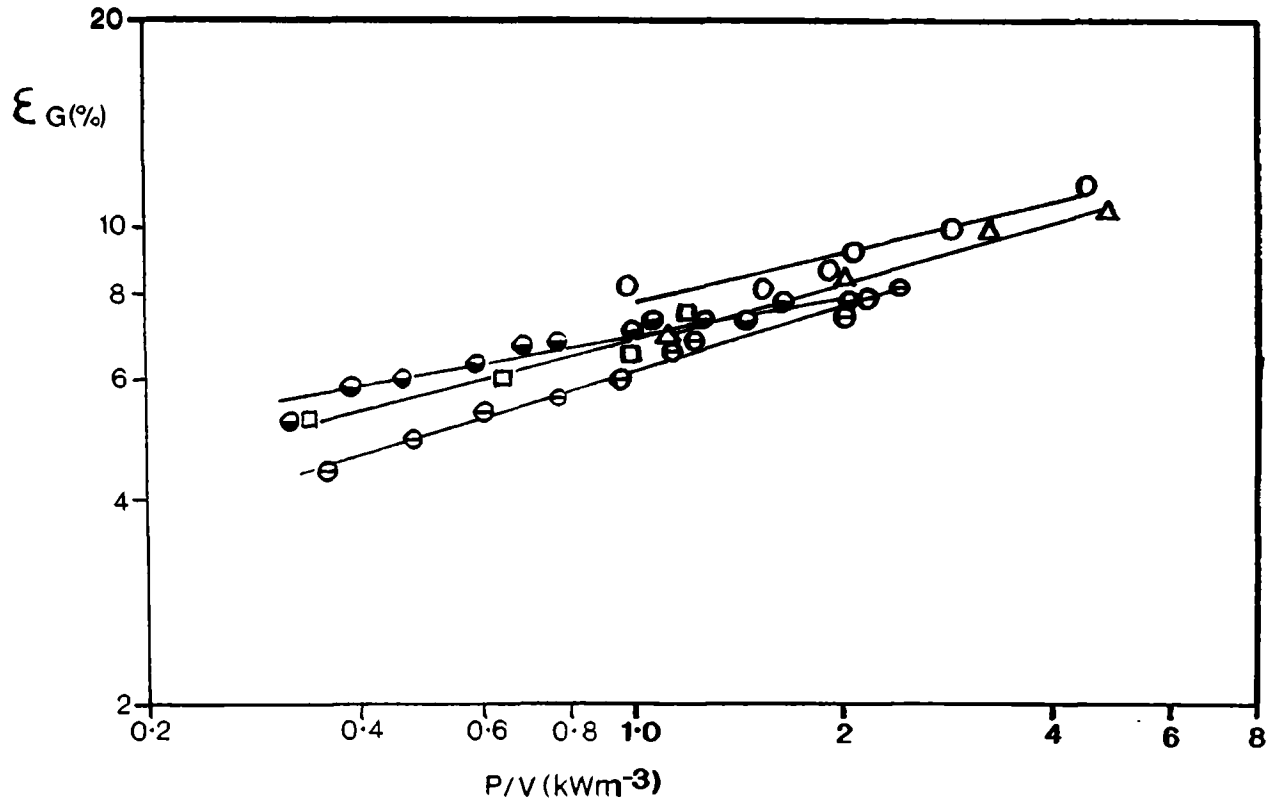

Figure 6.2 T72, ϵ_G v P/V, Water, v_s = 0.012 [m/s].

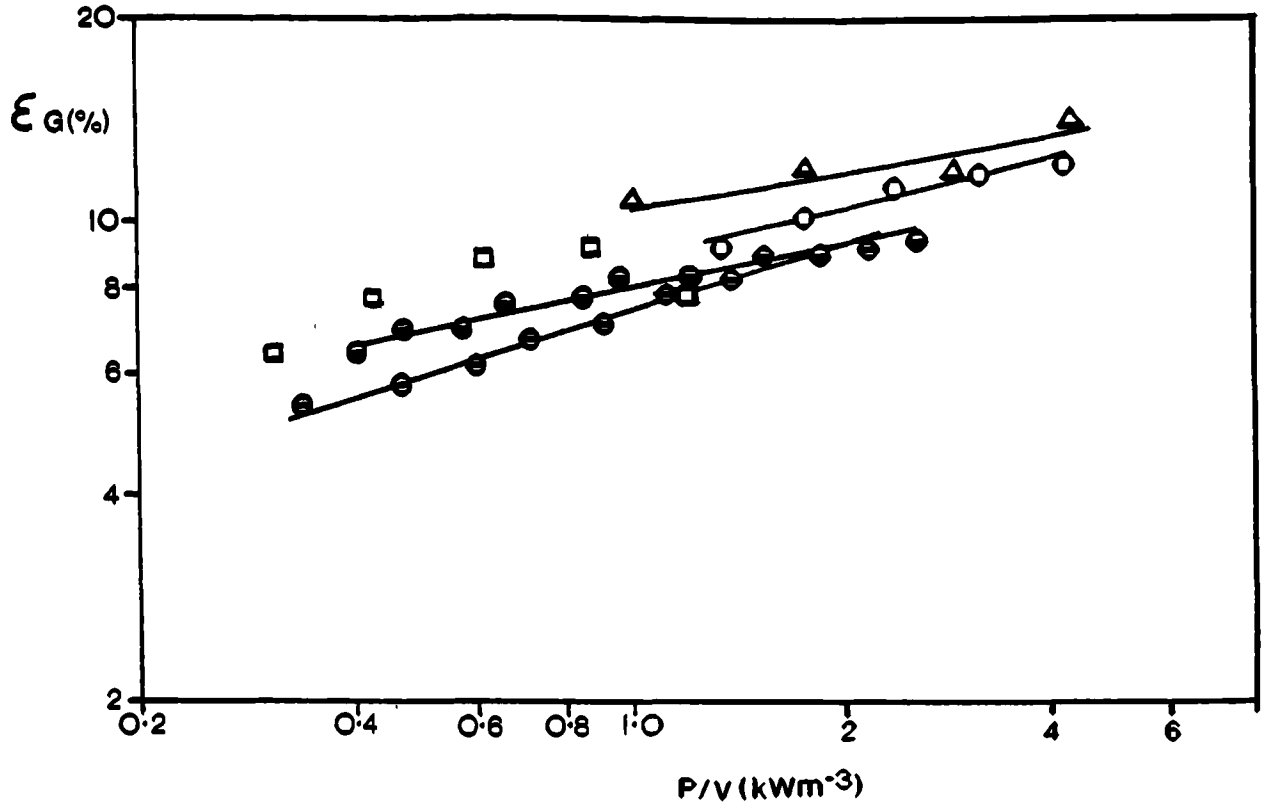

Figure 6.3 T72, ϵ_G v P/V, Water, v_s = 0.018 [m/s].

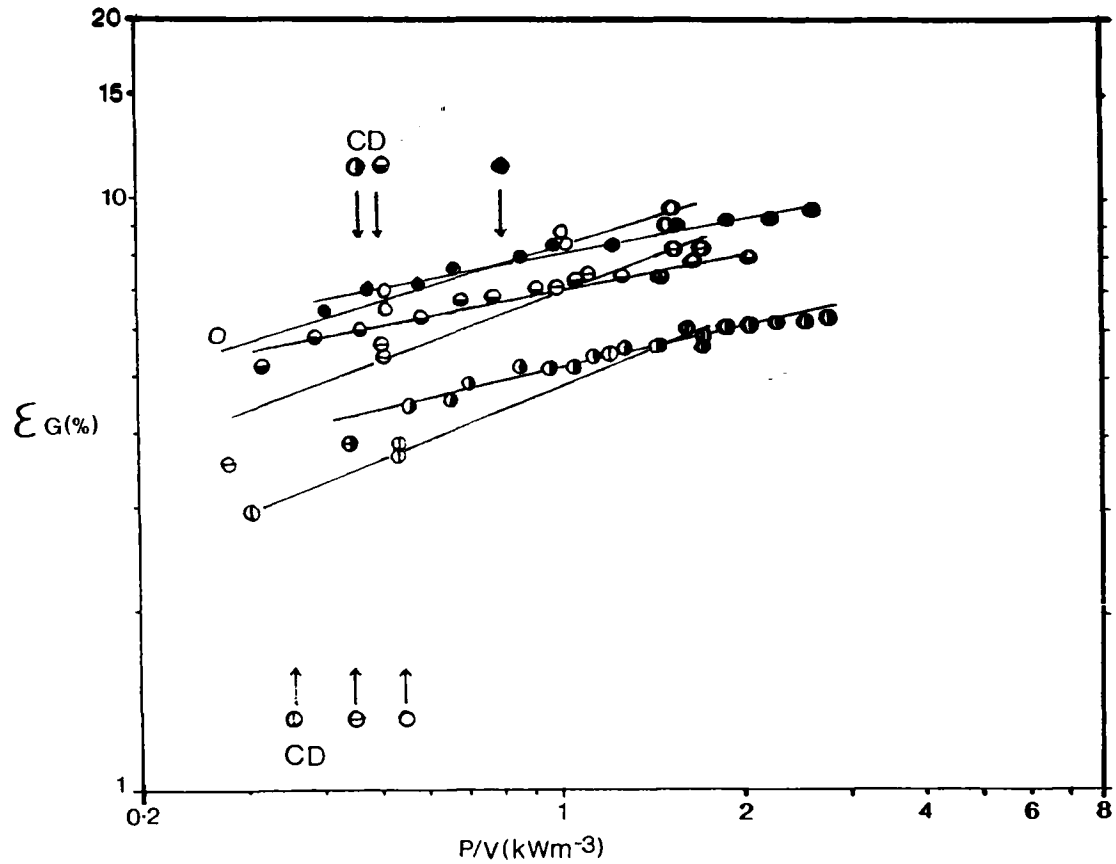

Figure 6.4 ϵ_G = P/V, Water, InterMIG (MRS), T45: o , T72: ● .

v_s = 0.006 [m/s]:⊕, 0.012 [m/s]: ⊖, 0.018 [m/s]:○.

Chapter 4. Figures 6.1 to 6.3 shows hold-up increasing with P/V at three gassing rates. Generally there was little difference between impeller types at constant P/V and v_s, although one or two exceptions were apparent. At v_s = 0.006 [ms^{-1}] the 6PSDT provided marginally higher hold-up than the 6DT over the entire power range. The A315 and IM (MRS and PS) corresponded closely at this gassing rate. When the highest gassing rate was considered the 6PSDT showed evidence of enhanced hold-up for 1 < P/V < 2 [kWm^{-3}].

Table 6.1 details the correlation coefficients obtained when hold-up was related to P/V and v_s using Eqn.2.23. Results for the 6DT show good agreement with correlations from the literature for that impeller[12,13,21,28]. The 6PSDT hold-up data shows a similar P/V dependence to that of the 6DT. However, the v_s exponent (β) was lower with the 6PSDT. The A315 exhibited a slightly lower P/V exponent and a similar v_s exponent, when compared with the 6DT. IM hold-up correlations at H/T = 1 in T72 show some variation in exponents α and β depending on the sparger used. The influence of sparger type is discussed in Section 6.2.4.

Correlation no. 11 in Table 6.1 was obtained by combining the data sets of all individual impeller correlations at H/T=1, in order to test statistically ('F' test) the 'fit' of the individual as opposed to 'overall' correlations. 'F' tests at a 5% significance level showed that the IM correlations (nos. 4 to 7) had significantly lower variance than the combined correlation no.11. Correlation no.16 combined A315, 6DT and 6PSDT data. 'F' tests showed no significant difference between the combined and individual correlations at the 5% level. The combined correlation can therefore be used to predict hold-up in water for 6DT, 6PSDT and A315, confirming their performance similarity. When using the IM impeller type the individual correlations are likely to be significantly more representative.

TABLE 6.1 GAS HOLD-UP CORRELATIONS IN WATER

$$\varepsilon_G = K\ (P/V)^{\alpha}\ (v_s)^{\beta}$$

Where ε_G [%]; P/V [$kW.m^3$]; v_s [$m.s^{-1}$].

No.	Impeller	H/T	Sparger	K	α	β	Points	R^2
1	6DT (T72)	1	PS	95.9	0.3	0.6	18	0.92
2	6PSDT (T72)	1	PS	62.4	0.28	0.47	13	0.84
3	A315 (T72)	1	RS	117.5	0.24	0.63	13	0.92
4	IM (T72)	1	PS	79.0	0.3	0.55	55	0.99
5	IM (T72)	1	SRS	78.8	0.29	0.54	48	0.98
6	IM (T72)	1	MRS	60.6	0.2	0.47	178	0.97
7	IM (T72)	1	LRS	156.1	0.25	0.69	88	0.98
8	IM (T45)	1	MRS	110.6	0.3	0.62	231	0.86
9	IM (T72)	2	PS	40.6	0.38	0.43	16	0.94
10	IM (T72)	2	MRS	77.9	0.13	0.55	136	0.91
11	Combine 1 to 7	1		77.5	0.24	0.53	413	0.94
12	Combine 6,8	1	MRS	84.9	0.28	0.56	409	0.87
13	Combine 4,9		PS	70.3	0.31	0.53	71	0.96
14	Combine 6,10		MRS	61.2	0.16	0.49	314	0.93
15	Combine 4 to 7	1		76.2	0.23	0.53	369	0.94
16	Combine 1 to 3	1		91.3	0.29	0.58	44	0.89

6.2.2 Effect of vessel scale on InterMIG hold-up

Hold-up results using 2 IM (MRS) in vessels T45 and T72 are compared in this section. Unfortunately exact geometric similarity was not maintained on scale-up, for reasons given in Section 4.1.

Fig.6.4 shows the hold-up increasing with P/V for three v_s in the two vessels. There appears to be little change in hold-up with increase in scale for $P/V > P/V_{CD}$. All data shown in these two figures is from the loading regime.

Correlations are shown in Table 6.1 for both vessels individually and combined (Nos. 6, 8 and 12). The correlations include all data obtained at the two scales for $P/V > P/V_F$. Correlations 6 and 8 show a difference in P/V and v_s exponents. This is probably caused by differences in IM D/T and sparger D_S/D at the two vessel scales (Section 4.1). Alternatively the effects of different measurement methods at the two scales may be responsible (Section 3.5). The correlation combining data for IM in the two vessels (no.12) shows a similar v_s and P/V exponent to the 6DT correlation. The variance of the combined correlation (F-test, 0.05 significance level) was significantly greater than the variance of the T72 correlation. This implies that vessel scale and/or slight geometric difference significantly effect IM hold-up performance.

6.2.3 Effect of aspect ratio on InterMIG hold-up

Hold-up results obtained at two H/T are shown in Figs. 6.5 and 6.6 for IM impellers. Under identical conditions of P/V and sparger type the hold-up remained roughly constant when doubling H/T. This implies little change in a when increasing aspect ratio using IM.

Table 6.1 gives the correlations obtained at the two aspect ratios. When using the point sparger the P/V exponent was higher at 2:1 whereas that of v_s lower. Correlation no.13 includes data for IM (PS) at both H/T = 1 and 2, an F-test at 5% significance level showed the variance of the

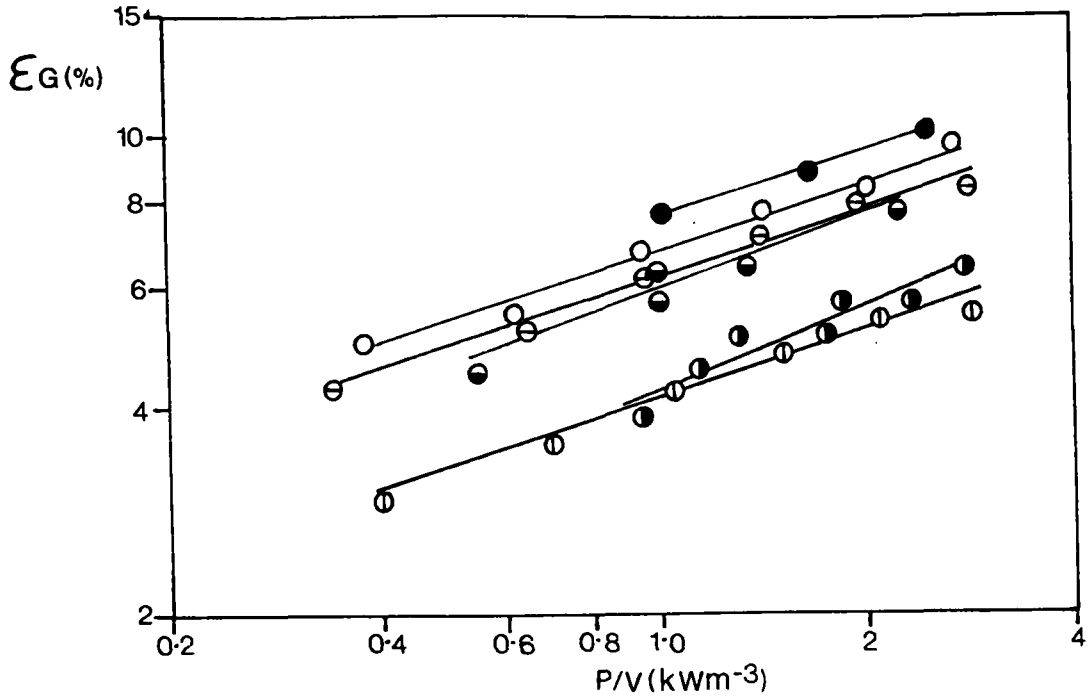

Figure 6.5 T72, ϵ_G v P/V, Water, InterMIG (PS).

H/T = 1: ● , H/T = 2: o .

v_s = 0.006 [m/s]: ◍◍ , 0.012 [m/s]: ⊖⊖ , 0.018 [m/s]: o● .

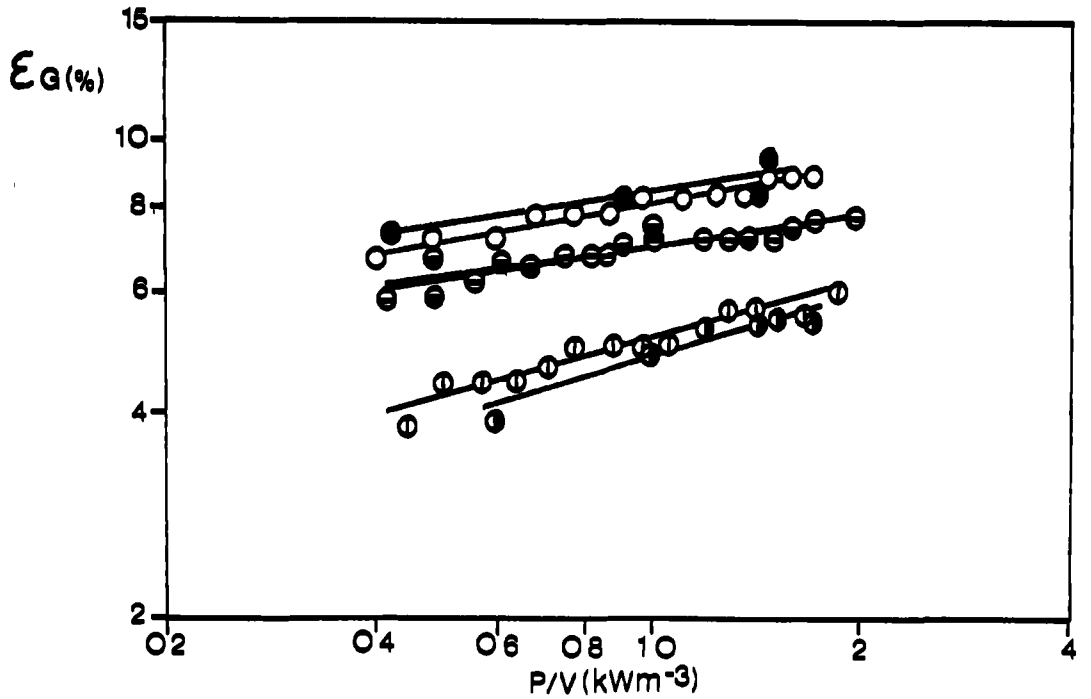

Figure 6.6 T72, ϵ_G v P/V, Water, InterMIG (MRS).

combined aspect ratio correlation was greater than that of no.4 but less than no.9. Correlation 14, combining IM (MRS) hold-up at the two aspect ratios showed the same results when tested against the individual aspect ratio correlations. These results therefore suggest little change of ε_G with H/T but are not conclusive.

6.2.4 The effect of sparger type on InterMIG hold-up.

Four sparger types were used with IM impellers in water. Gassed hold-up results are shown in Figs. 6.7 to 6.9 for three gas superficial velocities. These results are correlated with P/V and v_s in Table 6.1 both for individual sparger types and combined data.

Figure 6.7 shows a moderate influence of sparger type on hold-up. The Ds/D = 0.86 (MRS) exhibited a slightly higher hold-up at equivalent P/V than the other types. This diameter sparger ring introduces gas into the IM outer blades where the most intense turbulence and hence bubble break-up occurs.

As the aeration rate was increased to v_s = 0.012 [ms^{-1}] the various spargers began to show marked differences in hold-up at P/V < 1 [kWm^{-3}]. The PS and SRS (Ds/D = 0.43) gave the lowest hold-ups. The sparger types that introduce air into the IM inner blade region (PS, SRS) did not become loaded until P/V > 0.29 [kWm^{-3}], at this aeration rate, and therefore bubble sizes were larger and residense times lower than with the larger diameter rings. Complete gas dispersion occurred between P/V = 0.5 and 0.8 [kWm^{-3}] for all but the LRS (Ds/D = 1.22) heralding the convergence of hold-up performance.

It should be noted, (see Chapt.4), that with the centrally introducing sparger types some gas bypasses the outer vanes, rising up the shaft without dispersion. This phenomenon may explain the lower hold-up performances of the two central air introducers at power inputs slightly greater than those required for gas complete dispersion.

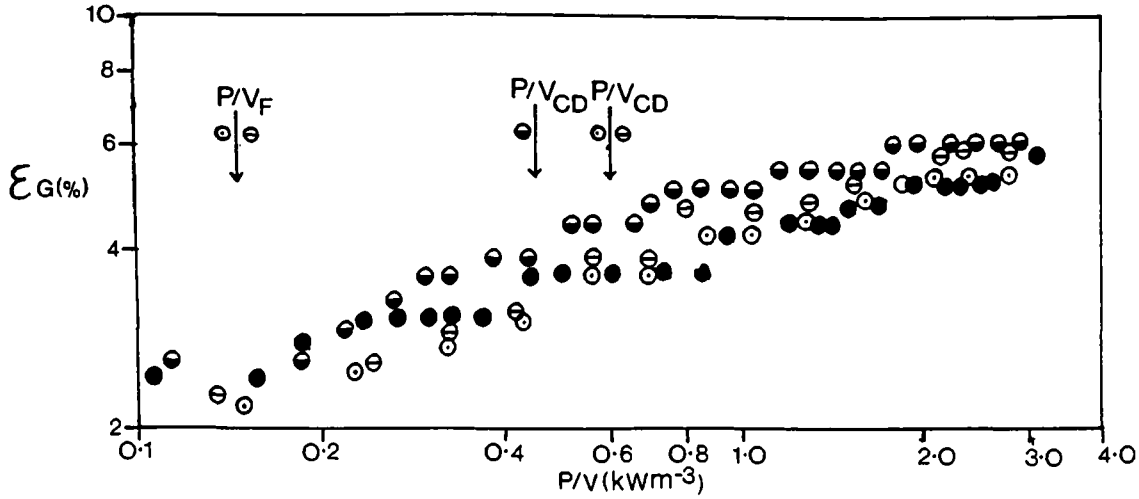

Figure 6.7 T72, ϵ_G v P/V, Water, InterMIG, v_s = 0.006 [m/s].

PS: ⊙ ,SRS: ⊖ ,MRS: ◒ ,LRS: ● .

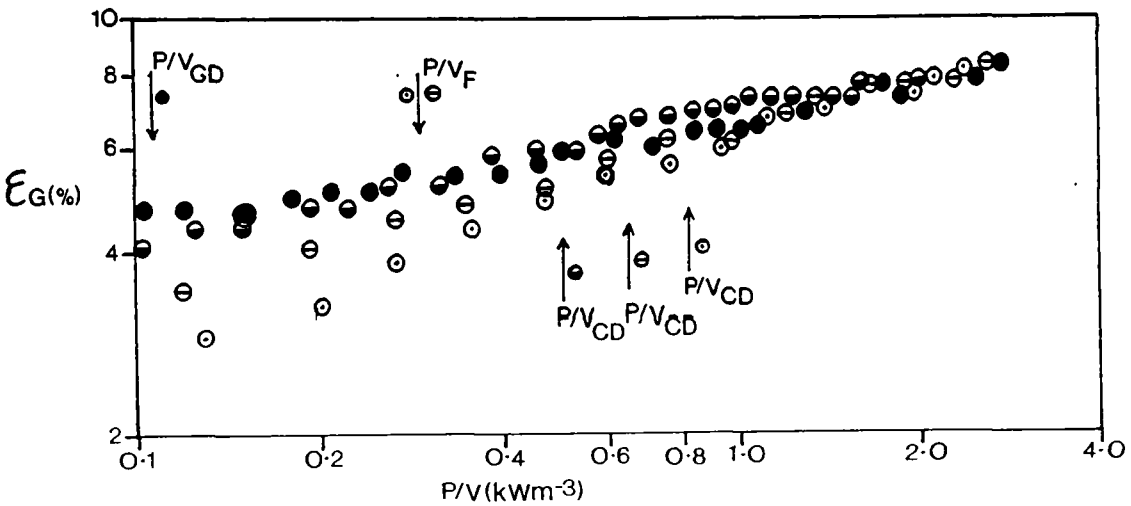

Figure 6.8 T72, ϵ_G v P/V, Water, InterMIG, v_s = 0.012 [m/s].

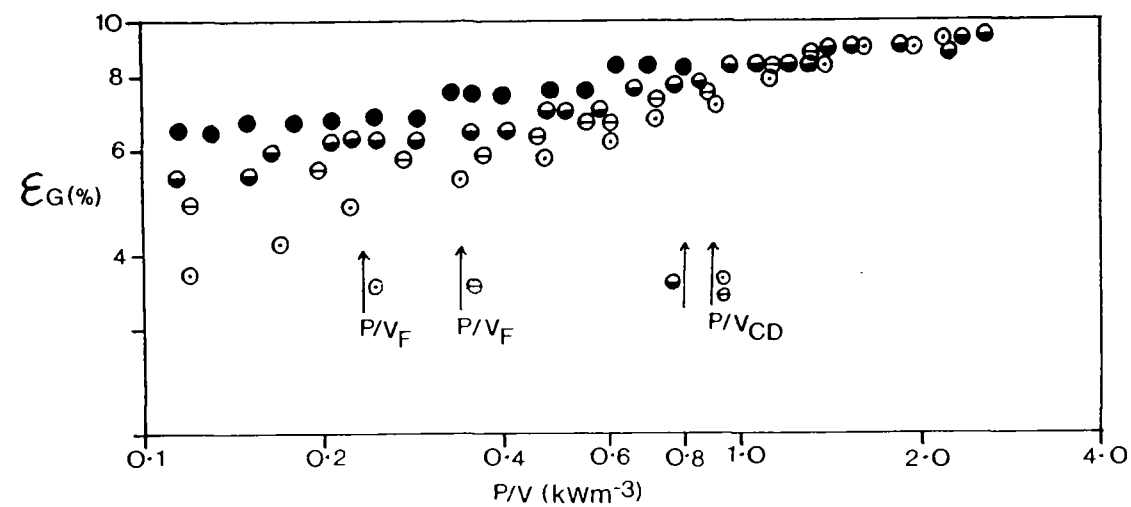

Figure 6.9 T72, ϵ_G v P/V, Water, InterMIG, v_s = 0.018 [m/s].

At the highest aeration rate used (Fig. 6.9) the hold-up results converged at P/V ≃ 0.9 [kWm^{-3}] corresponding to complete dispersion for all spargers but the LRS. Below this power input the LRS gave the highest hold-up followed by the MRS, SRS and PS.

Correlating the hold-up data for individual sparger types (Table 6.1) showed decreasing P/V and v_s exponents with increasing sparger diameter until the sparger diameter became greater than that of the impeller (Ds/D = 1.22). The individual sparger correlations (nos.4 to 7) all fit the data significantly better ('F' test, significance level 5%) than the combined data correlation (no.15). Sparger type therefore had a significant effect on IM hold-up. The correlation that combines all IM data from these experiments (no.15) reveals lower exponents for P/V and v_s than those found using the 6DT.

6.2.5 Non-coalescence and hold-up

Figure 6.10 indicates that the addition of an electrolyte to deionised water increases the hold-up at constant P/V and v_s. Observation confirmed that the average bubble size decreased on addition of ions leading to both a higher interfacial area and a higher hold-up. The increase in hold-up was caused by longer bubble residense time due to lower rise velocity for smaller bubbles. Smaller bubbles are also more easily entrained into the circulating liquid stream and so give higher recirculation of gas through the impeller than do larger bubbles. The above mentioned factors cause the area for interphase transfer to be enhanced greatly, leading to higher overall O_2 mass transfer coefficients (Section 7.2.3).

The NaCl concentration of 0.2M was chosen because a significant reduction in coalescence could be achieved (from 100% in pure water to 20% coalescence in 0.2M NaCl)[48]. Further increase in electrolyte concentration only slightly reduces coalescence (to 10% in 0.3M NaCl) but

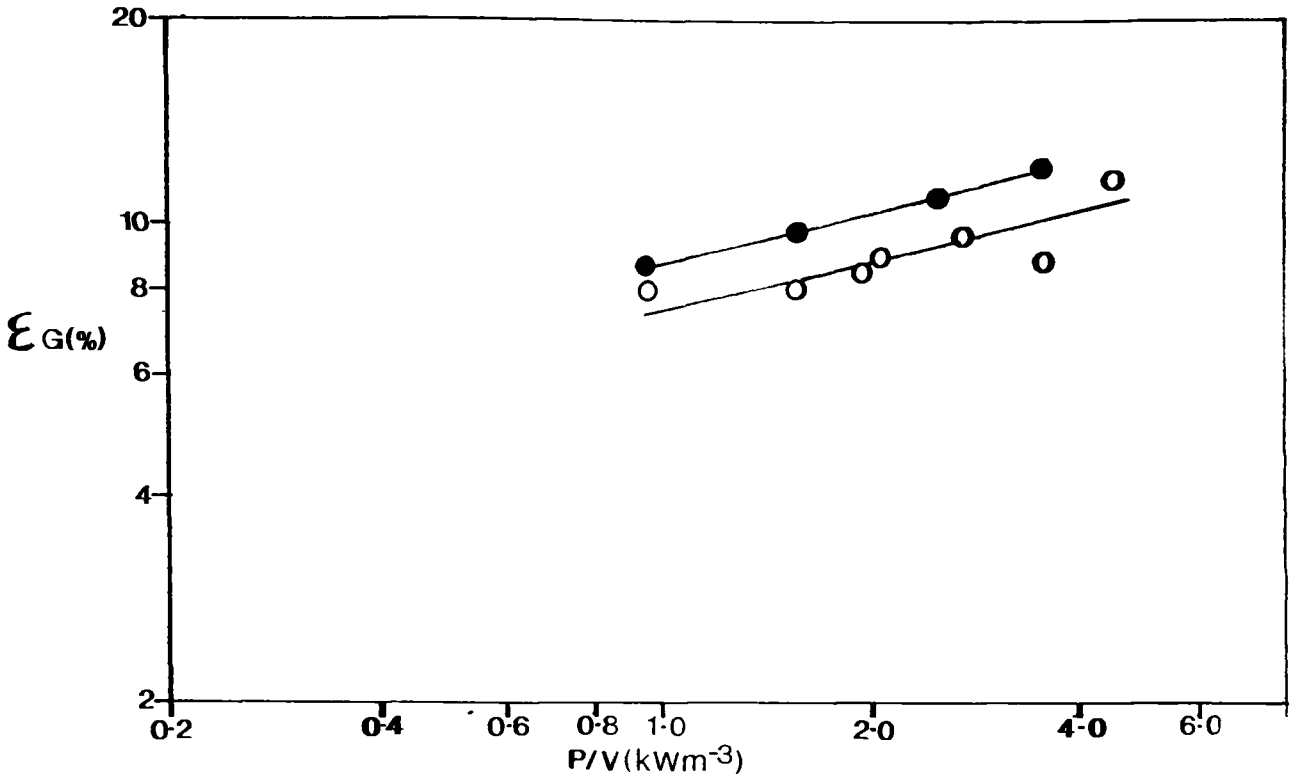

Figure 6.10 T72, ϵ_G v P/V, 6DT, Water: o , 0.2M NaCl: ● .

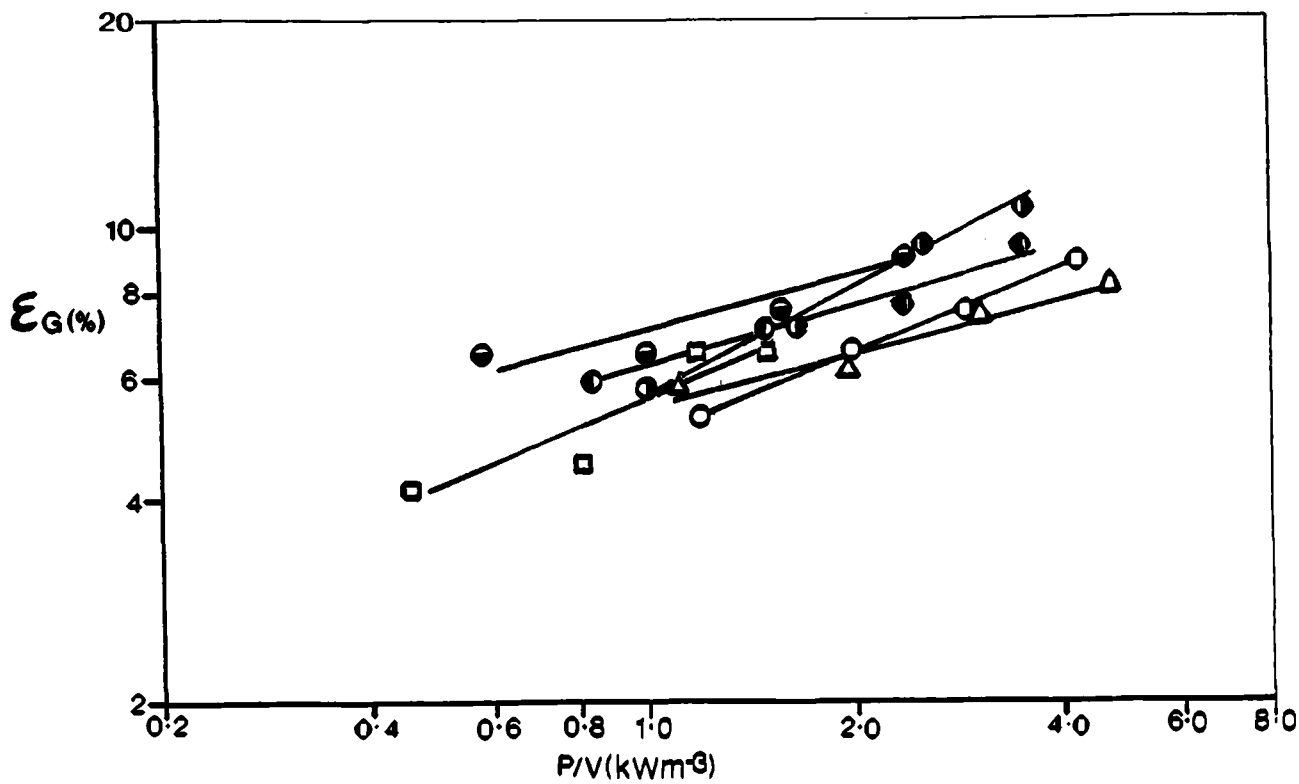

Figure 6.11 T72, ϵ_G v P/V, 0.07% CMC, v_s = 0.006 [m/s].

IM (MRS): ◆ , 6DT: o , 6PSDT: △ , A315: □ , 6MFD: ◐ , 6MFU: ◐ .

significantly reduces the activity of the enzyme catalase used during k_La measurements (Appendix II).

6.3 HOLD-UP IN NON-NEWTONIAN CMC.

The following section covers hold-up measurements made using three CMC concentrations in vessel T72 at H/T = 1 and 2. Results are compared on the basis of P/V and v_s for different agitator types graphically and in the form of tabulated correlations for each CMC concentration. Firstly low viscosity (0.07%; μa = 0.008-0.023 [Pa.s]) results are presented followed by intermediate viscosity (0.4%; μa = 0.06-0.12 [Pa.s] and 0.8%; μa = 0.17-0.4 [Pa.s]) results.

It is important, in the 0.8% and 0.4% CMC cases, to consider the effect very small bubbles have on the hold-up measurements. In these viscous solutions tiny bubbles rise very slowly, if at all, resulting in gradual hold-up decay subsequent to the cessation of aeration and agitation[89]. De-gassing the test fluid by gravity was very time consuming and therefore only partially achieved during experiments designed for k_La measurement where enzyme activity loss (Appendix III) with time was critical. However, hold-up values were recorded at peroxide induced equilibrium and were stable over this period. Even so hold-up results at higher viscosity exhibit a greater degree of scatter than those recorded in lower viscosity fluids.

In deionised water a relatively narrow size range of bubbles was observed with diameters in the order of 3-4mm. In CMC solutions a roughly bimodal bubble size distribution was seen. This comprised tiny bubbles of the order of 1mm or less and larger bubbles ranging from 3-5mm in 0.07% CMC to much larger cap shaped bubbles in 0.8% CMC. The increasing viscosity tending to promote an increase in size of these larger bubbles, a reduction in turbulence leading to poorer bubble break-up.

TABLE 6.2

GAS HOLD-UP CORRELATIONS IN 0.07% C.M.C.

$$\varepsilon_G = k\,(P/V)^{\alpha}\,(v_s)^{\beta}$$

Where ε_G [%]; P/V [kWm^{-3}]; v_s [ms^{-1}]

No.	Impeller	Sparger	k	α	β	No.Points	R^2
1	6DT	PS	66.6	0.27	0.49	15	0.93
2	6PSDT	PS	60.7	0.21	0.47	13	0.95
3	A315	Ring (Ds/D=0.6)	137.9	0.29	0.63	14	0.93
4	InterMIG 1:1	MRS (Ds/D=0.86)	53.7	0.2	0.4	15	0.9
5	InterMIG 2:1	MRS (Ds/D=0.86)	60.0	0.23	0.41	7	0.98
6	6 MFU	Ring (Ds/D=0.94)	65.0	0.43	0.47	13	0.93
7	6 MFD	Ring (Ds/D=0.94)	85.5	0.25	0.51	13	0.98
8	Combine 1,2	-	64.0	0.24	0.48	28	0.92
9	Combine 4,5	-	50.5	0.19	0.39	22	0.88
10	Combine 6,7	-	77.0	0.31	0.49	26	0.91
11	Combine 1 to 7	-	66.0	0.22	0.46	90	0.81

6.3.1 Effect of impeller type in 0.07% C.M.C.

Gassed hold-up results are presented graphically in Figures 6.11 to 6.13 and correlated in Table 6.2. Generally the hold-up was noticeably higher in this low viscosity solution than in deionised water under identical conditions, Hickman[20] and Machon et al[50] found similar effects. This can be explained by the non-coalescent behaviour of the CMC solution which leads to smaller mean bubble sizes than in water. Although CMC contains approximately 7% by weight sodium ions[20], the non-coalescent behaviour in 0.07% CMC cannot be ascribed entirely to the presence of Na^+ as their concentration is only 0.002 M which is insufficient to hinder coalescence significantly[47]. Mean bubble diameters (Sauter diameter) have been found to be lowered by a factor of two in 0.1% CMC compared with pure water[47]. The large number of bubbles generated in the impeller region rise more slowly than in water due to their smaller mean diameter and the higher liquid viscosity, the smaller bubbles are also recirculated more easily, this leads to a higher hold-up at given v_s and P/V.

Figure 6.11 shows hold-up results using six impeller types at v_s = 0.006 [ms^{-1}]. The variation in hold-up with impeller type is small and therefore similar to that in water . Figures 6.12 and 6.13 show hold-up values at v_s = 0.012 [ms^{-1}] and v_s = 0.018 [ms^{-1}] respectively, again variation due to impeller type is little changed from that found in water.

Correlating hold-up values for each impeller type resulted in a variety of exponents (α and β) and constants (K) delineated in Table 6.2. The 6DT hold-up exhibits a similar P/V dependency and a slightly reduced v_s dependence when compared with water. The 6PSDT shows a similar v_s exponent to the 6DT and to that observed in water, however, the P/V exponent was reduced. The A315 v_s exponent was greater than that of any other impeller tested. The 6MF hold-up correlation was sensitive to the pumping mode, the D.P.M hold-up being less responsive to P/V variation

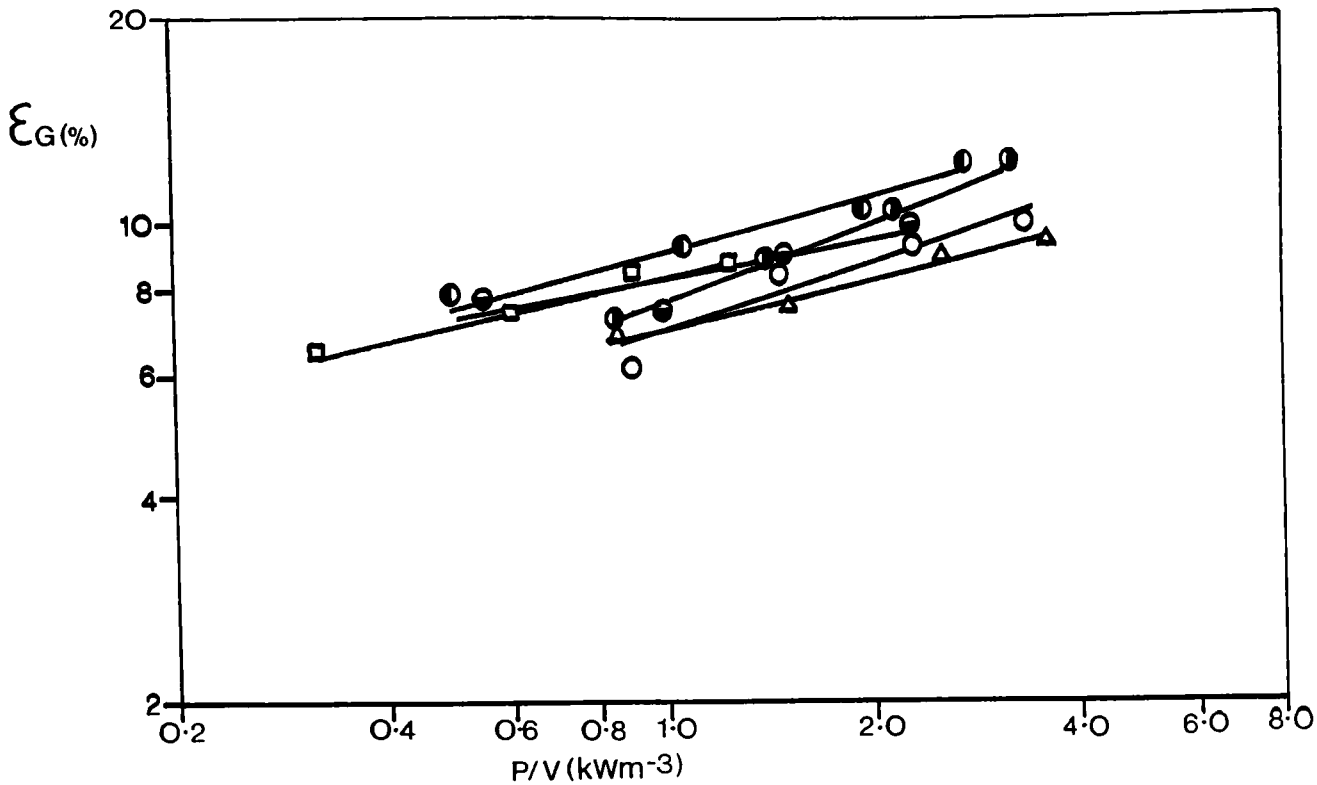

Figure 6.12 T72, ϵ_G v P/V, 0.07% CMC, v_s = 0.012 [m/s]. Key as before.

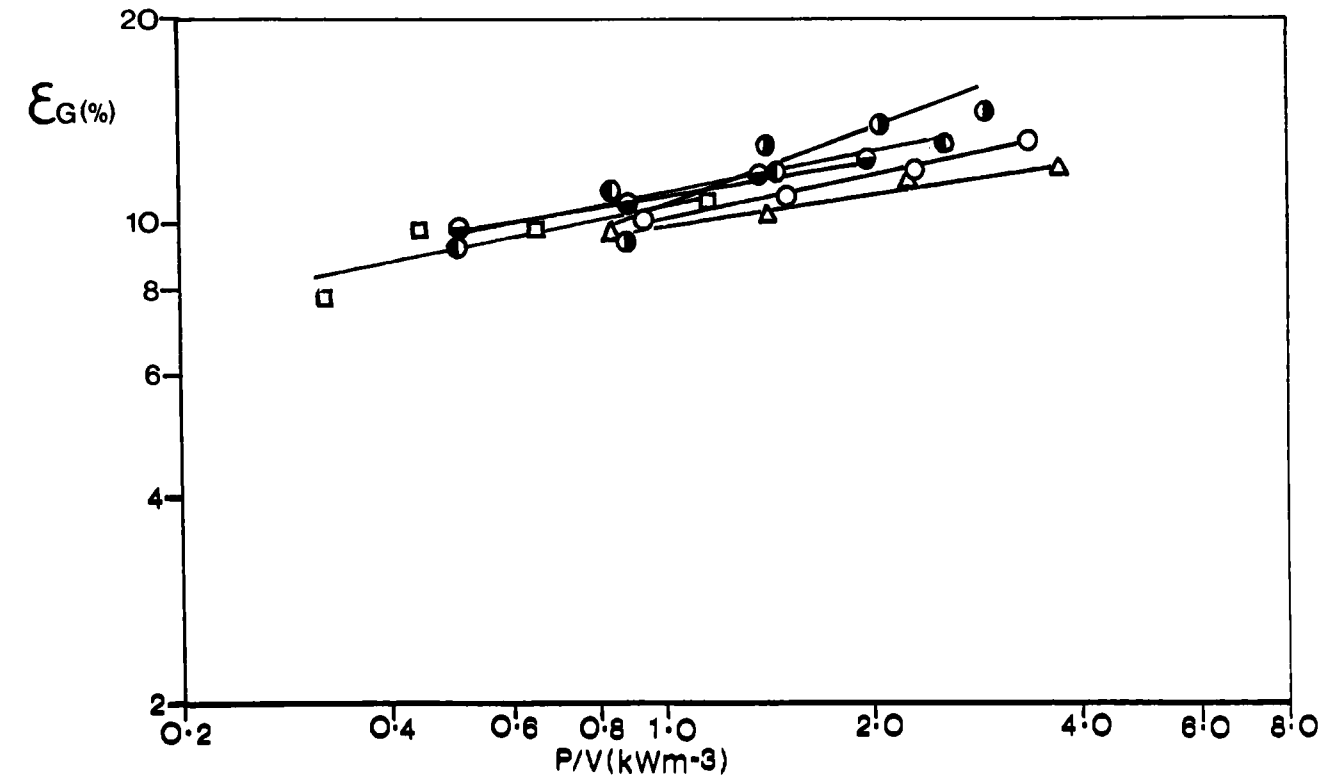

Figure 6.13 T72, ϵ_G v P/V, 0.07% CMC, v_s = 0.018 [m/s].

than the U.P.M.. The lower P/V exponent for the D.P.M. was also observed by Bujalski[12] in water, as was the higher v_s exponent for that pumping mode. Correlation no.10 was obtained by combining the 6MFU and 6MFD data, 'F' tests showed that at a 5% significance level the individual pumping mode correlations provided a better data fit than the combined one.

A combined correlation (no.8) including 6DT and 6PSDT data was found not to be significantly different from the individual ones (nos.1 and 2) at the 5% significance level, confirming their hold-up performance similarity. The IM exponent values were very similar to those found in water at H/T = 1 with the same sparger.

6.3.2 Effect of aspect ratio with InterMIG

Doubling H/T had a negligible effect on the exponents α and β when correlating ε_G [%]. Figure 6.14 indicates that the hold-up increased slightly on doubling H/T. A combined aspect ratio correlation is shown in Table 6.2 (no.9), an 'F' test showed a worse fit for the combined as opposed to individual correlations at the 5% significance level, but no difference between them at the 1% level.

6.3.3 Effect of impeller type in 0.4% and 0.8% C.M.C.

Hold-up recorded in 0.4% and 0.8% CMC solutions using six agitator types are described in this section. At both CMC concentrations the volume of entrained gas was reduced when compared with water and 0.07% CMC. The effect of impeller type on hold-up was also far greater in these more viscous fluids. The reduction in hold-up in 0.4% and 0.8% CMC can be ascribed to the formation of increasingly large slug like bubbles that are not broken up by the impeller(s). A very large number of tiny bubbles of almost zero rise velocity are also present. Results in 0.4% CMC are presented graphically in Figs. 6.15 to 6.18 and correlations listed in Table 6.3, those for 0.8% CMC in Figures 6.19 to 6.22 and Table 6.4.

TABLE 6.3

GAS HOLD-UP CORRELATIONS IN 0.4% C.M.C.

$$\varepsilon_G = K\ (P/V)^{\alpha}\ (v_s)^{\beta}$$

ε_G [%]; P/V [kWm^{-3}]; V_s [ms^{-1}]

No.	Impeller	Sparger	K	α	β	No.Points	R^2
1	6DT 1:1	PS	53.1	0.18	0.51	14	0.94
2	6DT 2:1	PS	53.1	0.22	0.56	14	0.95
3	A315	Ring (Ds/D=0.6)	142.8	0.3	0.73	13	0.93
4	InterMIG 1:1	MRS (Ds/D=0.86)	19.9	0.2	0.25	15	0.87
5	InterMIG 2:1	MRS (Ds/D=0.89)	17.5	0.19	0.22	14	0.96
6	6 MFU	Ring (Ds/D=0.94)	27.9	0.36	0.41	14	0.93
7	6 MFD	Ring (Ds/D=0.94)	34.9	0.15	0.38	13	0.9
8	6PSDT	Point	11.4	0.07	0.21	13	0.57
9	Combine 1 to 2	-	57.1	0.22	0.56	28	0.84
10	Combine 4 to 5	-	18.9	0.2	0.23	29	0.9
11	Combine 6 to 7	-	30.5	0.16	0.37	27	0.56

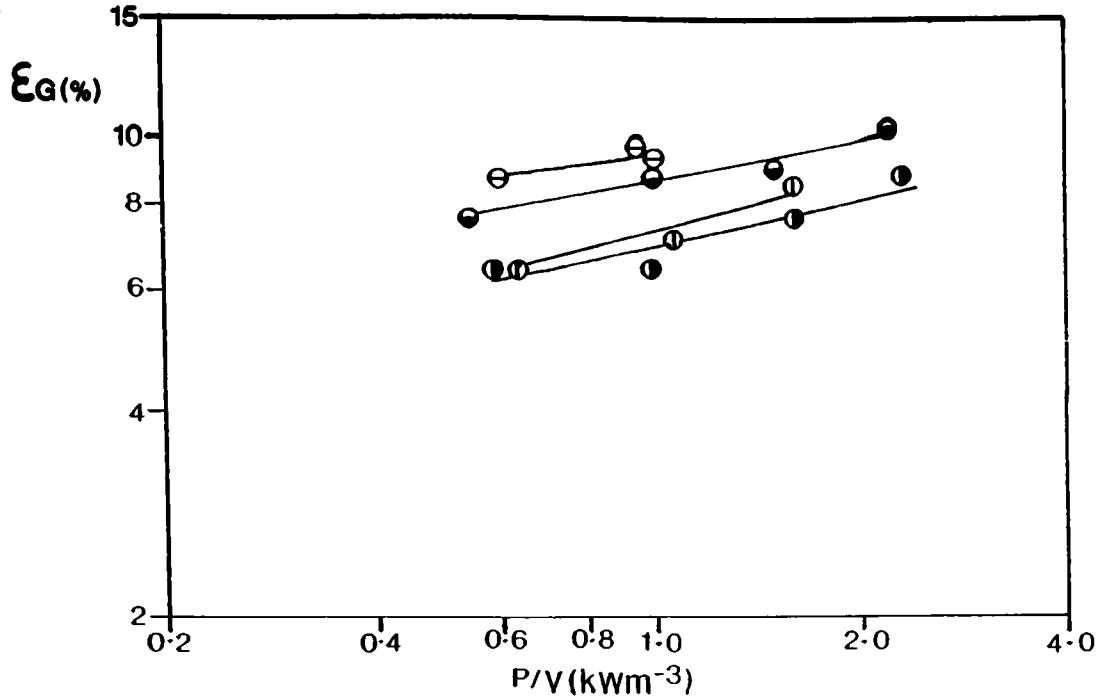

Figure 6.14 T72, ϵ_G v P/V, 0.07% CMC, InterMIG (MRS).

H/T = 1: ◒ , H/T = 2: ● .

v_s = 0.006 [m/s]:●● , 0.012 [m/s]:●●.

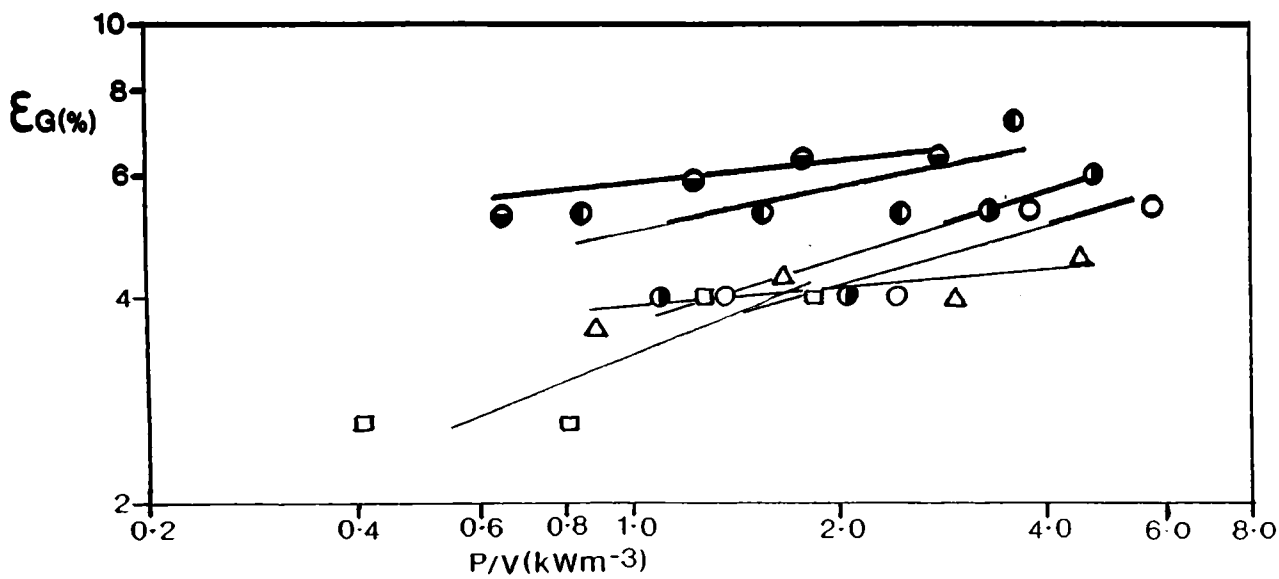

Figure 6.15 T72, ϵ_G v P/V, 0.4% CMC, v_s = 0.006 [m/s].

IM (MRS): ◒ , 6DT: ○ , 6PSDT: △ , 6MFD: ◐ , 6MFU: ◑ , A315: □ .

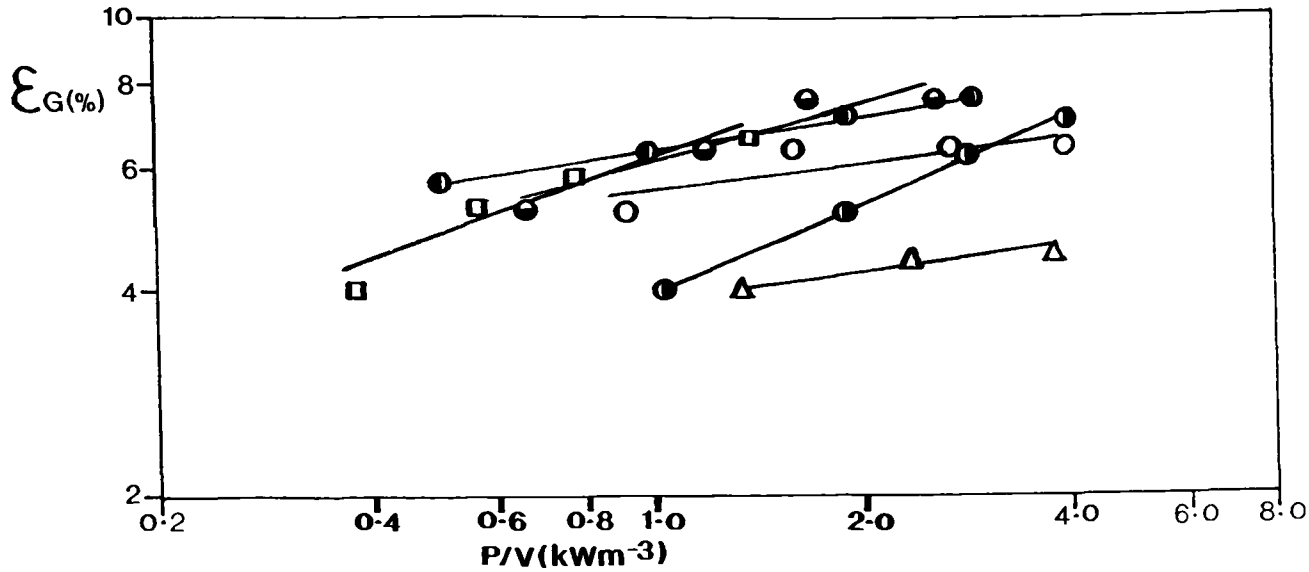

Figure 6.16 T72, e_G v P/V, 0.4% CMC, v_s = 0.012 [m/s].

Key as before.

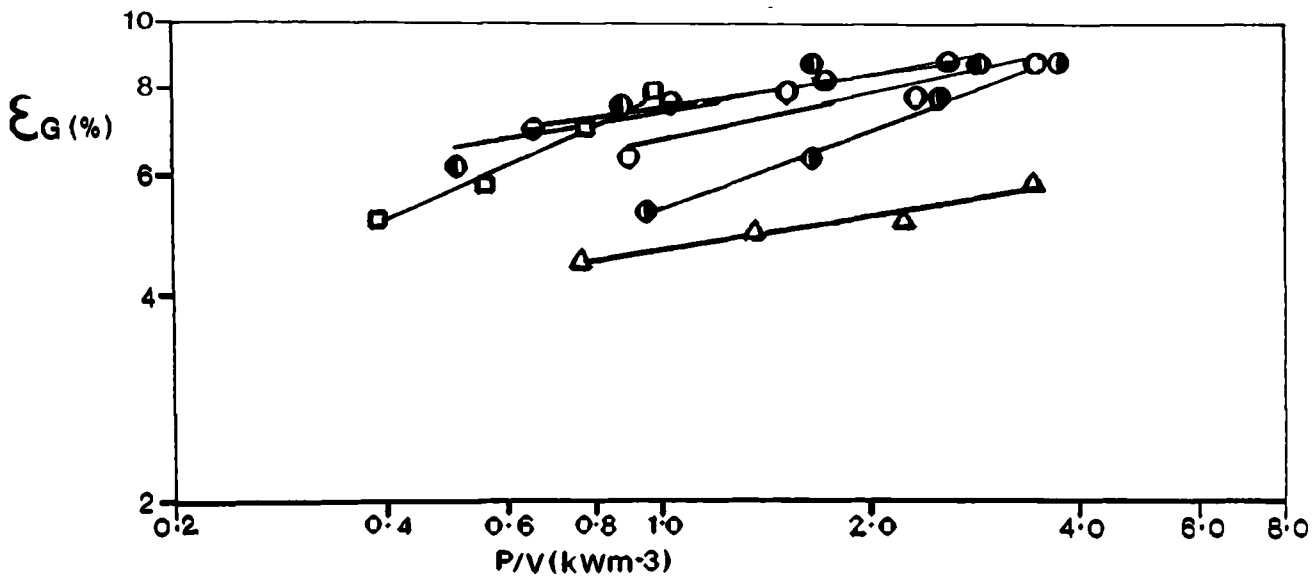

Figure 6.17 T72, e_G v P/V, 0.4% CMC, v_s = 0.018 [m/s].

Relative impeller hold-up in 0.4% CMC varied considerably. The highest hold-ups at 1:1 aspect ratio were provided by the IM and 6MFD types (lowest Pog impellers). The A315 hold-up improved relative to the other types with increasing v_s whilst the 6DT and 6MFU types provided similar hold-ups to each other at P/V > 2 kWm^{-3}. The 6PSDT hold-up performance degenerated relative to the other agitators with increasing v_s. Figure 6.18 shows IM and 6DT hold-up at H/T = 2, the IM provided higher hold-up values although it was effected less by v_s increase than the 6DT.

Correlations listed in Table 6.3 support the trends observed above. The 6DT data shows the influence of v_s was little altered from that found in water/0.07% CMC but the P/V exponent was noticeably reduced. The A315 once more exhibited the highest v_s exponent whilst the P/V exponent remained similar to that in less viscous fluids. The IM results indicated a marked reduction in the effect of v_s on hold-up at this concentration of CMC (as with Pog). The P/V exponent for IM was unchanged from the earlier cases. The 6MF hold-up exhibited a reduced dependence on both P/V and v_s when compared with 0.07% CMC. The pumping direction effected the v_s exponent to a small extent whereas the P/V exponent was much reduced for the D.P.M. (as seen in 0.07% CMC and water, both here and by Bujalski[12]).

Table 6.3 also includes a correlation combining the pumping modes of the 6MF. An 'F' test (5% significance level) showed that the combined correlation variance was significantly greater than the individuals. Therefore the individual correlations should be used to describe the different pumping modes. The 6PSDT correlation showed that variation of P/V had a negligible effect on hold-up, although the correlation coefficient (R^2) was very low (0.57), indicating a poor fit to the experimental data.

As in 0.4% CMC the various impellers tested showed considerable differences in hold-up in 0.8% CMC. The variation in impeller hold-up

TABLE 6.4

GAS HOLD-UP IN 0.8% C.M.C.

$$\varepsilon_G = K\,(P/V)^{\alpha}\,(v_s)^{\beta}$$

ε_G [%]; P/V [kWm^{-3}]; v_s [ms^{-1}]

No.	Impeller	Sparger	K	α	β	No.Points	R^2
1	6PSDT	PS	13.4	-0.06	0.22	12	0.82
2	A315	Ring (Ds/D=0.6)	42.9	0.28	0.54	13	0.75
3	6MFU	Ring (Ds/D=0.94)	17.8	0.35	0.31	12	0.87
4	6MFD	Ring (Ds/D=0.94)	15.9	0.24	0.33	12	0.88
5	InterMIG 1:1	MRS (Ds/D=0.86)	9.1	0.28	0.1	13	0.88
6	InterMIG 2:1	MRS (Ds/D=0.86)	12.9	0.31	0.18	13	0.96
7	InterMIG 1:1	PS	9.9	0.3	0.11	16	0.95
8	InterMIG 2:1	PS	16.0	0.33	0.27	17	0.95
9	6DT 1:1	PS	28.7	0.17	0.39	16	0.78
10	6DT 2:1	PS	9.514	0.45	0.26	15	0.91
11	Combine 3,4	-	16.6	0.32	0.32	24	0.71
12	Combine 5 to 8	-	13.2	0.28	0.19	59	0.67
13	Combine 7,8	-	15.0	0.29	0.22	33	0.59
14	Combine 5,6	-	10.8	0.3	0.14	26	0.91

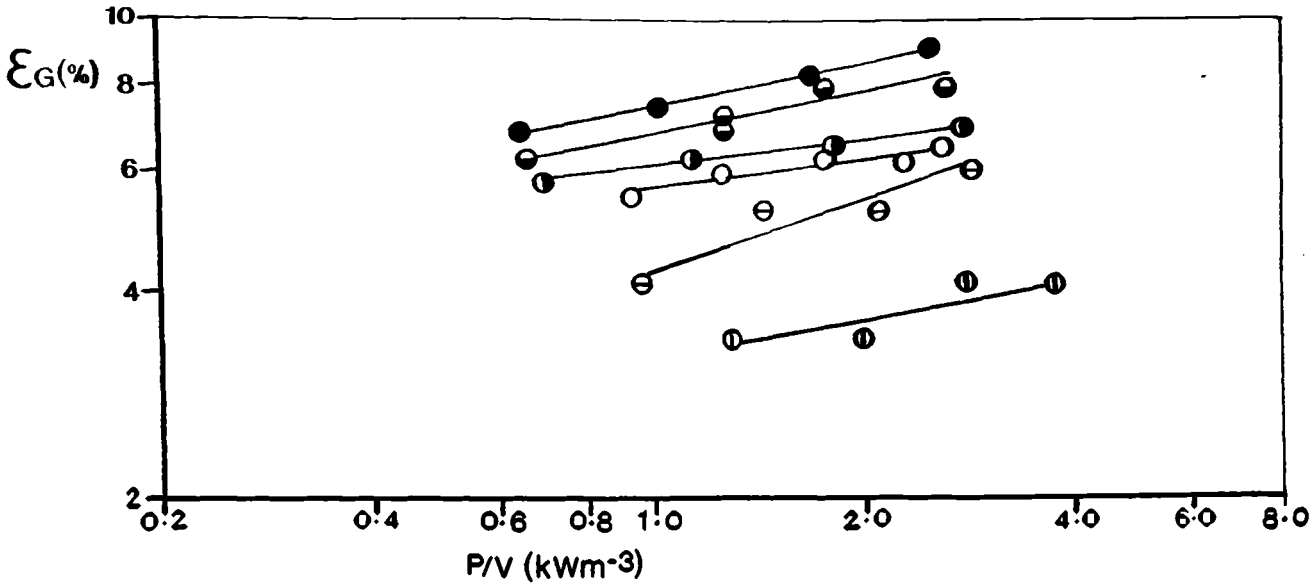

Figure 6.18 T72, e_G v P/V, 0.4% CMC, H/T = 2.

IM (MRS): ● , 6DT: ○ .

v_s = 0.006 [m/s]: ●◐ , 0.012 [m/s]: ●● , 0.018 [m/s]: ○● .

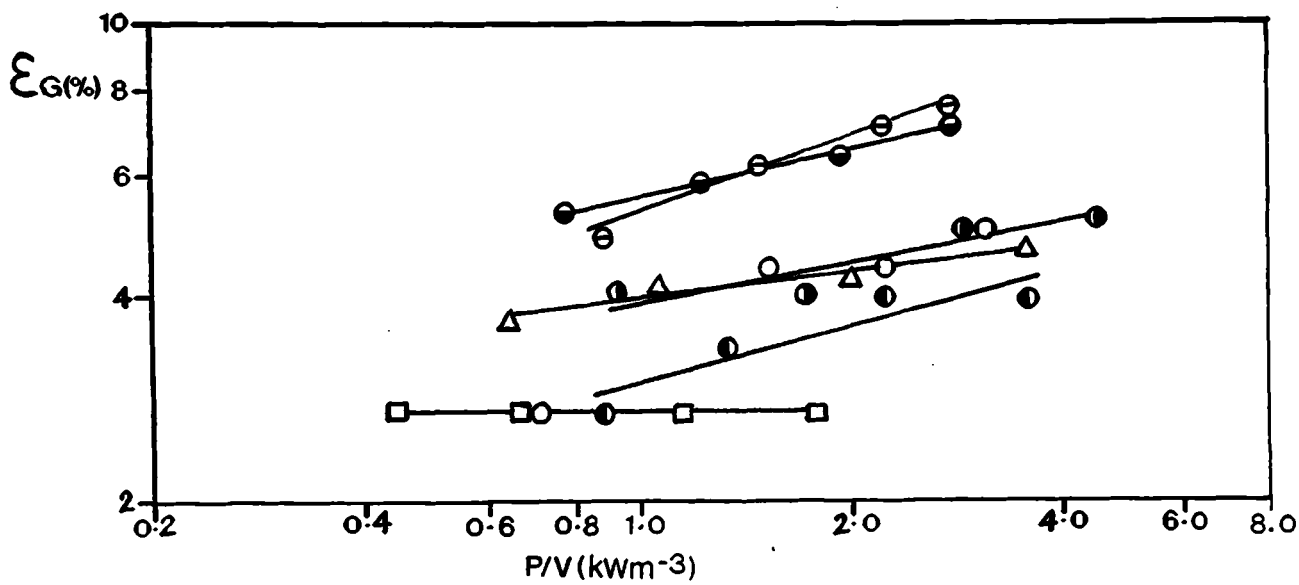

Figure 6.19 T72, e_G v P/V, 0.8% CMC, v_s = 0.006 [m/s].

Key as before.

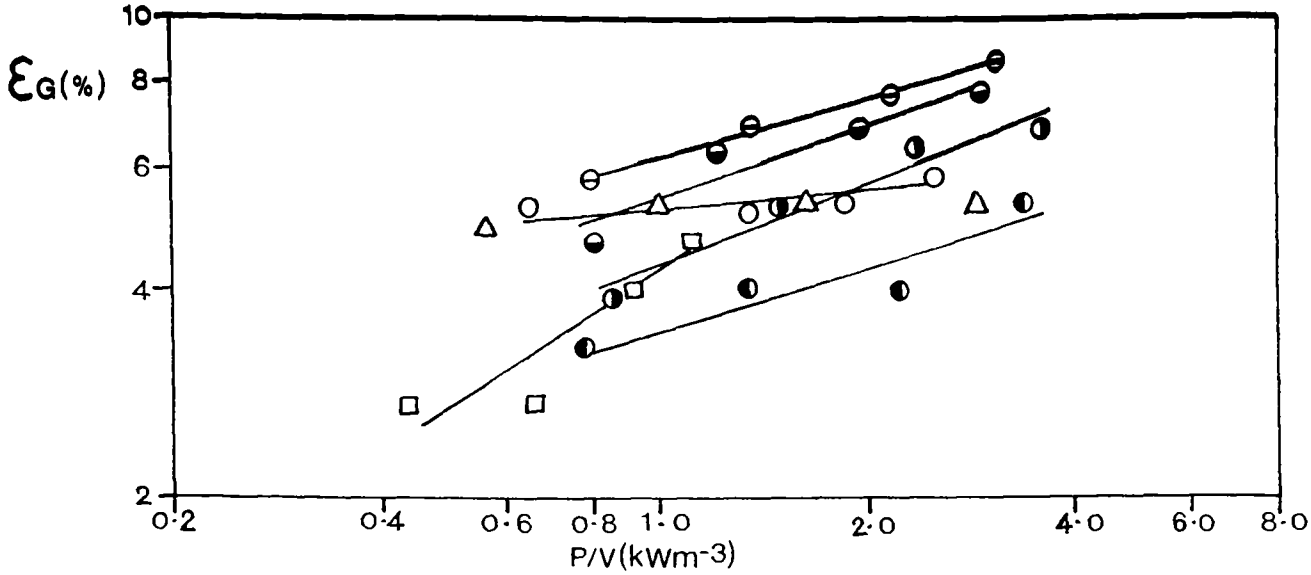

Figure 6.20 T72, ϵ_G v P/V, 0.8% CMC, v_s = 0.012 [m/s].

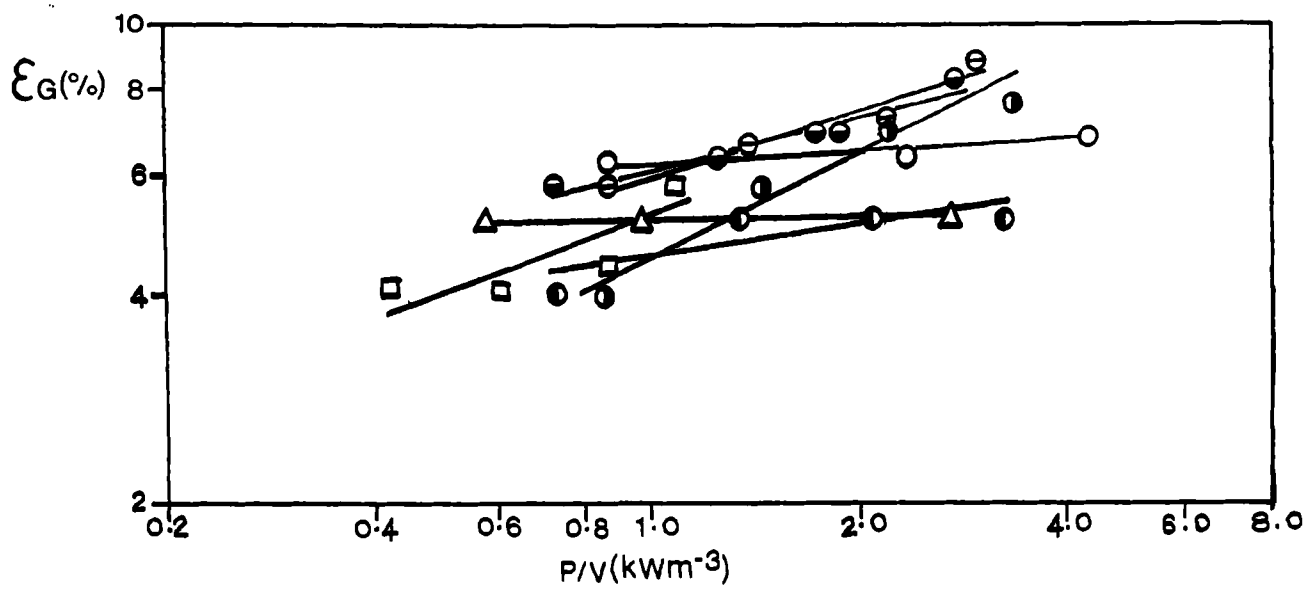

Figure 6.21 T72, ϵ_G v P/V, 0.8% CMC, v_s = 0.018 [m/s].

performance decreased with increasing v_s (Figs. 6.19 to 6.21). Overall, in 0.8% CMC, the IM provided the highest hold-up irrespective of sparger choice (again the lowest Pog impeller). The enhanced hold-up observed with IM was most evident at low v_s. Correlations shown in Table 6.4 for IM at 1:1 aspect ratio indicated a lower dependency of ε_G on v_s than for any other impeller tested (IM Pog was unaffected by v_s aswell).

The 6MFD and 6MFU configurations showed a reversal of relative performances at this the highest viscosity when compared with 0.4% CMC. The U.P.M. gave higher hold-up than the D.P.M., the latter exhibiting a far worse relative hold-up performance than in 0.4% CMC. This may be explained by the convergence of 6MF Pog values in 0.8% CMC. The 6PSDT and 6DT provided moderate hold-ups in 0.8% CMC although again the former exhibited a marked lack of P/V effect (see Table 6.4). Finally the A315 impeller which, as with all other concentrations, was characterized by poor hold-up at low v_s but rapidly improving relative hold-up with increasing v_s.

Figure 6.22 shows the H/T = 2 hold-up performance of IM and 6DT impellers. As was seen in 0.4% CMC the IM provided a considerably enhanced (100%) hold-up at this aspect ratio (as was the case at H/T = 1) when compared with the 6DT.

Table 6.4 gives hold-up correlations in 0.8% CMC. Generally the v_s exponents were reduced when compared with 0.4% CMC. The 6DT showed reduced dependence on v_s but similar dependence on P/V at H/T=1. The 6PSDT showed an almost identical performance to that in 0.4% CMC. The A315 impeller hold-up was the most dependent on v_s, although both v_s and P/V exponents were slightly reduced from 0.4%. The 6MF configuration hold-up was again more influenced by P/V in the U.P.M. although v_s exponents were similar irrespective of pumping mode. As was found in 0.4% CMC, the individual pumping mode correlations were a significantly better 'fit' than the combined correlation in 0.8% CMC.

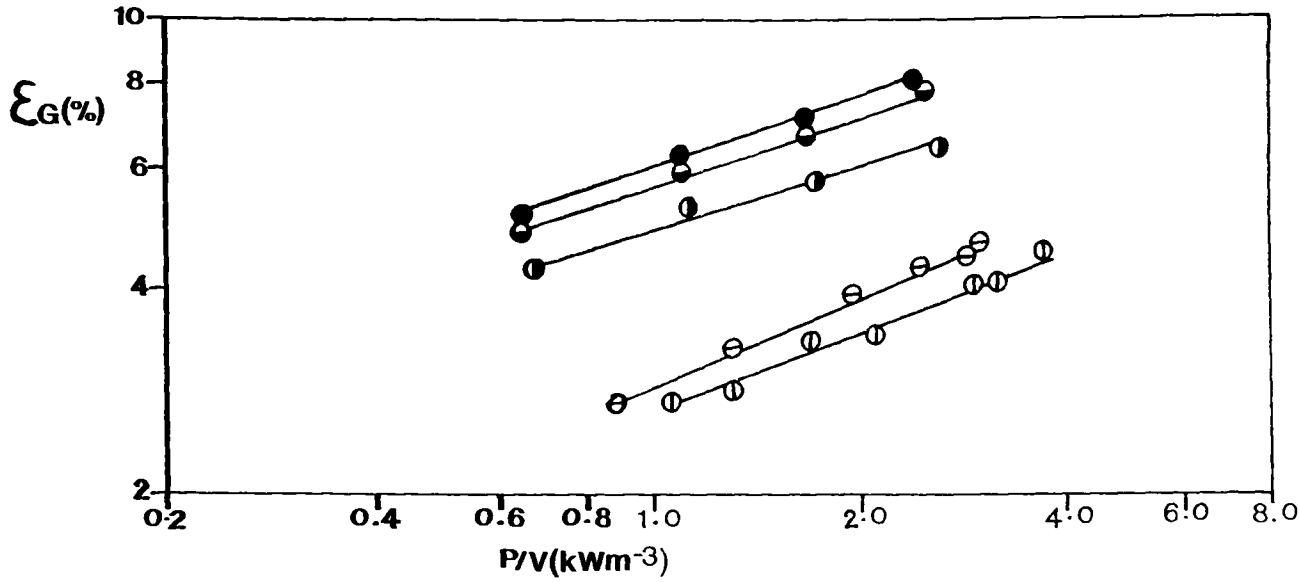

Figure 6.22 T72, e_G v P/V, 0.8% CMC, H/T = 2.

IM (MRS): ● , 6DT: ⊖ .

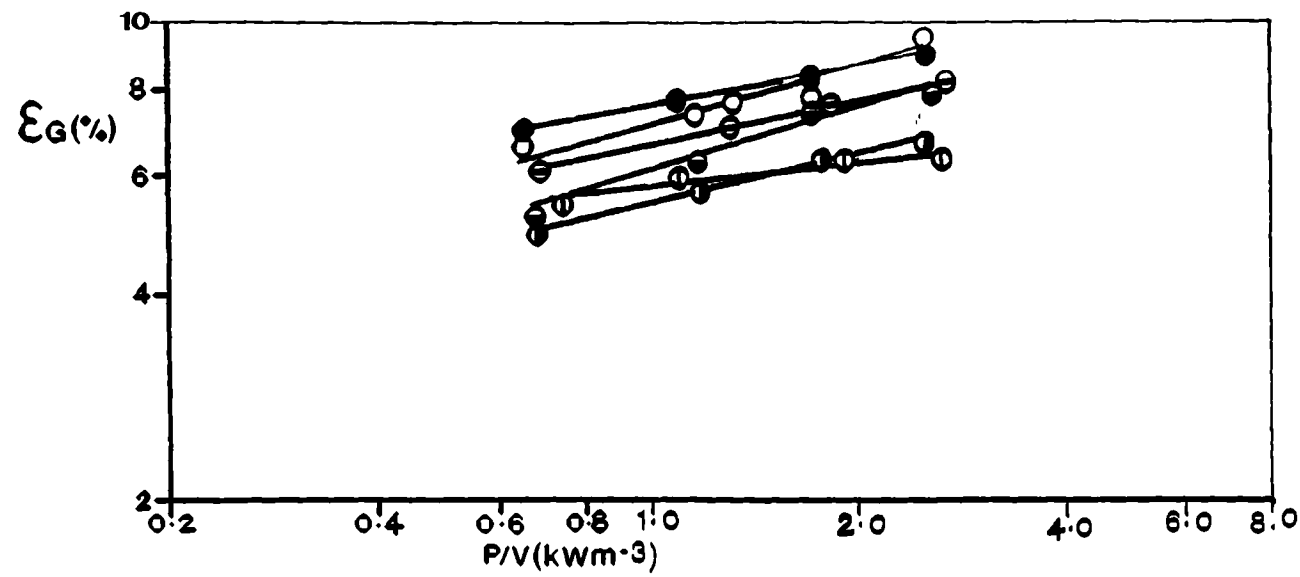

Figure 6.23 T72, e_G v P/V, 0.4% CMC, InterMIG (MRS).

H/T = 1: ◆ , H/T = 2: ○ . Key as before.

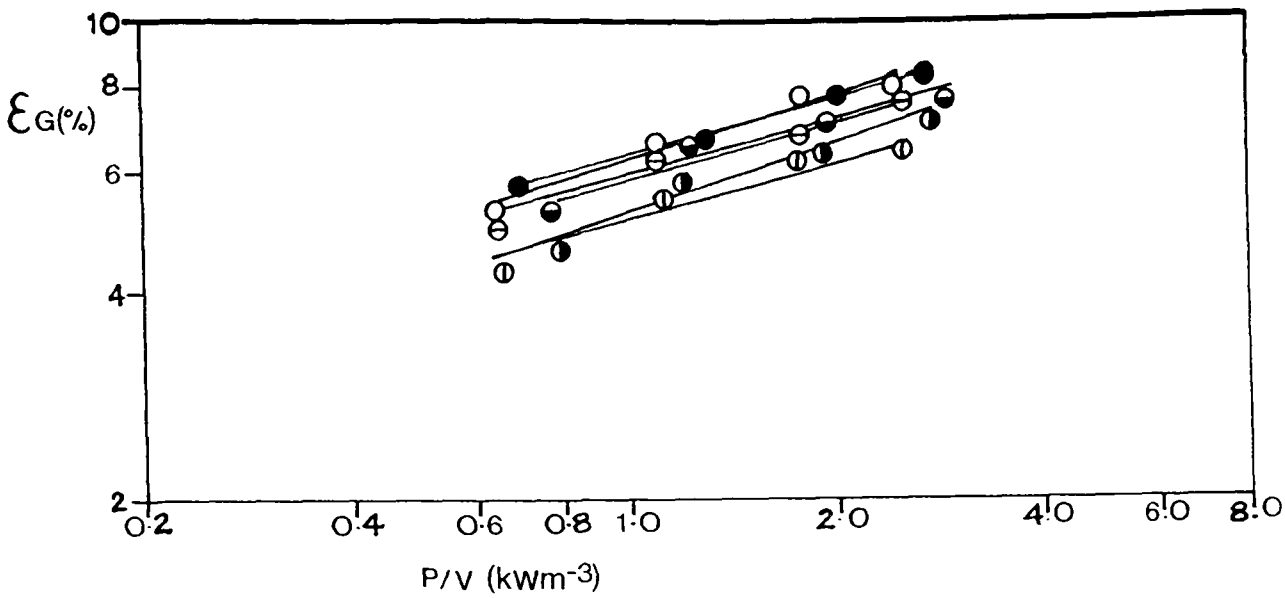

Figure 6.24 T72, ϵ_G v P/V, 0.8% CMC, InterMIG (MRS).

Key as before.

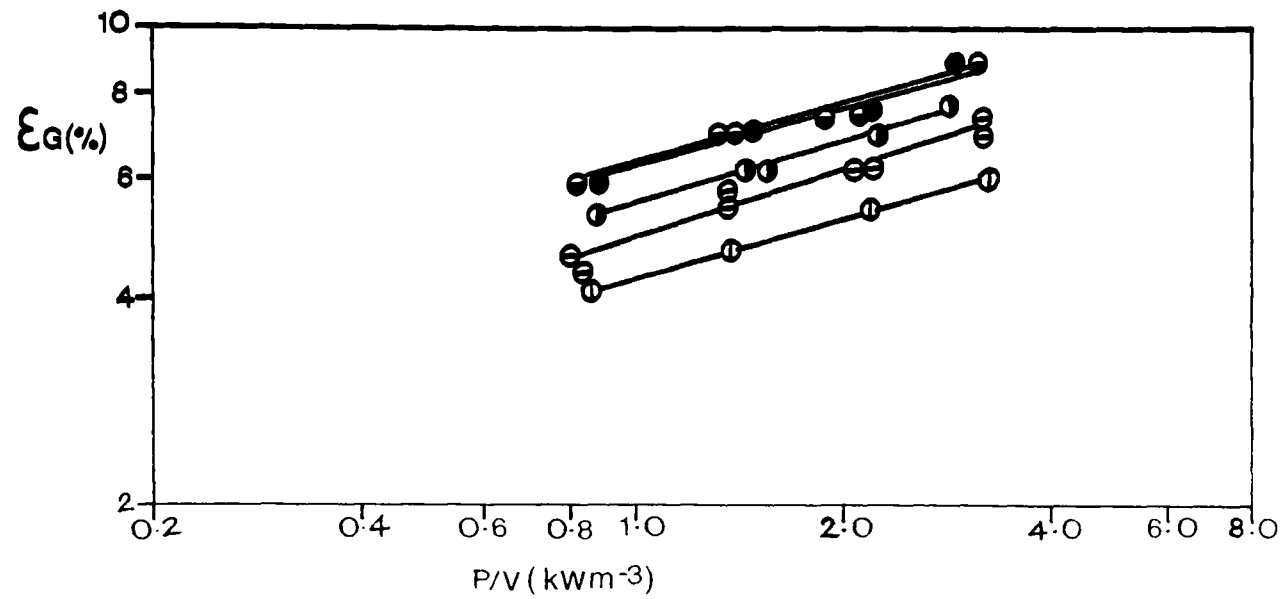

Figure 6.25 T72, ϵ_G v P/V, 0.8% CMC, InterMIG (PS).

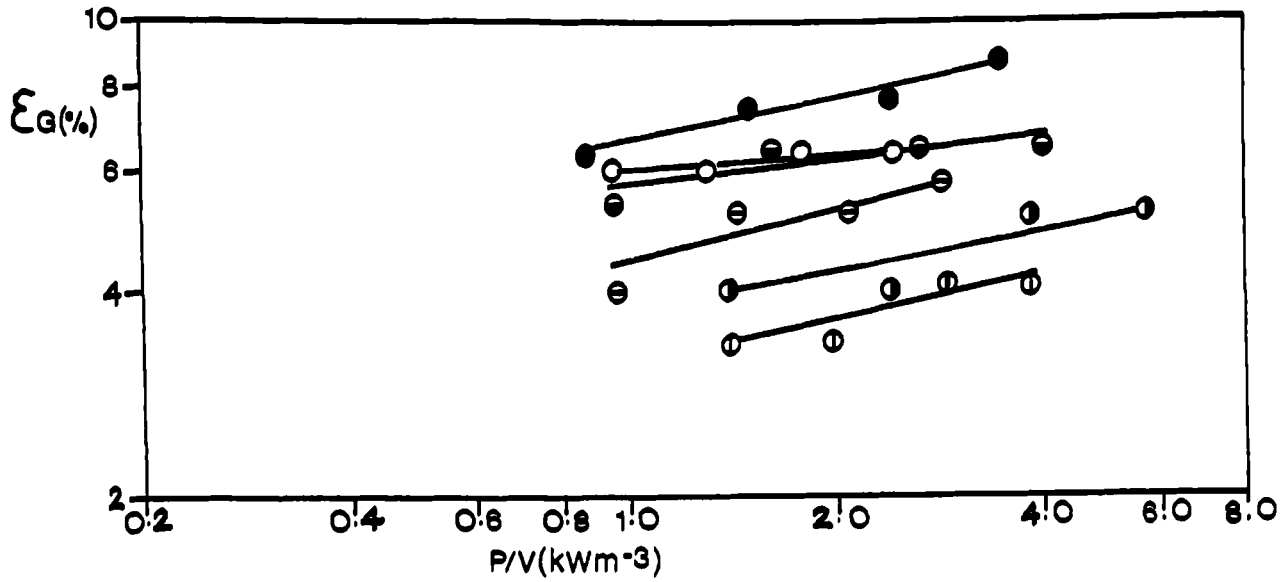

Figure 6.26 T72, ϵ_G v P/V, 0.4% CMC, 6DT.

Key as before.

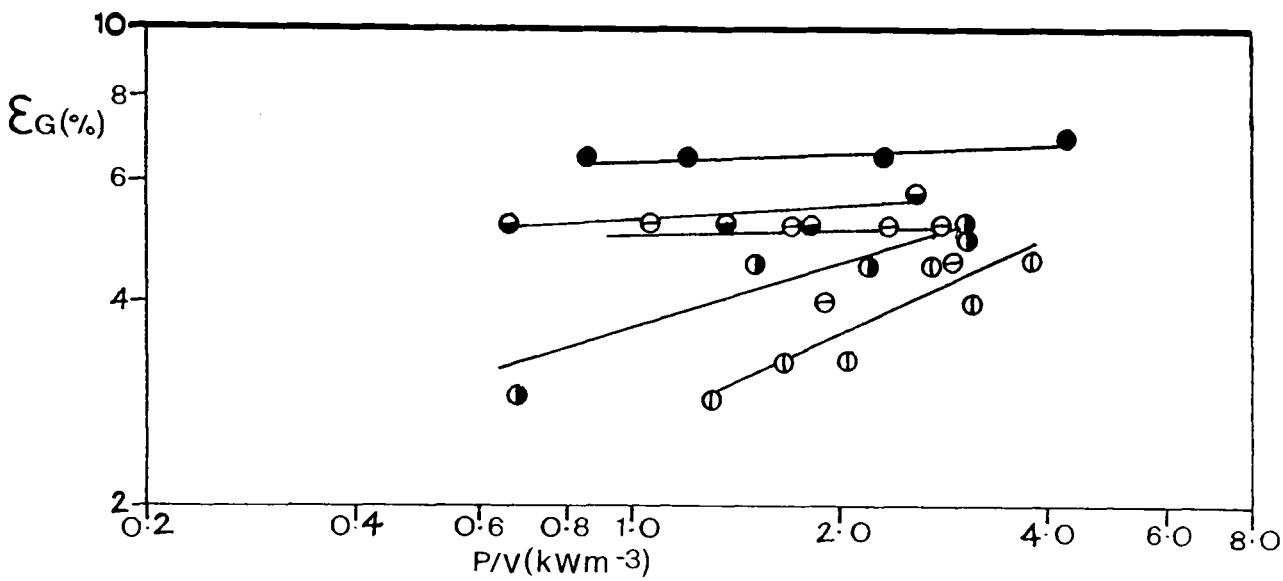

Figure 6.27 T72, ϵ_G v P/V, 0.8% CMC, 6DT.

6.3.4 Effect of aspect ratio in 0.4% and 0.8% C.M.C.

In this section hold-up results from experiments at H/T = 1 and H/T = 2 are compared for IM and 6DT agitators in the two concentrations of C.M.C. Results are shown in Figures 6.23 to 6.27 and correlations in Tables 6.3 and 6.4.

Firstly Figures 6.23 and 6.24 show hold-up increasing with P/V for IM (MRS) at H/T = 1 and 2 in 0.4% and 0.8% CMC respectively. In both CMC concentrations hold-up was unaffected by doubling H/T at equivalent power input. In 0.4% CMC (Table 6.3) the values of K, α and β are very similar for the two aspect ratios and a combined correlation showed no significant difference in variance at the 5% level from the individual ones. Similarly in 0.8% CMC the correlations for the two aspect ratios exhibit good agreement in terms of P/V and v_s exponents and at a 5% significance level a combined correlation (no.15 Table 6.4) gave as good a data fit as the individual correlations. The equivalent hold-ups at the two aspect ratios were obtained at equal v_s which implies increased hold-up if scale-up is attempted using constant vvm. IM hold-up at the two aspect ratios in 0.8% CMC when using a point sparger is shown in Figure 8.26. The hold-up was higher at H/T = 1 than at H/T = 2. No physical explanation for this can be put forward at the present time.

6DT hold-up results at H/T = 1 and 2 in 0.4% and 0.8% CMC are shown in figures 6.26 and 6.27. There is a high degree of scatter in the 0.8% data. In both 0.4% and 0.8% CMC the 2:1 aspect ratio hold-up is reduced when compared to the 1:1. From Tables 6.3 and 6.4 it is apparent that at H/T = 2 the 6DT hold-up is more dependent upon P/V. The individual aspect ratio correlation provide a better data fit than the combined correlations in both CMC solutions.

6.4 THE EFFECT OF VISCOSITY ON HOLD-UP IN CMC

When hold-up results from the preceding sections are combined the

TABLE 6.5

OVERALL GAS HOLD-UP CORRELATIONS

$$\varepsilon_G = k\,(P/V)^{\alpha}\,(v_s)^{\beta}\,(\mu a)^{\gamma}$$

No.	Fluid	Impeller (Aspect Ratio)	Sparger	K	α	β	γ	Pts.	R^2
1	CMC	6PSDT	PS	12.98	0.02	0.29	-0.19	38	0.83
2	CMC	6DT 1:1	PS	28.3	0.15	0.43	-0.17	45	0.88
3	CMC	6DT 2:1	PS	20.55	0.31	0.44	-0.18	30	0.76
4	CMC	A315	Ring Ds/D=0.6	38.1	0.25	0.58	-0.25	40	0.93
5	CMC	6MF(U)	Ring Ds/D=0.94	15.1	0.29	0.35	-0.22	39	0.82
6	CMC	6MF(D)	Ring Ds/D=0.94	15.7	0.16	0.36	-0.25	38	0.91
7	CMC	InterMIG 1:1	MRS Ds/D=0.86	15.4	0.21	0.25	-0.13	43	0.86
8	CMC	InterMIG 2:1	MRS Ds/D=0.86	12.6	0.22	0.22	-0.14	34	0.92
9	CMC	Combined 7 & 8	-	14.13	0.21	0.24	-0.13	77	0.88
10	CMC	Combined 2 & 3	-	26.4	0.18	0.46	-0.2	74	0.82
11	CMC	Combined 1 to 8	-	18.7	0.19	0.36	-0.19	339	0.71
12	Water	Combined From 6.1	-	77.5	0.24	0.53	-	413	0.94

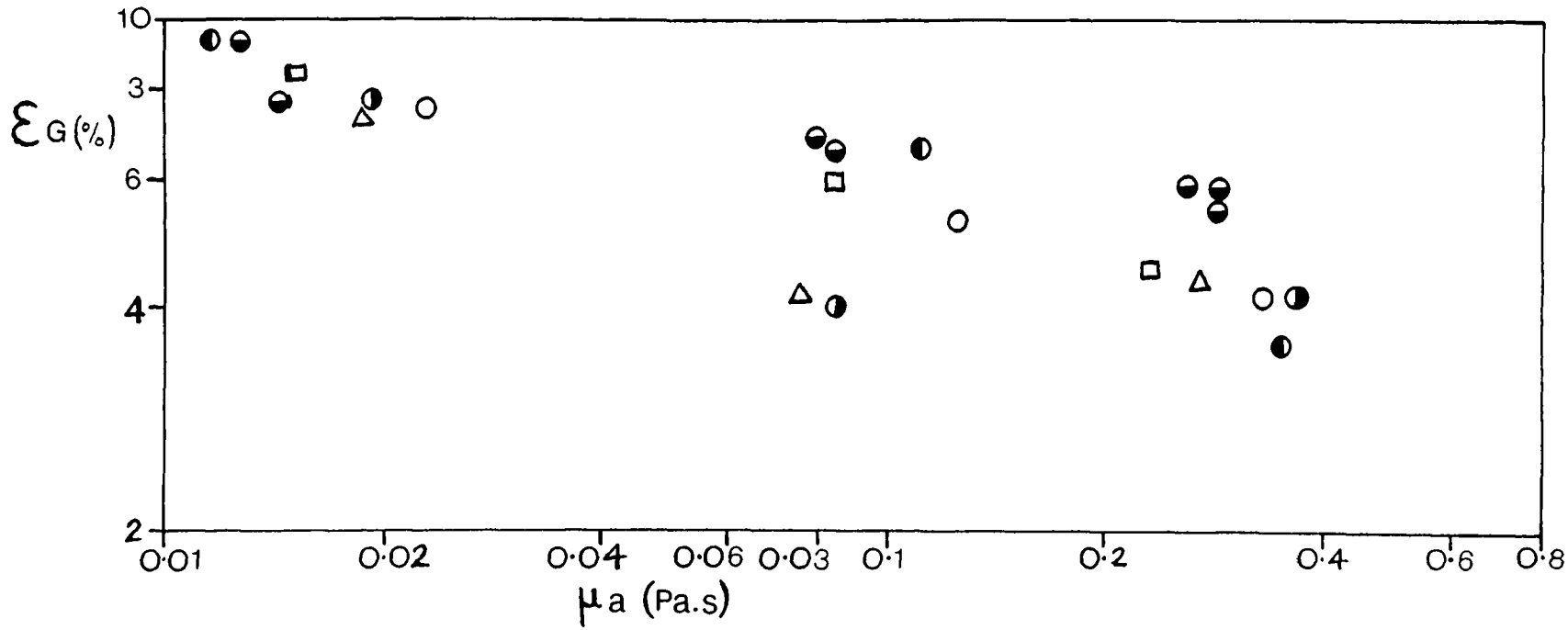

Figure 6.28 T72, ϵ_G v μ_a, v_s = 0.012 [m/s], P/V = 1 [kWm^{-3}].

IM (MRS): ◒ , 6DT: ○ , 6MFU: ◑ , 6MFD: ◐ , 6PSDT: △ , A315: □ .

effects of viscosity increase can be seen. It is clear that hold-up is reduced at constant P/V and v_s when viscosity is increased. However, the reduction in hold-up with increased viscosity is agitator dependent. Table 6.5 lists correlations for each impeller combining the data from 3 concentrations of CMC by inclusion of an apparent viscosity term. Moderately good correlation coefficients were obtained for each impeller. The apparent viscosity exponent (γ) values range from -0.13 (IM, MRS) to -0.25 (A315, 6MFD). IM at both H/T = 1 and 2 therefore provided higher relative hold-ups when viscosity was increased. The 6DT hold-up (γ = -0.17/-0.18) also showed a lower dependence on μa. The 6MFD and A315 hold-ups were both effected most by viscosity changes.

Figure 6.28 illustrates the decrease in hold-up with increasing viscosity at constant P/V and v_s, the lower dependence of IM hold-up on μa can be seen. The degree of gas recirculation into the impeller is likely to be reduced with increased viscosity due to lower local liquid velocities, lower liquid turbulence and changing flow patterns in the vessel. The effect of reduced gas recirculation will be to reduce hold-up, all other factors being equal. The bubble size distribution becomes increasingly bimodal in viscous non-Newtonian media, the break-up of gas bubbles is inhibited causing large slugs to pass up the centre of the vessel. The rupture of large bubbles at the surface and at the impeller also causes many very tiny bubbles to be formed[49,89].

The hold-up in CMC is therefore composed of hold-up due to large bubbles (ε_{LB}) and hold-up due to small bubbles (ε_{SB})[49]. Phillip et. al.[49] found that the hold-up due to large bubbles increased with increasing viscosity in CMC (as was the case with viscous Newtonian fluids) due to reduced rise velocities. The hold-up due to small bubbles (ε_{SB}) was, however, reduced in high viscosity CMC leading to a slight reduction in total hold-up with increased CMC concentration. The opposite effect (e.g. increased hold-up with increased viscosity) was seen in viscous Newtonian

fluids[49]. They also noted that although small bubbles contributed to roughly half the hold-up in viscous Newtonian fluids they contributed much less in non-Newtonian fluids.

Machon et. al.[50] studied hold-up with CMC in a stirred tank and observed a reduction in hold-up with increased CMC concentration. Unlike Phillip[49], Machon et. al. attributed this phenomenon to the increased rise velocity of the large slug like bubbles formed at higher CMC concentrations, which were not recirculated into the impeller but rose rapidly to the surface.

The variation in the rate of hold-up reduction with impeller type as viscosity is increased is likely to be due to the varying proportion of recirculated gas and variation in the ratio of small to large bubble hold-up. With the IM either a higher proportion of the inlet gas stream was recirculated and/or the large bubble hold-up was different to that of the impeller types that exhibited a higher reduction in total hold-up with increased viscosity.

At a given CMC concentration, P/V and v_s, impellers with low gassed power numbers (Pog) will operate at higher N and thus higher Metzner and Otto shear-rates. Under these conditions low Pog impellers will experience lower apparent viscosity and should therefore provide higher hold-up. The results in 0.4% and 0.8% CMC tend to support this conjecture.

Table 6.5 gives a number of correlations arrived at by combining data sets for differing impellers or geometries. 'F' tests at a 5% significance level indicated that the combined correlation (no.9) for IM at H/T = 1 and 2 was not significantly different from the individuals. The combined correlation (no.10) for 6DT at H/T = 1 and 2 was significantly worse than the individuals however.

6.5 COMPARISON OF HOLD-UP RESULTS WITH LITERATURE

In this section the results from preceding sections will be discussed with reference to studies on hold-up available in the literature.

No literature data is available for comparison of the effect of vessel scale on IM hold-up. Studies using other impeller types at differing scales in water have however been reported by Foust et.al.[113], Calderbank et.al.[43], Smith et.al.[114], Hassan and Robinson[115] and Bujalski[12], all used 6DT and in the case of the latter two six and four bladed paddles and mixed flow impellers. The results of these workers are shown in the form of correlations in Table 6.6.

An effect of vessel scale on hold-up was found by Bujalski[12] and Calderbank[43] who could not correlate varying scales together successfully using 6DT water data. Foust et.al[113], Smith et.al[114] and Hassan and Robinson[115] either correlated the data from varying scales together[113,114] or specifically stated no effect of scale[115]. Bujalski[12] clearly shows a decrease in both P/V and v_s exponents on scale increase and, as seen in this work, the differences were significant but not excessive.

Literature results in water using the 6DT impeller agree very well with those found in this work, particularly those of Van't Riet[28] and Chapman[21]. Bujalski's[12] results show a higher sensitivity to v_s, possibly due to different measurement methods (ultrasonic probe and visual) but show a similar P/V dependency. Hassan and Robinson[115] found an effect of impeller type on hold-up using 6DT, 6-bladed paddle and 4-bladed paddle in water and aqueous organics as did Calderbank and Figuereido[117] using 6DT with perforated and standard blades in water and 0.01% hexanol, their work is reviewed by Mann[54]. Bujalski[12] also found a significant difference between 6MF and 6DT using water in a 0.183m diameter vessel. Other studies have concluded that all water hold-up data may be correlated together satisfactorily irrespective of impeller type assuming $N > N_{CD}$

TABLE 6.6

LITERATURE HOLD-UP CORRELATIONS FOR 6DT IMPELLERS IN WATER AND C.M.C.

Impeller	D/T	T [m]	V [m^3]	Fluids	P/V Units	Correlation	Ref.
6DT	0.33	0.18 0.5	0.005 0.1	Water Ethanol Glycol		$\varepsilon_G \propto (P/V)^{0.4}(v_s)^{0.5}$	43
6DT	0.3	0.91	0.6	Water	Wm^{-3}	$\varepsilon_G = 0.34(P/V)^{0.25}(v_s)^{0.75}$	116
6DT	0.33			Water	Wm^{-3}	$\varepsilon_G = 1.43(P/V)^{0.31}(v_s)^{0.67}$	28
6DT	0.5	0.45	0.072	Water	kWm^{-3}	$\varepsilon_G = 1422(P/V)^{0.37}(v_s)^{1.17}$	12
6DT	0.5	0.61	0.178	Water	kWm^{-3}	$\varepsilon_G = 416(P/V)^{0.36}(v_s)^{0.95}$	12
6DT	0.5 0.33	0.56	0.14	Water	Wm^{-3}	$\varepsilon_G = 1.97(P/V)^{0.33}(v_s)^{0.66}$	21
6DT	0.33	0.56	0.14	CMC		$\varepsilon_G \propto (P/V)^{0.3}(v_s)^{0.7}$	50
6DT CBT	0.33	0.32 2.44	0.02	Water		$\varepsilon_G \propto (P/V)^{0.47}(v_s)^{0.53}$	113
6DT Various Blades	0.33 0.5	0.91 0.183	0.6 4.4	Water		$\varepsilon_G \propto (P_G/V)^{0.475}(v_s)^{0.4}$	114
6DT	0.3	0.91	0.6	Water 0.01% Hexanol	Wm^{-3}	$\varepsilon_G = 0.23(P/V)^{0.26}(v_s)^{0.68}$	117
6DT 6MF etc	0.5 to 0.7	0.305 0.286 1.79	0.02 0.06 4.3	Paper Fibre Suspen- sions	kWm^{-3}	$\varepsilon_G = 30.8(P/V)^{0.15}(v_s)^{0.54}(\mu a)^{-0.42}$	30

(or $P/V > P/V_{CD}$). Chapman et.al[21] found that 6DT, 4MFU/D, ADT and AFD of T/2 and T/4 diameter could be correlated together within ± 25%. The conflict in the literature concerning the impact of impeller size and design on hold-up may be related to differences in measurement method or lack of accuracy.

Generally, although differences between impellers are detectable in water and in certain cases have been shown to be significant, in other cases they have been insignificant and all water data has been usefully correlated together. In this work only the IM impeller showed significant differences from the other types tested in water even though individual correlations show varying exponents.

The effect of electrolyte addition on hold-up has been extensively studied by a number of workers[46-48]. Generally their exists a rather narrow concentration range of solutes over which a change from rapid coalescence in pure water to coalescence suppression takes place. This concentration range also governs an increase in hold-up from that in pure water to a maximum value beyond which further solute concentration increases have little or no effect. Typically above or below this narrow concentration range hold-up data may be satisfactorily correlated using separate 'coalescing' or 'non-coalescing' models. The use of 0.2M NaCl in this work demonstrated that the increase in hold-up due to the presence of electrolytes occurred irrespective of the presence of chemicals used in the NEL/Hickman k_La measurement technique. This would not have been the case if they enhanced coalescence themselves at the concentrations used.

The influence of sparger design on hold-up in water has been commented on by Bujalski[12] for 6DT impellers of two diameters with point and large ring spargers . Significant differences were found in both correlation exponents and absolute values of hold-up. The LRS (Ds/D = 1.22) gave higher hold-ups at low P/V whilst the data tended to converge at high P/V. Hickman[20] found higher hold-ups for IM with MRS in water.

The results of Bujalski[12] and Hickman[20] are in agreement with the more extensive IM data contained in this work. No reference to hold-up studies at H/T other than 1 could be found in the literature, for water.

Studies on hold-up in liquids of higher viscosity than water are uncommon in stirred tanks, particularly for non-Newtonian fluids. Machon et.al[50] assessed the effect of increasing CMC concentration on hold-up using a 6DT T/3 impeller in a tank of standard geometry. CMC concentrations used showed very similar K and n values to those found in this work. Their data is correlated in Table 6.6, values of constants are not given but P/V exponents are the same and v_s exponents higher than those found using 0.07% CMC in this work.

Machon et al[50] also found a hold-up increase from water to 0.015% CMC as was found in this work for 0.07% CMC. All further increases in CMC concentration led to a gradual decrease in hold-up. This occurred despite surface tension remaining constant at that of water throughout. It was postulated that the increase in hold-up in 0.015% CMC was due to the presence of tiny pin-head size bubbles. Further reductions in hold-up were due to the increasing size of the larger bubbles that comprise the other size range of the bimodal distribution. These large bubbles escape the liquid more rapidly and are recirculated with difficulty as viscosity increases. Machon et.al[50] also related the decrease in hold-up to increasing pseudo-plasticity.

Hickman[20] described hold-up measurements in CMC solutions of 0.04% to 1.4% in a 0.3m diameter vessel using a variety of agitators. As in this work and that of Machon[50] hold-up in 0.04% CMC was found to be higher than that of water. Further increases in CMC concentration led to hold-up reduction for IM but a more complex relationship between hold-up and viscosity at a given P/V for 6DT. At CMC concentrations greater than 0.5% the T/2 6DT hold-up showed regions of both of no change with increasing P/V and decrease with increasing P/V. In 0.8% CMC similar results were

found here, using the 6DT and 6PSDT agitators. Hickman[20] associated the 6DT behaviour with changing cavity size and structure in the transitional flow regime. He also found hold-up increased from 0.4% to 0.8% CMC which was not found to be the case here for 6DT, but was seen for 6PSDT. Hickman found the 6DT/MF combination gave higher hold-ups with the 6MF impeller pumping upwards in 0.8% and 1.4% CMC. The same was found to be the case in this work using 6MF in 0.8% CMC, but at lower CMC concentrations the opposite was true. In 1.4% CMC no increase in hold-up with increased gassing rate was seen.

Cooke et.al[30] reported hold-up measurements obtained using 6DT, 6MFD, A310, ICI Gasfoil, Scaba SRGT and PLENTY hydrofoil in three vessels of H/T = 1 and 3. The fluids under test were various paper fibre suspensions. Data was correlated using apparent viscosity calculated by the Metzner and Otto approach and is given in Table 6.6. The correlation includes all impeller and vessel data. Comparing correlation 11, Table 6.5 with that of Cooke et.al[30] reveals similar P/V exponents but higher v_s and μa exponents for the latter. The values of the constants are similar.

6.6 CONCLUSIONS

Different impeller types show only a small variation in ε_G[%] at constant P/V and v_s in deionised water. The inter-impeller variation is slightly greater in 0.07% CMC solution but is most severe in 0.4% and 0.8% CMC where differences of up to 100% were noted.

The IM impeller (MRS) gave the highest hold-ups over the range of test fluids. The dependence of ε_G[%] on v_s[ms^{-1}] was found to fall from $\varepsilon_G \propto v_s^{0.5-0.6}$ in water to $\varepsilon_G \propto v_s^{0.15}$ in 0.8% CMC. The dependence of ε_G[%] on P/V [Wm^{-3}] was $0.13 < \alpha < 0.32$. The influence of apparent viscosity (μa) for InterMIG was the lowest found, ε_G[%] $\propto \mu a^{-0.14}$.

The 6DT hold-up results in water agreed extremely well with literature values[21,28]. The overall hold-up performance of this impeller

was moderately poor. The P/V exponent 'α' fell from 0.32 to 0.24 and v_s exponent from 0.6 to 0.45 with increasing CMC concentration.

The 6PSDT hold-up results were similar to those of the 6DT in water (except at high v_s). The impeller provided the worst overall hold-up performance in CMC. The value of α fell from 0.3 in water to zero in 0.8% CMC, the value of β fell from 0.5 in water to 0.23 in 0.8% CMC. For the 6PSDT, $\varepsilon_G[\%] \propto \mu a^{-0.21}$.

The A315 hold-up was the most strongly influenced by gassing rate with $\beta = 0.67$ in water and $\beta = 0.56$ in 0.8% CMC. The influence of P/V varied little with test fluid, $\alpha = 0.26$ in water and $\alpha = 0.29$ in 0.8% CMC. A315 relative hold-up was poor at low v_s but good at high v_s. The A315 hold-up was more strongly effected by viscosity increase than most impellers with $\varepsilon_G \propto \mu a^{-0.27}$.

The 6MF(U)/(D) hold-up was found to be dependent upon pumping mode. For the D.P.M. α was between 0.28 and 0.17 whilst for the U.P.M. α ranged from 0.48 to 0.37 with increasing viscosity. The pumping mode had little effect on the v_s dependence of the hold-up, $\varepsilon_G[\%] \propto v_s^{0.54}$ in 0.07% CMC and $\varepsilon_G[\%] \propto v_s^{0.33}$ in 0.8% CMC. The hold-up was relatively strongly influenced by apparent viscosity with $\varepsilon_G \propto \mu a^{-0.24}$ (U.P.M.) and $\varepsilon_G \propto \mu a^{-0.27}$ (D.P.M.).

The addition on electrolyte (0.2m NaCl) to deionised water caused the gassed hold-up to increase by approximately 20%. The gassed hold-up in 0.07% CMC was found to be slightly higher than in deionised water due to coalescence suppression and hence the presence of a large number of tiny bubbles ≤ 1mm in diameter. The volume of entrained gas at constant P/V and v_s fell with increasing CMC concentration. $\varepsilon_G[\%]$ dependence upon μa was found to be $-0.17 < \gamma < -0.27$.

Hold-up using IM (MRS) was unaffected by doubling H/T in 0.4% and 0.8% CMC. Results in 0.07% CMC and water were inconclusive. Doubling the aspect ratio when using 6DT impellers caused a 20% to 40% drop in hold-up

in 0.4% and 0.8% CMC.

Sparger choice influenced hold-up strongly with IM when $N < N_{CD}$. The optimum sparger choice for IM was found to be an MRS (Ds/D=0.85) which discharged gas into the impeller outer blades. Both v_s and P/V dependence in deionised water were found to fall with increasing sparger ring diameter until the sparger diameter became greater than that of the impeller.

7. OXYGEN MASS TRANSFER RESULTS.

7.1 INTRODUCTION

This chapter presents k_La data obtained under a variety of conditions in vessel T72 using the NEL/Hickman measurement technique. The mass transfer data is compared firstly using P/V. This parameter is independent of vessel scale and geometry. Unlike the use of N, it allows impellers of different design to be compared. The aeration rate is described using the gas superficial velocity, v_s [ms^{-1}] which is independent of aspect ratio and vessel scale[73]. The use of Q_G (vvm) as a parameter does not allow differing aspect ratios or scales to be correlated together as accurately as the use of v_s[78,114,118]. v_s has also been used successfully for the correlation of k_La in bubble columns, allowing comparison with stirred tanks. Both P/V and v_s are important when considering process operating costs. Agitator selection can be made to optimise k_La under given operating conditions e.g retrofitting an existing vessel, or to minimise costs incurred when achieving a given k_La e.g. for a new bioreactor design.

Initially k_La results in deionised water are presented, enabling comparison to be made with literature correlations, as many water data are available. There follows sections describing data obtained using 0.07% CMC (μa = 0.008 to 0.023 Pa.s, Re = 1.5×10^4 to 1.1×10^5), 0.4% CMC (μa = 0.06 to 0.12 Pa.s, Re = 2×10^3 to 1.4×10^4) and 0.8% CMC (μa = 0.17 to 0.4 Pa.s, Re = 8.4×10^2 to 5×10^3). As well as comparison of agitator types, the influence of spargers and aspect ratio are also discussed. Results from the preceding sections are combined to investigate the effect of μ_a on kla. The hold-up results detailed in Chapter 6 are compared with k_La data obtained under identical conditions. The final chapter sections compare mass transfer correlations with those found in the literature.

7.2 OXYGEN MASS TRANSFER RESULTS IN WATER

7.2.1 Introduction

In this section k_La results obtained in deionised water using four impeller types are presented. Impeller types used were single 6DT, 6PSDT, A315 and 2 or 4 IM at H/T=1 or 2, each impeller was tested at v_s = 0.006, 0.012 and 0.018 [ms^{-1}]. The IM was also tested using both point (PS) and ring spargers (MRS). Aerated power input was in the range 0.5 to 5 [$kW.m^{-3}$], which is representative of industrial practice. The Reynolds number range in water was 3.6×10^5 to 1.2×10^6 (fully turbulent).

7.2.2 k_La results in deionised Water

Figure 7.1 shows k_La results in deionised water at a gas velocity of v_s = 0.006 [ms^{-1}]. In addition to k_La results from this work the van't Riet[73] correlations for coalescing and non-coalescing systems are shown. The data for A315, 6DT and IM shows similar dependence on P/V at this gas velocity and little scatter around the overall correlation line (Table 7.1 no.7). The 6PSDT data, however, lies noticeably above the correlation line. The k_La values from this work are situated between those predicted by the van't Riet[73] correlations at P/V > 1 [kWm^{-3}].

Figure 7.2 shows k_La results at v_s = 0.012 [ms^{-1}]. The scatter around the overall water regression line is greater than in the previous case. The data obtained using IM (PS) is significantly lower than that of the other types as the effect of v_s on k_La is negligible in water when using a point sparger (Section 7.2.3).

Figure 7.3 shows k_La values in water at v_s = 0.018 [ms^{-1}]. The scatter of data is even greater than in the previous case and indicates increasing divergence of impeller k_La with increasing v_s. The 6PSDT impeller showed a considerable enhancement of k_La over that obtained with 6DT at P/V < 2 [kWm^{-3}]. As in the v_s = 0.012 [ms^{-2}] case the IM (PS)

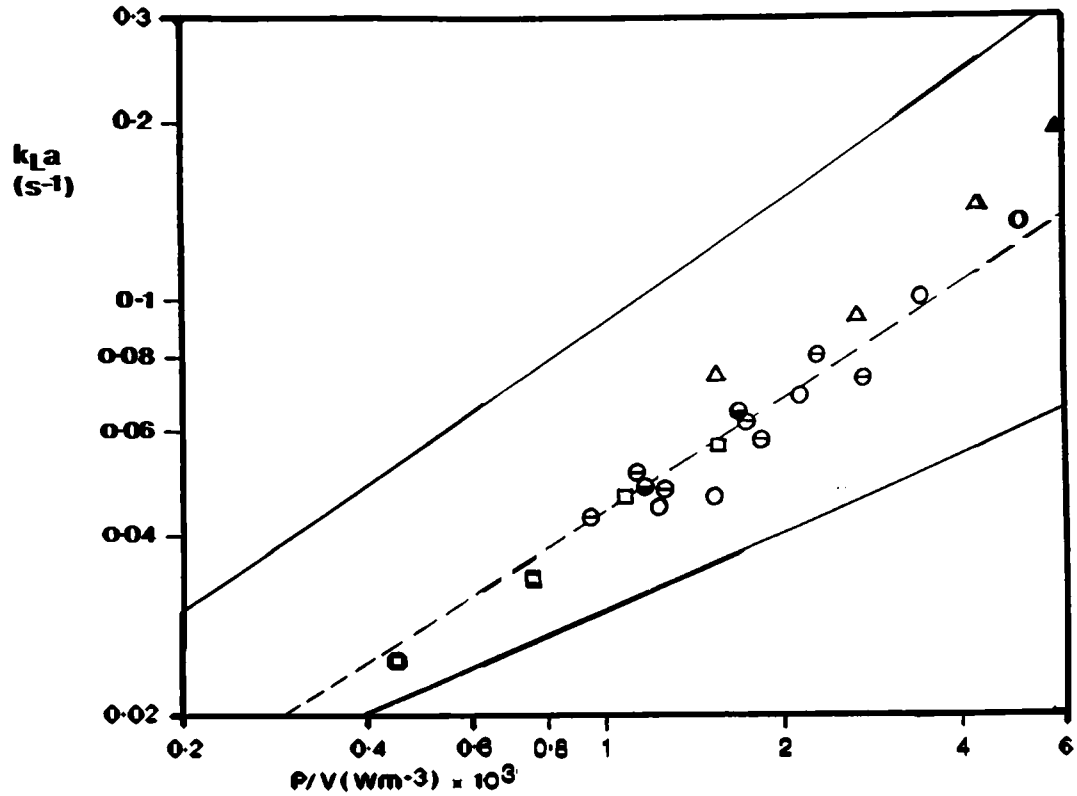

Figure 7.1 k_La v P/V, T72, Water, H/T = 1, v_s=0.006 [m/s].

InterMIG (MRS):⊖, InterMIG (PS): ⊖ , A315: □ , 6DT: ○ ,

6PSDT: △ .

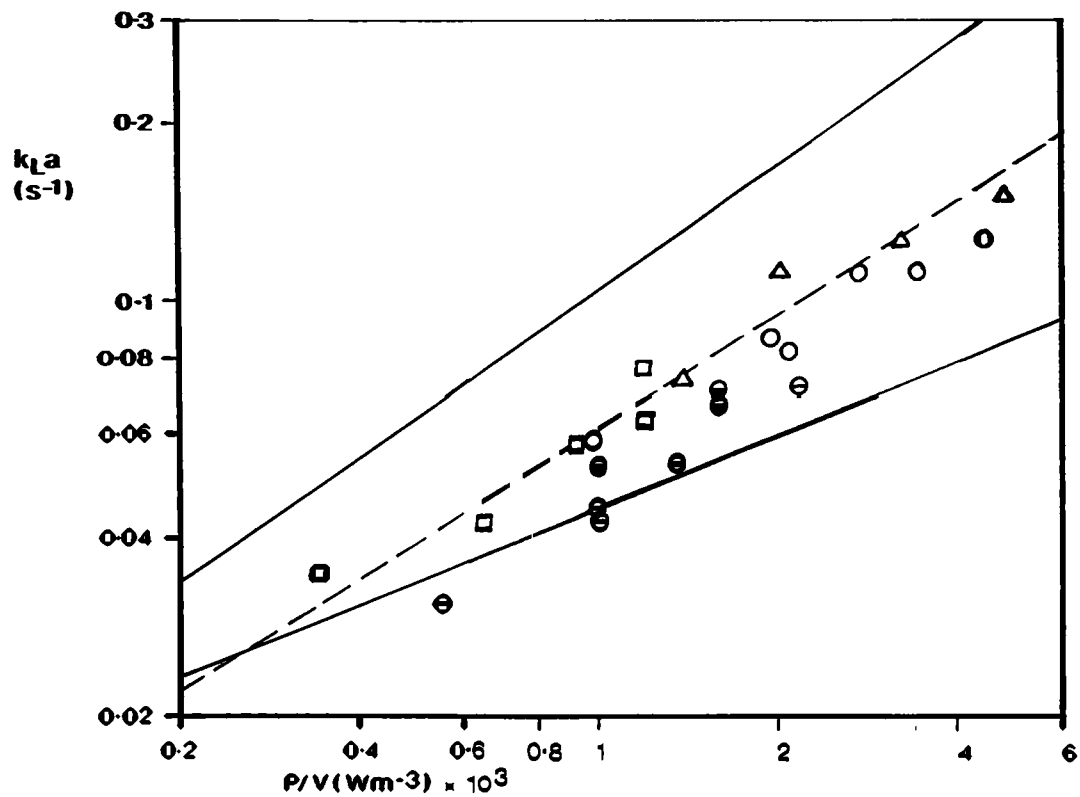

Figure 7.2 k_La v P/V, T72, Water, H/T = 1, v_s=0.012 [m/s].

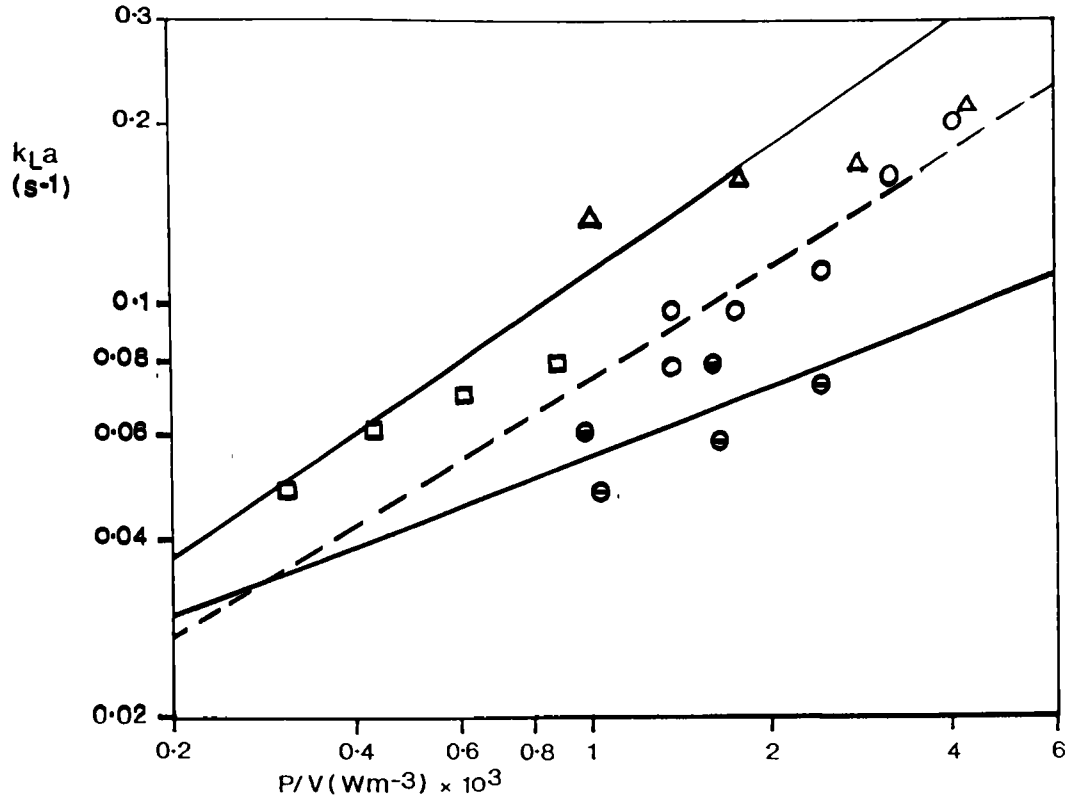

Figure 7.3 k_La v P/V, T72, Water, H/T = 1, v_s=0.018 [m/s].

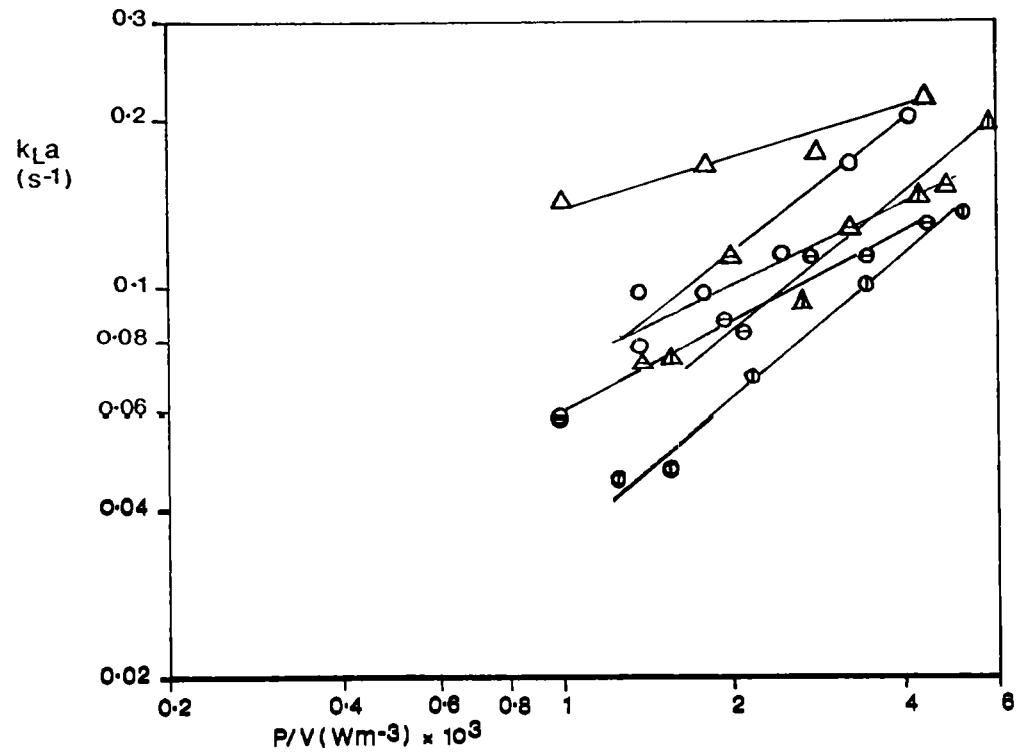

Figure 7.4 k_La v P/V, T72, Water, H/T = 1, 6DT: o ,6PSDT: Δ .

v_s=0.006 [m/s]: ⊕,0.012 [m/s]: ⊖,0.018 [m/s]: o .

exhibited considerably lower k_La values than the 6DT at $1 < P/V < 3$ [kWm^{-3}]. The k_La values obtained using the IM may be enhanced slightly with the use of an MRS (Section 7.2.3).

Hold-up results recorded during the same experiments are described in Section 6.2. Trends in the hold-up data were very close to those with k_La. At $v_s = 0.006$ [ms^{-1}] all impeller hold-ups were of similar magnitude, but as with k_La the 6PSDT hold-up was slightly above the rest. The IM (PS) hold-up at $v_s = 0.012$ [ms^{-1}] (Fig.6.2) was comparativeley low, an identical situation to that observed with k_La. Interestingly, the 6PSDT hold-up showed marked enhancement in the region $1 < P/V < 2$ [kWm^{-3}] corresponding to that found for k_La at $v_s = 0.018$ [ms^{-1}]. These findings imply that differences in impeller k_La in water are largely due to interfacial area differences linked to hold-up via bubble size distribution.

The k_La data measured in water are correlated with P/V and v_s for individual impeller types in Table 7.1. It can be seen from these correlations and Figs. 7.1 to 7.3 that the impeller type has a minimal effect on the P/V exponent, which for different stirrers ranges from 0.51 to 0.7. These findings agree with reports in the literature[73] concerning results in pure water and ionic solutions.

The effect of v_s on k_La does however vary with impeller type in water. Figures 7.4 to 7.5 illustrate the differing effects v_s changes on k_La. The 6DT (Fig. 7.4) exhibits $k_La \propto v_s^{0.5}$ (Table 7.1) and the 6PSDT (Fig. 7.4) $k_La \propto v_s^{0.45}$ although in the latter case the influence of v_s appears to decrease with increasing P/V. The A315 (Fig. 7.5) shows the most marked dependence of k_La on v_s ($k_La \propto v_s^{0.7}$) whereas the IM (Fig.7.5) shows a low influence of v_s, $k_La \propto v_s^{0.04-0.36}$, dependent on sparger (Section 7.2.3). It should be noted that in all cases k_La measurements were made under loaded conditions, ruling out any effect of flooding.

TABLE 7.1

$k_L a$ CORRELATIONS IN DEIONISED WATER

$$k_L a = K\,(P/V)^{\alpha}\,(v_s)^{\beta}$$

where P/V [Wm^{-3}]; v_s [ms^{-1}]

No.	Impeller Type	Sparger Type	K ($x10^{-3}$)	α	β	Number of Points	R^2
1	6DT	PS	4.1	0.7	0.5	17	0.93
2	A315	Ring	30.5	0.56	0.7	13	0.93
3	6PSDT	PS	19.0	0.51	0.45	13	0.73
4	IM	PS	0.86	0.6	0.04	16	0.96
5	IM	MRS	8.2	0.52	0.36	14	0.83
6	IM 2:1	PS	3.2	0.51	0.16	15	0.91
7	Overall 1:1	Various	6.0	0.63	0.47	73	0.8
8	Overall 1:1/2:1	Various	6.3	0.6	0.43	88	0.83

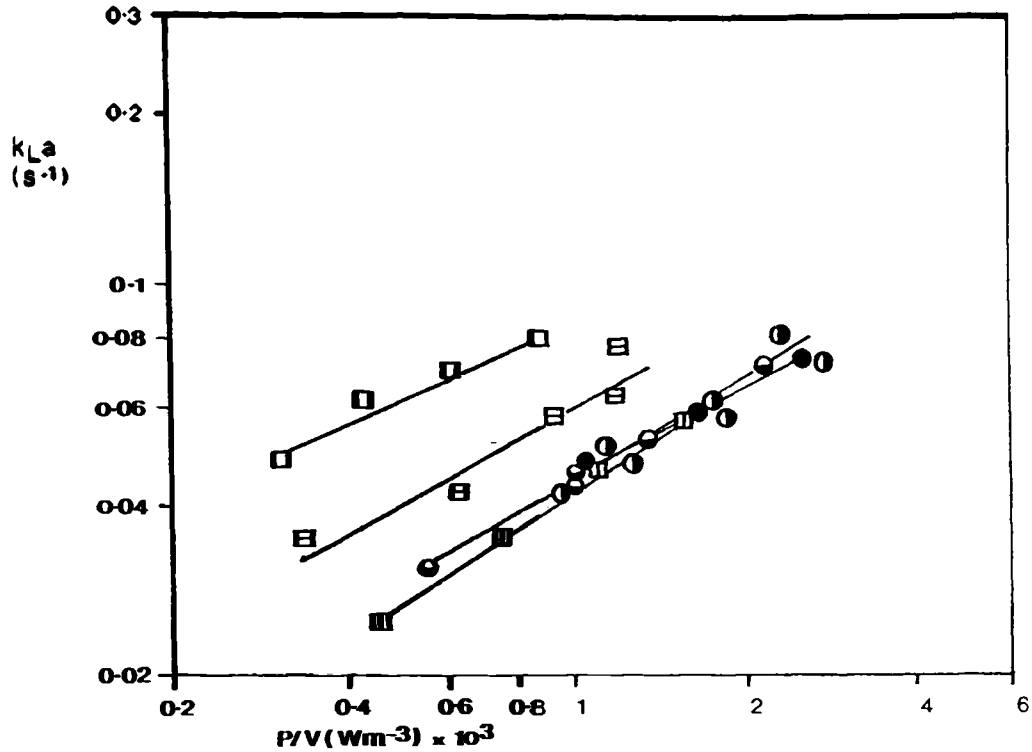

Figure 7.5 k_La v P/V, T72, Water, H/T = 1.

InterMIG (PS):●, A315: □ .

v_s=0.006 [m/s]: ■ ,0.012 [m/s]:⊟,0.018 [m/s]:□.

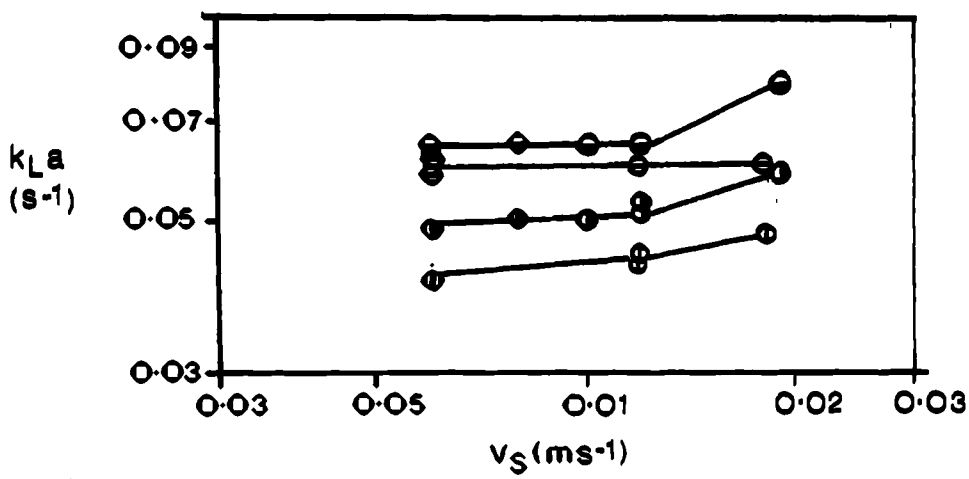

Figure 7.6 k_La v v_s, T72, Water, H/T = 1.

IM (MRS), P/V=1 [kW/m^3]: ◆ ,P/V=1.6 [kW/m^3]: ● .

IM (PS), P/V=1 [kW/m^3]: ◍ ,P/V=1.6 [kW/m^3]: ⊖ .

The hold-up results in deionised water showed only a small influence of impeller type, a finding which supports the trends observed with k_La.. As with k_La, the effect of P/V changes on hold-up for different agitators was similar. The hold-up with IM showed a strong effect of v_s irrespective of sparger choice, this was not found when k_La was measured. This implies that although hold-up increases with increased v_s the k_La does not, leading to the assumption that interfacial area remains constant and therefore mean bubble size increases with v_s for the IM. As v_s rises the IM appears incapable of breaking up the additional gas which may pass up the vessel centre as slug-like bubbles. This is particularly evident with a point sparger that discharges into the centre blades and is much reduced when a ring sparger is used to discharge gas into the impeller outer blade region. With the other impellers tested, both k_La and hold-up were influenced by v_s increase, this suggests that the k_La increase was due to a greater interfacial area for mass transfer, a.

Statistical 'F' tests were employed to ascertain whether the combined correlations (nos. 7 and 8, Table 7.1) were significantly different from the individual correlations (nos. 1 to 6, Table 7.1). The correlation combining all 1:1 water data (no.7) was found to be a significantly worse fit than any of the individual correlations at 1% and 5% levels, except for that of the 6PSDT. Similar results were found when testing correlation no.8. The water k_La data therefore cannot conclusively be shown to be independent of impeller type.

7.2.3 Effect of sparger on InterMIG mass transfer.

Figure 7.6 shows the influence of v_s on k_La at two power inputs using both PS and MRS. It is apparent that in the range $0.006 < v_s < 0.018$ $[ms^{-1}]$ the gassing rate has negligible influence on k_La values irrespective of sparger choice. The MRS however, gives higher k_La values

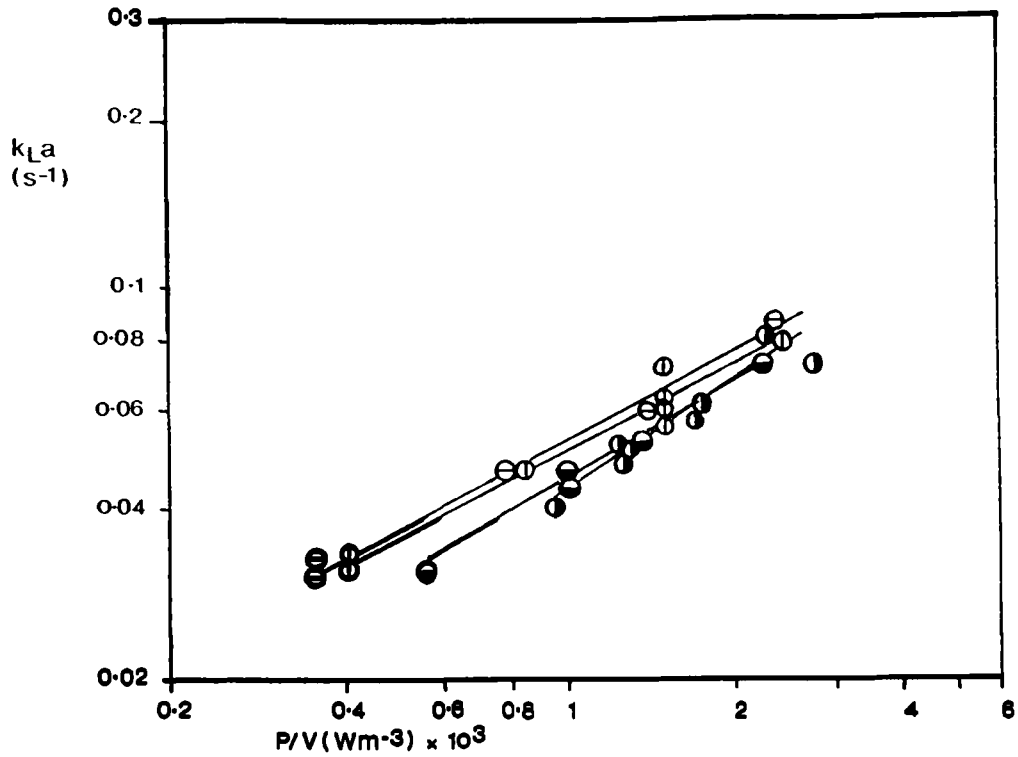

Figure 7.7 k_La v P/V, T72, Water, InterMIG (PS).

H/T = 1, v_s=0.006 [m/s]: ⊙ ,0.012 [m/s]: ● .

H/T = 2, v_s=0.006 [m/s]: ⊙ ,0.012 [m/s]: ● .

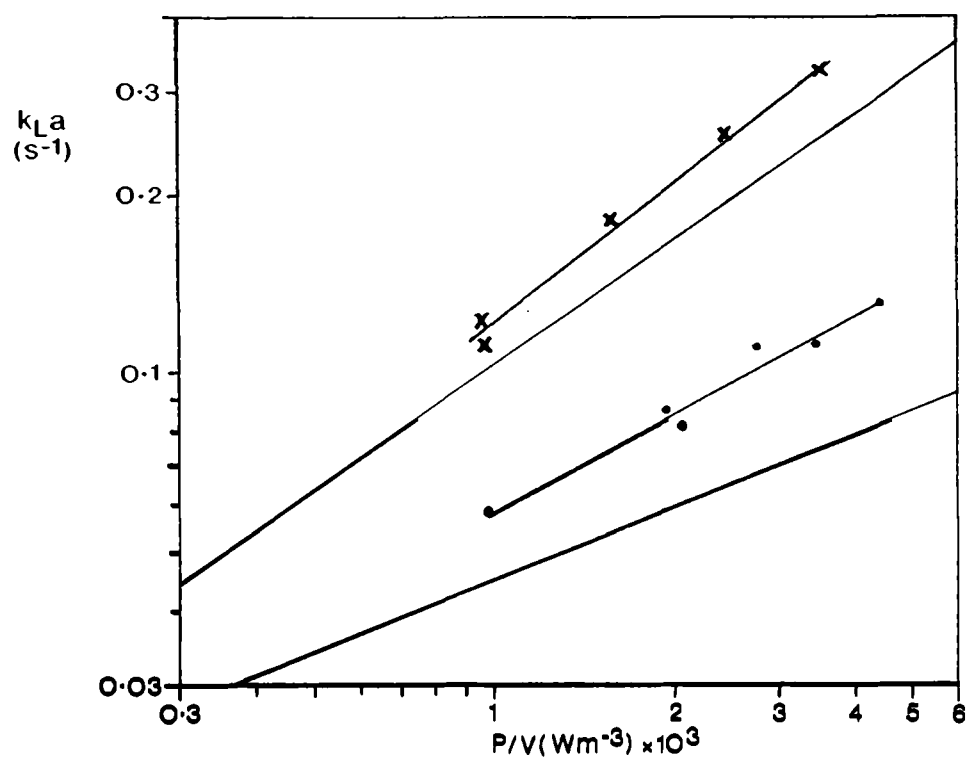

Figure 7.8 k_La v P/V, T72, 6DT, H/T = 1, v_s=0.012 [m/s].

Water: • , 0.2M NaCl: × .

than those obtained using the PS. This confirms the findings of Hickman[20]. Hold-up values were also higher when MRS were used. Improved bubble breakup leading to higher residence times can be achieved by discharging air into the IM outer blades. Sparger choice therefore affects the specific area, a, available for interphase O_2 transfer.

7.2.4 Influence of aspect ratio on InterMIG mass transfer

Figure 7.7 illustrates k_La results obtained using 2 IM at H/T = 1 and 4 IM at H/T = 2, two v_s are shown. At a given P/V, little effect of H/T can be seen on the k_La values. Results in Chapter 6 for IM at H/T = 1 and 2 using PS and MRS showed no change in hold-up when the two aspect ratios were compared on the basis of P/V and v_s. Under these conditions a vessel operated at H/T = 2 can be treated as two H/T = 1 vessels for k_La estimation purposes. From the results presented in this section it can be seen that the volumetric gas requirement for a given vessel volume (Q/V) is reduced when H/T is increased. In larger vessels this reduction can have an effect on the driving force for mass transfer as oxygen is stripped from the gas phase[119].

7.2.5 The effect of bubble coalescence on k_La.

Coalescence and its inhibition are phenomena of great importance for gas-liquid mass transfer because interfacial area, a, is directly affected. The mass transfer coefficient, k_L, is only slightly affected by changes in the concentration of coalescence inhibiting solutes[47,73]. As bubble diameter becomes smaller a decrease in k_L has generally been reported[73]. Increases in k_La of up to 7 times have been measured when coalescence was inhibited to its maximum extent[120]. The effect of turbulence on coalescence behaviour becomes stronger at high air flow rates which implies the effect of solutes will not be as high as for low air flowrates[47].

Figure 7.8 shows k_La data at H/T=1 using a single 6DT. Deionised water as coalescing and 0.2M NaCl as non-coalescing solutions were used. Also shown are the coalescing and non-coalescing correlations of van't Riet[73]. It can be seen that the addition of NaCl caused an increase of between 100% and 200% over the pure water k_La. The level of k_La enhancement found experimentally was very similar to that predicted by van't Riet[73]. The absolute k_La values were higher than predicted (Section 7.8). The k_La values for ionic solutions were more dependent on P/V than those for pure water. The hold-up of liquid was also increased when coalescence was suppressed, due to the longer residence time of the smaller bubbles (Section 6.2.) and increased recirculation.

7.3 OXYGEN MASS TRANSFER RESULTS IN 0.07% CMC

7.3.1 Introduction

There follows a description of k_La results using 0.07% CMC (μa 0.008-0.023 Pa.s) at H/T = 1 and 2 in the T72. Six impeller types were used: 6DT, 6PSDT, 6MFU, 6MFD, A315 and 2 or 4 IM. Only the IM was used at both aspect ratios. The Re range (including all impellers) was 1.5×10^4 to 1.1×10^5 (turbulent regime).

7.3.2 k_La results in 0.07% CMC

Figure 7.9 shows the k_La values at v_s = 0.006 [ms^{-1}]. They are similar to those at the same P/V and v_s in water. The inter-impeller variation is however noticeably greater than in water at equal v_s. At a given P/V, k_La is doubled when comparing 6MFD or IM with 6DT, the former two giving the highest and the latter the lowest k_La at this gas velocity. The influence of P/V is very similar for the various impellers. Bubble coalescence is suppressed in CMC indicating a likely similarity between P/V exponents in dilute CMC and ionic solutions[20].

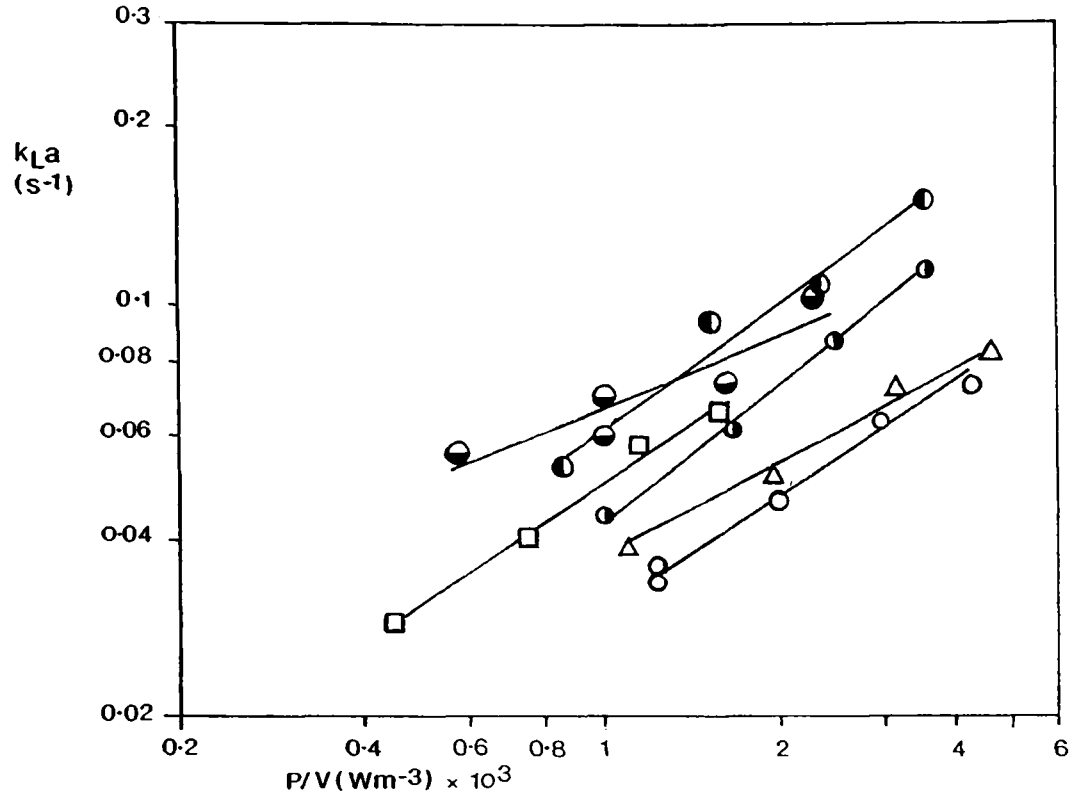

Figure 7.9 k_La v P/V, T72, 0.07% CMC, H/T = 1, v_s=0.006 [m/s].

6DT:o, 6MFU:◑, 6MFD:◐, 6PSDT:△, A315:□,InterMIG (MRS):● .

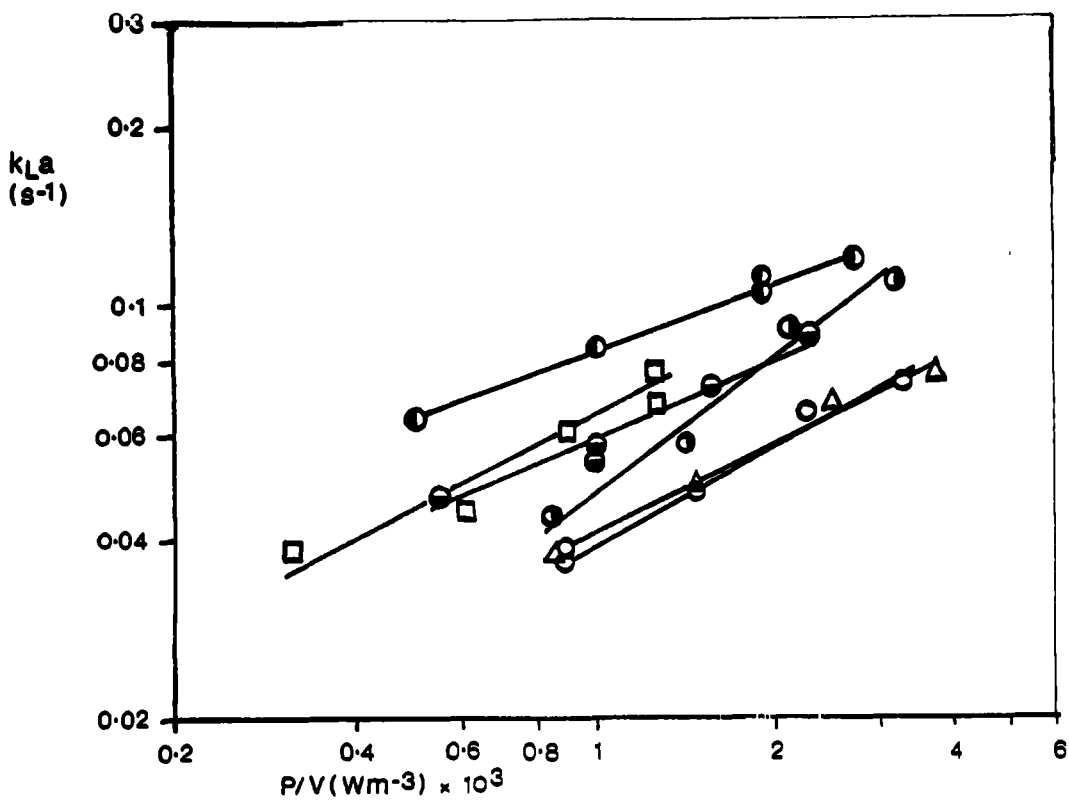

Figure 7.10 k_La v P/V, T72, 0.07% CMC, H/T = 1, v_s=0.012 [m/s].

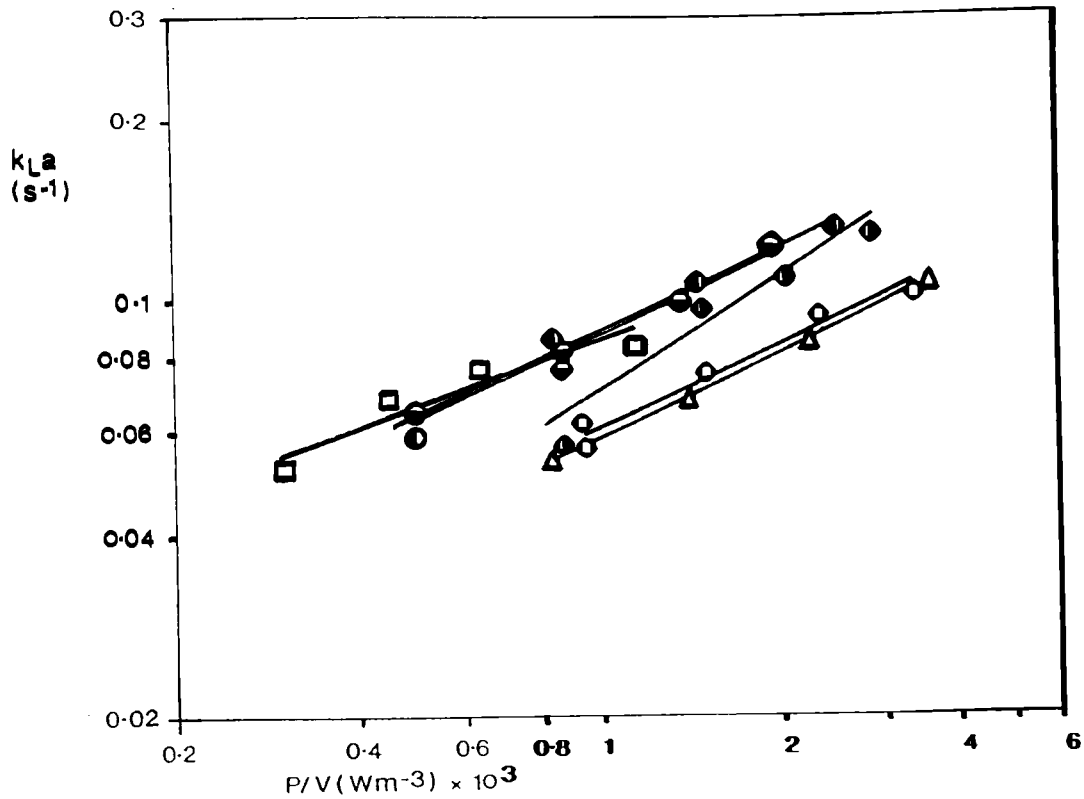

Figure 7.11 k_La v P/V, T72, **0.07% CMC, H/T = 1, v_s=0.018 [m/s].**

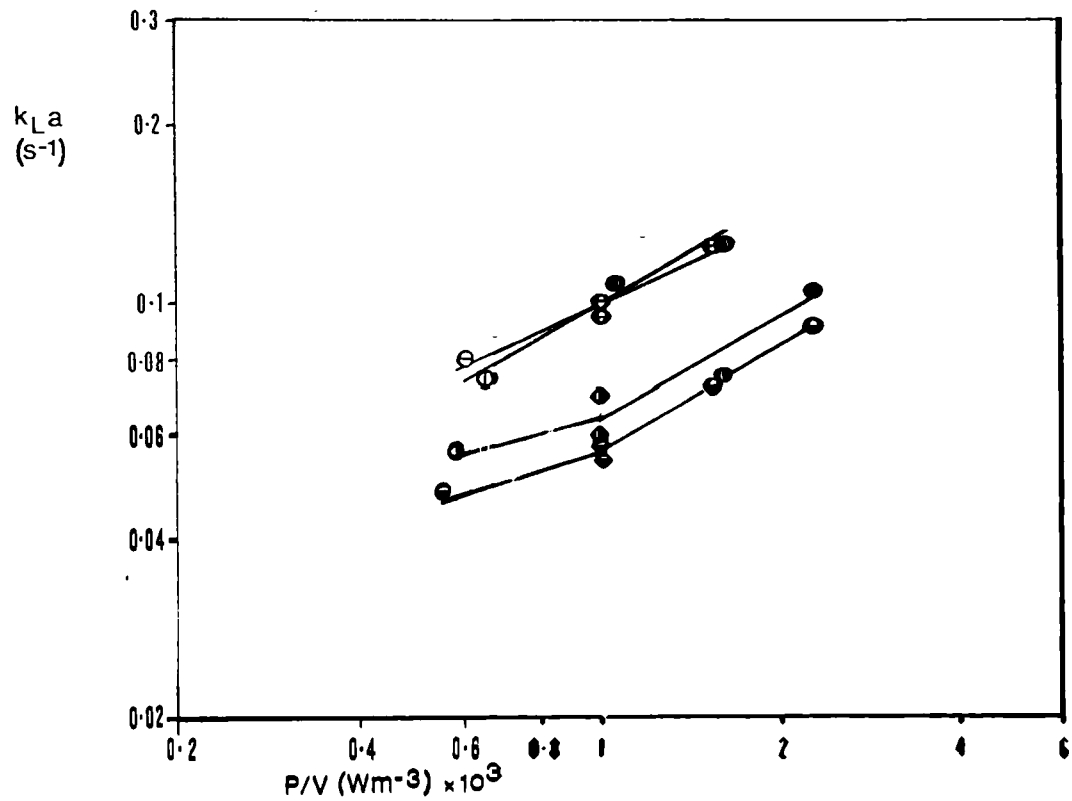

Figure 7.12 k_La v P/V, T72, 0.07% CMC, InterMIG (MRS).

H/T = 1, v_s=0.006 [m/s]:o,**0.012 [m/s]:●.**

H/T = 2, v_s=0.006 [m/s]:ɵ,**0.012 [m/s]:Ø.**

Figures 7.10 and 7.11 show the k_La results at v_s = 0.012 and 0.018 [ms^{-1}]. Unlike the findings in water, the inter-impeller variation fell with increasing v_s in 0.07% CMC. At v_s = 0.018 [ms^{-1}] the highest k_La was provided by the A315, IM and 6MFD and were some 50% higher than those with the 6DT and 6PSDT. Overall, at this CMC concentration the 6MFD performed best in terms of k_La, followed by IM, A315, 6MFU, 6PSDT and 6DT in that order. The 6PSDT and 6DT impellers provided very similar k_La at all v_s. The 6MFD provided consistently enhanced values when compared to the 6MFU. The relative performance of the A315 improved with increasing v_s. The IM was consistently better than the 6DT and 6PSDT .

Results from Chapter 6 indicate moderately good agreement between impellers which provide higher hold-up in 0.07% CMC and higher k_La. The hold-ups for 6DT and 6PSDT were the lowest as were their k_La values whilst the relative ε_G values for IM, A315 and 6MF were higher as was seen with k_La. The inter-impeller variation in k_La appears however to be more marked than that of ε_G.

Figure 7.12 shows k_La results using the IM at H/T=1 and 2. The results at H/T=2 were 40% higher than those at H/T=1. Section 6.3.3 showed that hold-up at H/T = 2 was 10% higher than at H/T = 1 for IM suggesting that under these conditions the k_La increase at the higher aspect ratio is due at least in part to an increase in interfacial area. No explanation for these results can offered at the present time.

Table 7.2 lists correlations for each impeller in 0.07% CMC. The impellers exhibit a similar dependency of k_La on P/V, except the 6MFU which shows a greater dependency. As with water the v_s exponent varies with impeller type. The IM at both H/T = 1 and 2 and 6MFD appear to be affected less by v_s than the other agitator configurations. Although 0.07% CMC shows non-coalescing behaviour the P/V exponents were less than or equal to those found in water. The exponents found for v_s were also less than or equal to those in water. The latter is consistent with

TABLE 7.2

$k_L a$ CORRELATIONS IN 0.07% CMC

$$k_L a = K\,(P/V)^{\alpha}\,(v_s)^{\beta} \qquad [wm^{-3}]\ [ms^{-1}]$$

No.	Impeller Type	Sparger Type	K ($x10^{-3}$)	α	β	Number of Points	R^2
1	6DT	PS	8.29	0.54	0.5	15	0.94
2	A315	Ring	24.7	0.49	0.54	14	0.88
3	6PSDT	PS	6.53	0.51	0.35	13	0.91
4	InterMIG 1:1	MRS	7.93	0.43	0.2	15	0.72
5	InterMIG 2:1	MRS	2.99	0.52	0.02	7	0.96
6	6MFD	Ring	5.67	0.49	0.16	13	0.91
7	6MFU	Ring	1.66	0.72	0.33	13	0.92
8	Combined 4,5		6.21	0.39	0.05	22	0.31
9	Combined 6,7		5.18	0.53	0.24	26	0.72
10	Combined 1,3		6.76	0.54	0.44	28	0.87

inhibited coalescence whereas the former is not.

Whereas all water data could be correlated relatively successfully using P/V and v_s, this was not the case for all 0.07% CMC data, indicating a greater variation in individual agitator performance. The data for 0.07% CMC could however be correlated more successfully by including an apparent viscosity term. This accounts for the variation in N and hence shear rate at a given power input for the differing impellers (see Table 7.5). Low Pog agitators experience lower μ_a at equal P/V than do higher Pog types and should therefore provide higher k_La values in shear-thinning liquids. This appears to explain the inter-impeller k_La variation found here.

Comparison of the trends in exponents α and β for the various impellers in Table 7.2 with those from Table 6.2 (hold-up) reveals some interesting parallels. The 6MFU shows both the strongest dependence of k_La upon P/V and the strongest dependence of ε_G on P/V. The α values when correlating either ε_G or k_La do not exhibit a high degree of variation for impellers other than the 6MFU.

When hold-up was correlated, the v_s exponent 'β' was only influenced to a minor extent by impeller variation, which was not the case with k_La. As in water, IM kla was barely effected by v_s changes whereas hold-up was influenced far more strongly in 0.07% CMC. A similar trend was also seen with the 6MFD. The A315 impeller hold-up was the most effected by v_s variation as was k_La.

Table 7.2 includes three correlations combining IM at 2 aspect ratios, 6MF using both pumping modes and 6DT/6PSDT. The variances of the combined correlations were tested ('F' test) against those of the individuals. As expected both the IM H/T = 1 and 2 and 6MF U.P.M. and D.P.M. results were correlated significantly better using the individual correlations. The 6DT/6PSDT correlation (no.10, Table 7.2) however showed no difference at the 5% significance level from the individual

correlations (nos.1 and 3 Table 7.2). This indicates that the two agitators may be treated as the same for k_La estimation purposes in 0.07% CMC.

7.4 OXYGEN MASS TRANSFER RESULTS IN 0.4% CMC

7.4.1 Introduction

As with the preceding section six impeller types were used at H/T=1 and two, the IM and 6DT at H/T=2. The apparent viscosity range in 0.4% CMC was 0.06 to 0.12 Pa.s and the Re range 2×10^3 to 1.4×10^4.

7.4.2 Effect of Impeller Type on k_La in 0.4% CMC

Figures 7.13 to 7.15 delineate the influence of P/V on k_La at three v_s for six agitator types. The k_La values found were reduced by approximately a factor of ten when compared with those in 0.07% CMC, due to the effect of increased viscosity (Section 7.6). As with 0.07% CMC the k_La results for the various agitators were most diverse at the lowest v_s. k_La enhancement of 150% to 200% was achievable by substituting the IM (best performer) for 6PSDT (worst performer) at v_s = 0.006 [ms^{-1}]. At the higher v_s this difference was reduced to 100% to 150% for best and worst performances.

Similar trends to those observed in 0.07% CMC were apparent in 0.4% CMC. The agitators providing the highest k_La's were the 6MFD and IM. The A315 showed an improving relative performance with increasing v_s. The 6MFU was consistently worse at providing k_La at a given P/V than the 6MFD. Unlike the situation in 0.07% CMC, the 6DT gave higher k_La values than the 6PSDT which was the poorest performer at this CMC concentration.

Hold-up results presented in Chapt.6 showed similar relative impeller performances to those seen for k_La in 0.4% CMC. The IM and 6MFD types gave the highest values of ε_G particularly at v_s = 0.006 [ms^{-1}] indicating that the enhanced k_La values for these agitators were achieved by

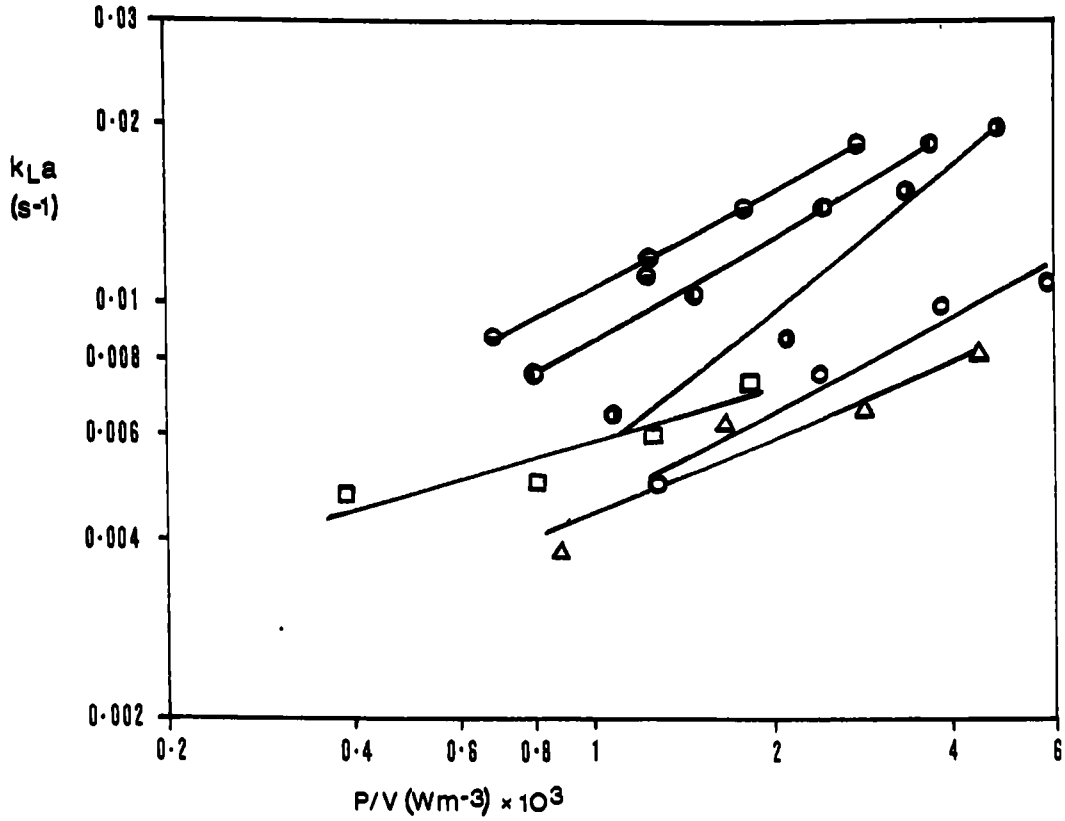

Figure 7.13 k_La v P/V, T72, 0.4% CMC, H/T = 1, v_s=0.006 [m/s].

6DT:○, 6MFU:◐, 6MFD:●, A315:□, 6PSDT:△, InterMIG (MRS):◒.

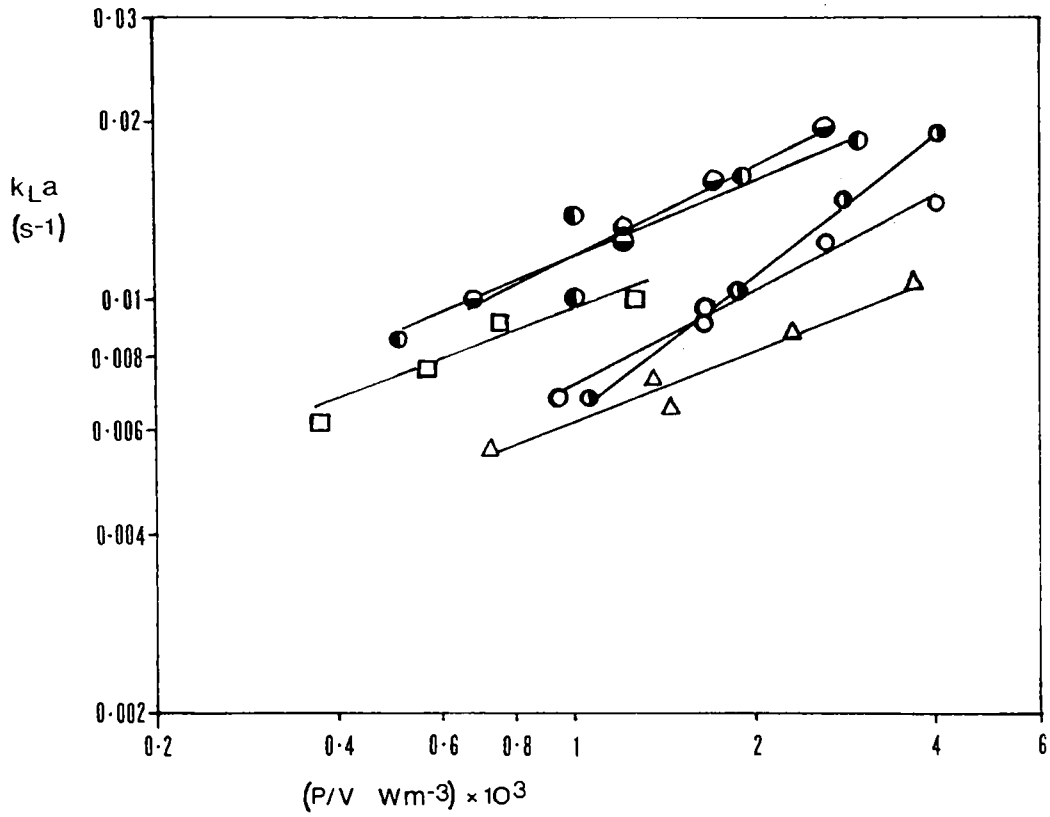

Figure 7.14 k_La v P/V, T72, 0.4% CMC, H/T = 1, v_s=0.012 [m/s].

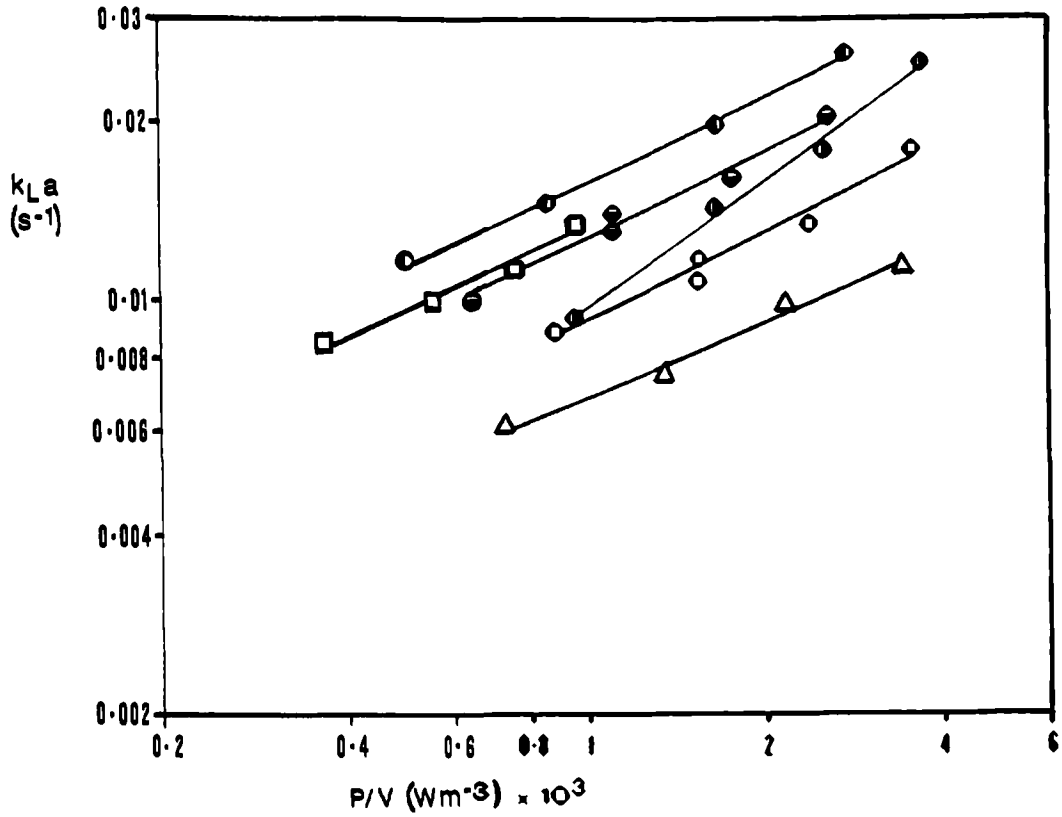

Figure 7.15 $k_L a$ v P/V, T72, 0.4% CMC, H/T = 1, v_s=0.018 [m/s].

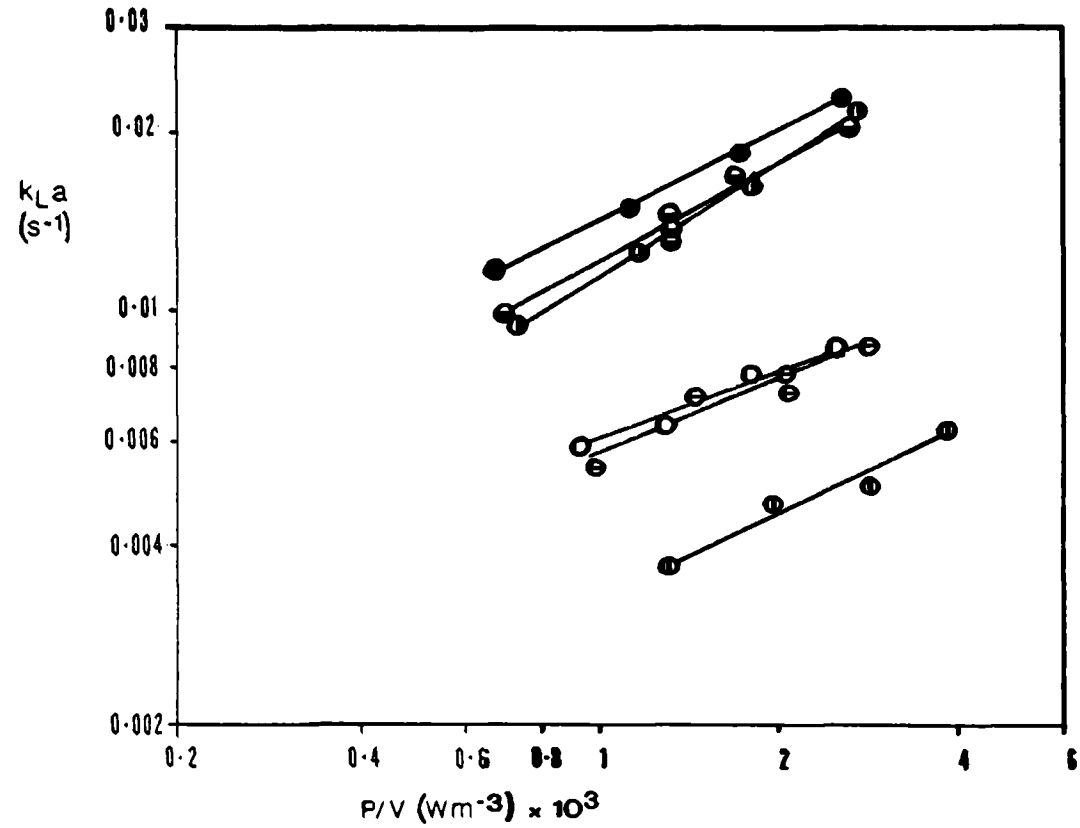

Figure 7.16 $k_L a$ v P/V, T72, 0.4% CMC, H/T = 2, 6DT: o, IM (MRS): ●

v_s=0.006 [m/s]: ⊙ , 0.012 [m/s]: ⊖ , 0.018 [m/s]: o .

enhancing interfacial area for oxygen transfer. The A315 hold-up improved relative to the other agitators with increased v_s, as did k_La. The 6PSDT gave both the lowest hold-up and k_La values overall in this concentration of CMC.

Table 7.3 gives the individual agitator correlations obtained in 0.4% CMC. The P/V exponents were similar to those found in 0.07% CMC in all cases except that of the A315 where the exponent was reduced from 0.49 to 0.3. The variation in P/V exponents was small when comparing the impellers tested in 0.4% CMC, the only significant deviations being the 6MFU where $k_La \propto P/V^{0.76}$ and A315 where $k_La \propto P/V^{0.3}$.

As previously noted, the variation in the v_s exponent was much more marked than that of P/V. The A315 again showed a stronger dependency of k_La on v_s than was the case for the other impellers tested. The IM at both H/T = 1 and 2 was only influenced to a small extent by variation in v_s; this was consistent with the results in all other fluids tested.

A variety of combined correlations are shown in Table 7.3. Firstly, combining 6DT and 6PSDT data (no.9) provided a significantly worse fit at the 5% and 1% levels than the individuals (nos.1 and 4), indicating a divergence in k_La at this CMC concentration. Secondly, combining 6MFU and 6MFD (no.11) also provided a significantly worse fit at the 5% level than the individuals. The pumping modes of the mixed flow impeller must therefore be considered separately for k_La estimation.

Hold-up correlations in 0.4% CMC are shown in Table 6.3, k_La values were seen to be more dependent on P/V than hold-up values. The 6PSDT for example, exhibited a strong dependence of k_La on P/V but negligible dependence of hold-up on P/V. The 6MFU hold-up was more strongly affected by P/V. The IM hold-up and k_La were both less influenced by v_s changes than other agitators whilst the A315 hold-up and k_La were both more influenced by v_s than the others.

TABLE 7.3

$k_L a$ CORRELATIONS IN 0.4% CMC

$$k_L a = K\,(P/V)^{\alpha}\,(v_s)^{\beta} \qquad [Wm^{-3}]\ [ms^{-1}]$$

No.	Impeller Type	Sparger Type	K ($x10^{-3}$)	α	β	Number of Points	R^2
1	6DT 1:1	PS	2.6	0.52	0.59	14	0.98
2	6DT 2:1	PS	2.6	0.42	0.51	14	0.89
3	A315	Ring	22.0	0.3	0.66	13	0.94
4	6PSDT	PS	2.1	0.42	0.42	13	0.95
5	IM 1:1	MRS	0.58	0.51	0.12	14	0.98
6	IM 2:1	MRS	0.5	0.55	0.14	14	0.96
7	6MFD	Ring	3.7	0.5	0.51	13	0.93
8	6MFU	Ring	0.25	0.76	0.42	14	0.94
9	Combined 1,4		2.22	0.5	0.53	27	0.87
10	Combined 5,6		0.53	0.54	0.13	29	0.94
11	Combined 7,8		2.4	0.5	0.44	27	0.74
12	Combined 1,2		1.8	0.56	0.61	28	0.69

7.4.3 Effect of aspect ratio on k_La in 0.4% CMC

Figure 7.16 compares the performances of IM and 6DT at H/T = 2. The 4 IM gave a considerably enhanced k_La when compared to that obtained using 2 6DT, although the influence of v_s was greater with the latter (as observed in other fluids at H/T = 1). Figure 7.17 shows IM k_La results at both H/T = 1 and 2, it can be seen from this figure that the k_La values obtained were unaffected by the increase in aspect ratio.

Hold-up was also greater for IM when compared with 6DT at H/T = 2, although the variation of ε_G with v_s was greater than the variation of k_La with v_s for InterMIG. Similarly ε_G at H/T = 1 and 2 remained a constant fraction of the vessel volume for IM supporting the k_La findings.

Combined correlations (Table 7.3 nos. 10 and 12) for IM and 6DT at H/T=1 and 2 both showed significantly worse data fits than the individuals at 5% significance level. However at the 1% level, correlation no.10 (IM H/T = 1 and 2) was not significantly different from the component correlations (nos. 5 and 6).

7.5 OXYGEN MASS TRANSFER RESULTS IN 0.8% CMC

7.5.1 Introduction

The most viscous CMC solution used in this study was 0.8% (μa 0.17 - 0.4 Pa.s). In this section, k_La results are presented for six impeller types at H/T=1 and two impeller types at H/T=2. The Re range was 8.4 x 10^2 to 5 x 10^3 (transitional regime).

7.5.2 Effect of impeller type on k_La in 0.8% CMC

The k_La results at H/T=1 are compared in Figs. 7.18 to 7.20, each describing a different gas velocity. The six impellers covered in the previous sections are represented, although the IM results are given for both PS and MRS. The inter-impeller k_La variation at constant P/V and v_s was considerable. The A315 exhibited a much improved performance relative

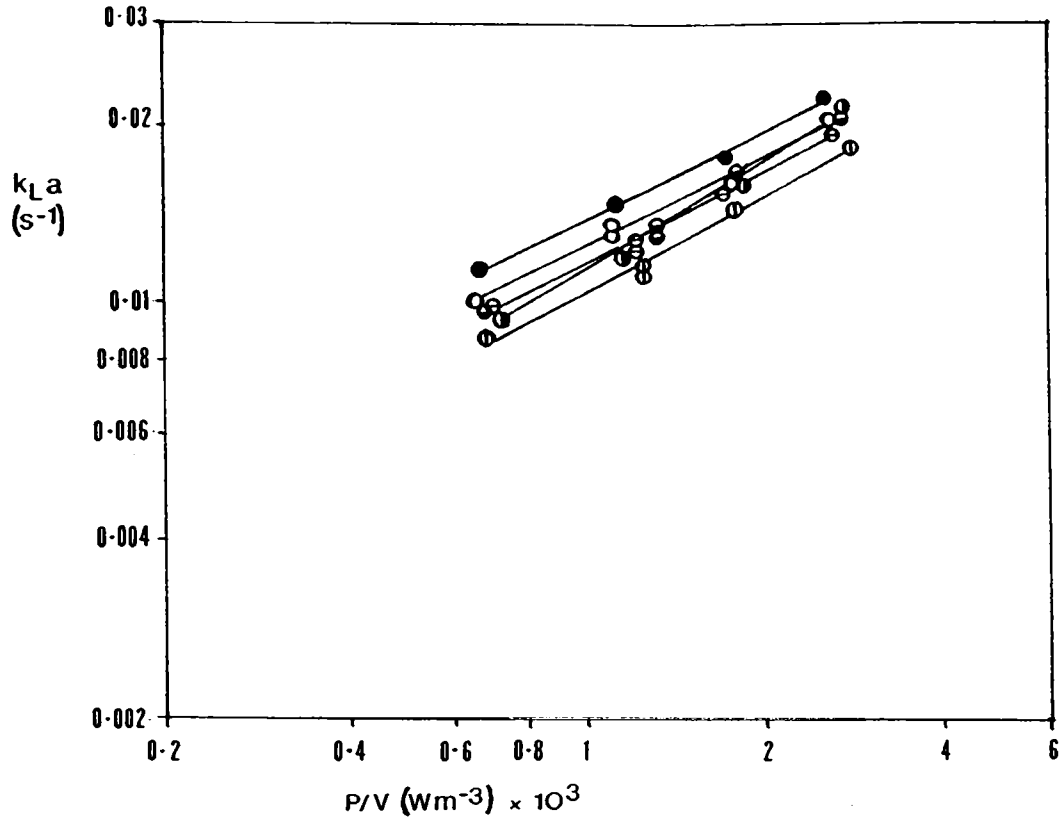

Figure 7.17 $k_L a$ v P/V, T72, 0.4% CMC, InterMIG (MRS).
H/T = 1, v_s=0.006 [m/s]: ◑ ,0.012 [m/s]: ⊖ ,0.018 [m/s]: ● .
H/T = 2, - : ◐ - : ⊖ - : o

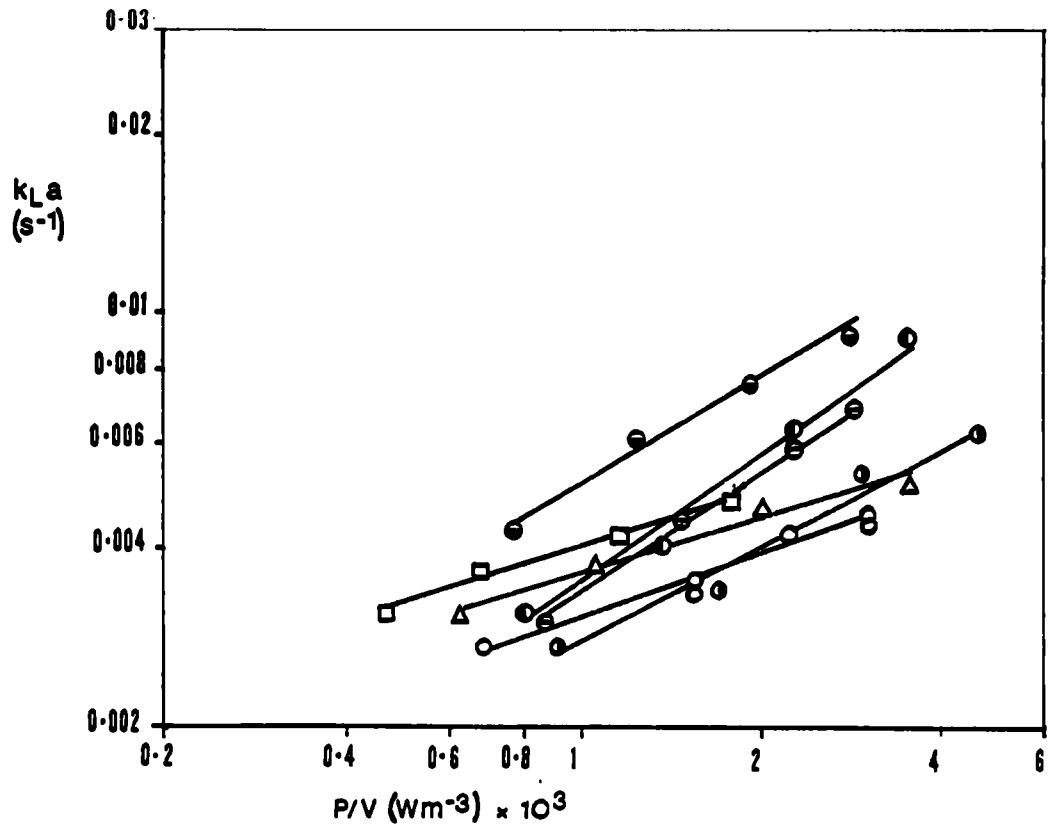

Figure 7.18 $k_L a$ v P/V, T72, 0.8% CMC, H/T = 1, v_s=0.006 [m/s].
6DT: o , 6MFU: ◑ , 6MFD: ◐ , IM (PS): ⊖ , IM (MRS): ⊖ .
A315: □ , 6PSDT: △ .

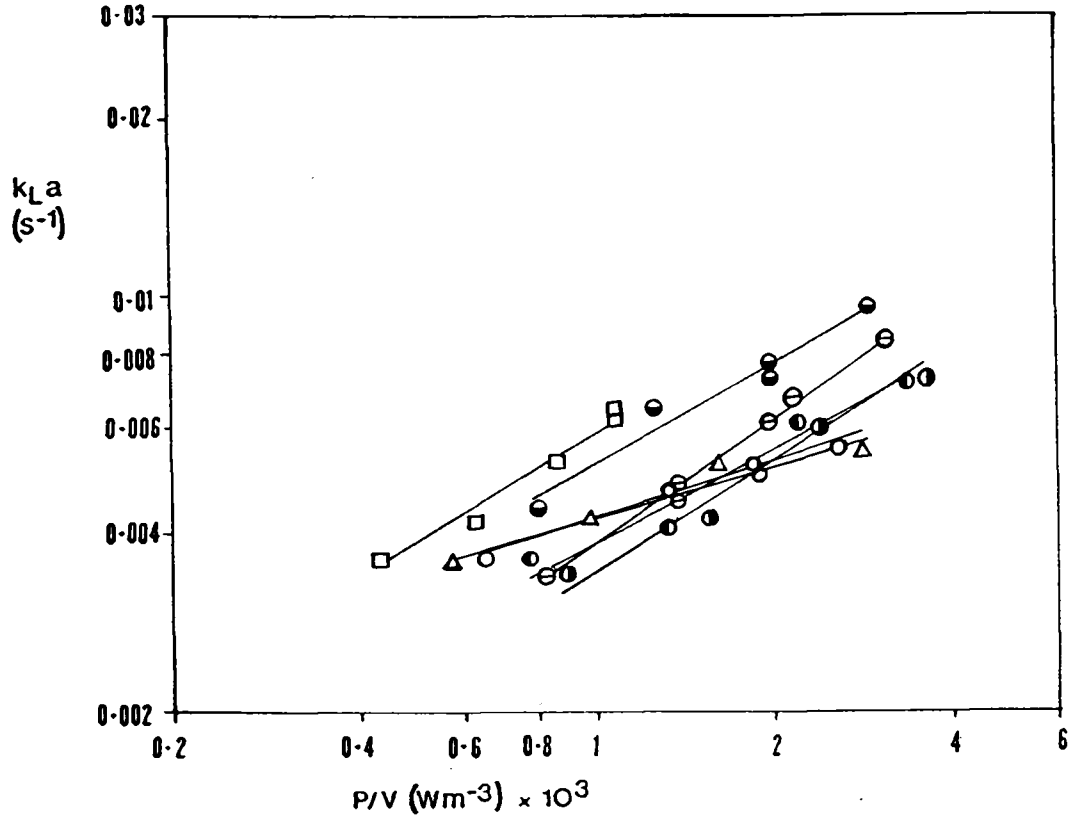

Figure 7.19 k_La v P/V, T72, 0.8% CMC, H/T = 1, v_s=0.012 [m/s].

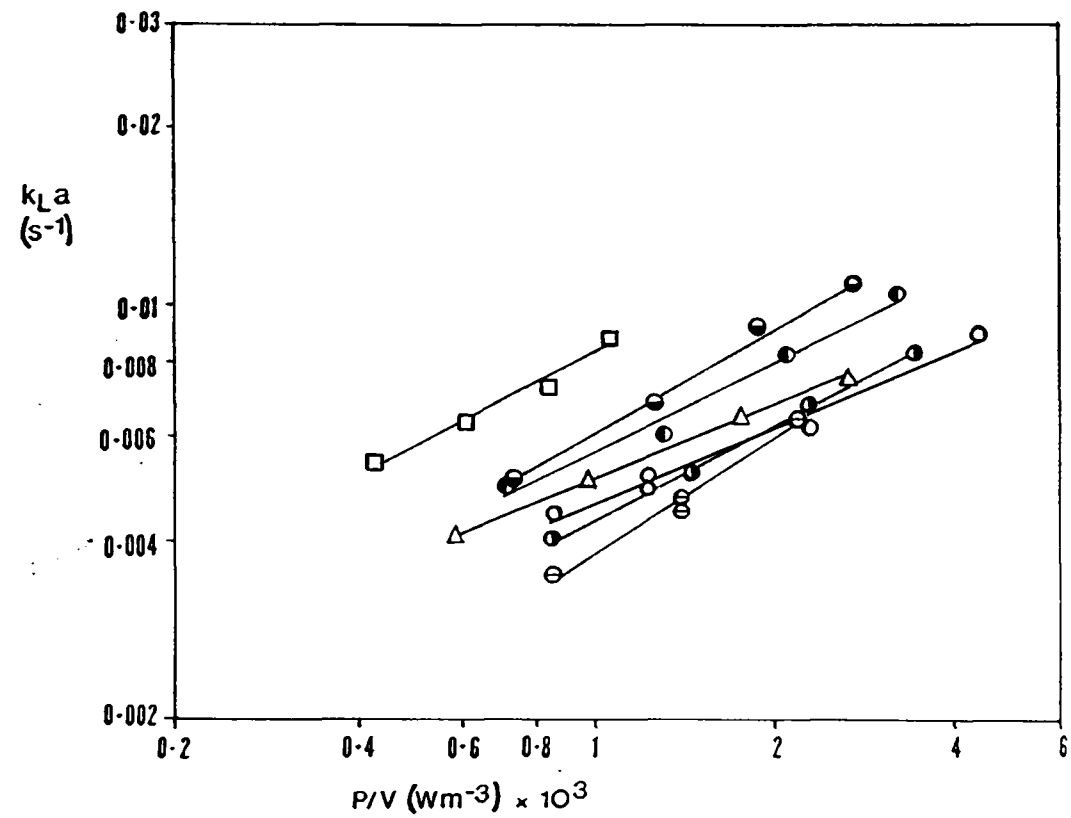

Figure 7.20 k_La v P/V, T72, 0.8% CMC, H/T = 1, v_s=0.018 [m/s].

to the other types at this CMC concentration. The A315 was also more strongly affected by v_s(as observed in other fluids), at both v_s = 0.012 [ms^{-1}] and v_s = 0.018 [ms^{-1}] the A315 gave the highest k_La values of the impellers tested. The IM with MRS provided a considerably enhanced mass transfer performance compared with the PS at all v_s, and gave the second highest performance overall. The 6MF again performed better in the D.P.M. and the 6DT and 6PSDT gave similar overall performances.

Figure 7.21 compares 2 6DT and 4 IM at H/T=2. The IM k_La results show a greater P/V dependence and a lesser $v_s$dependence than the 6DT. The IM k_La was greater than the 6DT at both v_s = 0.006 [ms^{-1}] and v_s = 0.012 [ms^{-1}] for P/V > 1 [kWm^{-3}]. These findings were consistent with those at a H/T=1.

Hold-up results for the various agitators in 0.8% CMC (Section 6.3.3) showed both similarities and significant differences from the k_La results. The IM (MRS) gave both the highest hold-ups and k_La values under given conditions (also seen in 0.4% CMC). The IM (PS) provided almost identical hold-ups to those obtained with the MRS but k_La results showed considerable reduction. This finding implies that the interfacial area available for oxygen transfer was reduced when using a PS. A significantly greater proportion of the PS hold-up consisted of large sluglike bubbles, due to the IM being unable to break-up bubbles effectively with the inner blades.

As previously mentioned, Fig.7.21 compares 6DT and IM k_La results at H/T = 2. The corresponding hold-up results are shown in Fig.6.23, the IM hold-up was greatly enhanced compared to the 6DT.

Table 7.4 lists correlations obtained in 0.8% CMC. There is a greater variation in P/V exponents than was found in other CMC concentrations and water. There is also a wide range of v_s exponents, as seen in the other fluids. Considering the 6DT results first, it can be seen that the P/V exponents were reduced at this CMC concentration; also,

TABLE 7.4

$k_L a$ CORRELATIONS IN 0.8% CMC

$$k_L a = K\,(P/V)^{\alpha}\,(v_s)^{\beta} \qquad [Wm^{-3}]\ [ms^{-1}]$$

No.	Impeller Type	Sparger Type	K ($x10^{-3}$)	α	β	Number of Points	R^2
1	6DT 1:1	PS	2.2	0.34	0.38	16	0.99
2	6DT 2:1	PS	6.2	0.33	0.6	16	0.93
3	A315	Ring	4.2	0.44	0.6	13	0.92
4	6PSDT	PS	2.0	0.33	0.33	12	0.95
5	InterMIG 1:1	MRS	0.18	0.58	0.13	13	0.95
6	InterMIG 2:1	MRS	0.14	0.65	0.22	13	0.92
7	InterMIG 1:1	PS	0.05	0.72	0.14	16	0.98
8	InterMIG 2:1	PS	0.03	0.73	0.02	17	0.89
9	6MFD	Ring	0.34	0.57	0.31	12	0.84
10	6MFU	Ring	0.51	0.54	0.4	12	0.98
11	Combined 9,10		0.5	0.53	0.35	24	0.81
12	Combined 1,2		3.25	0.33	0.46	32	0.93
13	Combined 5,6		0.13	0.64	0.18	26	0.9
14	Combined 7,8		0.036	0.74	0.09	32	0.9
15	Combined 1,4		2.39	0.32	0.36	28	0.93

there is good agreement between the two aspect ratios in this respect. The influence of v_s was reduced at H/T=1 when compared with the other test fluids. The A315 again exhibited a stronger dependency of k_La on v_s than on P/V. Comparing the 6PSDT exponents with those for other test fluids revealed a lower influence of both P/V and v_s at this CMC concentration. The exponents themselves were very similar to those for the 6DT.

IM results in 0.8% CMC showed a general increase in the influence of P/V on k_La which was more marked when using a point sparger. This finding differs from the general trend of decreased P/V effect at this CMC concentration. Again with IM only a small influence of v_s on k_La was apparent (as found under all conditions).

The 6MF gave similar P/V exponents in both pumping modes in 0.8% CMC, differing from results in 0.07% and 0.4% CMC where the U.P.M. showed a stronger influence of P/V on k_La. In the U.P.M. the dependence of k_La on v_s was little changed from 0.4% CMC. In the D.P.M. it was reduced. Statistical 'F' tests were used to show a worse fit at 5% significance level for combined correlations no.11 (6MFU/D) and no.15 (6DT/6PSDT) than the individual impeller correlations.

Hold-up correlations are given in Table 6.4 for this CMC concentration. As found in 0.4% CMC, the 6PSDT hold-up was unaffected by P/V increase. IM hold-up, like k_La, showed a reduced influence of v_s in 0.8% CMC. The A315 hold-up and k_La responded more to v_s increases than the other agitators.

7.5.3 Influence of aspect ratio in 0.8% CMC

Figures 7.22 and 7.23 show comparisons between IM (MRS) at H/T=1 and 2 and 6DT at H/T=1 and 2 respectively. The IM k_La values are similar at the two aspect ratios, however, the influence of v_s is marginally greater at H/T = 2. The results for 6DT at the two aspect ratios show little affect of H/T on the P/V exponent. Figure 7.24

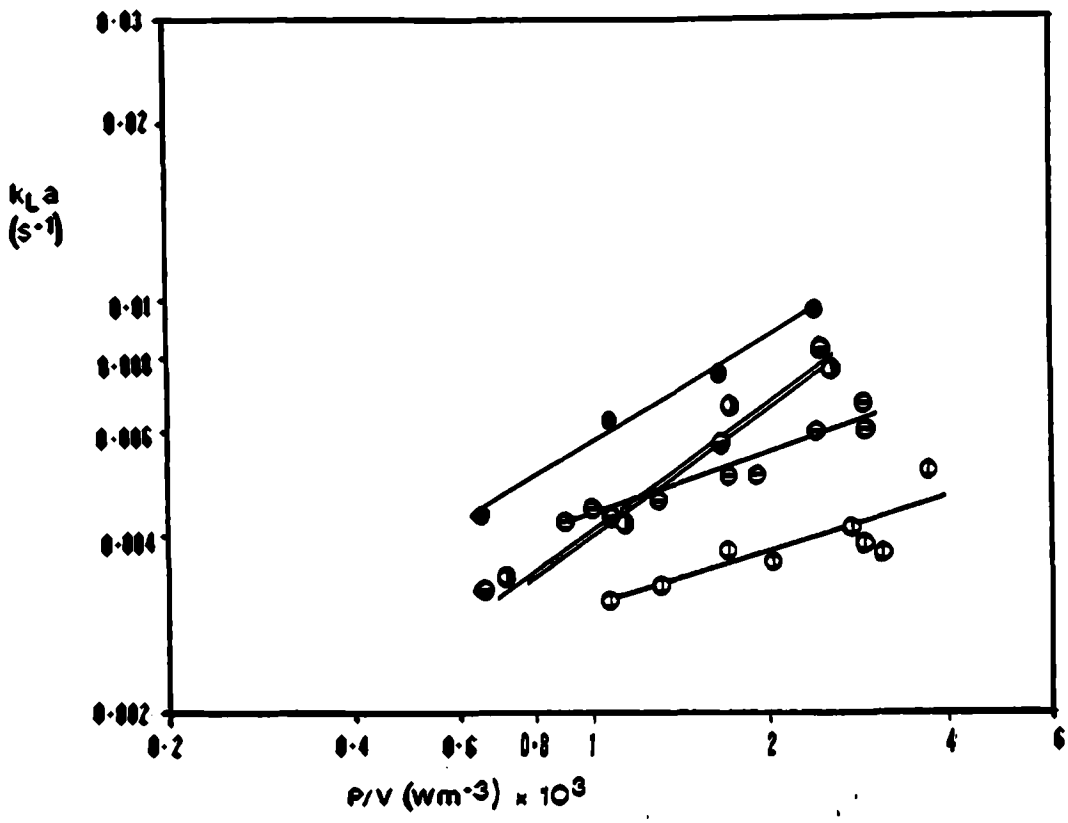

Figure 7.21 $k_L a$ v P/V, T72, 0.8% CMC, H/T = 2, 6DT:o,IM(MRS):◆ v_s=0.006 [m/s]:⊕, 0.012 [m/s]:●, 0.018 [m/s]:● .

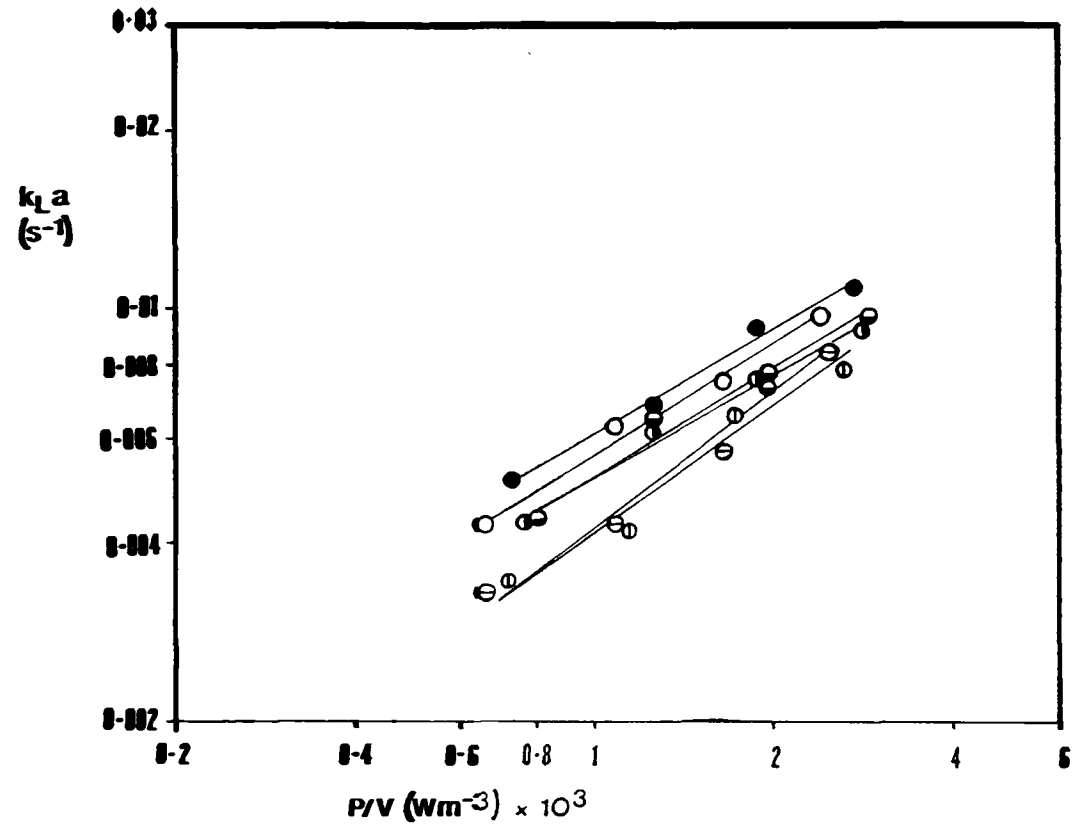

Figure 7.22 $k_L a$ v P/V, T72, 0.8% CMC, InterMIG (MRS).
H/T = 1, v_s=0.006 [m/s]:⊕ ,0.012 [m/s]:⊖ ,0.018 [m/s]:● .
H/T = 2, - :⊕, - :⊖, - :o .

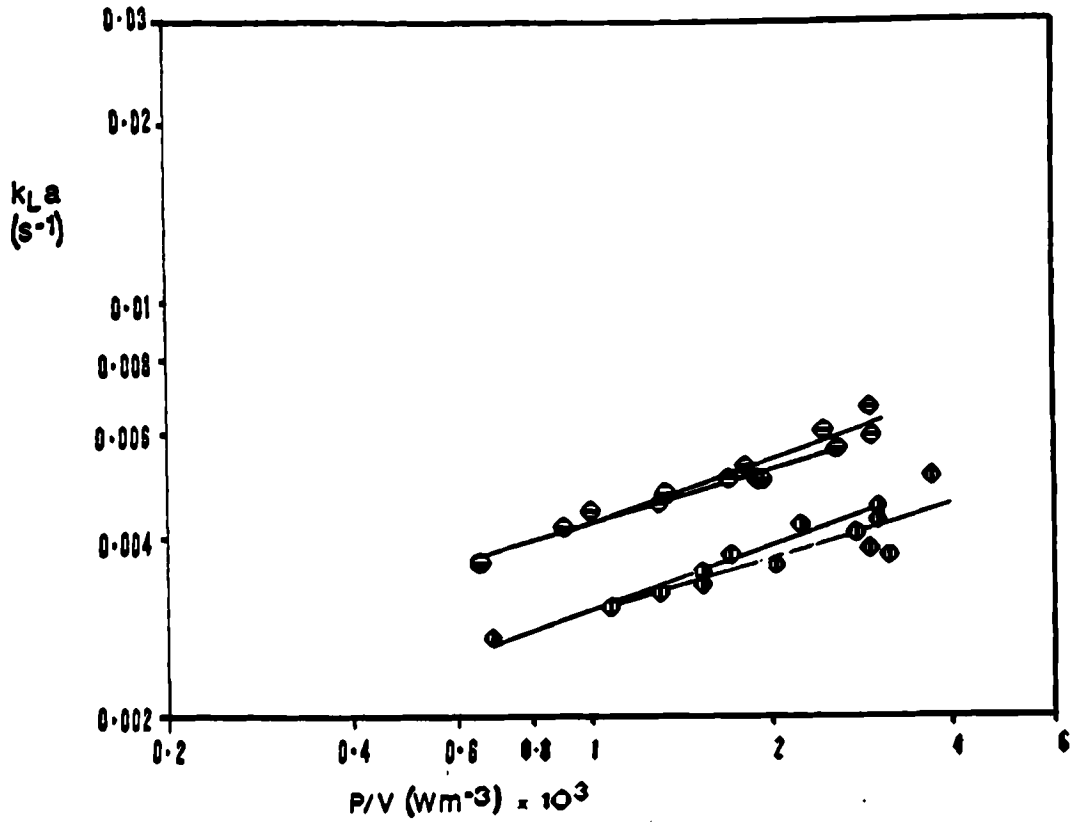

Figure 7.23 $k_L a$ v P/V, T72, 0.8% CMC, 6DT.
H/T = 1, v_s=0.006 [m/s]: ◆ ,0.012 [m/s]: ◆
H/T = 2, . : ⊕ , . : ⊖,

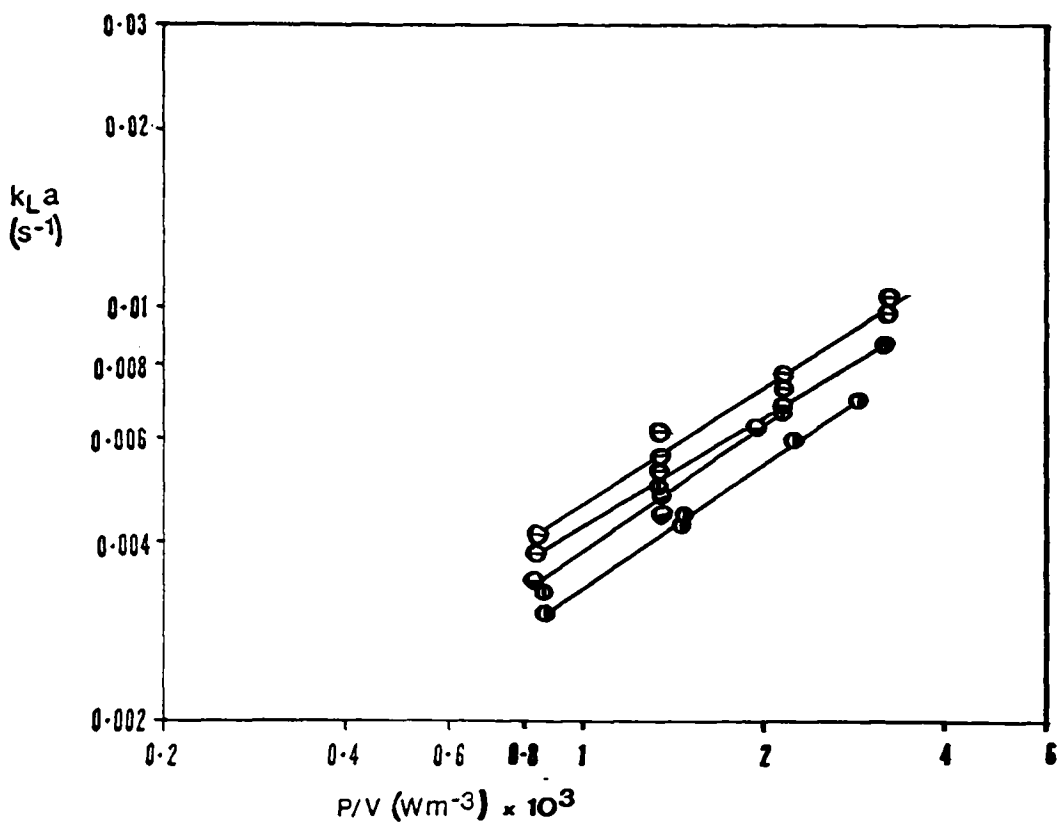

Figure 7.24 $k_L a$ v P/V, T72, 0.8% CMC, InterMIG (PS).
H/T = 1, v_s=0.006 [m/s]: ● ,0.012 [m/s]: ⊖ .
H/T = 2, . : ⊕ , . : ⊖ .

compares k_La values obtained at H/T=1 and 2 using IM impellers with a point sparger (PS). The P/V exponent was not affected by H/T increase. The results at H/T = 2 were close to those obtained at H/T = 1.

Reference to the corresponding hold-up results in Chapt.6 (Figs.6.24 to 6.27) indicated no affect of aspect ratio for IM (MRS). The 6DT hold-up at H/T = 1 and 2 showed a high degree of scatter, not evident in the k_La results. The two aspect ratios gave similar hold-ups at v_s = 0.012 [ms^{-1}] but not at v_s = 0.006 [ms^{-1}]. Statistical 'F' tests using individual and combined aspect ratio correlations from Table 7.4 showed no significant difference between IM (MRS) at H/T = 1 and 2 at the 5% significance level (nos.13, 5 and 6). The IM (PS) combined aspect ratio correlation (no.14) showed a significantly worse fit than the individuals at the 5% level as did the 6DT combined correlation (no.12).

7.6 THE INFLUENCE OF APPARENT VISCOSITY ON k_La

7.6.1 Introduction

The k_La results presented in Sections 7.2 for water and Sections 7.3 to 7.5 for viscous non-Newtonian CMC solutions indicate that k_La is strongly reduced with increasing viscosity. In this section, the relationship between apparent viscosity and k_La is investigated in the range 0.001 to 0.4 Pa.s.

It should be noted that when combining results from water and CMC solutions, the non-coalescence in CMC of low viscosity (0.07%), leads to an increase in interfacial area that counteracts the decrease in k_L due to viscosity increase. Therefore large errors in the assessment of k_La dependence on μa can occur by combining deionised water and CMC data. An improved approach involves the correlation of CMC k_La data with that obtained in electrolyte solutions with non-coalescent behaviour. Both methods are compared in the following section and their effect on the viscosity exponent commented upon.

TABLE 7.5

CONSTANT CMC CONCENTRATION CORRELATIONS

(ALL IMPELLERS) 1:1 ASPECT RATIO

$$k_L a = K\,(P/V)^{\alpha}\,(v_s)^{\beta}\,(\mu a)^{\gamma} \qquad [Wm^{-3}]\ [ms^{-1}]\ [Pa.s]$$

CMC Concentration	K ($\times 10^{-3}$)	α	β	γ	No. Points	R^2
0.07%	0.49	0.39	0.23	-0.73	84	0.74
0.4%	0.59	0.34	0.35	-0.87	82	0.75
0.8%	0.78	0.31	0.29	-0.82	93	0.76

TABLE 7.6

COMBINED CORRELATIONS

(Utilizing $k_s = 11.5$)

$$k_L a = K\,(P/V)^{\alpha}\,(v_s)^{\beta}\,(\mu a)^{\gamma} \qquad [Wm^{-3}]\ [ms^{-1}]\ [Pa.s]$$

No.	Impeller Type	K $\times 10^{-3}$	α	β	γ	Number of Points	R^2
1	A315	1.39	0.3	0.46	-0.86	40	0.97
2	InterMIG	0.14	0.42	0.06	-0.79	59	0.99
3	6MFU	0.12	0.45	0.22	-0.96	39	0.96
4	6MFD	0.2	0.43	0.19	-0.87	38	0.99
5	All, 1:1 CMC	0.52	0.34	0.27	-0.84	259	0.96

The calculation of μ_a in shear thinning CMC solutions requires a shear rate to be determined using values of k_s from the literature (Table 3.3). Two approaches were taken in this work; firstly the use of varying k_s depending on impeller type and secondly the use of k_s = 11.5 for all impellers. The results of these methods were compared in the form of correlations for each impeller type and for all impellers combined (see Tables 7.6 and 7.7).

The k_La correlations listed in Table 7.6 were tested statistically in order to discover whether the use of k_s as a constant (11.5) for all impellers significantly increased the variance of the data compared to the use of different k_s values for individual impellers. Correlations 1 to 4 Table 7.6 were tested against Correlations 2,4,5 and 6 Table 7.7. At the 5% significance level none of the constant k_s correlations showed a worse fit than the correlations using different k_s values. The overall correlations (no.7 Table 7.7 and no.5 Table 7.6) did not show a significant increase in variance either. Therefore the use of constant k_s values for the calculation of shear rate using the Metzner and Otto[4] approach did not significantly alter the correlation of k_La with P/V, v_s and μa for a range of impeller types. The relationship between k_La and μa for individual agitator types at constant CMC conc., P/V and V_s therefore depends almost entirely upon variations of N and not k_s in determining the shear rate.

7.6.2 k_La variation with apparent viscosity.

Fig.7.25 illustrates the k_La values obtained at constant P/V and v_s in 0.2M NaCl, 0.07%, 0.4% and 0.8% CMC solutions using six impeller types. The k_La with NaCl was higher than that with 0.07% CMC but not as much as the ten fold viscosity difference would suggest. The k_La values fell sharply with increasing viscosity in CMC.

It was apparent that the various impellers showed different values of

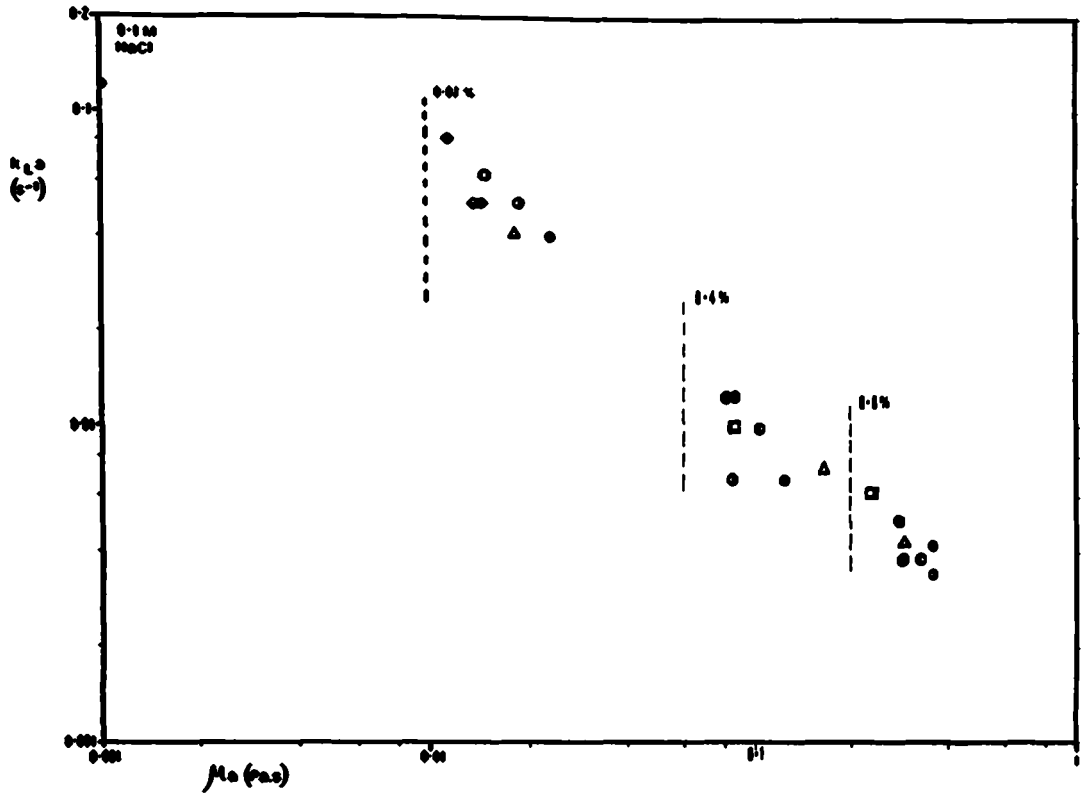

Figure 7.25 k_La v μ_o, T72, P/V = 1 [kW/m^3], v_s=0.012 [m/s].

A315:□, 6DT:●, 6PSDT:△, 6MFU:○, 6MFD:◐, IM (PS):◒,IM (MRS)◓

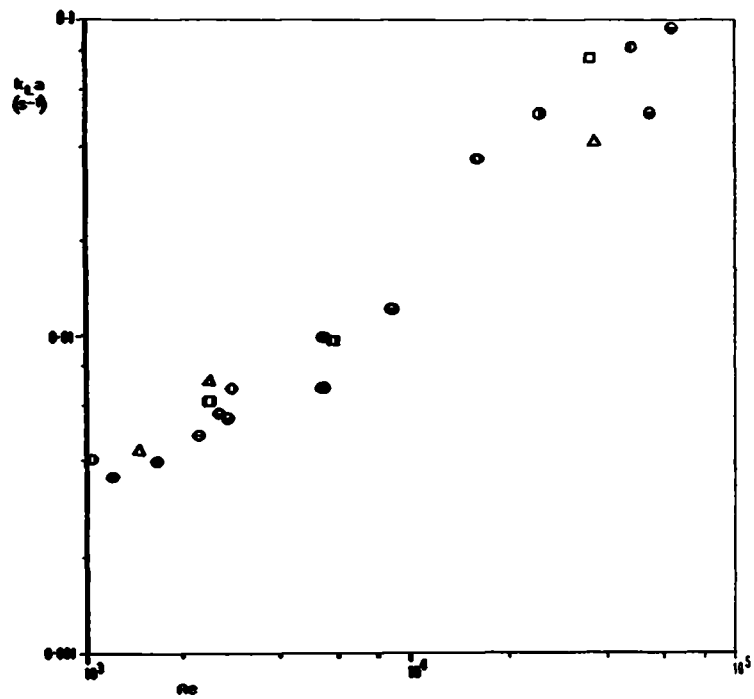

Figure 7.26 k_La v Re, T72, P/V = 1 [kW/m^3], v_s=0.012 [m/s].

Key as Fig. 7.25.

μa in the same concentration of CMC. This was due to both inter-impeller shear-rate variation and inter-batch K and n variation. At each CMC concentration the dependence of $k_L a$ on μa for all impellers combined is shown in Table 7.5. This dependence ($k_L a \propto \mu a^{-0.8}$) was close to that found when combining data using one impeller type at differing CMC concentrations (Table 7.7).

At constant P/V and v_s the various agitator types exhibit different Pog values due to differing design, D/T and cavity formation. Considering agitators of equal D/T but differing Pog, e.g. A315 and 6PSDT, those with lower Pog operate at higher N, higher shear-rates and therefore lower μa. This appears to be advantageous as $k_L a$ rises with decreasing apparent viscosity. Inspection of Pog values from Chapters 4 and 5 shows that those impellers with low Pog tended to provide higher $k_L a$ values at constant power input in shear-thinning liquids. The IM (Pog $\simeq$ 0.3) proved superior to the 6DT or 6PSDT (Pog $\simeq$ 2 to 3) in all concentrations of CMC. The advantage of low Pog impellers will only manifest itself when comparison is made on the basis of aerated P/V. Operation at equal N will not provide improved $k_L a$ performance for impellers such as the IM as the power drawn will be much lower. In order to improve $k_L a$ in an existing vessel, impeller retrofitting at equal P/V, N and torque is necessary unless motor and/or gearbox changes are made. In this situation low Pog impellers may be used by increasing D/T and/or number of stages so that the above conditions are met[121].

Fig.7.26 shows $k_L a$ v Re for the various impellers and CMC concentrations at P/V = 1 kWm^{-3} and v_s = 0.012 ms^{-1}. As was expected $k_L a$ increased with increasing Re for all impellers and no plateau regions were apparent. The Re range covers the transitional and turbulent regimes. From the data presented in Fig.7.26 little effect of different agitators on the Re - $k_L a$ relationship is apparent. Table 7.7 gives a correlation using Re instead of μ_a as a parameter with which to correlate $k_L a$.

TABLE 7.7

COMBINED CORRELATIONS

(Utilizing k_s From Table 3.3)

$$k_L a = K\,(P/V)^{\alpha}\,(v_s)^{\beta}\,(\mu a)^{\gamma} \qquad [Wm^{-3}],\ [ms^{-1}],\ [Pa.s]$$

No.	Impeller Type	K x 10^{-3}	α	β	γ	Number of Points	R^2
1	6DT	1.77	0.24	0.38	-0.81	45	0.97
2	A315	1.32	0.3	0.46	-0.87	40	0.97
3	6PSDT	1.01	0.31	0.37	-0.79	38	0.98
4	InterMIG	0.13	0.42	0.06	-0.81	59	0.99
5	6MFU	0.12	0.45	0.22	-0.97	39	0.95
6	6MFD	0.19	0.43	0.2	-0.88	38	0.99
7	All, 1:1 CMC	0.47	0.34	0.27	-0.85	259	0.96
8	All, 2:1 CMC	0.4	0.27	0.16	-0.91	81	0.88
9	All CMC	0.46	0.32	0.25	-0.86	340	0.95
10	All, 1:1 NaCl/CMC	0.55	0.33	0.27	-0.8	264	0.95
11	All NaCl/CMC	0.0116	0.12	0.21	$Re^{0.8}$	345	0.94
12	All NaCl/CMC	0.54	0.32	0.25	-0.81	345	0.94
13	All Data	1.16	0.39	0.39	-0.5	433	0.81

7.6.3 Overall Mass Transfer Correlations

Mass transfer results for each agitator type tested in this work are listed in Table 7.7 as are correlations combining various sets of data using differing fluids and aspect ratios. Comparing the overall correlations for each impeller type at H/T = 1 in CMC (nos.1 to 6 Table 7.7) shows P/V exponents ranging from 0.24 (6DT) to 0.45 (6MFU). The impellers with higher values of α exhibit lower K values (intercept) indicating a more rapid increase of k_La with P/V but lower k_La values at lower P/V than those impellers with higher K but lower α. The 6MFD, 6MFU and IM display very similar K and α values.

The variation in β (exponent of v_s) was greater than that of α with impeller type. The A315 impeller was the most sensitive to v_s changes, its relative performance improving rapidly with v_s increase. The 6DT and 6PSDT showed similar v_s dependence as did the 6MFU and 6MFD. Those impellers with lower P/V effect showed a higher influence of v_s. The IM k_La values were almost totally insensitive to v_s increase.

The apparent viscosity term used to correlate data from different CMC concentrations was successful in that the correlation coefficients for the various impellers were high. The exponent γ varies little between impellers although that of the 6MFU was higher. Increasing apparent viscosity therefore reduces k_La strongly irrespective of impeller type.

Correlation 7, Table 7.7, combines the data from the previous six individual correlations. The data fit was quite good and 'F' tests at the 5% significance level found only the InterMIG and 6MFD individual correlations to be significantly different from the overall correlation. Figure 7.27 shows the experimental data plotted against the correlation line obtained for all 1:1 aspect ratio CMC values.

Correlation 8 combines all 2:1 CMC data and is a worse fit than the 1:1 correlation with exponents α and β lower, possibly due to the greater proportion of IM data therein (all 2:1 data either 6DT or IM). Testing

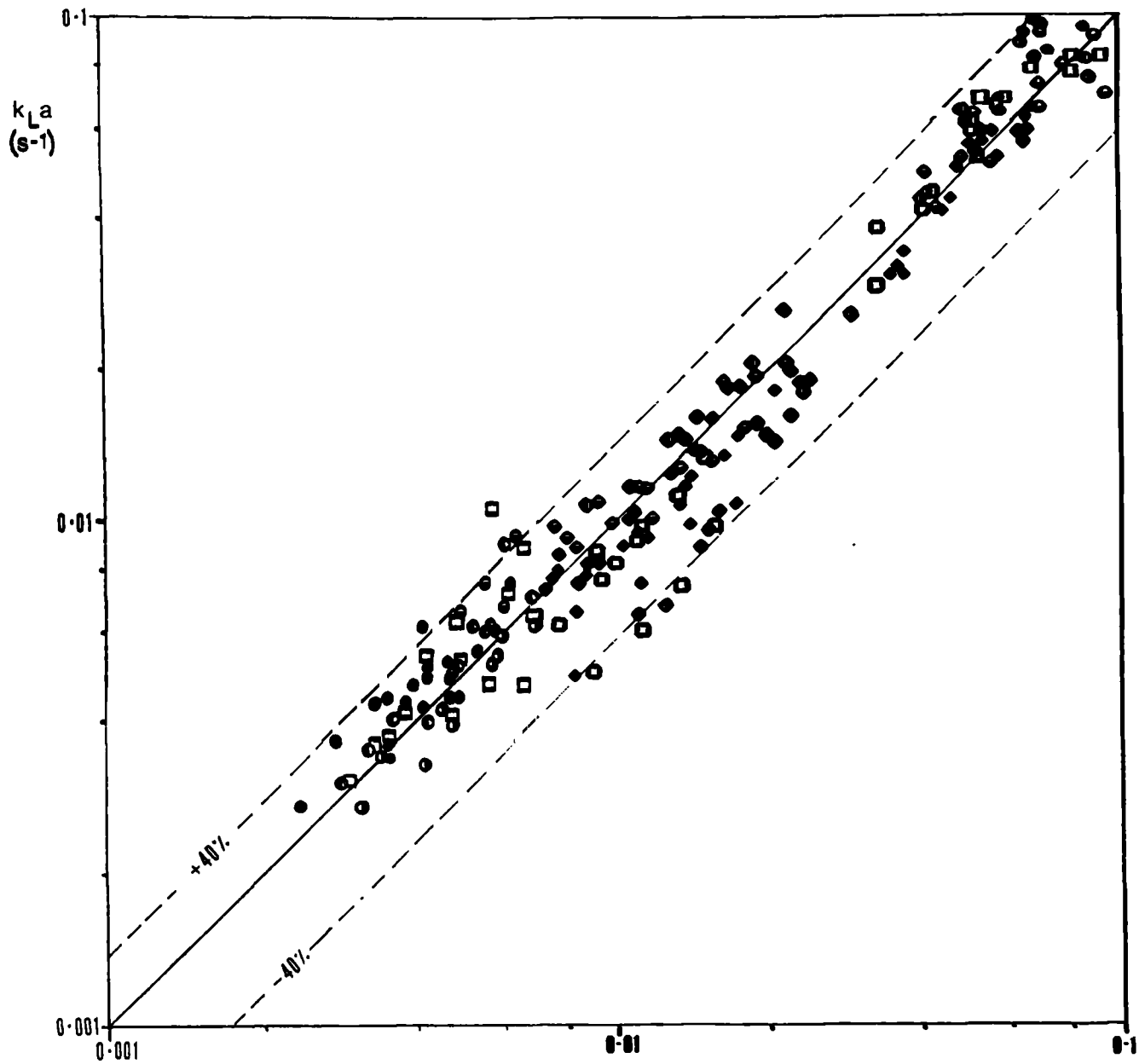

Figure 7.27 k_La v $4.7 \times 10^{-4} (P/V)^{0.34}(v_s)^{0.27}(\mu_a)^{-0.85}$

Key as Fig. 7.25.

the 1:1 and 2:1 correlations against a combined correlation (no.9) at 5% or 1% levels showed them to be significantly different.

Correlation 10 included NaCl data and can be compared with No.7 (CMC only) showing little change in exponents α and β but a slight reduction in γ (see Fig.7.25). Correlations 11 and 12 combine H/T = 1 and 2 in all CMC solutions and NaCl. The former uses Re as an independent variable whilst the latter uses μ_a. The two correlations fit the data as well as each other and the exponents found for Re and μa are of equal magnitude but opposite sign (Re α $1/\mu_a$). However the use of Re reduces the influence of the P/V term due to the incorporation of ND^2 in Re.

Finally correlation 13 amalgamates all k_La data irrespective of fluid, impeller or H/T. The incorporation of water increases the scatter about the correlation line and strongly reduces the influence of apparent viscosity when compared with data from NaCl and CMC alone. The influence of P/V and v_s are increased in this overall correlation.

7.7 GAS PHASE POWER INPUT AND MIXING MODEL SIGNIFICANCE

7.7.1 Power input associated with gas flow into vessel

For gas sparging into a vessel, the power used in compression to sparge a gas volumetric flow rate Q_G at pressure p_1 is [55,119]:

$$P_G = Q_G \rho_G \left[\frac{R.T.}{MW} \ln \frac{p_1}{p_2} + \alpha \frac{u_o^2}{2} \right] \qquad (7.1)$$

Where p_2= pressure at top of vessel.

u_o = gas velocity at sparger orifice.

α = Fraction of kinetic energy transferred to the liquid.

The first term in brackets represents work done in moving the gas through the static liquid head (assumed to occur isothermally) whilst the second refers to the kinetic energy of the gas stream at the sparger holes. The kinetic energy term is often neglected as being small compared to isothermal expansion[119]. The total power into the system can therefore

be calculated by use of :

$$P_t = P_G + P$$

P_t = Total power [kW]
P_G = Sparger gas power [kW]
P = Shaft power [kW]

Comparisons between k_La correlations involving P_t/V and P/V were made for all impellers at 1:1 aspect ratio in C.M.C. Including the sparger gas power increased the overall dependence of k_La upon P_t/V and decreased the influence of v_s, as would be expected. The correlations are shown in Table 7.8.

The magnitude of P_G is greatest relative to shaft power at high v_s and low N, under these conditions P_G may contribute up to 15% of P_t. At lower v_s and higher N, P_G contributes approximately 5% of P_t.

TABLE 7.8

COMPARISON OF OVERALL K_LA CORRELATIONS

INCLUDING P/V AND P_t/V RESPECTIVELY

$$k_La = K\,(P/V)^{\alpha}\,(v_s)^{\beta}\,(\mu a)^{\gamma} \qquad [Wm^{-3}]\ [ms^{-3}]\ [Pa.s]$$

Test Fluid	K ($\times 10^{-3}$)	α	β	γ	No. Points	R^2	Specific Power Term
All, 1:1 CMC	0.47	0.34	0.27	-0.85	259	0.96	(P/V)
All, 1:1 CMC	0.32	0.37	0.25	-0.85	259	0.96	(P_t/V)

Statistical 'F' tests on the two sets of showed that at the 5% significance level there was no difference between them.

7.7.2 Gas phase mixing model influence on results

In order to calculate an oxygen concentration driving force from the NEL/Hickman technique an assumed gas phase mixing model was required (see Appendix III). Previous workers in the field have used a variety of models to describe the gas residence time distribution[87,88]. In this work, two models were applied and their influence upon resultant k_La values assessed. Firstly the 'perfectly mixed gas phase' model was used which implies that all gas bubbles, regardless of their exposure time to the liquid phase, have the same oxygen concentration as the exit gas stream. Secondly the 'plug-flow' mixing model was used which uses a log-mean concentration difference (Appendix III).

TABLE 7.9

$$k_La = K\ (P/V)^{\alpha}\ (v_s)^{\beta}\ (\mu a)^{\gamma} \qquad [Wm^{-3}]\ [\ ms^{-1}]\ [Pa.s]$$

Mixing Model	Test Fluid	K ($x10^{-3}$)	α	β	γ	No. Points	R^2
Plug Flow	All, 1:1 CMC	0.56	0.33	0.29	-0.84	259	0.97
Fully Mixed	All, 1:1 CMC	0.47	0.34	0.27	-0.85	259	0.96

Table 7.9 shows two overall correlations for k_La using the 'fully back mixed' and 'plug flow' concentration driving forces. The two correlations exhibit marginal differences in both constant (K) and exponents (α, β and γ). The 'plug flow' driving force correlation also shows evidence of a slightly improved fit of the correlation to the data. The correlations were tested using an 'F' test at 5% significance level and were found not to be significantly different.

7.8 COMPARISON OF k_La RESULTS WITH THOSE FROM LITERATURE

7.8.1 Introduction

In this section the k_La results from this work are compared with those from literature and comments made. Firstly comparisons are made with studies using pure water and latterly with those using CMC or other non-Newtonian fluids. A vast body of research into mass transfer in agitated aerated vessels is available. However, much of the material is of limited value for comparison due to inaccuracy of the measurement technique, poor power measurement, differing correlation method or incomplete data presentation. The data or correlations used for comparison have been sifted with the above mentioned factors in mind and differences likely to affect the results commented on.

7.8.2 Comparison of water results

Mass transfer results in water are common as it is a useful standard with which to compare differing techniques, vessels, impellers etc. Care must be taken however as many workers do not state whether tap, deionised or distilled water was used. The variety of measurement techniques that have been used for k_La measurements in water are described in Chapter 2, most have associated drawbacks which effect the resultant data. In deionised water the fluid properties are relatively constant leading most workers to correlate using process variables alone.

Table 7.10 lists the constants and exponents obtained when correlating water data obtained using various measurement techniques. All authors used the 6DT impeller but some (including this work) present correlations combining other impellers tested. The range of power inputs and gas velocities used is generally very similar between studies (P/V = 0.1 to 5 kWm^{-3}, v_s = 0.002-0.02 ms^{-1}). Authors have used differing units for P/V and obtained differing values of constants, hence the data is also presented graphically. Fig.7.28 shows the correlations of Table 7.10 at a

TABLE 7.10

LITERATURE CORRELATIONS FOR WATER.

$$k_L a = K\,(P/V)^{\alpha}\,(v_s)^{\beta}$$

Ref.	Technique	Vessels D [m]	Imp.	P/V Units	K	α	β
[114]	Dynamic	0.44, 0.61 0.91, 1.83	6DT 6PSDT	Wm^{-3}	0.01	0.48	0.4
[73]	Dynamic, Separate	V = 0.002-2.6m^3	6DT	Wm^{-3}	0.026	0.4	0.5
[75]	Separate	0.18, 0.5	6DT	Wm^{-3}	0.025	0.4	0.5
[122]	Dynamic, 2-probe.	0.31-1.83	6DT	kWm^{-3}	0.17 0.49	0.64 0.76	0.22 0.45
[85]	Dynamic, Sulphite.	0.29	6DT	Wm^{-3}	0.005	0.59	0.4
[79]	NEL/Hick.	0.6, 2.0	6DT	Wm^{-3}	0.043	0.47	0.67
[30]	Dynamic	0.6	Var.	kWm^{-3}	0.2	0.7	0.3
[A.II]	Dynamic, NEL/Hick.	0.3	6DT	kWm^{-3}	0.24	0.7	0.3
THIS WORK	NEL/Hick.	0.72	Var.	Wm^{-3} kWm^{-3}	0.0063 0.41	0.6	0.43

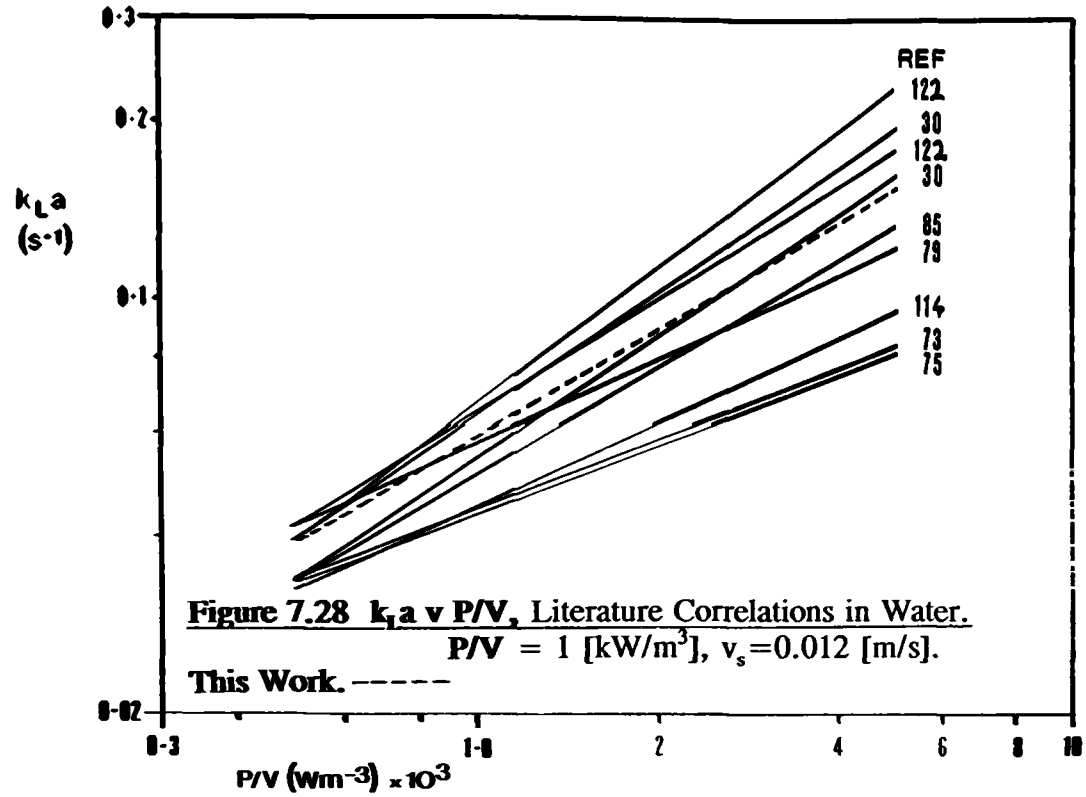

Figure 7.28 $k_L a$ v P/V, Literature Correlations in Water.
P/V = 1 [kW/m^3], v_s=0.012 [m/s].
This Work. – – – –

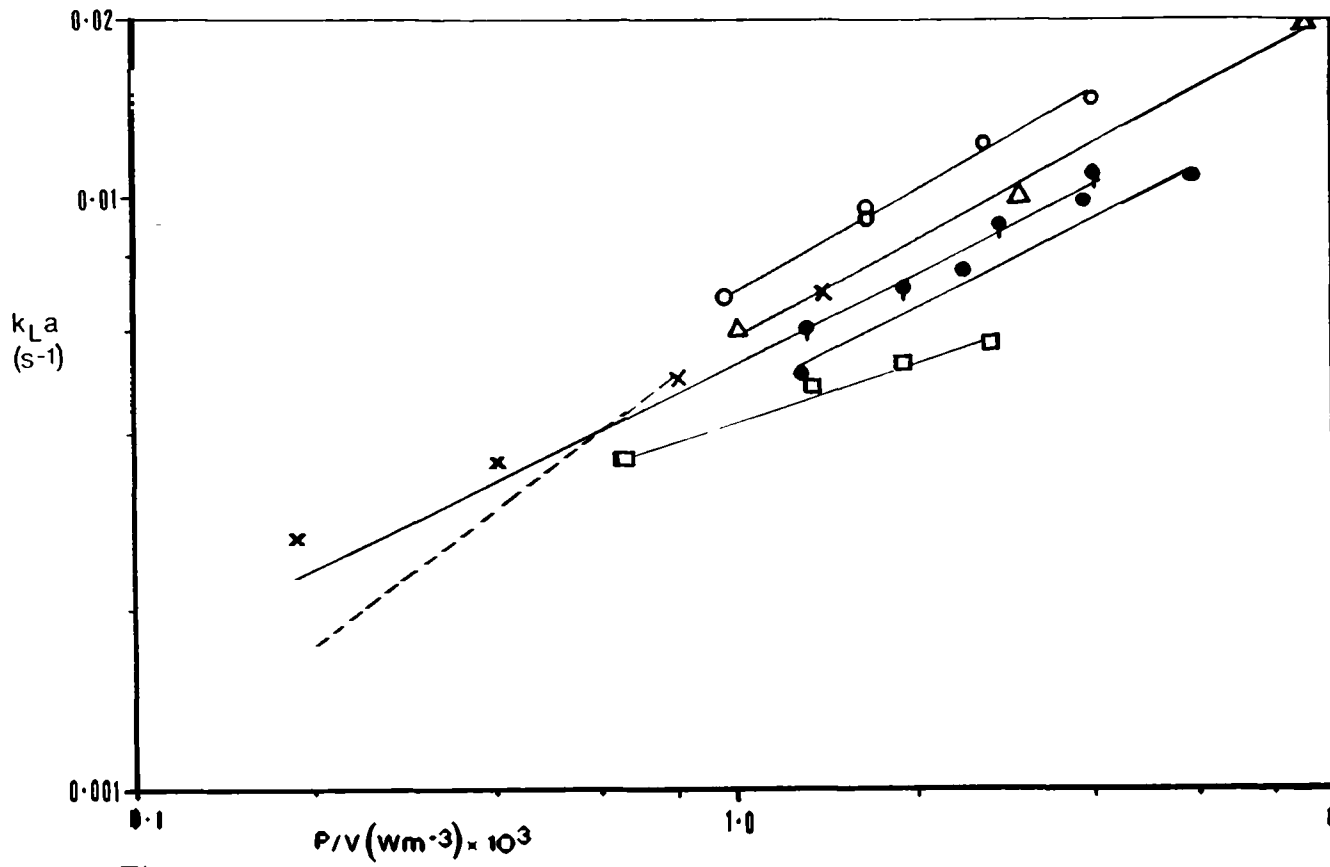

Figure 7.29 $k_L a$ v P/V, Literature Data in CMC, 6DT.
Yagi et. al.[95]: – – – – .
Kipke[41] (D=T/3), v_s=0.011 [m/s], μ_a=0.56[Pa.s]: ● .
This Work (D=T/2), v_s=0.012 [m/s], 0.4% CMC: o , 0.8% CMC: □ .
Hocker[7] (D=T/3), v_s=0.012 [m/s], μ_a=0.22 [Pa.s]: × .
Hickman[20], v_s=0.005 [m/s], 0.4% CMC: △ , 0.8% CMC: ◆ .

representative v_s of 0.012 [ms^{-1}]. It should be noted that presentation at different gas velocities will slightly alter the relative positions of correlation lines as the v_s exponent ranges from 0.22 to 0.67, although most are in the range 0.3 to 0.5.

Table 7.10 shows P/V exponent values from 0.4 to 0.76. Those obtained using the dynamic technique with no gas-phase O_2 depletion assumed[73,75,114] are lower (0.4 to 0.5) as are the regression lines (Fig.7.28). Results obtained using the dynamic method with gas phase mixing accounted for by use of 2-probes[30,122] show higher P/V exponents (0.6 to 0.7) and higher absolute k_La values. The combined water results obtained using the steady-state method in this work agree well with the latter data. Failure to account for gas-phase mixing when using dynamic techniques has previously been shown to result in underestimated k_La values[21]. Using the steady-state technique negates the influence of gas phase mixing assumptions and so results should correspond well with those using the 2-probe, double response method. As this is the case, the assumption that the low levels of chemical additives used in the NEL/Hickman technique do not effect the measured k_La values is supported.

Individual impeller correlation from this work show P/V exponents from 0.5 to 0.7 and v_s exponents from 0.04 to 0.7. The former correspond with the range obtained in the literature for the 2-probe dynamic technique whilst the latter show a greater range. Most impellers tested in the literature have been 6DT or modifications thereof. Literature v_s exponent values agree well with those found for 6DT and 6PSDT (0.5, 0.45) in this work. The IM and A315 impellers were found to exhibit the lower (IM) and higher (A315) β values. Unfortunately no literature water correlations for these impellers are available for comparison. The A315 data of Bakker[35] agrees well though. The agreement between literature values obtained at a variety of scales and those found here supports the use of correlations of the Eqn.2.23 type for scale-up purposes.

TABLE 7.11

LITERATURE STUDIES USING CMC

Ref.	D [m]	H/T	D/T	Imp.	Method	K [Pa.s^n]	n	μ_a
[95]	0.25	1	0.4	6DT	Dynamic	0.0117 - 1.32	0.95 -0.66	0.01 -0.33
[41]	0.4	1	0.33 0.4 0.6	6DT IM IM	Dynamic	1.5 -22	0.7 -0.4	0.22 -3.0
[7]	0.4	1+2	0.33 0.4 -0.7	6DT MIG	Dynamic	0.05 -1.47	0.8 -0.6	0.02 -0.3
[96]	0.15 -0.6	1	0.33 0.5	6DT	Dynamic	0.0073 -10.8	1 -0.59	0.007 -2.04
[20]	0.3	1	0.33 0.5 0.58	6DT IM	Steady -State	0.04 -25	0.8 -0.3	0.02 -1.5

7.8.3 Comparison of CMC mass transfer results.

Direct comparison of mass transfer results obtained by various workers using CMC solutions is complicated by both the range of non-Newtonian rheological characteristics and differences in data correlation techniques used. Where possible data was compared with the studies in which the apparent viscosity and Power-law parameters overlapped with those from this study, these are detailed in Table 7.11. In some cases comparison was only possible by adopting the correlation techniques of the relevant studies. It should be noted that all workers used vessels of smaller diameter than this study. Data available using the 6DT are compared with results from this work for similar viscosity CMC solutions and v_s in Fig.7.29. All the data exhibits a similar dependence of k_La on P/V (except for that of Yagi and Yoshida[95]) and similar absolute values of k_La. The data from this work agrees well with that of other workers, however, the basis for comparison is not exact as differing impeller diameters, vessel sizes, geometries, gas velocities and fluid rheological properties are shown together.

Although IM or MIG impellers were tested by Kipke[41], Höcker[7] and Hickman[20] only the latter provides raw data for comparison. The IM (0.58T) data from Hickman[20] is shown in Fig. 7.30 for two CMC concentrations using both ring and point spargers. The 0.8% CMC IM results from this work agree well with those of Hickman for both spargers, the 0.4% CMC results from this work are however marginally greater than Hickman's.

In order to compare results using CMC with those of Kipke[41] and Höcker[7] the dimensionless correlation technique of Zlokarnik[120] has been adopted, where:

$$k_La = f\ (\ \rho,\ \mu,\ \sigma,\ D_L,\ P/Q_G,\ Q_G/V,\ g,\ Si) \qquad (7.2)$$

Si is a measure of bubble coalescence behaviour. This gives rise to the following:

$$k_La^* = f\ (\ (P/Q_G)^*,\ (Q_G/V)^*,\ \sigma^*,\ Sc,\ Si^*\ ) \qquad (7.3)$$

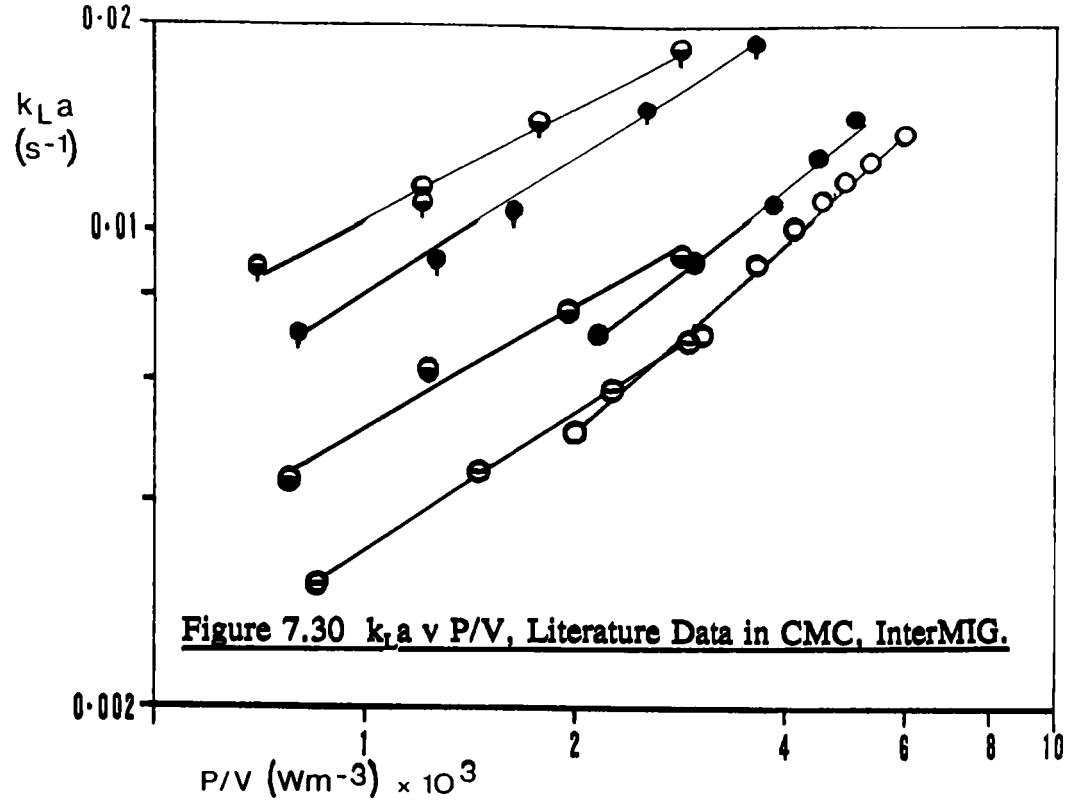

Figure 7.30 $k_L a$ v P/V, Literature Data in CMC, InterMIG.

Hickman[20], v_s=0.005 [m/s], 0.4% CMC, K=0.7, n=0.6,(MRS):◆.
" , " , 0.8% CMC, K=3.0, n=0.5,(MRS):●,(PS):○.
This Work,v_s=0.006 [m/s], 0.4% CMC,(MRS):◈ .
" , " ,0.8% CMC,(MRS): ⊖ , (PS):⊖ .

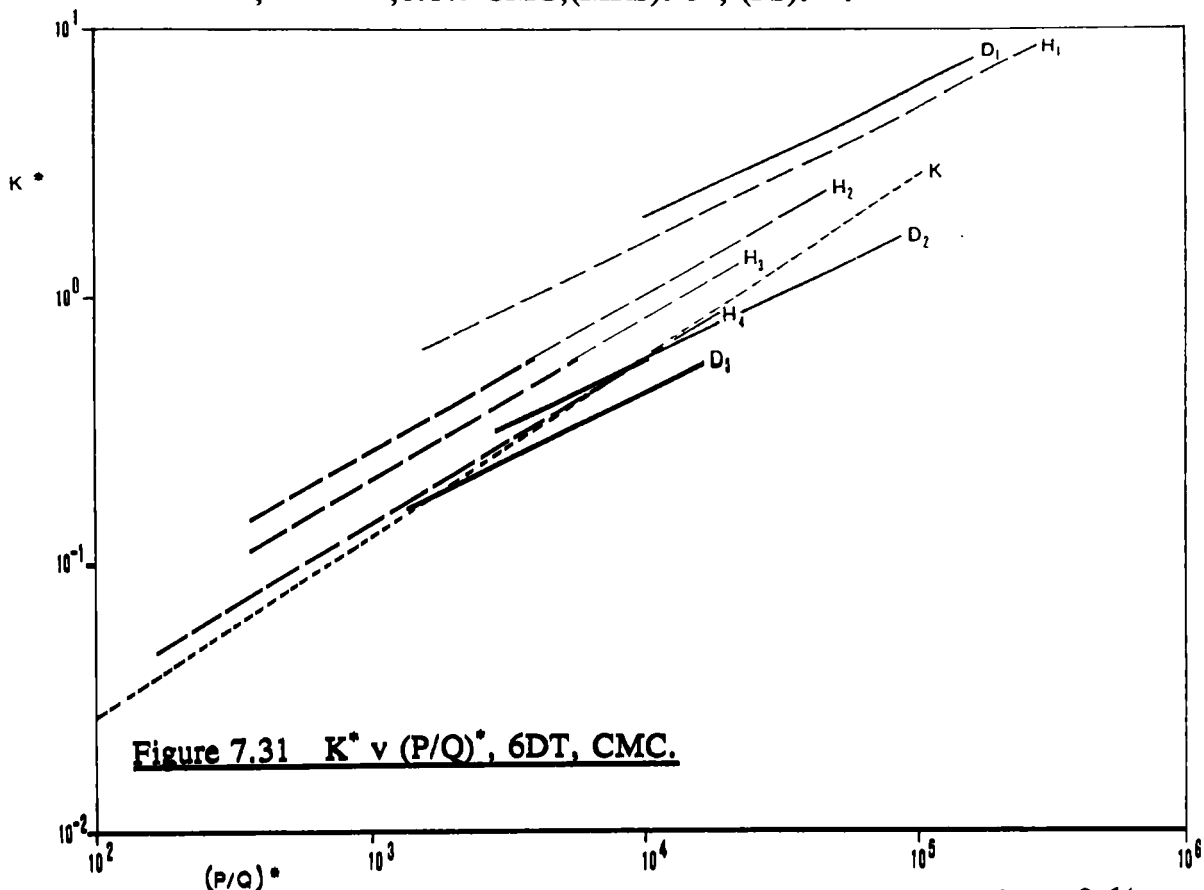

Figure 7.31 K^* v $(P/Q)^*$, 6DT, CMC.

Hocker[7], H_1,K=0.05, n=0.8. H_2,K=0.21, n=0.74. H_3,K=0.58, n=0.64.
" , H_4,K=1.47, n=0.6.
Kipke[41], K, μ_a=0.56-4.0 [Pa.s].
This Work,D_1, K=0.04, n=0.75,D_2, K=0.4, n=0.64,D_3, K=2.8 ,n=0.46.

where: $$k_L a^* = k_L a \left(\mu / \rho g^2 \right)^{1/3} \quad (7.4)$$

$$(P/Q_G)^* = P/Q_G \left[\rho \left(\mu_g/\rho\right)^{2/3} \right]^{-1} \quad (7.5)$$

$$(Q_G/V)^* = Q_G/V \left[\mu/\rho . g^2 \right]^{1/3} \quad (7.6)$$

$$\sigma^* = \sigma/\rho \left[\left(\mu/\rho\right)^4 g \right]^{1/3} \quad (7.7)$$

$$Sc = \mu / \rho D_L \quad (7.8)$$

Sc is the Schmidt number and Si^* a dimensionless group that describes the coalescence characteristics of the 2-phase mixture. The six dimensionless groups of Eqn.7.3 may be reduced to four by assuming that coalescence behaviour and surface tension do not vary significantly with CMC concentration (Si* and σ* removed). Surface tension has been shown not to be significantly reduced with increasing CMC concentration[2,95,96]. The diffusion coefficient, D_L, for the CMC solutions has been taken as 2.0 x 10^{-9}[$m^2 s^{-1}$] at 25°C as used by Höcker et.al[7] and Hickman[20] who cited the studies of Yagi et.al[95] and Nishikawa et.al[96].

Table 7.12 gives the results of multiple regression for the various geometries used in this study using Eqn.7.3. The fit of the data to the Zlokarnik correlation is worse than the fit to the correlation type used in the bulk of this work (Eqn.2.23). Table 7.12 also shows Hickman's[20] correlation coefficients for 1 T/2 6DT and 2 IM in the CMC concentration of 0-1.4%. This range included water and hence the assumption of invariable Si* is questionable. Hickman's exponents for P/Q* and Q/V* are similar to those found here, but the Sc exponent is negative here and slightly positive in Hickman's work. This implies a reduced effect of μa for Hickman, possibly due to the inclusion of water in the correlation (see 7.6.1).

TABLE 7.12

DIMENSIONLESS CORRELATIONS OF THE ZLOKARNIK TYPE (CMC ONLY)

$$k_L a^* = K\ (P/Q)^{*\alpha} (Q/V)^{*\beta} Sc^{\gamma}$$

No.	Impeller Type	K	α	β	γ	NOTE	R^2
1	6DT	0.632	0.28	0.67	-0.48	This Work	0.88
2	InterMIG	0.008	0.46	0.45	-0.4	"	0.95
3	A315	3.24	0.3	0.76	-0.59	"	0.92
4	6MF(U)	0.265	0.45	0.67	-0.56	"	0.92
5	6MF(D)	0.106	0.43	0.62	-0.47	"	0.98
6	6PSDT	0.477	0.31	0.68	-0.48	"	0.94
7	All Impellers	0.087	0.33	0.5	-0.48	"	0.88
8	6DT	0.0006	0.47	0.8	0.12	Hickman [0.001-0.34 Pa.s]	n/a
9	InterMIG	0.0003	0.45	0.62	0.13	Hickman [0.001-0.8 Pa.s]	n/a

TABLE 7.13

DIMENSIONLESS CORRELATIONS OF THE MODIFIED ZLOKARNIK TYPE

$$k_L a\ (V/Q) = K\ (P/Q)^{*\alpha}\ Sc^{\beta}$$

No.	Impeller Type	K	α	β	R^2	Reference
1	6DT	1.273	0.46	-0.44	0.91	This Work
2	InterMIG	0.047	0.79	-0.39	0.95	"
3	All Impellers	0.832	0.56	-0.48	0.92	"

TABLE 7.14

$k_L a$ DEPENDANCE ON μ_a , LITERATURE RESULTS.

$$k_L a \propto \mu_a^{\gamma}$$

Ref.	Impeller	Fluid	μ_a Range [Pa.s]	γ
[20]	6DT	CMC Water	0.001 -1.5	-0.26
[20]	IM	CMC Water	0.001 -1.5	-0.29
[79]	6DT	CMC	0.006 -0.15	-0.6
[30]	Various	Paper Fibre	0.15 -0.6	-1.0
[123]	6DT	PEG 6000	0.004 -0.03	-1.0
[2]	6DT	CMC	0.001 -0.0053	-0.41
[96]	6DT	CMC Millet -Jelly	0.001 -2.04	-0.5
[95]	6DT	CMC	0.001 -0.33	-0.4

Both Höcker et al[7] and Kipke[41] modified Zlokarnik's[120] correlation by connecting $(k_La)^*$ multiplicatively with $(Q/V)^{*-1}$ to give a new number K*. Höcker then plotted K* v (P/Q)* for each CMC concentration whilst Kipke showed one line for all concentrations. Although Table 7.12 indicates that (Q/V)* exponents were less than unity in this work, the procedure of Höcker and Kipke was followed to give the correlations shown in Table 7.13. Fig.7.31 shows 6DT data from this work with that of Höcker et.al[7] and Kipke[41]. For CMC solutions with similar Power-law indices, the data of Höcker[7] agrees well with this work. Kipke[41] shows data from various CMC concentrations scattered around one correlation line, which is shown here. The lowest viscosity used by Kipke was 0.56 Pa.s which was greater than the highest viscosity here. However as seen in Fig.7.31 there is moderately good agreement between this work and Kipke.

Although the dimensionless correlations of Zlokarnik[120] and their derivatives have been used to compare data from this work with that from the literature, none of them provide as good a fit to the experimental results as $k_La = f\ [P/V,\ v_s,\ \mu_a]$. Comparison on the basis of the latter have been made with a number of literature studies, these are shown in Table 7.14. Researchers have previously obtained μ_a exponents in the range -0.4 to -0.6, it appears however that their correlations have included water data. As shown previously, this has the effect of reducing the dependence of k_La on μa. More recent studies by Cooke et.al[30] and Nienow and Brocklehurst[123] have indicated that $k_La \propto 1/\mu_a$, these workers did not include water in their correlations. The results from this work indicate a k_La dependence on μa only slightly lower than that found by Cooke[30] and Nienow[123].

8. CONCLUSIONS AND FURTHER WORK.

8.1 CONCLUSIONS

Conclusions concerning IM and the other impeller power, fluid dynamics and gassed hold-up are located at the end of their respective chapters. In this chapter the results from the k_La studies are combined with power and hold-up results in order to draw overall conclusions.

The NEL/Hickman steady-state k_La measurement method proved to be relatively cheap, simple to use and effective. It gave reproducible results in water and CMC, providing the concentration of active catalase was maintained at a level of approximately fifteen times the stoichiometric requirement. In water the maximum catalase concentration must be less than the concentration at which bubble coalescence is suppressed. Therefore only a relatively narrow range of catalase concentrations are useable in water.

The k_La measurements in deionised water using the NEL/Hickman technique agreed closely with 2-probe dynamic technique results from the literature. Both of these methods gave higher k_La results in water than the commonly used van't Riet correlations[73] (single probe dynamic technique data). The discrepancy arises because the steady-state technique is insensitive to the gas-phase mixing model, the two-probe technique accounts for it but the single probe method is both sensitive and does not account for gas-phase mixing.

For the measurement of k_La in systems containing numerous tiny bubbles (e.g. CMC), a steady-state experimental method was essential because dynamic methods will underestimate k_La.

At constant aerated P/V and gas velocity in deionised water (turbulent flow), both ε_G and k_La varied little with changing agitator type. The influence of P/V upon k_La and ε_G was also similar irrespective of agitator type. The strong dependence of k_La on P/V was therefore

largely due to changing interfacial area, a. Inter-impeller k_La results in water exhibited varying dependance on v_s. This was particularly evident with the IM/point sparger combination, where increased gas velocity influenced hold-up more than k_La. At high v_s, IM were not able to break-up and disperse the additional gas, because it bypassed the outer blades. This led to an increase in bubble size, so that although hold-up rose, interfacial area and k_La did not.

At constant P/V and v_s in shear-thinning CMC solutions, inter-impeller hold-up and k_La variation was much greater than in water. In 0.07% CMC (turbulent flow) the highest k_La and hold-up were provided by the lowest Pog impellers (e.g. IM and 6MFD). The 6DT and 6PSDT impellers gave similar k_La values to each other but lower ones than the IM, 6MF etc.

In 0.4% and 0.8% CMC (transitional flow), the performance of the various impellers diverged further. At constant P/V and v_s, low Pog impellers consistently provided considerably enhanced k_La values. IM, 6MFD and A315 gave the highest overall and 6DT and 6PSDT the lowest. Inter-impeller k_La variation was greater than hold-up variation, implying an effect of impeller type on bubble size distribution or k_L. The dependence of k_La and hold-up on P/V was reduced strongly for 6DT and 6PSDT in the transitional flow regime, an effect not seen with IM for example. Sparger choice had some effect on bubble size distribution with IM, but k_La was almost independant of v_s for IM in CMC irrespective of sparger. The A315 hydrofoil k_La and hold-up were consistently more strongly dependent on v_s than the other agitators tested in CMC. Generally inter-impeller v_s dependence variation was greater than inter-impeller P/V dependence variation.

Correlation of k_La results for different agitators in each concentration of CMC was markedly improved by the inclusion of an apparent viscosity term. For equal aerated power input, low Pog impellers operate at higher N and shear-rate thus lowering the apparent viscosity in

shear-thinning CMC. This supports the use of the Metzner and Otto shear-rate determination method for viscosity dependent k_La correlation in non-elastic shear-thinning fluids. Combining k_La results from different CMC concentrations (μ_a from 0.008 to 0.4 Pa.s)for each impeller showed that $k_La \propto \mu_a^{-0.79to-0.97}$, the exponent being slightly dependent on impeller type. Hold-up was less strongly effected by viscosity increase ($\varepsilon_G \propto \mu_a^{-0.13to-0.25}$). The influence of μ_a on k_La reported here is higher than in many previous works (Section 7.8). It was shown that the inclusion of water data into the correlation reduces k_La dependance on μ_a. This is inadmissable as deionised water is a coalescing system and CMC suppresses coalescence. A more valid procedure is to correlate CMC data with that obtained in non-coalescing salt solutions, as has been done in this work. The use of different values of the Metzner and Otto constant, k_s, for different impellers had a negligible effect on the overall k_La correlation when compared with constant k_s=11.5. Data from this work was correlated far more successfully using P/V, v_s and μ_a than when using dimensionless correlation techniques of the Zlokarnik type[120].

Power, hold-up and k_La values were measured and compared at both H/T=1 and H/T=2 for the IM and 6DT impellers. Unaerated power draw at H/T=2 with four IM or two 6DT was almost exactly double that for two IM or one 6DT at H/T=1. Multiple IM impellers drew optimum power at a lower S/T than 6DT. Reduction in S/T to below the optimum caused a smaller reduction in power draw for IM than 6DT. The IM therefore lends itself well to retrofitting and multi-stage use. No effect of aspect ratio on IM Pog/Po at constant v_s was found in water or CMC. The 6DT Pog/Po was higher at H/T=2 due to different upper impeller gassing characteristics. Under identical conditions of P/V and v_s, IM hold-up and k_La were found to be virtually independent of aspect ratio in water, 0.4% and 0.8% CMC. 6DT results at the two aspect ratios were not as consistent. Four IM at H/T= 2 provided higher k_La than two 6DT in all concentrations of CMC, this

agreed well with findings at H/T=1. As k_La remained constant when doubling H/T at constant P/V and v_s with IM, a reduction in Q_G for a given k_La is implied.

The choice of impeller type for use in mechanically agitated gas-liquid reactors is complex. The impeller type has been shown to influence unaerated flow pattern, Po, $P/V_{F/L}$, P/V_{CD}, Pog/Po and torque instability aswell as ε_G and k_La in non-Newtonian liquids. No one agitator type is superior in every respect under all conditions, so that impeller choice must be based on the design criteria for a particular process. In order to optimise k_La it is important to ascertain whether agitators are to be compared on the basis of equal unaerated P/V, aerated P/V or N. In this work comparison has been principally conducted on the basis of aerated P/V. Under these conditions 6DT and 6PSDT gave similar k_La values, 6MFD typically gave higher k_La than 6MFU, A315 intermediate values and IM (MRS) high relative k_La in CMC. However, comparison on the basis of unaerated P/V, a common but conservative approach, would change the relative impeller performances. Those agitators with higher Pog/Po will transfer more power to the gas-liquid system. Under these circumstances in CMC, the 6PSDT would give higher k_La than the 6DT and the 6MFD advantage over the 6MFU would be reduced or dissapear. The A315 relative performance would improve considerably whilst the IM relative performance would deteriorate.

Comparison on the basis of equal N alone would favor high Pog impellers such as the 6PSDT and 6DT as opposed to low Pog types. When replacing 6DT at equal N with low Pog types such as A315 or IM, more stages and increased diameter are required in order to obtain equal torque. Power characteristics are now available for large D/T IM at low S/T, but the same cannot be said for the A315 as no data is available for multiple impellers, effect of S/T or for D/T > 0.5. Until this data is available IM are a better choice for retrofitting than A315.

8.2 FURTHER WORK

The oxygen mass transfer work presented in this thesis considers overall vessel parameters such as k_La, ε_G, P/V, v_s etc.. It is recognized that this type of approach is somewhat simplistic, but the currently available experimental techniques and measurement methods make it neccessary to treat the vessel as well mixed and homogeneous. Significant spatial and temporal variation in energy dissipation rate, bubble sizes, hold-up and therefore k_La become increasingly likely with increased viscosity and scale. This may lead to damaging O_2 or substrate gradients. For viscous non-Newtonian liquids the impeller type has been shown to influence k_La and ε_G at constant P/V and v_s. The relationship between these parameters is highly complex for differing equipment geometries. A long-term aim should be to achieve greater understanding of phenomena such as local energy dissipation rates, local bubble size and residence time distributions, coalescence and break-up rates etc.. This would enable multi-compartment models to be used instead of the single compartment model used at present.

Techniques such as Laser Doppler Anemometry (L.D.A.) can be used to obtain local energy dissipation rates in single-phase systems. There is clearly a requirement for their application to gas-liquid reactors, but considerable technical difficulties must be overcome first. Discrete probes for measurement of local hold-up and bubble size also need to be developed, in order to easily determine local interfacial area. Improved local measurement techniques will need to be combined with greater automated data handling capability in order to analyse results. Empirical work of this sort may be used to aid the construction of accurate gas-liquid computerised fluid dynamics (C.F.D.) models.

Other objectives for investigation include the effect of increased D/T on hydrofoil flowpattern, power draw, gas dispersion, hold-up and k_La.

Results from such work would allow the effectiveness of replacing 6DT impellers with A315 at equal speed and torque to be assessed. The effect of S/T variation on hydrofoil power draw is required before multi-impeller agitated systems can be accurately designed with these types. To this end, investigation at $H/T \geq 2$ is necessary.

Further novel agitator designs for gas-liquid contacting purposes in viscous non-Newtonian fluids should include features such as low Po, high Pog/Po, minimized torque instability, low P/V_{CD} and high D/T. Proprietry designs should be independently tested under realistic conditions whenever possible.

The Metzner and Otto[4,5] approach to shear rate determination appears to correlate power, viscosity and k_La data from this work well inspite of the extrapolation of the method outside the laminar flow regime. Further work is required in order to assess the effect of different shear rate estimation methods on the correlation of non-Newtonian gas-liquid data. This work should include the use of viscous Newtonian and non-Newtonian liquids of roughly equal viscosity in order to investigate the effect of consistency and power-law indices on fluid dynamic and oxygen mass-transfer performances.

The data obtained using the mixing vessel T72, are intended for use in improving the agitator selection for fermentation applications. Fermentation research vessels of similar scale are available, often with variable speed motors, so that selected findings from the mixing vessel may be confirmed using microbial broths.

Further data is required at both larger and smaller scales using the NEL/Hickman technique, in order to quantify any scale effects when using a variety of agitator types in non-Newtonian liquids at H/T=1 and H/T=2.

APPENDIX I: INTERMIG AND MIG LITERATURE SURVEY.

1. Introduction.

This appendix is concerned with information available in the literature with respect to two types of impeller, the MIG and InterMIG. Both were designed and are manufactured by Ekato G.m.b.h. of Schopfheim, West Germany. Much of the performance data available concerning InterMIG and particularly MIG impellers originates from the manufacturers themselves. Independent sources are therefore especially valuable in order to corroborate the manufacturers data.

The name MIG is a shortened form of Mehrstufen Impuls-Gegenstrom, meaning multi-stage impulse counter-current impeller[42]. The name InterMIG has the same meaning except that it utilises the interference effect (see later), hence Inter-MIG. In this work InterMIG is abbreviated to IM. Figure 1 shows a typical MIG impeller stage. The impellers are referred to as multi-stage because they are always mounted in at least pairs for each H/T = 1. In practice all sources show each stage fixed on the shaft at 90^{o} to the preceding stage (with the exception of one study involving only one IM stage[124]). Countercurrent refers to the flow induced by the inner and outer MIG/IM blades. Generally the impellers are rotated in the direction which allows the outer blades to pump fluid downwards whilst the inner blades pump fluid upwards. Following the nomenclature used by previous authors[20,91,98] this rotation direction is referred to as U.P.M. (Upwards Pumping Mode) and describes the inner blade action. All the available manufacturers literature refers to this rotation direction as do most other sources with the exception of studies at Birmingham University[20,91,98] and the National Engineering Laboratory, East Kilbride[124,125] which also cover the D.P.M. (Downward Pumping Mode).

The interference effect referred to in the name IM relates to a design improvement applied to the earlier MIG impeller in order to

FIGURE 1

MIG® IMPELLER

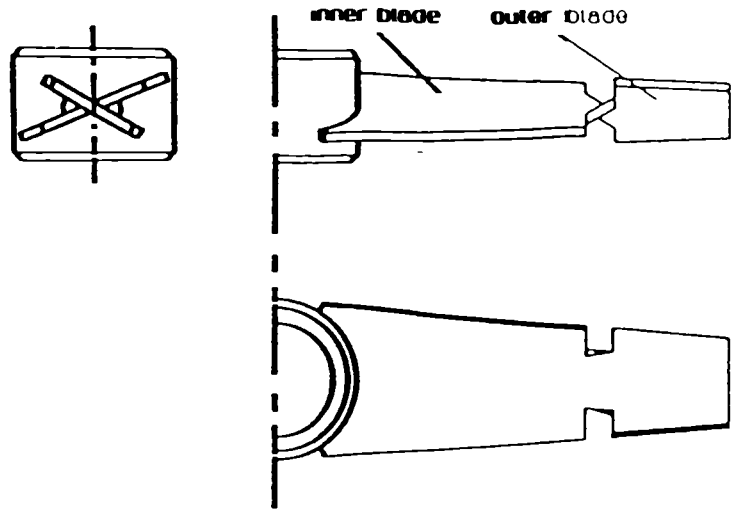

FIGURE 2

InterMIG® **IMPELLER**
(Slotted variant)

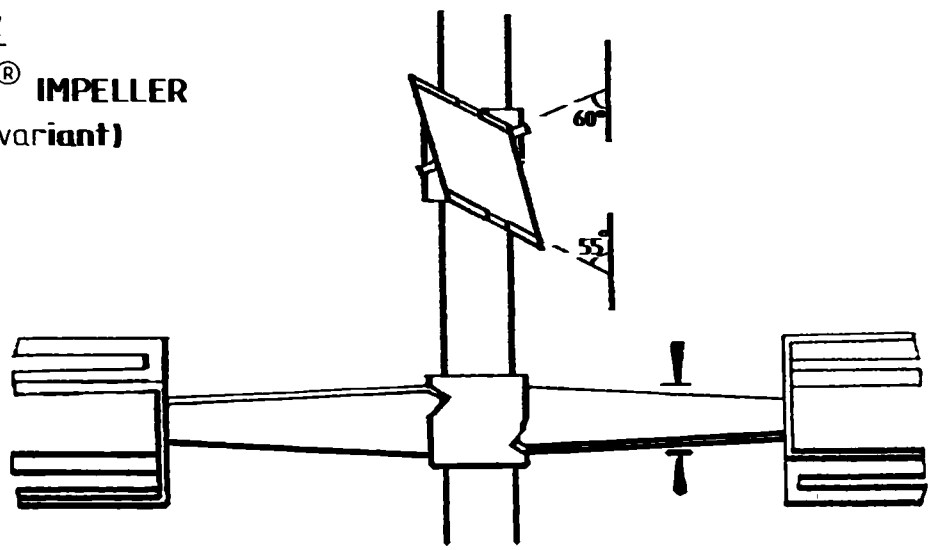

FIGURE 3

InterMIG® IMPELLER
(Un-slotted variant)

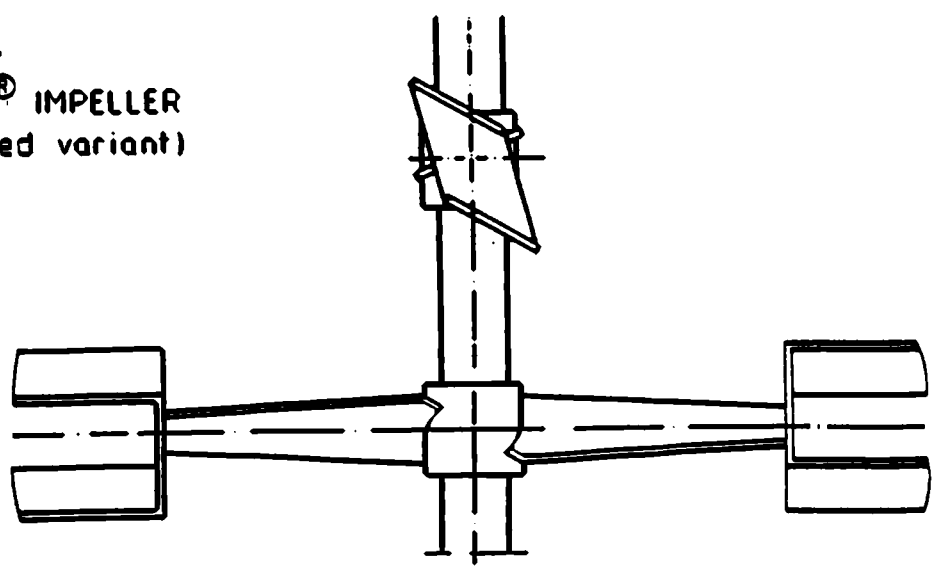

increase the stirring intensity of each stage. Instead of the single outer blades of the MIG, the IM has twin outer blades. These utilise the effect of fluid mechanical interference to increase the axial flow considerably whilst only slightly increasing the drag. Kipke[126] delineates the theory behind this design, and compares MIG and IM performance with respect to solid suspension and fermentations.

Two variants of the IM design exist, one has slotted outer blades whilst the other has unslotted outer blades (see Figs. 2 and 3). Although some sources recorded whether the IMs were bifurcated or not, none (including Ekato) indicate why the variants exist or what effect they have on performance. A very recent impeller design from Ekato is called the InterPROP. This impeller utilises the interference effect but differs from the IM due to a more streamlined blade construction akin to a propeller. No independent data is available concerning this impeller.

2. Dimensions.

The manufacturers[97] stipulate D/T ratios of 0.5 to 0.95 for MIG and IM. Generally baffled vessels require D/T < 0.7 (turbulent or transitional flow) and unbaffled vessels D/T > 0.7 (laminar flow). However a number of sources[7,40,101,127] have used smaller diameter ratios (D/T = 0.4). Baffling of vessels when using IM is usually by 2 or 4 baffles each of 8% of the tank diameter with a 2% gap between baffle and vessel wall[97]. The manufacturers and other sources refer to an IM with D/T = 0.6 as an InterMIG 06. The majority of independent literature refers to IM impellers in the D/T range 0.55 to 0.7 in baffled vessels.

The recommended separation of MIG and IM stages is given by Ekato[97] as S/T = 0.28 and S/T = 0.5 respectively. The increase in recommended separation being due to improved axial mixing from the twin outer blades of the IM. Most sources of IM data used a separation of S/T = 0.5 giving two stages for vessels with H/T = 1. Hocker[40] used the recommended

separation of S/T = 0.28 for MIG impellers to agitate a vessel of H/T=1 (i.e. 3 stages) but doubled the separation for investigations at H/T=2 (S/T = 0.56).

Ekato[97] recommended a lower impeller clearance from the vessel base of C/T = 0.16 for MIG and C/T = 0.22 for IM. Studies at Birmingham University[12,20,91,98] have used C/T = 0.25 to 0.3 for IM. Again Hocker[40] used the recommended MIG clearance at H/T = 1 but doubled it at H/T = 2. Nearly all independent investigations of IM/MIG performance have been conducted in vessels with H/T = 1. Exceptions are Hocker[7,40] MIG at H/T = 1 and 2 (geometric similarity not maintained), Himmelsbach[100] IM at H/T = 1 and 2, Henzler[106], MIG, H/T = 2 and Phillip et.al.[105] H/T = 1 to 4.

3. Flow patterns.

A principle area of interest when studying agitator performance is the flow pattern generated. This depends strongly on agitator type, agitator positioning and configuration of the vessel as well as the fluid used. Typically the flow patterns of impellers can be observed in transparent perspex vessels by using the 'light plane' or 'collimated light' method. This involves illuminating the vessel with a thin vertical sheet of light and adding numbers of neutral buoyancy tracer particles. Photographs are then taken which indicate the relative tracer movements and hence the flow pattern. This method was used by Perfect[98] in a 0.45 m tank for both U.P.M. and D.P.M. with IM. The IM and MIG impellers produce primarily axial flow with a radial component. Kipke[126] and Ekato[97] also showed light plane photographs of IMs. These results revealed a complicated flow pattern, in the U.P.M. the inner blades produced a relatively uniform upwards diagonal flow whilst the outer blades produced a more violent downwash from which eddies break off towards the vessel wall. Dead zones are restricted to the area where the shaft enters the liquid and are only present at low N or high viscosity. The IM imparts

the highest velocity on the fluid at the outer blades which aids mixing in the region of the vessel wall and base. Perfect's[98] results for D.P.M. showed surface aeration occurring at a lower speed than for U.P.M. due to vortex formation around the shaft, aided by the inner blades pumping downwards; Allsford[91] confirmed this. In the D.P.M. mixing at the vessel base is worse as the impeller outer blades pump up. Perfect[98] found the unaerated flow behaviour to be consistent throughout the speed range used. The above mentioned light plane investigations were all conducted in the turbulent flow regime.

4. Velocity fields.

For exact analysis of flow behaviour, measurement of velocity fields in the axial, radial and tangential directions are required. This may be achieved by either Hot-wire Anemometry or Laser-Doppler Anemometry. A number of studies have used the L.D.A. to determine both mean velocities, $\bar{u}$ (often normalised as $\bar{u}/u_{tip}$) and the instantaneous fluctuating velocities u' (and u'_{rms}) of the liquid in radial, axial and tangential directions. Kipke[128] showed axial and radial mean velocities for IM in the turbulent regime at H/T=1. He also showed fluctuating velocities in axial and radial directions to obtain information on the local distribution of energy dissipation or shear stress. The measurement of fluctuating velocities revealed a relatively uniform distribution of energy dissipation purported to be due to the large D/T ratio, high number of stages and countercurrent nature of the impellers. The uniform shear field may provide a better environment for micro-organisms than that for a 6DT for example.

Laufhutte et.al.[104] measured the distribution of fluctuating velocities, in a H/T=1 turbulent system for 6DT, 3-blade propeller, 2 IM 06 and 2 IM 07. The smaller diameter IM were found to give a more uniform flow field. The highest normalised rms fluctuating velocities were found

in the plane above the lower stirrer (u'_{rms}/u_{tip} = 0.12) whereas the lowest (u'_{rms}/u_{tip} = 0.05) were observed in the vicinity of the liquid surface. A comparison of maximum normalised fluctuating velocities was given (6DT the highest u'_{rms}/u_{tip}) and their location.

TABLE 1

IMPELLER	D/T	u'_{rms}/u_{tip}
6DT	1/3	0.35
3-blade Prop	1/3	0.2
	1/2	0.11
2 InterMIG	0.6	0.2
	0.7	0.2

Plots of isoenergetic lines ($\varepsilon/\bar{\varepsilon}$ = constant) showed again a very uniform energy dissipation distribution for IM when compared with 6DT or 3-bladed propellers.

TABLE 2

IMPELLER	D/T	Re x10^4	$\varepsilon/\bar{\varepsilon}$ range
6DT	1/3	3.1	0.08 to 7.7
3-blade Prop	1/3	5.3	0.5 to 10
	1/2	5.3	0.1 to 3
2 InterMIG	0.6	5	0.5 to 2
	0.7	5	0.1 to 1

Crozier[125,129] investigated IM impellers in a 0.25 m vessel at H/T=1 and 2 using both U.P.M. and D.P.M. Tangential velocities were found to be the largest component but lower than those of 6DT. Normalised mean velocities were similarly lower than those of the 6DT, as found by other workers.

TABLE 3

IMPELLER	$\bar{u}_{max}/\pi ND$
Rushton turbine	0.75
2 InterMIG 06	0.15

Axial flow was found to dominate with radial flow highest in the impeller tip region. Ekato[97] provided the only reference to MIG L.D.A. data, showing a uniform turbulent fluctuating velocity field as with IM. Phillip et.al.[105] showed isoenergetic curves for IM and 6DT and again noted the even nature of the IM energy dissipation, commenting that undesired coalescence was suppressed in peripheral regions, more mass transfer area was available and mean effective viscosity lowered.

TABLE 4

IMPELLER	Range $\varepsilon/\bar{\varepsilon}$
6DT	0.1 to 8
2 InterMIG 06	0.5 to 2

Gerstenberg et.al.[130] commented that improved energy dissipation achieved by the use of multi-stage stirrers in polymerisation reactors slowed the reduction in the overall heat transfer coefficient, U, by reducing fouling. Kipke[41,126,128] commented that the IM imposes less shear stress on the stirred material and is therefore advantageous in shear sensitive biological operations.

5. Unaerated power characteristics.

A range of k_s values have been reported in the literature for MIG and IM.

TABLE 5 : InterMIG and MIG k_s values

REFERENCE	AGITATORS	k_s	LIQUID USED
Allsford 91	2 InterMIG 06	16 23	Carbopol C.M.C.
Hocker 40	2 InterMIG 06/04 and 09	11	C.M.C.
Henzler 106,131	2 InterMIG 065	17.5	C.M.C.
Himmelsbach 100	2 InterMIG 06	15	Xanthan
Matthew Hall 132	D not stated InterMIG	25	not stated

From the table it can be seen that a k_s value of 15 to 17.5 appears to be a reasonable assumption for IM 06.

Allsford[91] obtained power curves for 2 IM 06 in two concentrations of Corn Syrup (Newtonian), two Boger fluids (PAA in glucose), two concentrations of CMC and two Carbopol solutions. Both U.P.M. and D.P.M. were used and the power drawn was measured for each impeller individually. In Corn Syrup the overall power was unaffected by the direction of rotation. However in the U.P.M. the lower impeller drew less power than the upper and the upper less power in the D.P.M.. With Corn Syrup the combined Po fell to 0.7 at the highest Re (1000) attainable and was still falling. The power curves in the shear thinning fluids (Carbopol and C.M.C.) lay below the Newtonian curve over the whole Re range, falling to Po = 0.5 at Re = 1000. In the transitional regime the data for C.M.C. was located above that for Carbopol. In the case of the Boger fluids at Re > 100 (transitional) the Po were considerably greater than those for the Newtonian fluid, with increasing viscoelasticity causing an increase in Po. At Re = 1000 a Po of 1.5 was obtained for the lower concentration Boger fluid. No unaerated Power numbers were obtained in the turbulent flow regime. In the laminar regime Allsford found Po.Re ≃ 90 (see Fig. 4).

Hickman[20] measured unaerated power consumption in a 0.3 m diameter vessel using 2 IM 058. Fluids studied were 1.4%, 0.8% and 0.6% C.M.C. Rotation direction was found to have no effect on total power drawn and the power curve exhibited no minima in the transitional flow regime. He compared his C.M.C. data with Newtonian and viscoelastic (P.A.A. in water) data of Hocker[134] and found the C.M.C. curve well above the Newtonian curve for the whole Re range covered (10 to 2000) but coinciding with that for P.A.A. This comparison does not appear valid as Hocker[134] utilised MIG impellers (with lower Po) as opposed to IM. As previously mentioned Allsford's[91] C.M.C. data was below his Newtonian data. Hickman's[20]

FIGURE 4 POWER NUMBER vs REYNOLDS NUMBER (UNAERATED)
LAMINAR / TRANSITIONAL FLOW, H/T = 1

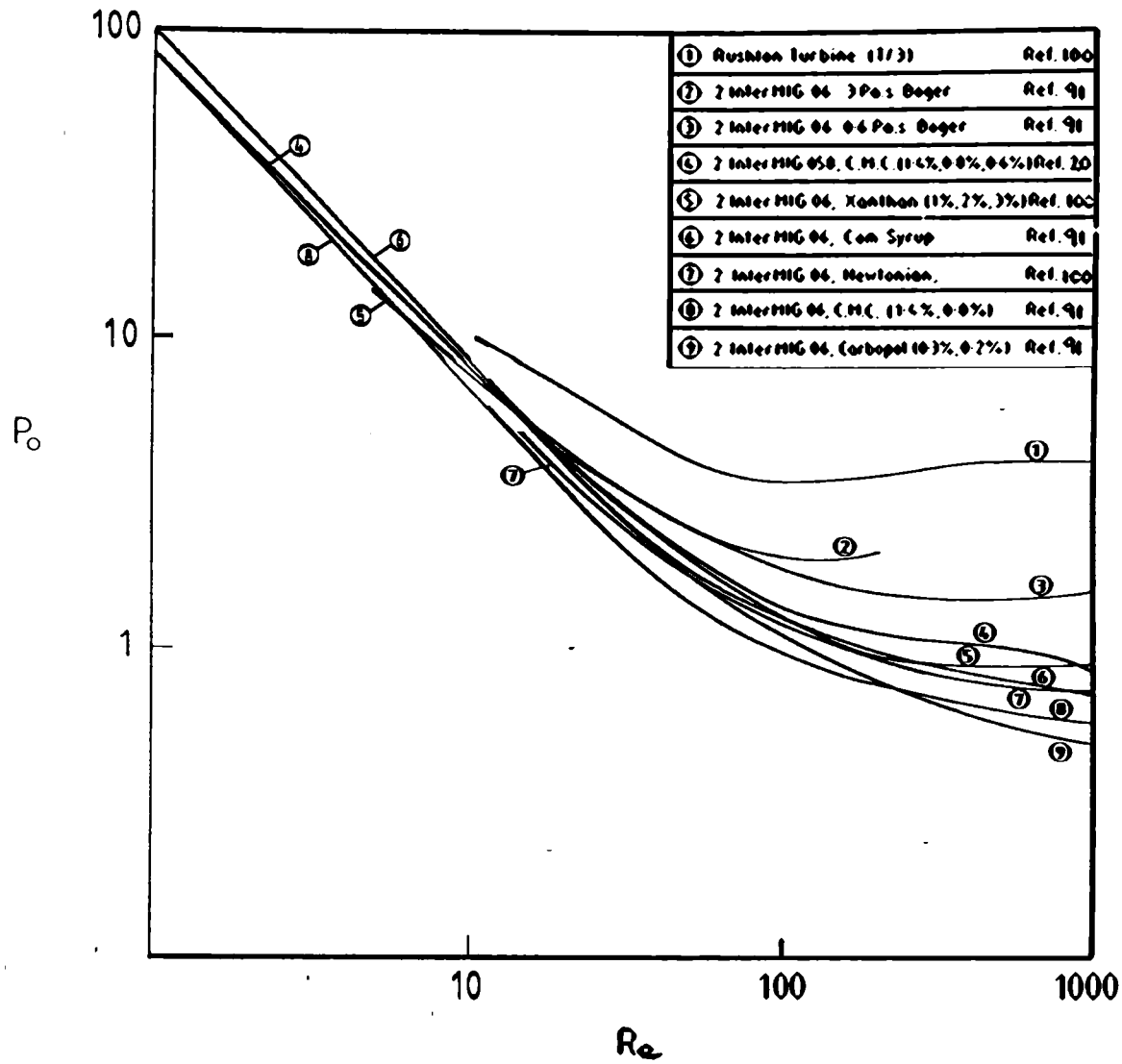

combined Po was between 0.8 and 1.0 (0.4 to 0.5 per stage) at Re 100 to 1000 (see Fig. 4).

Himmelsbach[100] showed an unaerated power curve for 2 IM 06 in 1% and 3% Xanthan. The Re range covered was 10 to 1000, no minima were apparent in the power curve and the Xanthan concentration showed no effect on Po. The data for Xanthan (pseudoplastic,viscoelastic) lay above a Newtonian curve shown for comparison. At Re = 1000 total Po = 0.7 to 0.8 (Xanthan) and Po = 0.6 to 0.7 (Newtonian) (see Fig. 4).

Man and McEwan[124] tested 1 IM 067 in water in the U.P.M. and D.P.M. For the U.P.M. the Po was 0.25 to 0.36 at Re $1.2x10^5$ to $1x10^6$ and for the D.P.M. Po = 0.36. Kipke[126] gave total unaerated Po for 3 MIG 07 and 3 IM 07 in a 0.4 m vessel between Re = $1.75x10^5$ and $4.4x10^5$ (turbulent). The values of Po were 3 IM 07 = 0.84 (0.28 per stage) and 3 MIG 07 = 0.55 (0.18 per stage) (see Fig. 6). Ekato[97] stated Po = 0.65 (2 stages, turbulent, D/T < 0.7) for IM giving Po = 0.325 per stage. In the laminar regime for D/T > 0.7, Po.Re = 110. For 3 MIG impellers (D/T < 0.7) in the turbulent flow regime Po = 0.55 (0.18 per stage) and Po.Re = 100 in the laminar regime. (see Fig. 6). Matthew Hall[132] gave a Po for IM of 0.8 in the turbulent regime but did not indicate the number of stages (3 probably).

The most thorough investigation of power consumption in Newtonian and non-Newtonian fluids was completed by Hocker et al.[40] MIG 04, MIG 06 and MIG 07 were used at H/T=1 and 2, although spacings and clearances were doubled at H/T=2. Liquids used were glycerol and glucose syrup (Newtonian), C.M.C. (pseudoplastic, shear thinning and inelastic over the $\dot{\gamma}$ range used) and P.A.A. in water (viscoelastic). Results obtained by Hocker[40] are tabulated below for Newtonian fluids.

FIGURE 5 POWER NUMBER vs REYNOLDS NUMBER (UNAERATED)
LAMINAR / TRANSITIONAL FLOW, H/T = 1

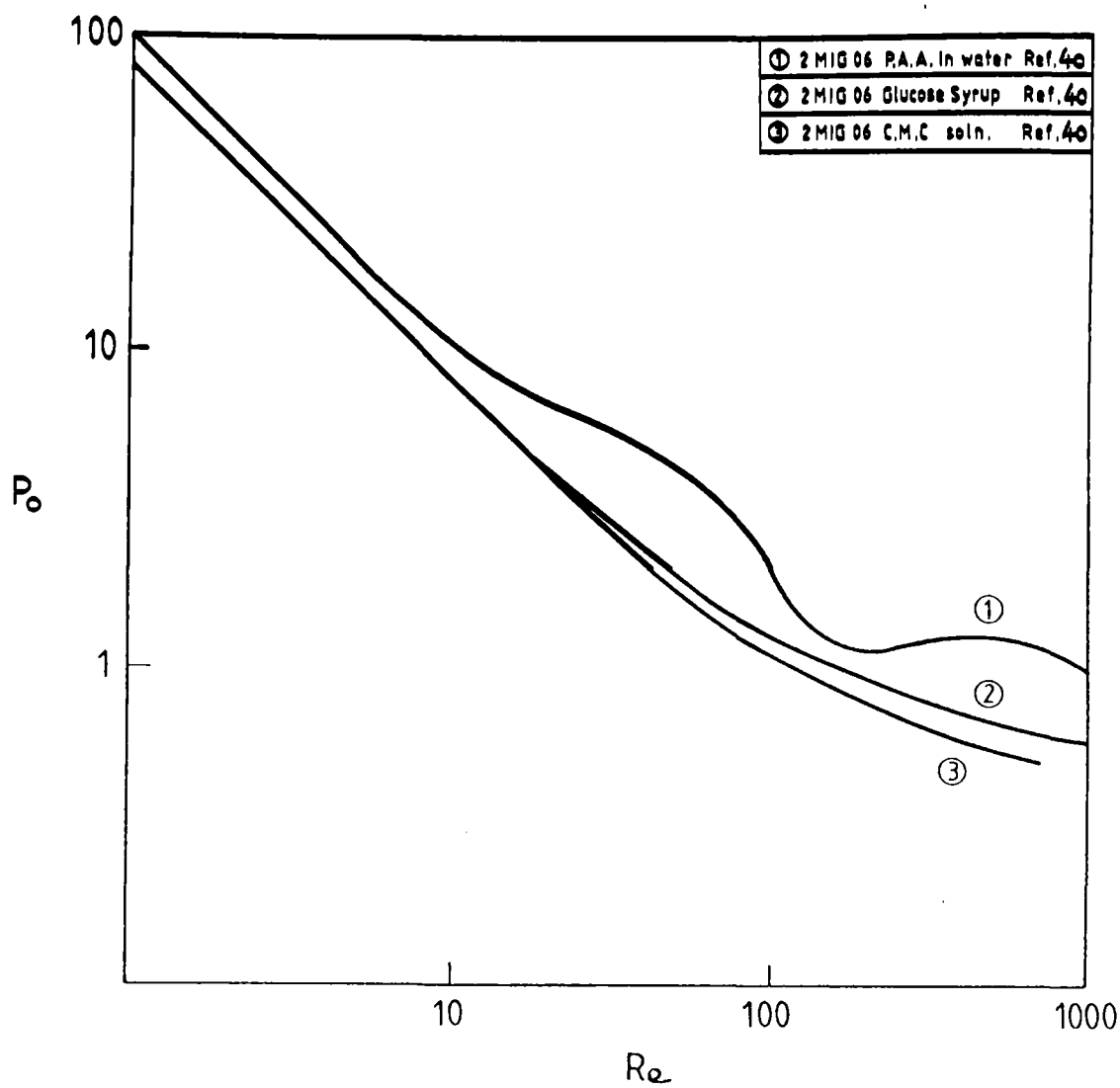

ASPECT RATIO	IMPELLERS	LAMINAR REGIME	TURBULENT REGIME	TURBULENT PER STAGE
1:1	3 MIG 04	Po.Re = 63.1	Po = 0.68	Po = 0.227
1:1	3 MIG 06	Po.Re = 52.5	Po = 0.55	Po = 0.183
1:1	3 MIG 07	Po.Re = 47.0	Po = 0.525	Po = 0.175
2:1	3 MIG 06	Po.Re = 72.4	Po = 0.63	Po = 0.21

The power curves showed no minima in the transitional region and Po was constant in the turbulent regime. The results indicated decreasing Po with increasing impeller diameter and an increase in Po when stage separation was increased from S/T = 0.28 to S/T = 0.56. Hockers[40] results for MIG in C.M.C. showed no difference from the Newtonian case in the laminar regime. The power numbers for C.M.C. in the transitional region were universally lower than those for the Newtonian fluids. Hocker[40] postulated that this was caused by a reduced liquid volume exposed to inertia forces due to pseudoplasticity. An extended laminar region was therefore apparent. At Re > 1000 no difference in Po was noted from the Newtonian case.

When P.A.A. solutions were investigated, no well defined laminar flow was achieved and hence no calculation of k_s possible. The k_s value (11) found for C.M.C. was therefore used. For all geometries in the Re 1 to 100 range, power numbers in P.A.A. were greater than for comparable Newtonian liquids due to viscoelasticity. At Re > 100 only 6DT showed a power reduction (from Newtonian), all MIG types showed an increase in Po. The different behaviour would appear to be connected with the diference in flow produced by the 6DT and MIG, the possible causes are discussed in detail by Hocker[40] (see Figs. 5 and 6).

Bujalski[12] investigated 2 IM 06 in water and glucose using vessels of

FIGURE 6

POWER NUMBER vs REYNOLDS NUMBER
TURBULENT FLOW, H/T = 1

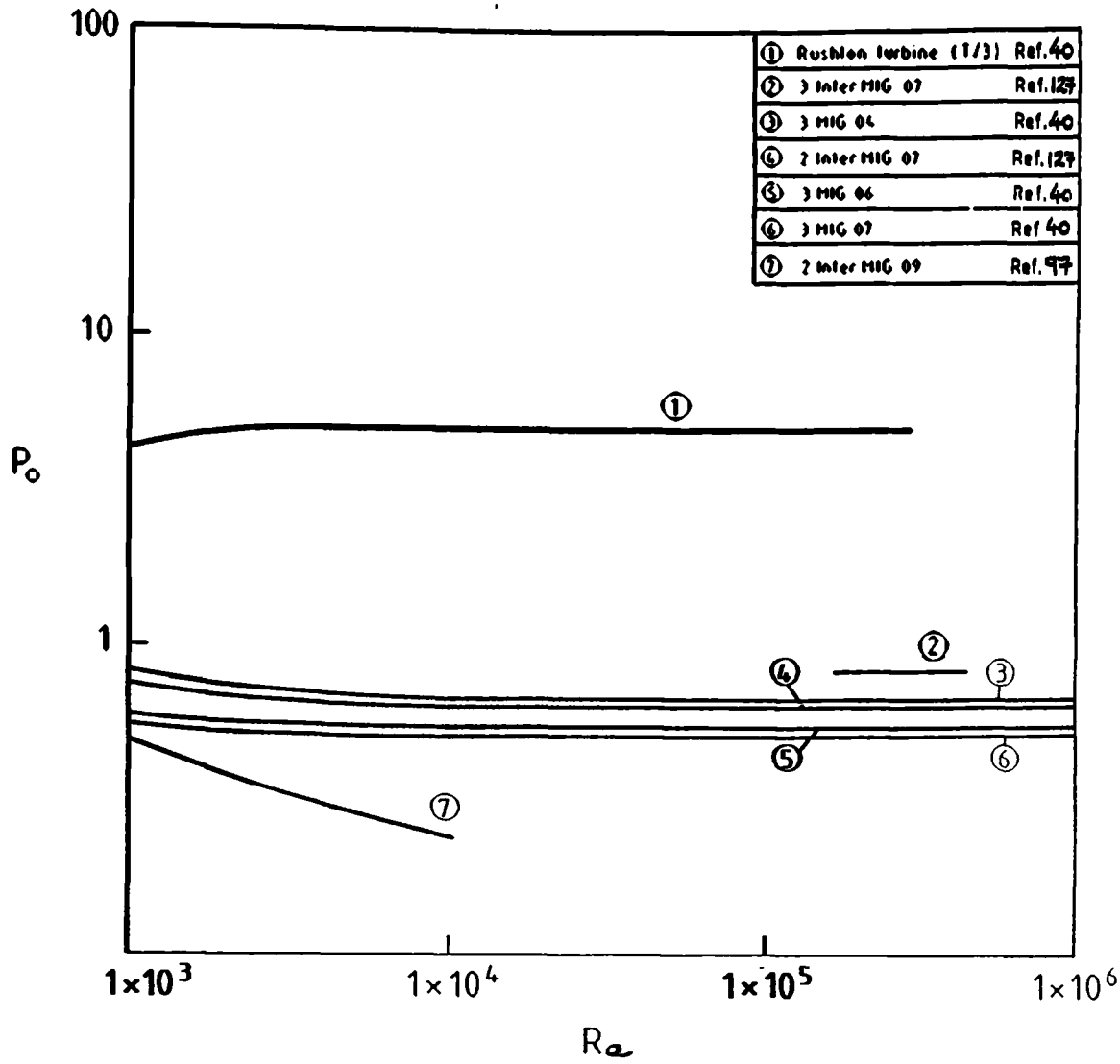

T=0.29m, 0.45m and 0.61m diamter. The Po was found to be constant for $Re \geq 2x10^3$. Values of Po = 0.65 (0.325 per stage) were found for all three vessels indicating no effect of scale for IM for this range of vessel sizes.

Summarising the non-aerated power results for MIG and IM indicates the following. Direction of rotation (UPM or DPM) has little or no effect on Po until surface aeration occurs. Power numbers are very low compared with other stirrer types such as 6DT. There is no minima in the power curve for Newtonian fluids with MIG or IM. In the turbulent regime for Newtonian fluids IM impellers give a Po per stage of 0.225 to 0.35 (depending on source of data). Under the same conditions MIG impellers give a power number of 0.175 to 0.23 per stage reflecting their lower drag. In the laminar regime for Newtonian fluids, Po.Re = 90 to 110 for IM and Po.Re = 50 to 100 for MIG. Strongly viscoelastic fluids such as Xanthan and P.A.A. caused a Po increase for both MIG and IM in all flow regimes except possibly the laminar over Newtonian fluids. Shear thinning fluids such as Carbopol and C.M.C. exhibited lower Po than those for Newtonian fluids in the transitional and turbulent regions for IM[91] and transitional regime for MIG[40]. Individual stage power measurement (Birmingham University) indicated a slightly lower Po for the bottom impeller in the U.P.M. and the opposite for D.P.M. The effect of increasing MIG diameter appeared to reduce Po, whilst increasing separation increased Po. No effect of vessel scale was been found for IM impellers over the range T=0.29m to T=0.61m.

6. Aerated power characteristics.

The authors mentioned when discussing unaerated power generally used the same equipment to investigate aerated power consumption. The most extensive study was completed by Hocker[7] using 6DT, disc, MIG 04, MIG 06 and MIG 07. Glycerol solutions as Newtonian, C.M.C. as pseudoplastic and

P.A.A. as viscoelastic were investigated. The power input was considerably influenced by aeration of the media. Po was plotted as a function of Ga at various Fl for constant Fr (see Figures 7, 8 and 9).

For 6DT in Newtonian fluids 3 distinct regions were discernible (see Fig. 7), the first at high Ga (low μ) of horizontal curves showed decreasing Po with increasing Fl as gas cavities were formed behind the blades. The cavities pass through various intermediate states before flooding occurs. This occurs when the pumping capacity of the impeller is not sufficient to overcome the upward flow of gas.

The second region of the 6DT Po vs Ga plot (Fig. 7) showed the convergence of curves for different Fl as even at low gas rates large cavities are formed behind the blades. The third region showed curves for various Fl converging at one Po, this happens at low Ga (high μ) and was characterised by extremely stable gassed cavities. The C.M.C. solutions showed very similar behaviour to the Newtonian but the P.A.A. exhibited different characteristics. The horizontal curves at constant Po converge at higher Ga than with glycerol or C.M.C. The elastic properties of P.A.A. appear to promote stable cavity formation at lower viscosities than in the Newtonian case. Overall the gassed power of the 6DT depends on both Fl and the rheological properties of the fluid.

The MIG 06 operated at H/T=2 exhibited different characteristics to the 6DT. Hocker[7] shows data plotted for C.M.C. at 3 Froude numbers (Fig. 8). The results indicated only a slight dependence of Pog on gas throughput, the largest effect of gas rate being at the lowest Fr and high Ga. As with the 6DT the curves converge at $\sqrt{Ga} \simeq 1000$ (albeit from a smaller spacing). Unlike the 6DT however the convergence corresponds to a slight increase in power as opposed to a decrease. This implies (as with the ungassed case) an increase of power with increased viscosity (again unlike 6DT). Hocker[7] maintained that the wide spacing of the MIG blades (180^{o}) was the reason for the absence of stable cavities even at high

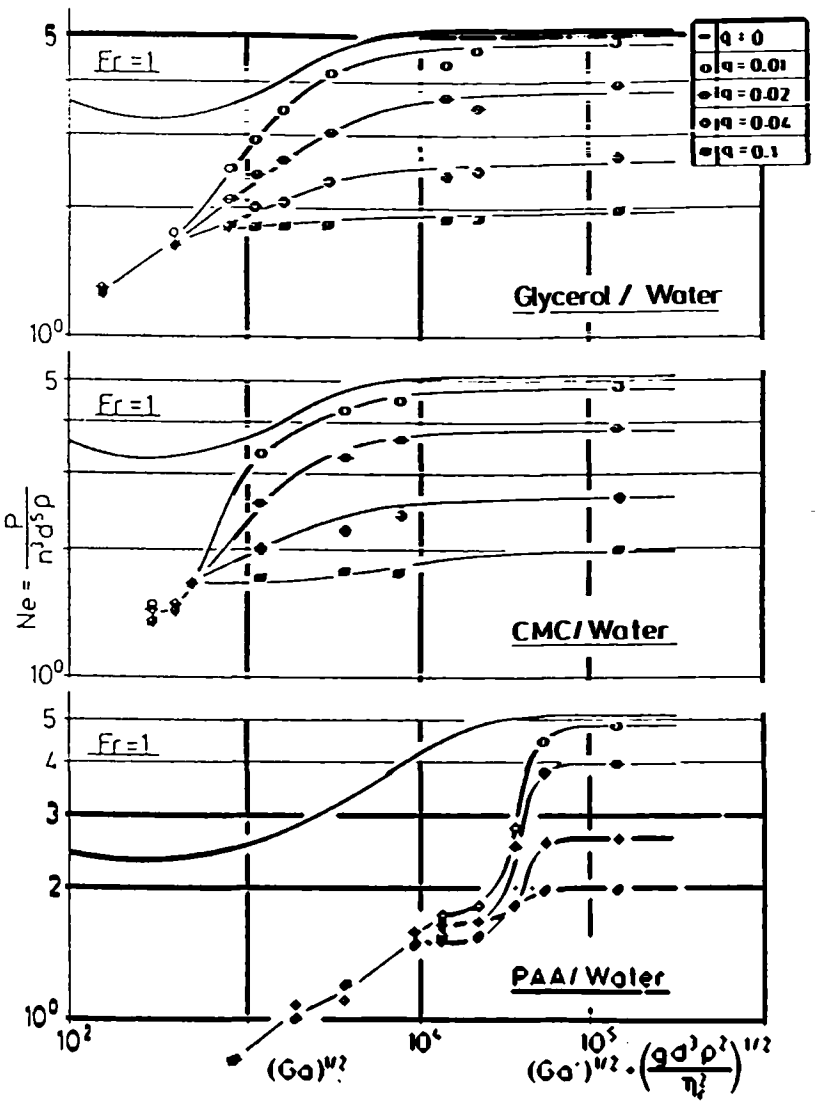

Fig. 7. Power characteristics of flat blade disc turbine Ne = f(Ga) for Fr = 1. Liquids: glycerol/water; CMC/water; PAA/water.

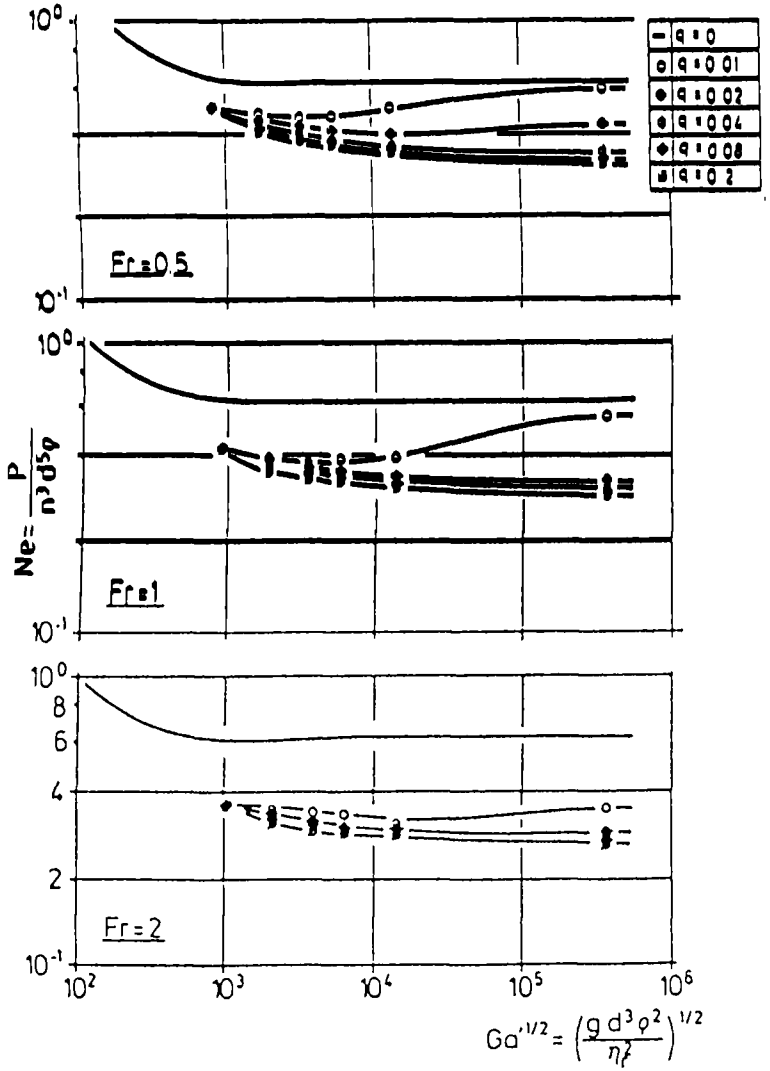

Fig. 8. Power characteristics as a function of Galileo number. Agitator type: MIG-6, H/T = . Liquids: CMC/water solutions.

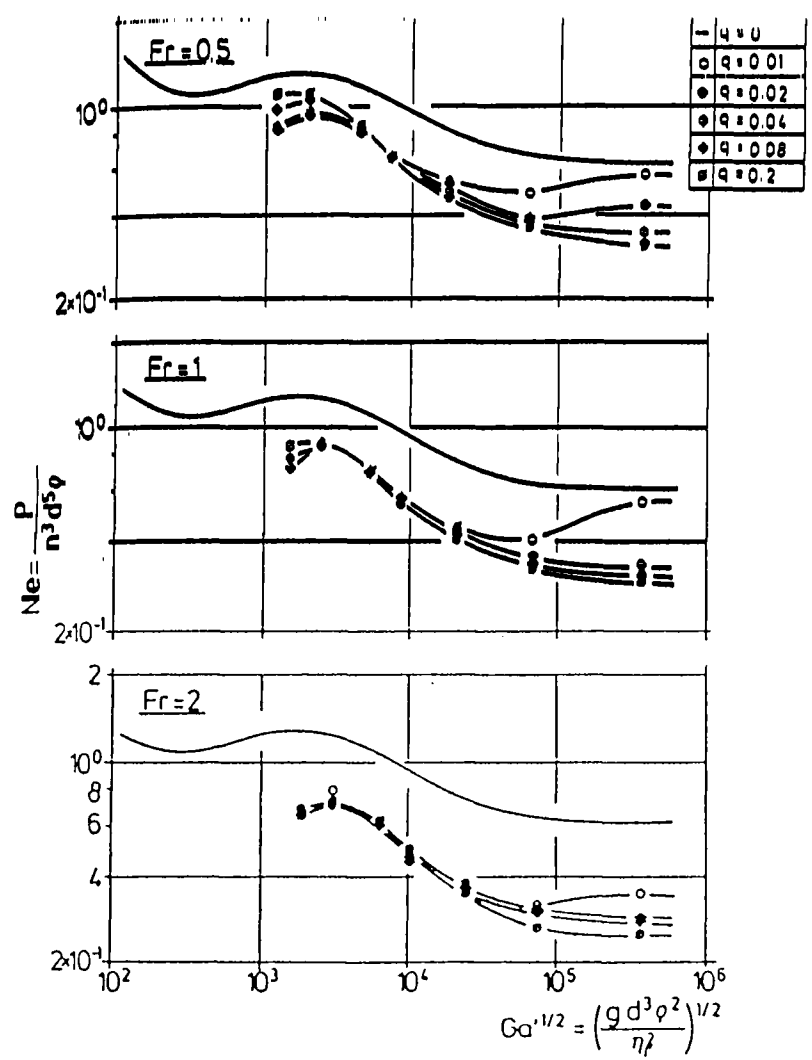

Fig. 9. Power characteristics as a function of Galileo number. Agitator type: MIG-6, H/T = 2. Liquids: PAA/water solutions.

viscosities, hence no reduction in power, though similar results have in fact been found with other impellers.

MIG 06 data is also shown at 3 Froude numbers for P.A.A. solutions (Fig. 9), again the results in P.A.A. were noticeably different from those obtained with C.M.C. As in the unaerated case, the aerated power increased markedly with decreasing $Ga^{\frac{1}{2}}$. The MIG type appears increasingly independent of Fl with increasing N and Fr.

In summary, Hocker[7] observed that at constant speed the 6DT power consumption decreased with increasing viscosity whereas the MIG power consumption remained constant or rose. Also the MIG power consumption was only affected to a small degree by changes in gas flowrate (although it is reduced from the unaerated case). These phenomena may be beneficial during fermentations where the rheological properties of the broth change and/or the air flow may be altered as the MIG impellers would continue to draw roughly the same power.

Kipke[41] reported the power characteristics of IM in C.M.C. solutions (see earlier for geometry etc.) He commented that because the MIG/IM design has only two blades per stage it was not possible for the gas cavities of one blade to interfere with that of the other. Furthermore Kipke[41] assumes that because of the lack of cavity bridging it is not possible to flood a MIG/IM in a manner analogous to a 6DT. This assumption is contentious as the two-phase flow in the vessel may still be gas dominated and hence the stirrer flooded even if bridging cavities are not present. Kipke's flooding definition seems misleading. He shows a Po vs Fl plot for 2 IM 04 at various Froude numbers for μ_a = 1 Pa.s C.M.C. The data indicated that gassed power depends primarily on Froude number (hence N) and there is little or no influence of Fl (hence gas rate) in the range $0.004 < Fl < 0.1$. Although data was shown only for μ_a = 1 Pa.s, Kipke stated that the data applies to both the low and high viscosity range and therefore Pog is independent of μ_a as well as Fl. These

findings agree with Hocker[7] for MIG in various fluids.

Himmelsbach[100] worked with IM and 6DT in Xanthan and reported power consumption decreasing with increasing Froude number as a result of formation of large cavities behind the blades. Himmelsbach also commented that in the viscoelastic Xanthan flooding does not occur in the same way as in less viscous fluids in the turbulent regime. In the turbulent regime flooding happened at constant speed if the gas flowrate was increased, but in Xanthan the impeller may become flooded at low gas rate by an increase in liquid viscosity as cavities become larger and more stable. This he added occurrs easily with 6DT but cannot occur with IM due to the blade separation (180^{o}). Himmelsbach noted the reduction in IM dispersion and circulation capacity in Xanthan when compared with less viscous media. Both Himmelsbach and Kipke appear to call the IM unfloodable only with respect to bridging cavities in high viscosity liquids and not in the turbulent regime for lower viscosity liquids. Henzler[106] provided a figure showing the flooding characteristics of various impellers including 3 MIG 06 and 3 MIG 07 at $Re > 10^{4}$ with respect to Fr (x-axis) and Fl (y-axis). The MIG data was obtained from Hocker[133], it showed the MIG flooding at lower Fl and higher Fr than T/3 6DT.

Schugerl[42] reviewed power data for the MIG and included much of Hockers[7] data. He commented on the point that flooding occurs at higher Fl for MIG but omitted to mention whether this was in high or low viscosity fluids. He included pictures of IM cavities from Kipke using a rotating camera but wrongly calls the impellers MIG. Schugerl stressed that the aerated power requirement does not depend on the gas flow rate either in water or in highly viscous liquids. It should be noted that there is no evidence to support the assertion that gas rate does not influence aerated power requirement in water. The influence of gas rate in water may be low but is certainly present. Also, due to the large distance between blades the gas cavity formation is suppressed and power

input increases with increasing viscosity.

Matthew Hall[132] mentioned that the IM does not have a well defined flooding point and stated that it is less prone to flooding than the 6DT.

Allsford[91] used IM in a range of fluids (see earlier). On the introduction of gas the power was found to fall gradually to Pog/Po = 0.7 for almost all fluids. In viscous fluids (e.g. Corn Syrup) the power was independent of gas flowrate as found by Hocker, Kipke etc. The fall in power on gassing was attributable to the formation of large cavities attached to the split vanes of each agitator blade. The cavities increased in size with increasing speed, stretching up to 75% of the distance to the following blade in Corn Syrup and further still in C.M.C.. The gassed power falls to a value relatively less than that generally exhibited by other impellers. The gassed power of individual stages was found to be roughly equal. The gassed power curve diverges from the ungassed in Corn Syrup at Re≈50. The relative fall on gassing was similar for Corn Syrup, Carbopol and C.M.C. so that the power curves lay in the same relative positions as the ungassed ones (e.g. C.M.C. gassed curve above Carbopol gassed curve).

The constant viscosity Boger fluids used showed different behaviour. In the high viscosity Boger, Pog was always higher than Po at $N \leq 3\ s^{-1}$ (the highest N attainable). However when using other fluids large cavities did not develop until speeds higher than $N = 3\ s^{-1}$ were attained, so a significant drop in power may be seen in Boger fluids at higher N, or so Allsford postulated. No explanation was offered concerning the increase in power on aeration. From the data shown no minima could be seen in the Pog curves for any fluid, they fell steadily over the whole Re range.

Allsford[91] studied the gas dispersion performance of various impeller types and combinations. He commented that IM despite their high D/T exhibited a very poor gas dispersion performance until very high

rotational speeds had been reached. At lower N very large cavities could be observed trailing almost to the following blade as no gas dispersion obscured the view. Allsford also showed a table comparing the gas dispersion performance in 0.8% C.M.C. of the various impeller configurations in terms of both N and P/V. When IM were compared with other twin agitator systems in terms of P/V required for both impellers to disperse gas the following results were obtained. Only the T/2 (6DT + MFU) required marginally less power than the IM 06, all T/3 impeller combinations and T/2 (6DT + MFD) required more power. Single impellers required less power for gas dispersion apart from the T/2 MFD.

Hickman[20] also compared the performance of IM with other impellers at a gas flow of 1/2 vvm, in terms of P/V, N and Re for both bubble cloud formation and complete gas dispersion. IM required more power than any other impeller system used (e.g. 1 or 2 T/2 6DT, 1 or 2 T/3 6DT and T/2 6DT/MF combinations). These findings were in 0.8% C.M.C. and are totally at odds with Allsfords[91] findings in the same fluid and at the same concentration. The power required by IM to disperse gas was however reduced by the use of a ring sparger as opposed to a point sparger (see later).

Hickman found no minima in the IM gassed power curves which were shown for 0.2%, 0.4%, 0.6%, 0.8% and 1.4% C.M.C. solutions. Gas dispersion began at Re = 300 to 500 but complete dispersion could not be attained at all in 1.4% C.M.C. Ring spargers are thought to aid gas dispersion in IM as they deliver gas to the blade tips which are the fastest moving parts of the impeller and therefore produce the highest shear stress and bubble breakup. Hickman also noted a fall in Pog/Po with increasing Re as the gassed power fell faster than the ungassed power. No effect of C.M.C. concentration on aerated power was seen in the range 0.2% to 0.6%, however the 0.8% C.M.C. power curve was slightly lower and the 1.4% showed drastically reduced Pog at equivalent Re.

In 0.6% C.M.C. Hickman's data showed the effect of rotation direction on Pog, D.P.M. drawing more power than U.P.M. until Re > 1500. The gassed hold-up also appeared to be unaffected by both rotation direction and a change in gas rate from 0.5 vvm to 1 vvm in all concentrations of C.M.C. except 0.2%. In the 0.2% C.M.C. solution the hold-up was increased by an increase in Q_G.

In summary the addition of gas to a vessel agitated by MIG/IM causes a marked reduction in power drawn. The two-phase regime may be gas dominated (flooded), gas partially dispersed (loaded) or gas completely dispersed throughout the vessel. A number of authors (Hocker[7], Kipke[41]) claim MIG/IM cannot be flooded, others (Henzler[106], Hickman[20], Allsford[91]) demonstrated that it can and indeed may be flooded at higher N and lower Q_G than the T/3 6DT, for example. This difference may stem from a variation in the definition of 'flooding'. Gas dispersion with MIG/IM requires higher speeds than with 6DT although authors differ as to whether higher power inputs are required (Hickman[20], Allsford[91]). All authors comment on the small or non-existent effect of gas flowrate variation on the aerated power drawn by MIG/IM. Hocker[7] found the largest effect of Q_G at low N and low μ. Hickman[20] observed an effect of Q_G at high N. Hocker[7] found Pog rose with increasing μ and Kipke[41] supported this. Hickman[20] found no effect of C.M.C. concentration until 1.4% was reached when Pog was strongly reduced, which appears to contradict Hocker[7]. All sources indicated the absence of minima in the aerated power curve.

7. Spargers.

Various sparger types have been tested with MIG/IM. Hocker[7] assessed the performance of the following types with respect to mass transfer (k_La vs P/V) performance using 6DT and MIG 06; ring sparger, point sparger, 3-concentric rings and sintered plates. Tests in 1.5% C.M.C. with 6DT indicated little or no effect of the sparger. When using MIG 06 however

the 3-ring nozzle and sintered plate types gave higher k_La values than the centrally located types. Hocker commented that the centrally located ring and point spargers perform worse because gas preferentially rises in the region of the shaft without being fully dispersed.

Hickman[20] indicated that complete gas dispersion occurs at a lower power input when a ring sparger is used. He also compared mass transfer performance in 0.8% C.M.C., the ring sparger was found to increase k_La by a small amount at low P/V. The two types of sparger were found not to affect the gassed power drawn.

8. Vessel vibration.

A range of sources commented that when using MIG/IM strong vibrations of the vessel were apparent during aerated agitation. These vibrations were of a magnitude not normally encountered with other impeller types in two phase operation. Sittig[135] commented that the MIG caused vibration but that the IM should give a smoother performance (although still vibratory). He noted that fermenters mounted on load cells were particularly prone to vibrate as they have a lower natural frequency which lies in the range of the stirrer speed. He also commented that the phenomenon is very weak when no gas is present. Matthew Hall[132] stated that vibration is a problem with large diameter impellers such as MIG/IM and that it could affect load cell performance. Hickman[20] observed severe vibrations with all fluids tested under gassed conditions at high impeller speeds.

Kipke studied the hydraulic forces on different impeller types in order to predict vibration effects on scale-up. Firstly he discussed unaerated conditions[102]. When filling or emptying an agitated vessel shaft deflection was not only dependent on approach to its natural frequency but also on the degree of submergence of the impeller. When run in air only local resonance occurs (due to bearings, gear teeth etc.).

When submerged the system damping is normally increased but this may not be sufficient to suppress local resonance.

Pressure fluctuation in the fluid in front of the impeller blades means forces on individual blades are always of differing magnitudes, leading to a residual force on the shaft in a radial direction. This force is in addition to the unbalanced force normally associated with shafts which may be determined from the shaft speed, critical speed and distance from the C of G. of the piercing point of the shaft on the impeller. Kipke[102] aimed to isolate the unbalanced force from the total radial force and hence estimate hydraulic forces for different agitators. Propellers, 3 MIG and pitched blade turbines were tested in the turbulent regime in water. Hydraulic forces in the tangential and radial directions showed differing behaviour. Tangential forces were found to increase linearly with speed on a double log plot. Radial forces stayed constant in the sub-critical speed range but rose sharply as the critical speed was approached. A maximum was detected at the critical speed. In the supercritical range radial forces fell slightly and then steadily increased. The maximum was caused by an interaction between the vibrating blade (due to shaft deflection) and oscillating flow in front of the blade (due to turbulence). Conclusions were that hydraulic forces are influenced by baffle type/number but that the degree of influence depends on the impeller type. Influence of shaft shape on hydraulic forces was low. Maximum dynamic load on impeller blades were 1.5 to 2.8 times the mean value depending on impeller type.

Kipke[101] went on to consider the influence of gassing on radial impeller forces and resulant tank forces for both 6DT and a range of IM impellers in both water and C.M.C. solutions. Hydraulic radial forces were evaluated by estimating shaft bending moments measured using shaft strain gauges. Tank deflections were measured using displacement pick-ups, the vessels being mounted on rubber-buffers so that the spring

constant and damping could be varied.

Tank vibrations were found to be amplified by aeration. In water at stirrer speeds of 5 to 7 Hz and aeration rates of 0.5 to 3 vvm, tank vibration was 8 to 20 times higher than the unaerated case. The natural frequency of the water filled tank was 6.1 Hz, implying that as the impeller speed approaches the tank natural frequency strong vibrations should occur. The tank vibrations were considerably reduced if the ratio f/f_N was smaller than 0.8 (achieved by altering the tank natural frequency). When radial impeller forces were compared with tank forces the former were found to be much smaller. This implies that the impeller forces were amplified by an internal mass spring system related to the two phase mixture between the impeller tip and baffle/wall.

Kipke[101] assumed a transfer function scheme involving the exciting radial force, internal exciting force and measured tank force interconnected by two internal amplification factors. The effect of P/V (and hence bubble size), gas rate and impeller diameter on the internal amplification factor was assessed. Results showed little effect of impeller diameter (IM 04, 06 and 07) or gas rate but a strong influence of P/V at values greater than 0.3 kW m^{-3} (impeller flooded at < 0.3 kW m^{-3}) with amplification factors up to 15 at 3 kW m^{-3}.

Unaerated tank forces showed a small peak at the tank natural frequency, aerated tank forces showed this peak and a much larger one at the impeller frequency. No reasons were given as to why the impeller frequency does not produce a tank force in the unaerated case. In the aerated case it can be seen that if the impeller frequency approaches the tank natural frequency resonance will occur. When $f/f_N=1$ the impeller diameter <u>does</u> have an effect on tank forces with IM. The T/3 6DT showed only a small increase in tank forces when $f/f_N = 1$.

Conclusions drawn by Kipke[101] included the following. In aerated agitated liquids strong tank vibrations occur if the impeller speed

approaches the tank natural frequency. Gassed reactors vibrate at a frequency equivalent to the impeller speed, non-gassed reactors at their natural frequency. The internal amplification factor between exciting radial force and tank force is mainly influenced by P/V. Influence of impeller shape is weak but the diameter ratio has a strong effect on resultant forces. The viscosity of the liquids did not have a significant influence on impeller or tank forces (Re > 500).

The findings of the two previously mentioned papers [101,102] were drawn together with additional information concerning baffle loading with 3 impeller types including MIG 07[127]. Pressure distribution on the baffle was measured and plotted in dimensionless form against baffle height. Surprisingly both the one stage propeller and T/3 6DT produced a relatively uniform pressure distribution with height whereas the MIG 07 (3 stages) produced a baffle load distribution which increased strongly towards the bottom part of the tank. Absolute baffle load was greater with the small high speed impellers but large diameter stirrers were more influenced by impeller speed. Baffle vibration was found to be composed of both high and low frequency components. The maximum load was roughly double the mean baffle load. If the characteristic baffle frequency is approached by the impeller speed on scale-up, resonance and hence possible baffle flutter or breakage may occur. This may be aggravated by thin wall baffles for heat exchange purposes. The mean baffle load decreased somewhat with an increase in the number of baffles.

9. Mass transfer.

References associated with the manufacturer are Phillip et al.[105], Kipke[41,128] and Himmelsbach[100]. Other German sources are Hocker[7], Henzler[131], and Schugerl[42]. Hickman[20] studied the mass transfer performance of IM at Birmingham University and remains the only U.K. reference other than Matthew Hall[132].

Kipke[41] presented mass transfer data for both T/3 6DT and 2 IM 04 in C.M.C. solutions of varying viscosity. Measurements of k_La was by a dynamic gassing out method. Kipke found a stronger influence on k_La from P/V than from gas rate. No difference between stirrer types was commented on in this paper.

Himmelsbach[100] compared the mass transfer performance of 2 IM 06 and 09 with T/3 6DT in water, 1% and 3% Xanthan using a dynamic gassing out technique. In water and 1% Xanthan the impeller type had no influence on k_La at a given P/V. However in 3% Xanthan the 6DT could not disperse the gas sufficiently and homogenisation suffered, this reduced k_La values to 1/4 of those obtained with IM 06 at equivalent P/V. Kipke[128] utilised the 3% Xanthan data of Himmelsbach[100] but omits the water and 1% Xanthan data.

Phillip et al.[105] tabulated the exponent w, ($k_La \propto (P/V)^w(v_s)^x$) for 1 6DT T/3, 2 IM 06 and 2 InterPROP 05 in water, 1% and 1.7% C.M.C. for H/T from 1 to 4. The tabulated results showed in water little variation in exponent w until H/T = 3 or 4 when it was reduced to half the 2 IM 06 values of 0.38. In 1% and 1.7% C.M.C. the 6DT exponent was roughly half that of the 2 IM 06. The P/V exponent universally increased with increasing H/T.

Hocker[7] studied mass transfer in aerated Newtonian and non-Newtonian fluids using a range of MIG, 6DT and disc agitators in vessels H/T = 1 and 2. The influence of agitator type in a given system was negligible although with highly psuedoplastic fluids an agitator capable of transferring power uniformly into the liquid appeared advantageous. Gas distributors that supplied gas over the whole bottom cross-section were preferable only in conjunction with large diameter impellers.

Schugerl[42] reviewed mass transfer correlations obtained by various workers including Hocker, Henzler et al. and showed no effect of impeller type at similar P/V. Hickman[20] used a steady state k_La measurement technique in water and a number of C.M.C. solutions to compare a number of

agitator configurations (including 2 IM 06) with respect to mass transfer performance. k_La values obtained were found to be dependent on liquid rheology, power input, gassing rate and number/type of impellers. In solutions of low viscosity (0.4% to 0.8% C.M.C.) T/3 6DT gave higher k_La at low P/V than larger impeller types. At high P/V in all solutions the various impeller types gave similar k_La values with the exception of the T/2 6DT/MF combination and the IM which vibrated severely.

10. Fermentation.

Hickman[20] measured the respiratory quotient (R.Q.) of a Bakers yeast culture in a 20 ℓ, H/T=1 vessel using a variety of impeller types. The dry yeast was added to a number of concentrations of C.M.C. and R.Q. measured at different air rates and power inputs. The R.Q. gives an indication of the state of the culture and availability of oxygen. The power input required to produce the lowest R.Q. was recorded for various impeller types. In 0.8% C.M.C. at 1/2 and 1 v.v.m. 2 T/3 6DT provided the required R.Q. at the lowest power input followed by 2 T/2 6DT and 6DT/6MF combination and finally 2 IM at the highest P/V. In 1.4% C.M.C. IM still did not compare favourably with the 2 6DT combinations although it required slightly less power than the T/2 6DT/6MF combination. Hickman concluded that the IM showed a poorer mixing performance than their large diameter and high speed at low power inputs would suggest. He went on to mention that the IM may reveal advantages at H/T > 1.

Griot et al.[136] studied mixing times and mass transfer in bioreactors using an oxygen sensitive microbial culture (Bacillus subtilis). For given operating conditions the product ratio (acetoin/butanediol) could be used to define mixing performance. Comparison of the performance of 2 6DT and 2 IM for viscous non-Newtonian broths was made by using Xanthan as a thickening agent. In 2% Xanthan IM gave roughly constant product ratios at P/V from 2 to 11 kW m^{-3}. 6DT gave lower Ac/Bu ratios at 2 kW m^{-3} but

higher at > 4 kW m^{-3}. Therefore at the lower stirring rate the IM performed best. It was observed that the vertical bulk mixing of the IM was suppressed at high N. Under these conditions caverns formed around each stirrer, a condition observed for 6DT at all speeds.

Buckland et al.[121] discussed improvements in viscous mycelial fermentation performance by agitator retrofitting. In low viscosity broths, if impellers operated above the flooding limit, similar oxygen transfer efficiencies were obtained regardless of impeller type at the same P/V. In high viscosity shear-thinning broths bulk blending was poor due to a tendency to form caverns. Under these conditions large diameter impellers were more energy efficient in achieving bulk blending and were able to achieve better oxygen transfer efficiencies. Improvement in O_2 transfer by changing agitator types was assumed to be primarily due to improvements in bulk mixing. Results were tabulated for replacing two T/3 6DT with either 2 or 3 IM or Prochem impellers that drew the same power and torque and ran at the same speed. Best results may be achieved by using low Po agitators with good top to bottom flow patterns. Changing agitator type represents a cost effective means of process improvement.

RETROFITTING FOR EQUAL SPEED, N; TORQUE, M AND POWER, P[121].

IMPELLER TYPE	NUMBER OF STAGES	D/T
6DT	2	0.33
InterMIG	2	0.58
InterMIG	3	0.54
Prochem	2	0.47
Prochem	3	0.43

Sittig[135] in his review of fermentation, showed a plot of P/V vs V for various industrial fermenters using either MIG/IM or 6DT impellers.

The IM/MIG type were used in protein, antibiotic, ascorbic acid, enzyme and fruit sludge fermentations. The majority were 50 to 100 m^3 in volume with P/V between 0.5 and 2 kW m^{-3}. Two protein fermentations agitated by MIG were 200 and 350 m^3 volume with P/V of 1.5 and 1 kW m^{-3}. Maximum P/V shown by Sittig for any impeller was 2.5 kW m^{-3}.

Ekato[137] listed industrial process plant agitated using MIG, IM, 6DT etc. Most MIG agitated reactors fell within the volume and P/V range given by Sittig[135]. Exceptions were one 30 m^3 antibiotic bioreactor operated at 3 kW m^{-3}, a 20 m^3 enzyme fermenter at 3.5 kW m^{-3} and a 100 m^3 Xanthan fermenter at 4 kW m^{-3}, all with IM.

MASS TRANSFER IN AERATED AGITATED VESSELS : ASSESSMENT OF THE NEL/HICKMAN STEADY STATE METHOD

Cooke, M	ICI Chemicals and Polymers Ltd, U.K.
Dawson, M.K.	The University of Birmingham, U.K.
Moody, G.	National Engineering Laboratory Executive Agency, U.K.
Nienow, A.W.	The University of Birmingham, U.K.
Whitton, M.J.	British Hydromechanics Research Group Ltd, U.K.

1. INTRODUCTION

Many industrial chemical and biochemical processes are limited by the rate at which oxygen can transfer from a gas phase to a liquid phase. The optimisation of gas liquid mass transfer rates in stirred tank reactors, which are commonly used for these processes, is therefore of great interest to industry. The hydrodynamics of this type of process are very complicated and the majority of development work to date has been based on empirical research. A number of experimental methods for investigating these systems have been developed but each method has its limitations.

The majority of published data is confined to the air-water system. Industrial fluids, however, are usually more viscous than water and quite often of non-Newtonian rheology. There is therefore a need for researchers to extend their work into more industrially relevant fluids. One of the stumbling blocks to achieving this is that the experimental methods developed for measuring oxygen transfer rates in the air-water system cannot easily be applied to rheologically-complex systems.

Hickman (1,2) published a novel experimental technique for measuring oxygen transfer rates in gas-liquid dispersions. This technique is potentially simple, low cost and applicable to rheologically-complex fluids.

However, following the instructions given in (2) researchers from Birmingham University, British Hydromechanics Research Group and ICI, have experienced a number of difficulties with the experimental method.

The aims of this paper are to describe the problems encountered with this method, provide solutions to these problems, and clarify the optimum conditions for achieving accurate oxygen transfer measurements.

2. MASS TRANSFER MEASUREMENT

The equation describing oxygen transfer between a gas and a liquid is:

Mass transfer rate = $k_L a (H_e c_G - c_L)$

The parameters of interest are k_L, the liquid film transfer coefficient, and a, the interfacial area per unit volume of liquid. However, it is very difficult to separate a from k_L so usually the combined parameter $k_L a$ is measured.

Experimental methods for measuring $k_L a$ can be divided into transient and steady state methods.

2.1 Transient methods

One example of a transient method is the dynamic gassing out technique which consists of sparging the vessel with pure nitrogen until all oxygen has been stripped from the liquid.

The sparge gas is then rapidly changed from nitrogen to air. By recording the oxygen concentration of the liquid with time, k_La can be calculated (3). However, this calculation requires an assumption about the degree of gas phase mixing, which can lead to large errors (4). However, this error can be reduced (4,5) if the off gas concentration is also recorded (two-probe technique).

2.2 Steady state methods

In this case the concentration of oxygen in each phase is constant with time, as oxygen transfers between the two phases. To achieve this steady state, oxygen must be continuously generated in one phase and continuously removed, at the same rate, from the other phase.

Two examples of steady state techniques are the sulphite method (6), and the yeast culture method (7). In both cases the chemicals used, and/or produced during the experiments, can alter the bubble size distribution and mass transfer characteristics of the system under study. Additional problems include the difficulty of determining the reaction order with the sulphite method (11), and the poor reproducibility of yeast fermentations (7).

3. NEL/HICKMAN TECHNIQUE (1,2)

3.1 Description

Hydrogen peroxide (BDH Ltd, GPR, 30% wt./vol.) is continuously added to the liquid phase where it is broken down by the enzyme Catalase (BDH Ltd or Sigma Chemicals Ltd, bovine liver extract, 2×10^5 enzyme units (EU) /ml).

$$2H_2O_2 \rightarrow 2H_2O + O_2$$

$$r = k\,[H_2O_2]^A\,[cat]^B$$

This reaction rate is first order with respect to hydrogen peroxide (i.e. A=1) and independent of catalase concentration over a wide range (i.e. B=0).

Thus oxygen is continuously produced in the liquid phase. This oxygen is then stripped from the liquid by a continuous flow of air through the vessel. Initially hydrogen peroxide and oxygen accumulate in the liquid phase until a steady state is reached where the reaction rate is balanced by the peroxide addition rate and the rate of oxygen production is equal to the rate of oxygen transfer from the liquid phase to the gas phase.

i.e. $r = Q / V_L$

and $r/2 = OTR = k_La\,\Delta c$

The oxygen concentration driving force is estimated from the liquid dissolved oxygen level and an assumed gas phase mixing model.

For the calculation of k_La the only parameters required are

- Concentration and feed rate of hydrogen peroxide
- Dissolved oxygen concentration at steady state
- Gas flow rate and pressure
- Liquid volume
- Temperature
- Henry's law constant

Hickman (2) claimed that the k_La values obtained from this method were independent of peroxide feed rate and catalase concentration over a wide range of test conditions.

3.2 Experimental equipment and test fluids

Figure 1 shows a typical experimental set up. The range of scales studied was 5l to 5000l.

The authors have used the NEL/Hickman method in the following liquids:

- Deionised water
- 0.1M KCl, or NaCl, solution
- 25 ppm Poly Propylene Glycol solution
- Sodium Carboxy Methyl Cellulose solutions
- Celbi Eucalypt paper fibre suspensions

Two or more dissolved oxygen probes (Electrosense or Schott Gerat (model CG867) polarographic probes) were zeroed and spanned in the agitated, aerated vessel.

A metering pump was used to give an accurate and steady flow of peroxide into the vessel. The peroxide was discharged beneath the liquid surface into a well mixed region.

A suitable amount of catalase enzyme was added to the liquid, see Section 5.1.1. Peroxide was metered into the vessel at a fixed rate until a dissolved oxygen steady state was achieved. The experiment could then be repeated over a range of conditions.

The dissolved oxygen level at steady state (controlled by the peroxide feed rate) was always in the range 130% to 300% of the saturated dissolved oxygen level (8).

The production of water and/or the presence of hydrogen peroxide can affect the rheology of some model fluids. Regular rheological tests are therefore recommended.

The oxygen concentration of the exit gas may also be measured, this gives a check on the oxygen balance of the system.

4. PROBLEMS ENCOUNTERED

4.1 Catalase activity

There has to be a minimum concentration of active catalase in the vessel for the assumption of first order reaction rate, with respect to hydrogen peroxide, to hold. If there is insufficient active catalase either a pseudo steady state will be achieved or no steady state will be achieved at all. A pseudo steady state is a steady dissolved oxygen level which is lower than that which would be obtained in the presence of sufficient catalyst. This leads to an over estimation of k_La.

This problem can manifest itself either through insufficient initial active catalase or through loss of catalase activity with time.

Catalase activity loss can be caused by the following:

Temperature
pH
ionic strength
fluid dynamics
Substrate inhibition

Within the temperature range studied, 10 to 25°C, no significant effect on catalase activity was found.

Departure from neutral pH will result in increased activity loss.

In 0.1M NaCl and KCl solutions a significant loss of activity was observed, compared to deionised water. In 0.1M K_2SO_4 solution, total activity loss occurred immediately.

We have no real evidence to suggest that fluid dynamics affect catalase activity.

High standing concentrations of peroxide have been shown to accelerate catalase activity loss.

In addition, catalase active life has been found to vary significantly with composition of the test medium.

4.2 Probe membrane effects

4.2.1 Mechanical integrity

The mechanical integrity of the dissolved oxygen probes is an essential prerequisite for accurate measurements. We have found that damaged/old membranes or a poor membrane seal to the probe will lead to errors. Where peroxide can contaminate the probe electrolyte, the probe response is found to drift steadily upwards even in the absence of catalase.

This problem will result in a high dissolved oxygen reading, leading to an underestimation of k_La.

4.2.2 Catalase attachment to probe surfaces

The following beaker tests were conducted with the dissolved oxygen probes:

TEST	ACTION	PROBE RESPONSE
1.	a) Expose to peroxide	No change
2.	a) Expose to catalase b) Wash with water c) Expose to peroxide	No change Probe reading increased

Test 1 shows that the probe membrane is not permeable to peroxide.

In test 2, the probe reading increased on exposure to peroxide because of the action of catalase. This catalase became attached to the probe during step 2(a) and was not removed by the water wash. The catalase, which also deposits on the vessel internals, can be deactivated using a 0.1M H_2SO_4 wash, after which the probes no longer respond to peroxide.

As above this problem can lead to the under estimation of k_La.

4.2.3 Position and orientation

As in all k_La measurement techniques, incorrect dissolved oxygen readings can result from poorly positioned probes. This can be caused by either local depletion of oxygen (polarographic probes consume oxygen) due to poor local mixing when compared with the bulk mixing, or air bubbles attaching to the probe membrane. The former gives low dissolved oxygen readings, i.e. over estimated k_La, the latter gives high dissolved oxygen readings, i.e. under estimated k_La. A suitable probe position is in the impeller discharge stream as shown in Fig.1.

5. SOLUTIONS TO TECHNICAL PROBLEMS

5.1 Catalase activity

5.1.1 Estimation of required initial catalase concentration

The minimum catalase concentration required for the break down of peroxide can be calculated as follows:

The first stage is to estimate the maximum k_La likely under the range of experimental conditions.

The maximum oxygen transfer rate is then calculated from:

$$OTR_{MAX} = k_La_{MAX} (c_L - H_ec_G)$$

At the maximum k_La, the peroxide induced equilibrium must be at least 130% of the air equilibrium, Section 3.2.

i.e. $c_L = 1.3 * c_{L\,(\text{AT AIR EQUILIBRIUM})}$

$c_{L\,(\text{AT AIR EQUILIBRIUM})}$ is easily measured.

H_e is estimated using literature data for the air- water system.

c_G is estimated from an ideal gas phase mixing model. The simplest assumption is the no depletion/enrichment model.

i.e. $c_G = c_{G\,(\text{AIR INLET})}$

The required peroxide feed rate is then calculated:

$Q_{MAX} = OTR_{MAX} * 2V_L$

The concentration of catalase required to break down a peroxide feed rate of Q_{MAX} in one minute can be calculated using the following information:

Catalase activity = $2x10^5$ EU/ml, and 1 EU decomposes 1 μmol H_2O_2 /min, (9).

In practice, the authors have found that to achieve a steady state in a reasonable time and to avoid high standing concentrations of peroxide, the actual catalase concentration needs to be at least fifteen times this calculated value. Since the initial catalase concentration required is proportional to k_La, fig. 2, it is obviously very system dependent.

At high catalase concentrations (high k_La), surface effects due to catalase deposition are exacerbated. The coalescence behaviour of the system may also be affected.

5.1.2 Activity loss

Activity loss is minimised by avoiding large standing concentrations of peroxide in the liquid. This is achieved by running experiments at a high catalase concentration and the minimum allowable peroxide feed rate.

The standing peroxide concentration can be checked by adding a small quantity of catalase to the liquid during an experiment. The dissolved oxygen level will rapidly increase and then it should return to the original steady state level. If the resulting peak is very large, it shows that the standing concentration of peroxide is too high. If this occurs, more catalase should be added to the system. High concentrations of peroxide can be avoided by making periodic small additions of catalase to balance the activity loss.

In extreme cases of activity loss, k_La will be over-estimated, see Section 4.1. To avoid this situation, it is useful to measure the off gas oxygen concentration as this allows a check on the mass balance of the system. Any disagreement between the mass balance calculations and the oxygen concentration measurements indicates a problem.

A set of base line experimental conditions should be chosen and repeated at regular intervals to check the reproducibility of the results.

5.2 Probe care and checks

5.2.1 Mechanical integrity

The probes can be checked before use by starting the peroxide feed to the agitated, aerated vessel before adding any catalase (N.B. if the vessel has recently contained catalase, all traces of this must be deactivated with a 0.1M H_2SO_4 wash) . A significant increase in the probe dissolved oxygen reading indicates that peroxide is contaminating the probe's electrolyte. The probe must be completely stripped down and reassembled with a new membrane.

Improved reproducibility has been obtained, with the Electrosense probes, by using heavy duty (25 μm) polypropylene membranes (supplied by Uniprobe Ltd) rather than thin (10 μm) PTFE membranes. The heavy duty membranes also reduce the probe's consumption of oxygen helping to avoid the problems described in Section 4.2.3.

6. EXPERIMENTAL RESULTS

Experimental data for a Rushton turbine in a range of test liquids are given in figures 3 to 6.

In deionised water, fig. 3, and KCl solution, fig. 4, the steady state method gave good agreement with the transient two probe method. This indicates that the chemicals used in the NEL/Hickman method do not significantly affect the k_La of the test medium.

In PPG solution, fig. 5, and CMC solution, fig. 6, the steady state method gave k_La values significantly higher than the transient method. This was the result of the large hold up of tiny bubbles in these liquids.

The transient method described cannot be applied to systems which contain a large hold up of tiny bubbles (i.e. < 1mm in diameter) which have a long residence time compared with their equilibrium time. These bubbles act as an additional oxygen sink which slows down the transient response of the liquid phase, (10). Therefore, the transient method will always underestimate k_La.

A steady state method avoids the problem caused by the tiny bubble hold up because there are no transients to inhibit. Thus the steady state technique gives a better estimate of the system k_La.

7. CONCLUSIONS

1. The NEL/Hickman steady state method is relatively simple, effective and gives reproducible results if the correct procedures are followed.

2. For the measurement of oxygen mass transfer rates from air in systems containing very small bubbles a steady state experimental method is essential because the two-probe transient method will under estimate k_La.

3. The mechanical integrity and positioning of dissolved oxygen electrodes is vital to the successful implementation of the NEL/Hickman technique.

4. The concentration of active catalase in the system must be maintained at a level of at least fifteen times the stoichiometric requirement.

5. The technique has been successfully used to measure k_La values up to 0.5 s^{-1}. The high catalase concentrations required for these measurements increase the level of catalase deposition on vessel and probe surfaces.

8. ACKNOWLEDGEMENTS

Support from the following is gratefully acknowledged: NEL for work at the University of Birmingham (including M.K. Dawson) and members of the FMP consortium for work at BHR Group Ltd.

9. NOMENCLATURE

a	Specific interfacial area	m^2/m^3
c_G	Gas phase oxygen concentration	$kmol/m^3$
c_L	Liquid phase oxygen concentration	$kmol/m^3$
H_e	Henry's law constant	-

k	Reaction rate constant	$kmol/m^3s$
k_L	Liquid film transfer coefficient	m/s
OTR	Oxygen transfer rate	$kmol/s$
P_t	Impeller power input	kW/m^3
r	Reaction rate	$kmol/m^3s$
Q	Peroxide feed rate	$kmol/s$
V_L	Liquid volume	m^3
Δc	Concentration driving force	$kmol/m^3$
Vs	Superficial gas velocity	m/s
[cat]	Catalase concentration	$kmol/m^3$
$[H_2O_2]$	Peroxide concentration	$kmol/m^3$

10. REFERENCES

1. Hickman, A.D., Bioreactor Design Club Report, FOTP/D/06, NEL, Scotland, (1987).
2. Hickman, A.D., Proc. 6th Euro. conf. mixing, Pavia, Italy, (1988), BHR Group, Cranfield, 369.
3. Dang, N.D.P., Karrer, D.A., Dunn, I.J., Biotech. & Bioeng., 19, (1977), 853.
4. Chapman, C.M., Gibilaro, L.G., Nienow, A.W., Chem. Eng. Sci., 37, (1982), 891.
5. Cooke, M., Proc. Particle Processing in Liquid Suspension, UCL, (1989), 125.
6. Midoux, N., Charpentier, J.C., Proc. 3rd Euro. conf. mixing, York, England, (1979), BHR Group, Cranfield, Paper F4.
7. Hickman, A.D., Nienow, A.W., Int. conf. on bioreactor fluid dynamics, Cambridge, England, (1986), BHR Group, Cranfield, Paper 22.
8. Dawson, M.K., Bioreactor Design Club Report, NEL, Scotland, (1990).
9. BDH Ltd, chemical supply data.
10. Heijnen, J.J., Van't Riet, K., Wolthuis, A.J., Biotech. & Bioeng., 22, (1980), 1945.
11. Thibault, J., Leduy, A., Davies, A., Can. J. Chem. Eng., 68, (1990), 324.

Figure 1: Experimental set up

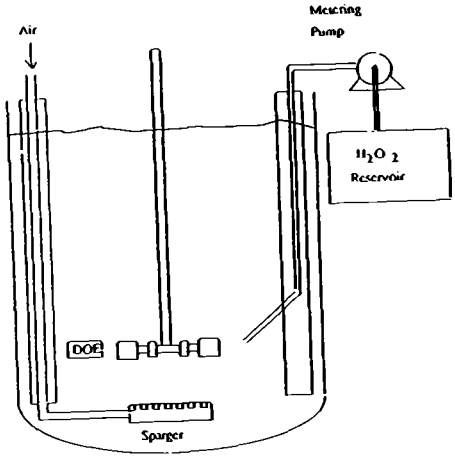

Figure 2: Minimum recommended catalase concentration

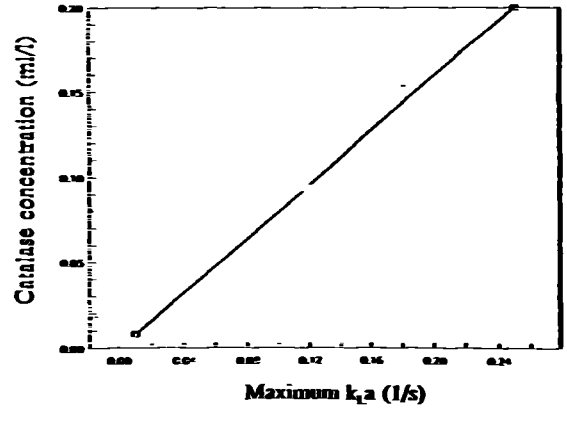

Figure 3

Air-Water Mass Transfer in a 0.3m Diameter Tank

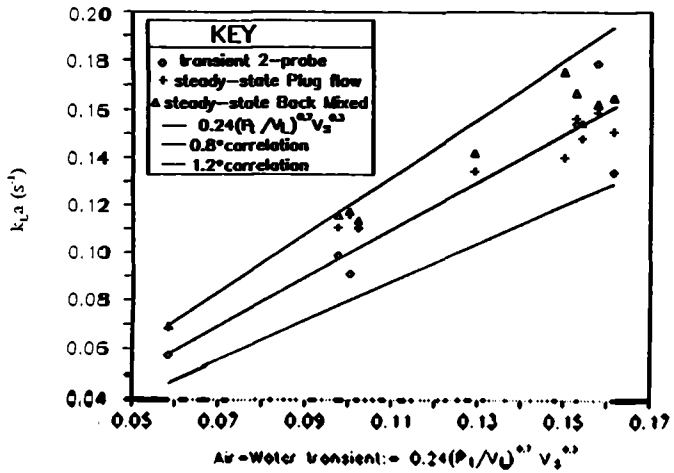

Figure 4

Air-0.1M KCl Mass Transfer in a 0.3m Diameter Tank

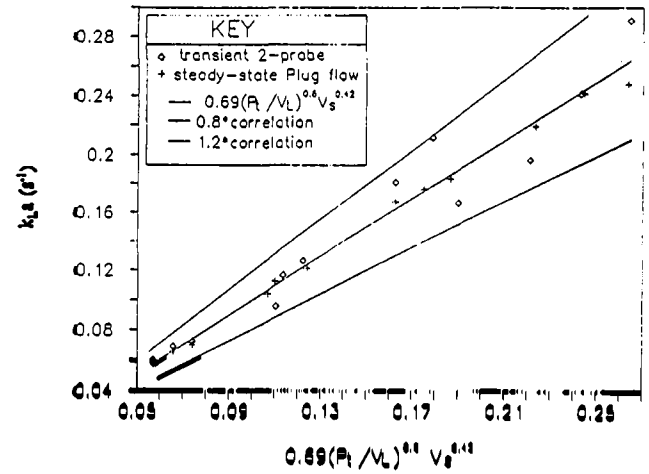

Figure 5

Air-25ppm PPG Mass Transfer in a 0.286m Diameter Tank

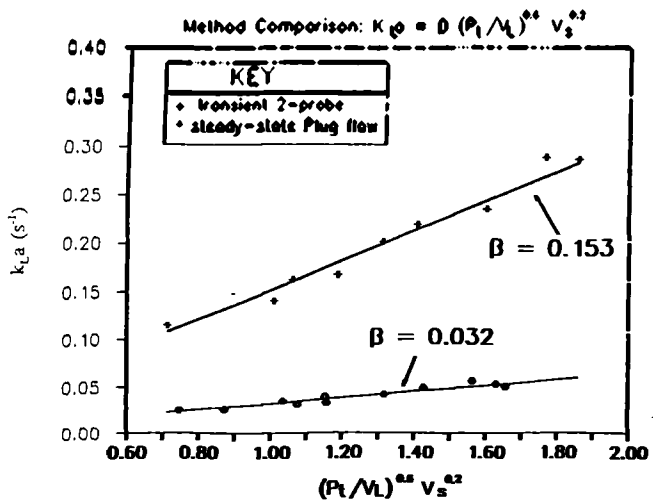

Figure 6

Air-0.4%CMC Mass Transfer in a 0.3M Diameter Tank

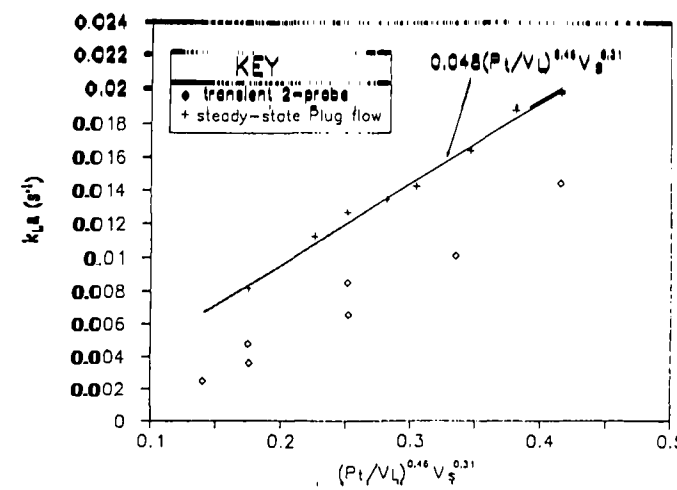

APPENDIX III: NEL/HICKMAN TECHNIQUE.

1. Catalase concentration, activity and interbatch reproducibility.

During early trials using the NEL/Hickman technique the initial catalase concentration ([cat.]) was calculated from the literature[79]. In Hickman's paper a plot of k_La v [cat.] at constant N and Q_G showed no variation in k_La for 0.005 ml ℓ^{-1} < [cat.] < 0.03 ml ℓ^{-1} in water. An enhanced k_La value at [cat.] = 0.075 ml ℓ^{-1} was attributed to changes in the system interfacial properties caused by the high [cat.]. The catalase concentration can be calculated from the stoichiometry for a given O.T.R., but this gives much lower values than Hickman[79] (see Appendix II).

As catalase was supplied in a solution containing both ethanol and glycerol (Section 3.6.3), the concentration at which coalescence may be suppressed was investigated by reference to the literature[47,48]. Kietel and Onken[47] defined a limiting concentration (Co), above which the Sauter mean bubble diameter (measured in an airlift reactor) was reduced in water. For ethanol, Co = 0.002 mol ℓ^{-1} which, if considered as the sole coalescence suppressor, gives Co = 1.14 ml ℓ^{-1} for catalase. For glycerol (Propane-1,2,3-triol) no coalescence data was available so data for Propane-1,3-diol was used instead. This gave Co = 0.001 mol ℓ^{-1}, so considering only glycerol content, Co = 0.24 ml ℓ^{-1} for catalase. Although both lower limiting concentrations are higher than [cat.] used in this work or by Hickman, the coalescence supression of glycerol, ethanol and catalase combined may be influential at lower catalase concentrations. Hence a minimum effective catalase concentration was sought.

Experiments were conducted with 2 IM 055 at constant N, v_s and peroxide addition rate, using water and CMC solutions as test fluids. Water was used because the highest k_La values, O.T.Rs and hence [cat.] were expected, whilst the interfacial properties of water are sensitive to trace chemicals making [cat.] choice more critical. Tests were carried

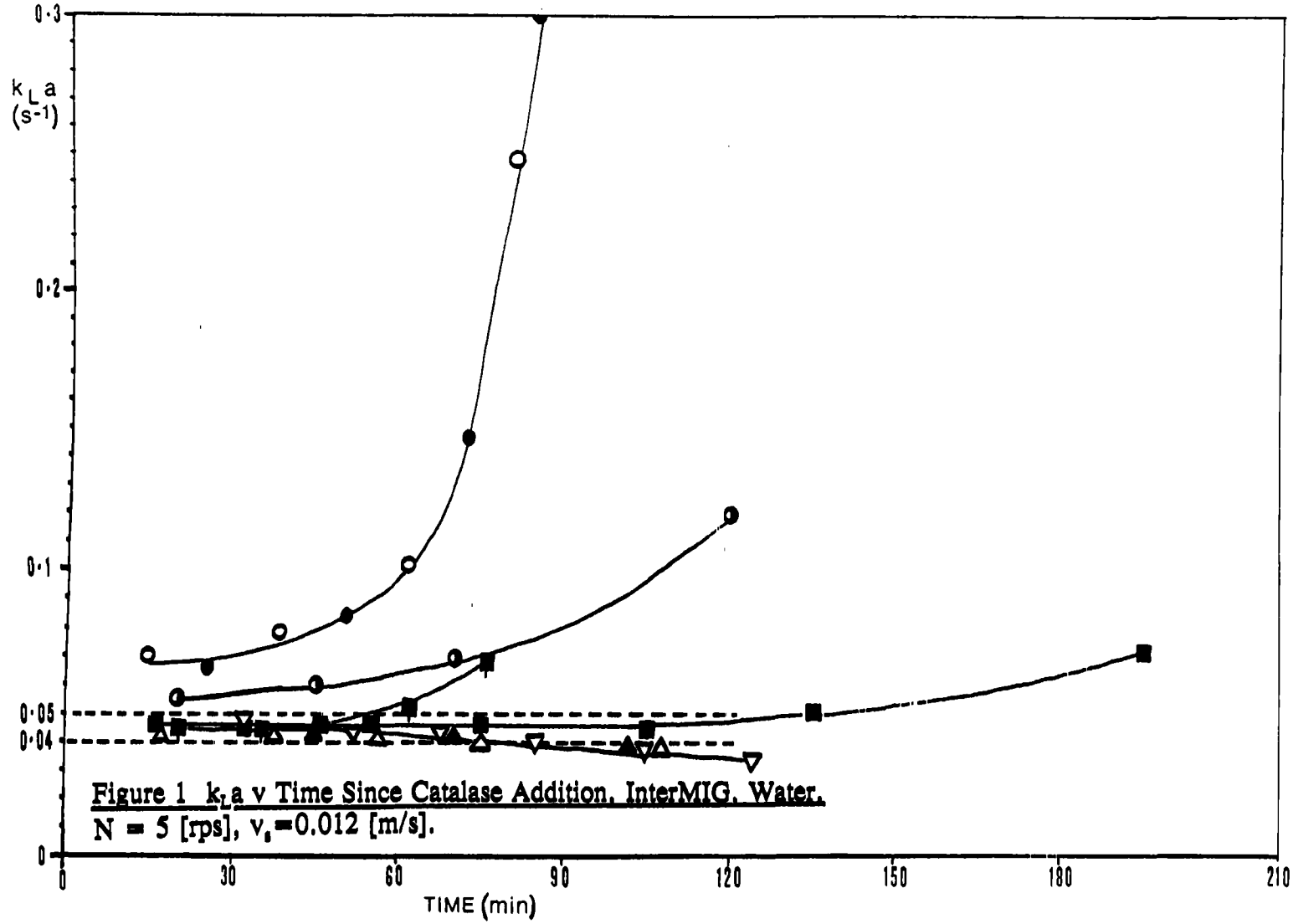

Figure 1 $k_L a$ v Time Since Catalase Addition, InterMIG, Water. N = 5 [rps], v_s=0.012 [m/s].

Deionised Water,[cat.] = 0.017(ml/l): ● .
" " 0.033(ml/l): ▼ , ■ .
" " 0.05(ml/l): △ , ▲ .
" " 0.067(ml/l): ▽ .
0.04% CMC, " 0.017(ml/l): ◑ .
Tap Water, " 0.017(ml/l): ○ .

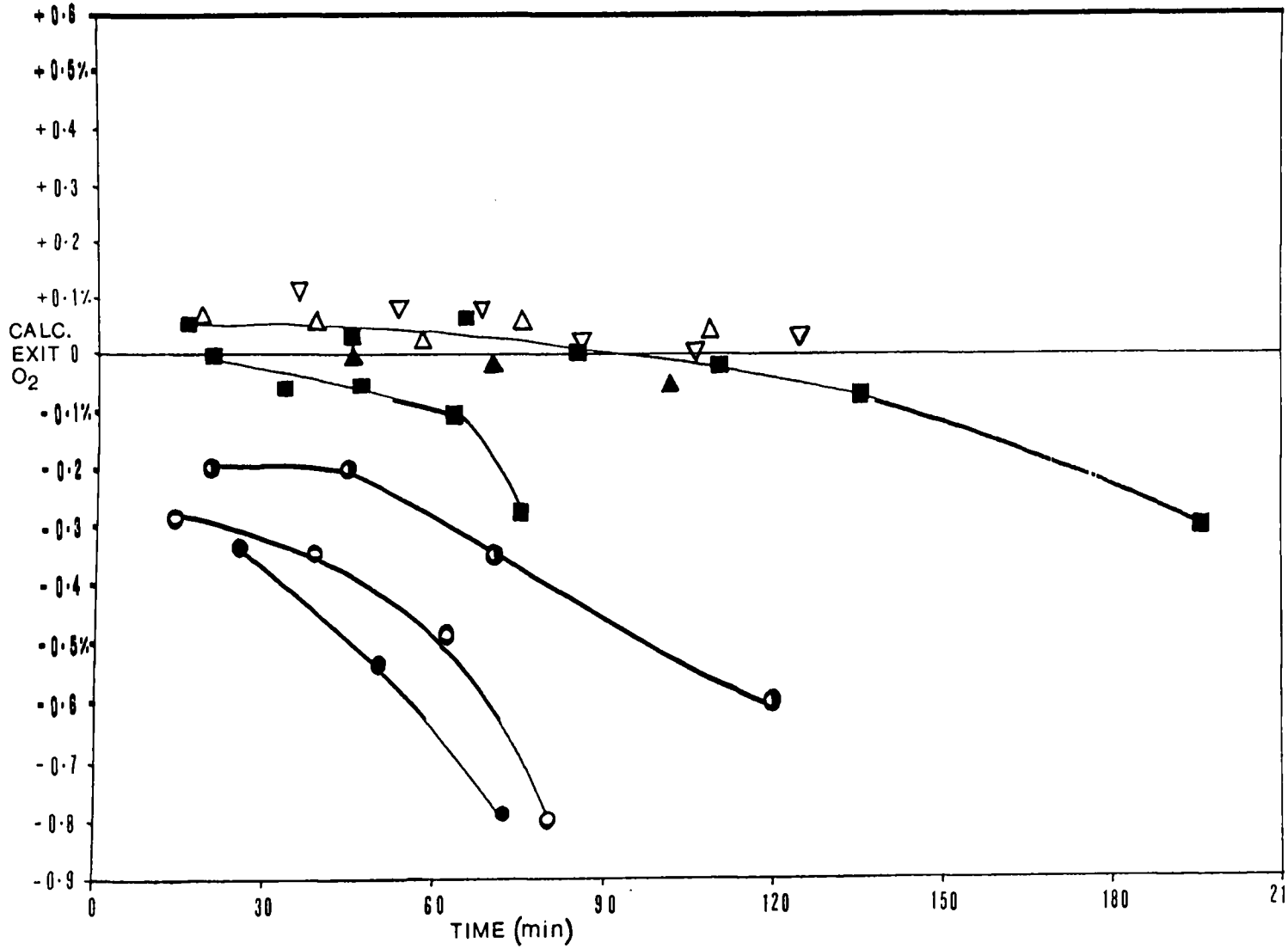

Figure 2 Comparison of Calculated and Measured Exit O_2 Values.

Key as Fig. 1.

out by adding a set amount of catalase and repeating readings for up to four hours to test enzyme activity with time.

Figure 1 shows k_La v time since catalase addition for 4 initial catalase concentrations. Figure 2 shows the difference between measured exit oxygen values and those calculated from the assumed O.T.R. (Appendix III.5) for the corresponding runs as oxygen fraction v time. At [cat.] = 0.017 ml ℓ^{-1}, k_La increased dramatically with time in both deionised and tap water. It was postulated that this effect was due to catalase activity loss. Appendix II details possible causes for activity loss which results in O.T.R. being increasingly overestimated for constant ΔC, giving increased k_La. Evidence in support of the activity loss theory was provided by an increasingly slow reduction in dissolved oxygen when peroxide pumping ceased. Also the measured exit oxygen concentration fell relative to that calculated from the assumed O.T.R. (Fig.2). A [cat.] of 0.017 ml ℓ^{-1} was insufficient for even initial k_La readings in water (Figs. 2 and 6).

The same initial [cat.] provided a less steep increase of k_La with time in 0.04% CMC, possibly due to a stabilizing effect of the polymer. In 0.8% CMC (Figures 3 and 5), 0.017 ml ℓ^{-1} [cat.] provided repeatable k_La results for up to 7 hours, due to lower levels of peroxide (lower k_La) and increased stability.

Increasing initial [cat.] to 0.033 ml ℓ^{-1} gave constant k_La for at least 60 minutes in water, but inconsistent results after a longer period. Initial [cat.] of 0.05 and 0.067 ml ℓ^{-1} gave k_La values very close to those obtained at 0.033 ml ℓ^{-1} but k_La gradually decreased for $t > 60$ minutes. This effect was tentatively ascribed to catalase attachment to and weakening of dissolved oxygen probe membranes (also Appendix II). The effect was of much smaller magnitude than the activity loss (Figures 1 and 2).

In order to avoid the problems of catalase activity loss and high

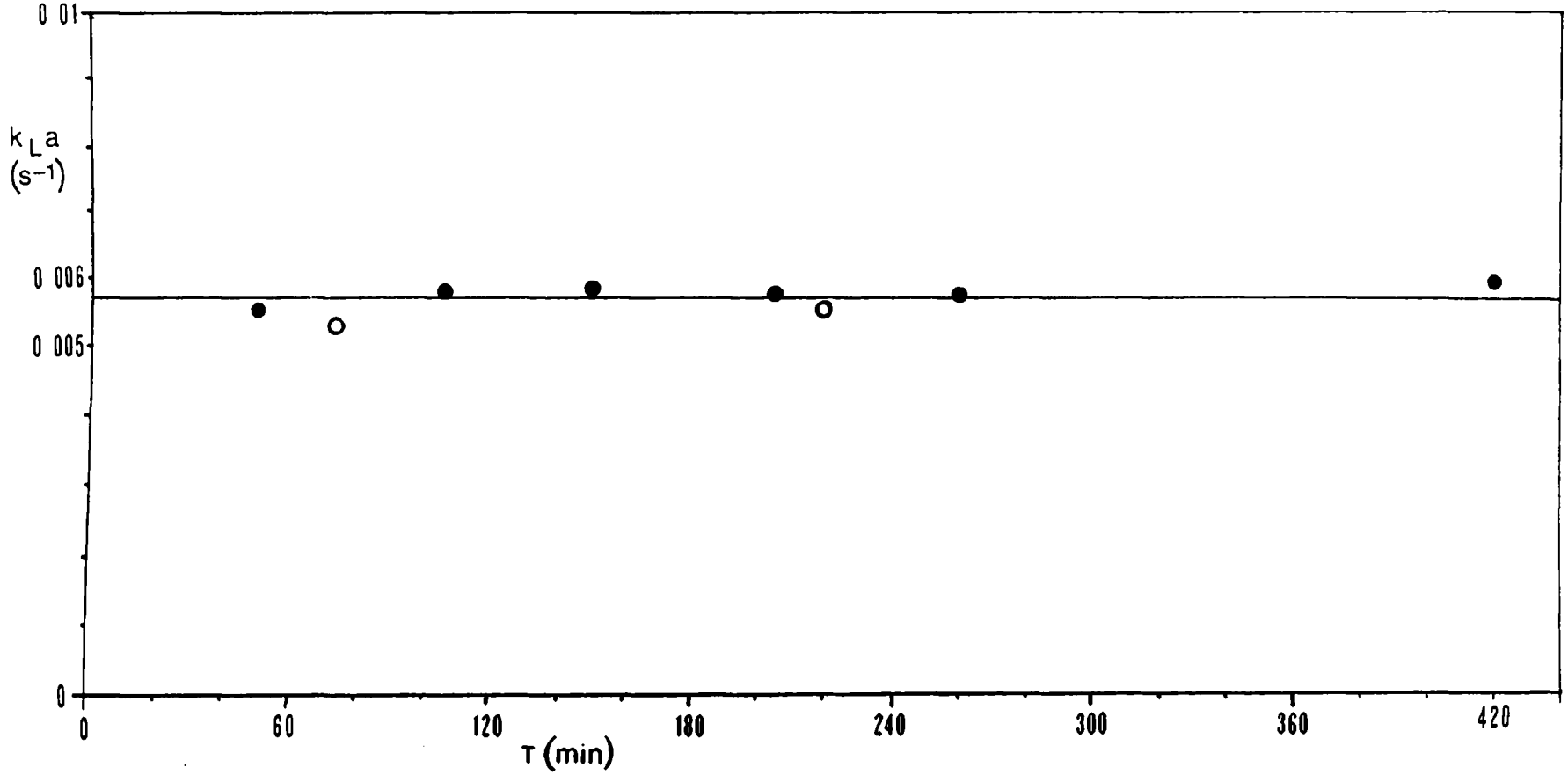

Figure 3 $k_L a$ v Time Since Catalase Addition, InterMIG, 0.8% CMC.

N = 5 [rps], v_s=0.012 [m/s].

Run 1:o, Run 2:●.

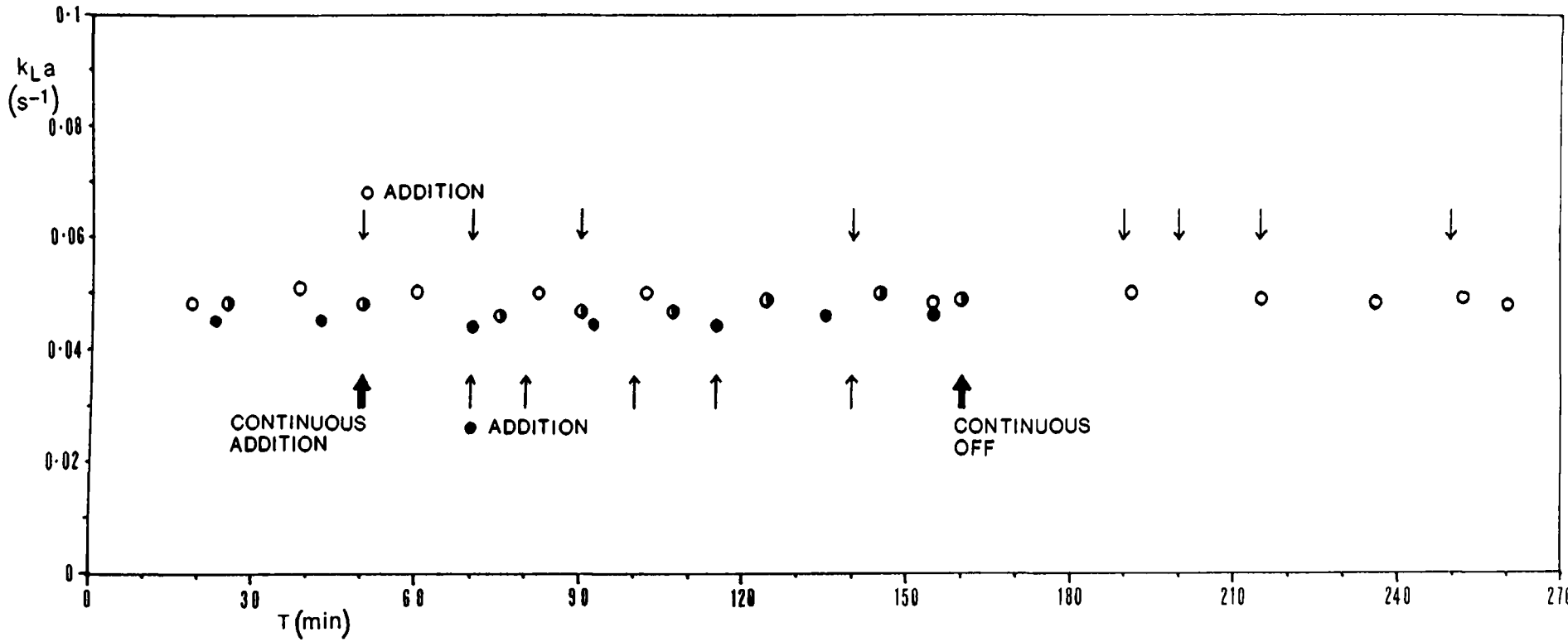

Figure 4 k_La v Time Since Catalase Addition, InterMIG, Water.

N = 5 [rps], v_s=0.012 [m/s].

[cat.]=0.033(ml/l) with Fed Batch Addition, Run 1: o, Run 2: ●.

[cat.]=0.033(ml/l) with Continuous Addition: ◑ .

initial [cat.] additions, both fed-batch and continuous catalase addition methods were tried. The results of these tests are shown in Figures 4 and 5, both of which involved initial addition of 0.033 ml ℓ^{-1} followed by subsequent additions at t > 50 minutes. Repeatable results were obtained for up to 4 hours. The total catalase added to the system never exceeded 0.1 ml ℓ^{-1}.

By combining the initial k_La measurements (within 30 mins of catalase addition) from 15 deionised water batches at constant N and Q_G, both day to day reproducibility and the effect of initial [cat.] can be seen (Fig. 6). For 0.03 < [cat.] < 0.07 ml ℓ^{-1}, all k_La values were within ±10% of the mean value. For [cat.] < 0.02 ml ℓ^{-1}, k_La was overestimated due to insufficient active catalase. At the higher concentrations, (but still less than 0.1 ml ℓ^{-1}), no k_La enhancement due to coalescence suppression was seen.

Recommendations for minimum [cat.] are system dependent. Appendix II details the calculation procedure based on an assumed k_La. Multiplying the resultant value by a factor of 15 (AII.5.1), for the standard N and Q_G, gave a minimum recommended [cat.] of 0.03 to 0.04 ml ℓ^{-1}. This agrees with Fig.6 but ignores activity loss with time.

Generally [cat.] should be calculated using the above mentioned method, but with checks to ensure no activity loss with time and subsequent catalase additions if this occurs. In coalescing systems concentrations of > 0.2 ml ℓ^{-1} should be avoided due to possible coalescence supression, giving a maximum measurable k_La of approximately 0.25 s^{-1} in these systems.

2. Hydrogen peroxide concentration.

Hydrogen peroxide (30% w/v) was used undiluted to minimise changes in vessel liquid volume on addition. Hickman[79] demonstrated a lack of effect of peroxide addition rate on measured k_La in water. High addition

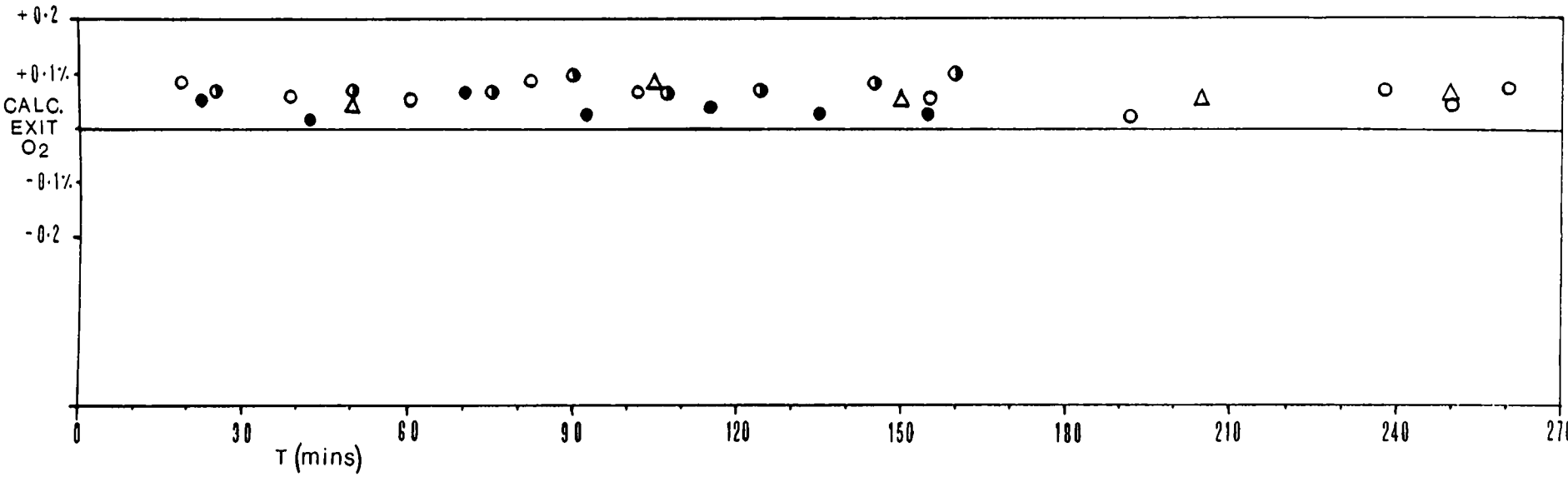

Figure 5 Comparison of Calculated and Measured Exit O_2 Values.

Key as Fig.4 and [cat.] = 0.017(ml/l), 0.8% CMC:Δ.

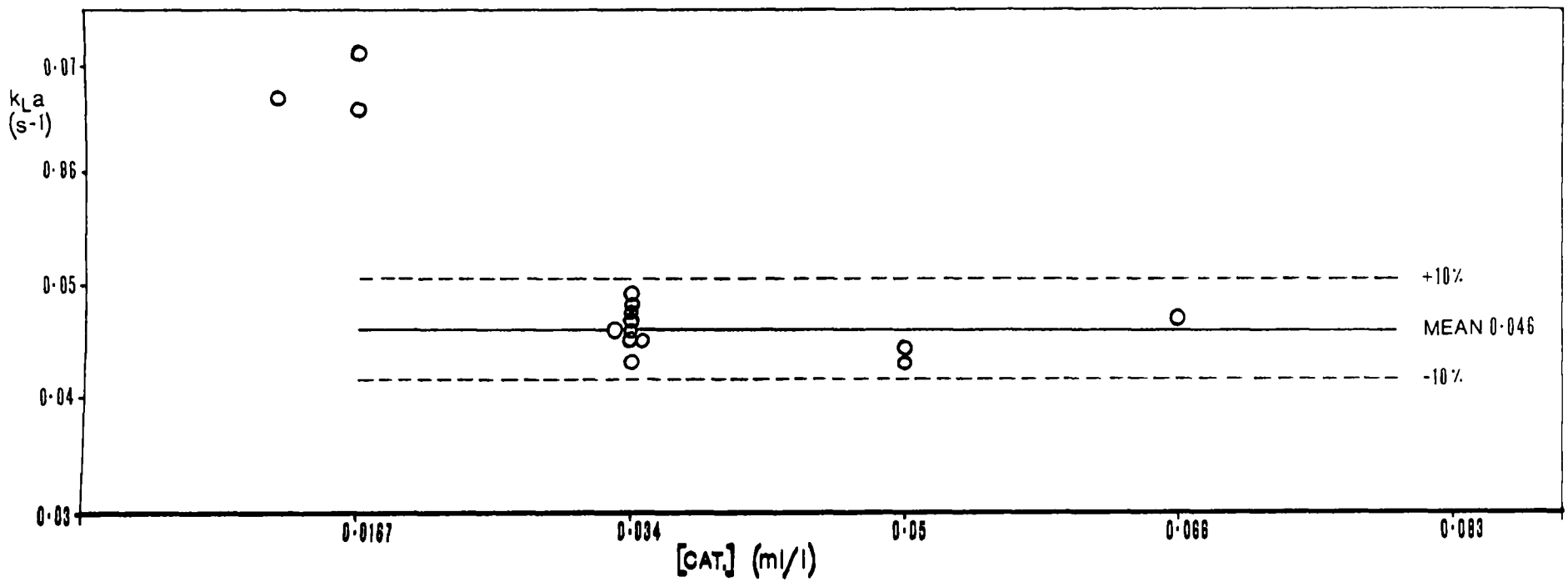

Figure 6 k_La v Catalase Concentration, InterMIG, Water.

N = 5 [rps], v_s = 0.012 [m/s].

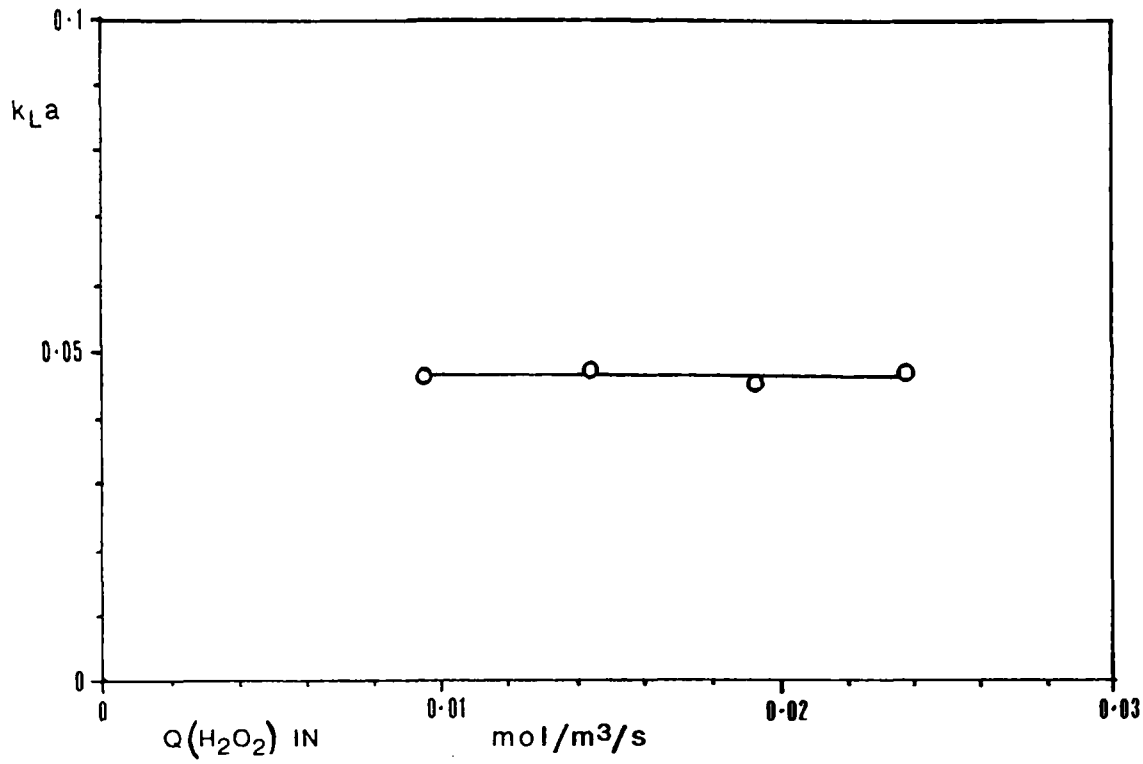

Figure 7 $k_L a$ v Peroxide Flowrate, InterMIG, Water.

[cat.]=0.033(ml/l), N = 5 [rps], v_s = 0.012 [m/s].

rates raise dissolved oxygen in the liquid phase, thus reducing the effect of dO_2 measurement errors on ΔC calculation. On the other hand high standing concentrations of peroxide lead to a faster loss of catalase activity due to substrate inhibition. Choice of peroxide addition rate (adjusted at the pump) is therefore a compromise. Fig.7 shows k_La v specific H_2O_2 molar flowrate in water under standard conditions of agitation and aeration. The [cat.] used was 0.033 ml ℓ^{-1} with subsequent additions to maintain activity. The k_La value was not effected by altering $[H_2O_2]_{in}$. The variation in k_La was of the order of that seen over time since catalase addition (Fig.4) and less than that from day to day (±10%).

3. Multiple dissolved oxygen electrodes.

Multiple dissolved oxygen electrodes were used in order to provide more consistent measurements. When probe readings disagreed the calibration was checked by ceasing peroxide addition and allowing dO_2 to fall to equilibrium. Early warning was therefore given of any probe malfunction. The assumption of a well mixed liquid phase was also tested by multiple dO_2 probe use. Differing probe readings would indicate one or more of the following; probe malfunction, gas bubble attachment, cavitation behind one probe or spacial variation in liquid phase dissolved oxygen.

Generally probe agreement was very good for all agitator geometries in all test fluids. If the ratio of the 2 (or 3) probe signals is defined as $dO_{2(1)}/dO_{2(2)}$ then $0.95 < dO_{2(1)}/dO_{2(2)} < 1.05$. Figs.8 and 9 show A315 k_La calculated from each probe signal in water and 0.8% respectively. This data is intended as a sample to demonstrate the proximity of the multiple probe signals. The k_La data presented in Chapter 7 was calculated by taking the arithmetic mean dO_2 value. The multiple electrode results indicated that the liquid phase could be treated as well

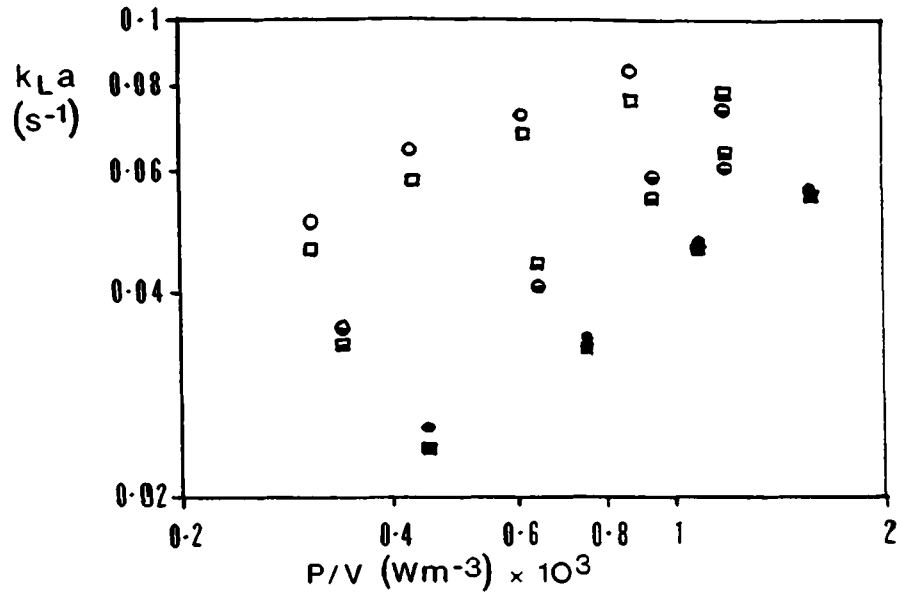

Figure 8 k_La v P/V , A315, Water, Multiple Probe Readings.

Probe 1, v_s = 0.006 [m/s]: ■ ,0.012 [m/s]:◙,0.018 [m/s]: □ .
Probe 2, · :● , · :◒, · : o .

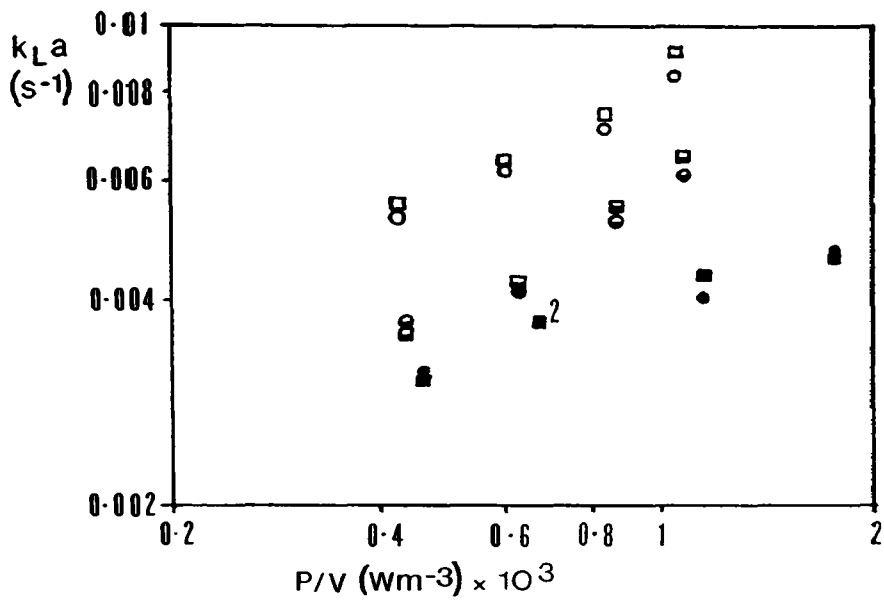

Figure 9 k_La v P/V , A315, 0.8% CMC, Multiple Probe Readings.

Key as Fig.8.

mixed. The only exception to the general probe signal similarity was observed when using either the 6DT or 6PSDT. At the highest speed used for a constant v_s the no.1 (impeller discharge stream) probe signal tended to oscillate wildly in most test liquids. This phenomenon ceased as speed was reduced. The cause was probably the formation of a gas cavity behind the probe due to its location in a region of very high liquid velocity. No other impeller types tested exhibited similar behaviour due to lower discharge stream liquid velocities and hence lower ΔP across the probe.

4. Calculation of $k_L a$ from experimental data.

The determination of $k_L a$ is based on equation 2.33, derived in Chapter 2:

$$Q_{02} = k_L a \ (C^* - C_L) \qquad (2.33)$$

where: Q_{02} = Oxygen Transfer Rate (O.T.R.) per unit reactor volume [mol $m^{-3}s^{-1}$]

C^* = Liquid phase O_2 concentration in equilibrium with the gas phase [mole m^{-3}]

C_L = Actual liquid phase O_2 concentration [moles m^{-3}]

The NEL/Hickman steady-state technique reverses the usual direction of oxygen transfer, so that:

$$Q_{02} = k_L a \ (C_L - C^*) \qquad (A.1)$$

The following calculations assume:-

a) Ideal gas behaviour

b) Well mixed liquid phase

c) The volume fraction of oxygen in air = 0.2095

4.1 Calculation of Q_{02} (O.T.R.)

At steady state, ($dC_L/dt = 0$), the addition rate of hydrogen peroxide is equal to the rate of hydrogen peroxide decomposition, so that:

$$Q_{H_2O_2} \cdot [H_2O_2] \; / \; V = r_1 \qquad (A.2)$$

where $Q_{H_2O_2}$ = Peroxide flowrate [m^3s^{-1}]

$[H_2O_2]$ = Peroxide concentration [$mol.m^3$]

V = Vessel volume [m^3]

r_1 = Rate of peroxide decomposition [$mol.m^{-3}s^{-1}$]

One mole of oxygen is produced by the decomposition of 2 moles of peroxide. At steady state the production rate of oxygen is equal to the rate of oxygen transfer from the liquid to the gas phase.

$$r_1/2 = O.T.R. = k_La\,(C_L - C^*) \qquad (A.3)$$

EXAMPLE

Typical values: $Q_{H_2O_2} = 36.6$ [ml/min]

$= 6.1 \times 10^{-7}$ [m^3s^{-1}]

$[H_2O_2] = 8.8 \times 10^3$ [$mol.m^{-3}$]

$V = 0.293$ [m^3]

$$O.T.R. = \frac{(6.1 \times 10^{-7} 8.8 \times 10^3/0.293)}{2} = 9.16 \times 10^{-3} \text{ [mol.m}^{-3}\text{s}^{-1}\text{]}$$

4.2 Calculation of the driving force ($C_L - C^*$)

The dissolved oxygen probes were spanned (100% reading) at vessel temperature, T_v [K] and vessel pressure, P_v [atm.]

$$P_v = P_h + P_s + 1 \text{ [atm.]}$$

where

P_h = Head pressure [mm.Hg/760]

P_s = Static pressure [m H_2O/10.33]

Static pressure, (P_s), was assumed to be equivalent to H/2 [m H_2O].

At T_v, one atmosphere of water saturated air comprises:

w% water vapour + (100-w)% dry air. Tabulated values of w were used[138].

The pressure of oxygen in the gas phase at probe calibration conditions, (T_v, P_v), is given by:

$$pO_2^{cal} = P_v . 0.2095 . \frac{100-w}{100} \qquad (A.4)$$

The liquid phase oxygen concentration is:

$$C_L = pO_2^{cal} H \frac{C_{LO2}}{100} \qquad (A.5)$$

where H = Henry's coefficient [mol O_2/m^3/atm. O_2]

C_{LO2} = Dissolved oxygen probe reading [%]

From Chapter 2, Henry's Law relates gas (p_i) and liquid (c_i) phase oxygen concentrations at equilibrium:

$$Hc_i = p_i \qquad (2.24)$$

where H = Henry's law coefficient.

For water, from the International Critical Tables[139]

H = 0.2663 moles O_2/m^3 water/atm. air at 25°C

Temperature correction : Add 1.56% for each drop of 1 °C

$$H = 0.2663 \left(\frac{100 + ((25 - T_v)\ 1.56)}{100} \right)$$

In terms of oxygen partial pressure:

$H = \frac{0.2663}{0.2095} = 1.271$ moles O_2/m^3 water/atm. O_2 at 25°C

Wasan et.al.[140] presented data indicating a solubility reduction in

deionised water of from 1.4% in 0.06% CMC to 2.9% in 0.5% CMC. Hickman[20] presented the following solubility data (at 25°C):

0.8% C.M.C.: $H = 1.22 - 1.268$ mol.$O_2/m^3/atm.O_2$

1% C.M.C.: $H = 1.225$ mol.$O_2/m^3/atm.O_2$

This gives a maximum reduction in solubility of 3.6% for 1% CMC. For the CMC concentrations used in this work, the literature indicates a negligible reduction in solubility from that of water. The solubility of oxygen in water was therefore used when calculating results in CMC.

For NaCl solution (1.93 M) from the International Critical Tables[139]

$H = 0.141$ moles O_2/m^3 water/atm.air at 25°C

Therefore 0 M NaCl : $H = 0.2663$ mol/m^3/atm.air

1.93 M NaCl : $H = 0.141$ mol/m^3/atm.air

For 0.2 M NaCl

$$H = 0.2663 - \left(\frac{0.2663 - 0.141}{1.93} \, 0.2 \right) = 0.2533$$

In terms of oxygen partial pressure:

$$H = \frac{0.2533}{0.2095} = 1.209 \text{ mol.} O_2/m^3/\text{atm.} O_2 \text{ at } 25^\circ C$$

In order to calculate the driving force, values of C^*_{out} (liquid phase O_2 concentration in equilibrium with exit gas) and C^*_{in} (liquid phase O_2 concentration in equilibrium with inlet gas) are needed. The latter may be calculated from:

$$C^*_{in} = pO_2^{cal} \; H \qquad (A.6)$$

Determination of the exit gas oxygen concentration was as follows:

For an ideal gas: $\frac{P_1 V_1}{T_1} = \frac{P_2 V_2}{T_2}$

Also at 273.15 K and 1 atmosphere, 1 mole ideal gas occupies 0.02241 m^3. To find the volume of air containing 1 mole oxygen at probe calibration conditions.

$$V_2 = P_1 V_1 T_2 / P_2 T_1 \qquad (A.7)$$

$$V_2 = 1\ 0.02241\ T_v / pO_2^{cal}\ 273.15 \qquad [m^3]$$

Oxygen concentration at probe calibration conditions in the gas phase:

$$C_G^{cal} = 1/V_2 \qquad [mol.m^{-3}]$$

The volumetric flowrate of air leaving the vessel:

$$Q_{G(out)} = Q_{G(in)} + \left(\frac{O.T.R.\ V\ R\ T_v}{P_v} \right) \qquad (A.8)$$

where R = Universal gas constant $[JK^{-1}mol^{-1}]$

$Q_{G(in)}$ = Volumetric air flowrate into vessel at T_v, P_v $[m^3 s^{-1}]$

O.T.R. = Oxygen transfer rate $[mol/m^3/s]$

V = Vessel volume $[m^3]$

The oxygen concentration in the exit gas stream is:

$$C_{G(out)} = \frac{(C_G^{cal}\ Q_{G(in)}) + (O.T.R.\ V)}{Q_{G(out)}} \qquad (A.9)$$

The partial pressure of oxygen in the exit stream is:

$$P_2 = P_1 V_1 T_2 / V_2 T_1 = pO_2^{out} \qquad (A.10)$$

where $V_2 = 1/C_{G(out)}$

$P_1 = 1$ [atm]

$V_1 = 0.02241$ $[m^3]$

$T_2 = T_v$

$T_1 = 273.15$ K

$$C^*_{out} = pO_2^{out}\ H \qquad (A.11)$$

The concentration driving force can be calculated on the basis of:

a) Fully back-mixed gas phase, exit O_2 applies to whole vessel.

b) Plug flow gas phase, log mean driving force

For case a): $$\Delta C = C_L - C^*_{out} \qquad (A.12)$$

For case b): $$\Delta C = \frac{(C_L - C^*_{in}) - (C_L - C^*_{out})}{\ln\left(\frac{C_L - C^*_{in}}{C_L - C^*_{out}}\right)} \qquad (A.13)$$

Finally $$k_L a = O.T.R./\Delta C \qquad (A.14)$$

EXAMPLE $R = 8.314\ [JK^{-1}mol^{-1}]$

Typical values $T_v = 24^oC = 297.15K$

$P_h = 52\ [mm\ Hg] = 0.06842\ [atm]$

$P_s = 0.36\ [m\ H_2O] = 0.03485\ [atm]$

$w = 0.02982\ [bar] = 0.02942\ [atm]$

$C_{Lo2} = 180\%$

$Q_{G(in)} = 0.004\ [m^3s^{-1}]$

$P_v = 1 + 0.06842 + 0.03485 = 1.1033\ [atm]$

$pO_2^{cal} = 1.1033\ 0.2095\ 0.9706 = 0.2243\ [atm]$

$$H = \left(\frac{0.2663\left(\frac{100 + (25-24)\ 1.56}{100}\right)}{0.2095}\right) = 1.291\ [mol\ O_2/m^3/atm\ O_2]$$

$C_L = 0.2243\ 1.291\ (\frac{180}{100}) = 0.5212\ [mol\ O_2/m^3]$

$V_2 = (1.0.02241\ 297.15)/(0.2243\ 273.15) = 0.1087\ [m^3]$

$C_G^{cal} = 1/0.1087 = 9.201\ [mol\ m^{-3}]$

$$Q_{G(out)} = 0.004 + \left(\frac{9.16 \times 10^{-3}\ 0.293\ 8.314\ 297.15}{1.1033.101325}\right) = 4.059 \times 10^{-3} \quad [m^3 s^{-1}]$$

$$C_{G(out)} = \frac{(9.201\ 4.0 \times 10^{-3}) + (9.16 \times 10^{-3}\ 0.293)}{4.059 \times 10^{-3}} = 9.728 \ [mol\ m^{-3}]$$

$$p0_2^{out} = (1.0.02241\ 297.15)/\ ((1/9.728)\ 273.15) = 0.2372 \ [atm]$$

$$C^*_{out} = 0.2372\ 1.291 = 0.3062 \ [mol\ m^{-3}]$$

$$C^*_{in} = 0.2243\ 1.291 = 0.2896 \ [mol\ m^{-3}]$$

Fully back-mixed case

$$\Delta C = 0.5212 - 0.3062 = 0.215 \ [mol\ m^{-3}]$$

$$k_L a = 9.16 \times 10^{-3}/0.215 = 0.0426 \ [s^{-1}]$$

Plug flow case

$$\Delta C = \frac{(0.5212 - 0.2896) - (0.5212 - 0.3062)}{\ln\ (\frac{0.5212 - 0.2896}{0.5212 - 0.3062})} = 0.223 \ [mol\ m^{-3}]$$

$$k_L a = 9.16 \times 10^{-3}/0.223 = 0.0411 \ [s^{-1}]$$

5. Estimation of errors.

The equation (Eqn.2.33) defining $k_L a$ makes certain assumptions discussed in Chapter 2 which are generally accepted here. These are a well mixed liquid phase, $1/k_L >> 1/H\ k_g$, and the applicability of Henry's law. Other assumptions are that the volume fraction of oxygen in air is 0.2095 and that air and oxygen behave as ideal gases. Section 3 demonstrated the general agreement of dissolved oxygen probe readings, supporting the well mixed liquid phase assumption. The following section considers maximum estimated errors and their effect on subsequent derived variables and hence $k_L a$. The probability of maximum errors occurring for all parameters in an additive fashion is very low.

From Eqn. A.2, errors in O.T.R. estimation are caused by those from V, $Q_{H_2O_2}$ and $[H_2O_2]$. Liquid volume was measured by visual level check. Initial measurement was 0.72 m ± 0.002 m giving a maximum error of ±0.3%. During a days experimentation with water as a test fluid, up to 5ℓ of water could be produced by decomposition of peroxide. When using CMC test fluids less than 0.1ℓ of water was typically produced. Therefore the maximum error in volume (at H/T = 1) in water was +1.7% at the end of a days experiments. Sample removal, periodic checks and evaporation reduce this error to +1% maximum. This could be reduced further by pumping liquid out of the vessel at a rate equal to the peroxide addition rate, at the expense of added experimental complexity.

The peroxide concentration measurement was reproducible to within ±2% on the same sample. This ignores possible variation of $[H_2O_2]$ over the course of a day. Sample test of $[H_2O_2]$ before and after use of the bulk for k_La experiments showed all results within ±3%. Therefore the maximum error in $[H_2O_2]$ was taken as ±3%.

The peroxide flowrate was measured by weight loss of the peroxide reservoir over a period varying from 10 minutes (water) to 30 minutes (0.8% CMC). Typically from 100g to 400g of H_2O_2 solution was added to the vessel. Balance accuracy was 0.01g, however, rig vibration caused a flickering final digit. Hence measurement accuracy was taken as ±0.1g giving a maximum error of ±0.1% (0.8% CMC) or ±0.04% (water). Run duration was measured using an analogue timer with an assumed accuracy of ±1 s giving a maximum error of ±0.17% over 10 minutes. Maximum flowrate error was therefore ±0.2% in water.

The combination of maximum overestimation of $Q_{H_2O_2}$, $[H_2O_2]$ and underestimation of volume leads to an overall error of +3% or -4% in O.T.R. This degree of error is very unlikely as component errors will cancel each other out to some extent.

The discussion of error arising during the calculation of ΔC is divided into three parts: errors in C_L, in C^* and in driving force ΔC. Firstly, considering errors likely to effect C_L estimation, which are associated with probe calibration pressure, P_v, temperature, T_v, Henry's coefficient and steady state dissolved oxygen measurement. Pressure at the probe is the sum of atmospheric, vessel head pressure and static head due to the liquid depth. When the vessel headspace was pressurised, (only during catalase longevity tests) mercury manometer readings with ±1 mm Hg accuracy gave maximum error of ±2% for a typical 50 mm Hg head pressure. The pressure due to static head varies for each probe. This introduces a maximum error of roughly ±0.2 m water for H/T = 1 where static head was assumed to be constant at 0.36 m H_2O. Atmospheric pressure errors due to changing weather conditions were estimated at ±2%. Maximum error in P_v at probe calibration conditions was therefore approximately ±4%.

Temperature measurement accuracy was ±0.1°C, including variation from probe to probe. An error of 0.1°C introduces a negligible error into the calculation of pO_2^{cal} due to changing water vapour content. Maximum error possible in calculation of pO_2^{cal} was therefore ±4%.

Accuracy of dissolved oxygen probe initial calibration (zero and span) was estimated as ±1%. Drift of the dO_2 signal was never greater than ±2%, unless probe membranes were damaged. Both initial accuracy and lack of drift were aided by careful probe maintenance, calibration and frequent equilibrium dO_2 level checks. Hence overall dissolved oxygen measurement accuracy was ±3%. Probe reading variation from position to position was never greater than ±5% (Appendix III.3), this variation also incorporates the calibration and drift errors.

The solubility of oxygen in deionised water was assumed to be within ±1% of the literature value. In CMC solubility was assumed to be equal to that of water, introducing an error of up to -4%.

The concentration of oxygen in the liquid phase, C_L, can therefore

include a maximum error of ±8% in water and from +7% to -11% in CMC. These errors represent an additive sequence of maxima, typical error in C_L is likely to be within ±4%.

Calculation of C* requires a value of $Q_{G(out)}$ from a mass balance. The volumetric flowrate into the vessel, $Q_{G(in)}$ is therefore required (Eqn. A.8). The inlet flowrate was measured at 10 psig and ambient temperature, maximum error due to calibration, temperature and pressure variation was estimated at ±2%. This error was maintained when converting the volumetric flowrate to vessel temperature, T_V and pressure, P_V. Error in the right hand term in equation A.8 is ±7% maximum. Under typical operating conditions this leads to a maximum error of ±2% in $Q_{G(out)}$.

Calculation of the oxygen concentration in the exit gas stream, $C_{G(out)}$, required a value to be found for $C_{G(cal)}$. From equation A.7 the maximum error introduced into $C_{G(cal)}$ is ±4%. $C_{G(out)}$ error is therefore ±3.8%, as errors in $Q_{G(in)}$ and $Q_{G(out)}$ cancel (Eqn. A.9). Finally the greatest error in C^*_{out} will be ±4.8% (Eqn. A.11).

The example in III.4 shows that the assumption of plug flow or fully back mixed gas phase composition introduces a very small error when using the steady-state technique. The recirculation of gas under most experimental conditions is highly likely, indicating divergence from ideal plug flow behaviour. The assumption of a fully back mixed gas phase implies that all bubbles oxygen concentration is equal to that of the exit gas stream, this is unlikely. Therefore neither model exactly describes the gas phase oxygen composition. In this work the backmixed model has been used for presented data. An overall comparison of the backmixed model with the plug flow model is given in Chapter 7.

Errors incorporated into ΔC depend not only on the errors in C_L and C* but also on the absolute value of C_L. Maximum component error in C* and C_L are ±4.8% and ±8% respectively. The largest single factor causing these potential errors is due to vessel pressure error (up to ±3% and ±4%

respectively). Therefore C* and C_L errors are likely to be of the same sign and hence cancel each other out when calculating ΔC. Henry's coefficient errors will also cancel in ΔC calculation.

At low concentration driving force errors in C_L and C* will have a greater influence than at high ΔC. For example if C_{LO2} = 130% a +2% error in C_L (and hence +1% error in C*) will result in a +6% error in ΔC. However if C_{LO2} = 200%, the same errors in C_L and C* give a ΔC error of only +3%. Therefore the hydrogen peroxide flowrate was adjusted to give high driving forces and thus minimise errors in ΔC.

Assuming the worst possible case, maximum error in ΔC was roughly 20% for C_{LO2} = 130%. A more typical error is approximately ±5%. In this case combined with an O.T.R. error of ±3% the resultant error in k_La would be ±8%. This seems very reasonable considering that the worst case errors have been included (except ΔC) and in comparison with accuracy quoted in the literature. Appendix III.I shows k_La results reproducible to within ±10% on different days with varying [cat.] and H_2O_2 feedrate.

NOMENCLATURE

a	- Interfacial area per unit volume of liquid.	[m^{-1}]
A'	- Gas-liquid interfacial area.	[m^2]
C	- Impeller clearance from vessel base.	[m]
c	- Shaft diameter.	[m]
[cat]	- Catalase concentration.	[$mol.m^{-3}$]
C^*	- Liquid phase O_2 concentration in equilibrium with the gas phase.	[$mol.m^{-3}$]
C_2	- Impeller to liquid surface clearance.	[m]
c_i	- Interfacial O_2 concentration (liquid phase).	[$mol.m^{-3}$]
C_L	- Liquid phase O_2 concentration.	[$mol.m^{-3}$]
C_s	- Sparger clearance from impeller centre line.	[m]
D	- Impeller diameter.	[m]
D_D	- Impeller disc diameter.	[m]
d_h	- Sparger hole diameter.	[m]
D_i	- IM inner blade diameter.	[m]
D_L	- Gas-liquid molecular diffusion coefficient.	[$m^2.s^{-1}$]
DPM	- Downward pumping mode.	[-]
D_s	- Ring sparger diameter.	[m]
d_s	- Sauter bubble diameter.	[m]
d_z	- Sparge pipe diameter.	[m]
e	- Impeller hub outer diameter.	[m]
f	- Frequency.	[s^{-1}]
f_N	- Natural frequency.	[s^{-1}]
g	- Gravitational acceleration.	[$m.s^{-2}$]
H	- Liquid height.	[m]
$[H_2O_2]_{IN}$	- Inlet H_2O_2 concentration.	[$mol.m^{-3}$]
H'	- Henry's law constant.	[mol O_2/m^3/ atm.O_2]
H_g	- Gas-liquid mixture level.	[m]

I	- Impeller hub height.	[m]
K	- Consistency index.	[$N.s^{n}.m^{-1}$]
k_G	- Gas phase mass transfer coefficient.	[$m.s^{-1}$]
k_L	- Liquid phase mass transfer coefficient.	[$m.s^{-1}$]
k_La	- Volumetric mass transfer coefficient.	[s^{-1}]
k_S	- Metzner and Otto constant.	[-]
L	- Impeller blade length.	[m]
M	- Torque.	[N.m]
MW	- Molecular weight.	[$kg.kmol^{-1}$]
N	- Shaft rotational speed.	[s^{-1}]
n	- Flow behaviour index.	[-]
n	- Number of sparger holes.	[-]
OTR	- Oxygen transfer rate.	[$mol.m^{-3}.s^{-1}$]
P	- Pressure.	[$N.m^{-2}$]
P	- Power.	[W]
Pg	- Gassed power.	[W]
p_G	- O_2 partial pressure (gas phase).	[atm.]
P_G	- Power input due to gas stream.	[W]
p_i	- Interfacial O_2 partial pressure (gas phase).	[atm.]
P_t	- Total power.	[W]
Q_G	- Volumetric gas flowrate.	[$m^3.s^{-1}$]
$Q_{H_2O_2}$	- Volumetric flowrate of H_2O_2.	[$m^3.s^{-1}$]
Qo_2	- O_2 transfer rate.	[$mol.m^{-3}.s^{-1}$]
R	- Universal gas constant.	[$J.K^{-1}mol^{-1}$]
r	- Mass transfer rate.	[$mol.s^{-1}$]
RQ	- Respiratory quotient. (moles CO_2 formed / moles O_2 consumed)	
S	- Impeller separation.	[m]
s	- IM outer vane slot width.	[m]
T	- Temperature.	[^{o}K]
T	- Vessel diameter.	[m]

t_c	- Contact time.	[s]
$\bar{u}$	- Mean velocity.	[$m.s^{-1}$]
u'	- Fluctuating velocity.	[$m.s^{-1}$]
u_o	- Velocity of gas at sparger orifice.	[$m.s^{-1}$]
u_{tip}	- Blade tip velocity.	[$m.s^{-1}$]
UPM	- Upward pumping mode.	[-]
V	- Liquid volume.	[m^3]
v_{bs}	- Single bubble rise velocity.	[$m.s^{-1}$]
v_s	- Superficial gas velocity.	[$m.s^{-1}$]
W	- Impeller blade width.	[m]
w	- Water vapour pressure.	[atm.]
x_1	- Blade thickness.	[m]
x_2	- Blade thickness.	[m]

SUBSCRIPTS

F	- Flooding.
CD	- Complete dispersion.
R	- Recirculation.
SA	- Surface aeration.
G	- Gassed or gas.
LB	- Large bubble.
SB	- Small bubble.
V	- Vessel.

GREEK SYMBOLS.

ε	- Local energy dissipation rate.	[$W.kg^{-1}$]
ε_G	- Gassed hold-up.	[%]
ρ	- Density.	[$kg.m^{-3}$]
τ	- Shear stress.	[$N.m^{-2}$]

GREEK SYMBOLS.

ε	- Local energy dissipation rate.	[$W.kg^{-1}$]
ε_G	- Gassed hold-up.	[%]
ρ	- Density.	[$kg.m^{-3}$]
τ	- Shear stress.	[$N.m^{-2}$]
τ_p	- Probe response time.	[s]
δ	- Film thickness.	[m]
μ	- Dynamic viscosity.	[$Ns.m^{-2}$]
μ_a	- Apparent viscosity.	[$Ns.m^{-2}$]
$\dot{\gamma}$	- Shear rate.	[s^{-1}]
$\dot{\gamma}_{AV}$	- Average shear rate.	[s^{-1}]
α	- Fraction of kinetic energy dissipated as turbulence.	[-]
σ	- Surface tension.	[$N.m^{-2}$]

DIMENSIONLESS NUMBERS.

Fl_G	- Gas flow number. (Eqn.2.12)	[-]
Fr	- Froude number. (Eqn.2.11)	[-]
Ga	- Galilei number. (Eqn.2.13)	[-]
Po	-Power number. (Eqn.2.10)	[-]
Pog	- Gassed power number.	[-]
Re	- Reynolds number. (Eqn.2.8)	[-]
Sc	- Schmidt number. (Eqn.7.8)	[-]

ABBREVIATIONS

6DT -Six bladed disc turbine (Rushton turbine).

6MFU -Six bladed mixed flow impeller, pumping up.

6MFD -Six bladed mixed flow impeller, pumping down.

6PSDT -Six bladed pipe section disc turbine.

A315 -Lightnin' A315 hydrofoil.

CMC -Carboxymethylcellulose.

DPM -Downward pumping mode.

UPM -Upward pumping mode.

IM -InterMIG impeller.

T72 -0.72m diameter vessel.

T45 -0.45m diameter vessel.

REFERENCES

1. Barnes, H.A., Hutton, J.F. and Walters, K., "An Introduction to Rheology", Elsevier, (1989).

2. Ranade, V.R. and Ulbrecht, J.J., A.I.Ch.E.Journal, 24, No.5, 796-802, (1978).

3. Ranade, V.R. and Ulbrecht, J.J., 2nd European Conf. on Mixing, Cambridge, BHRA, F6, 83-98, (1977).

4. Metzner, A.B. and Otto, R.E., A.I.Ch.E.Journal, 3, No.3, (1957).

5. Metzner, A.B., Feehs, R.H., Ramos, H.L., Otto, R.E. and Tuthill, J.D., A.I.Ch.E.Journal, 7, 3, (1961).

6. Ducla, J.M., Desplanches, H. and Chevalier, J.L., Chem.Eng.Comm., 21, 29. (1983).

7. Hocker, H., Langer, G. and Werner, U., Ger.Chem.Eng., 4, 51, (1981).

8. Rushton, J.H., Coshck, E.W. and Everett, H.J., Chem.Eng.Prog., 46, 395, (1950).

9. Bates, R.L., Fondy, P.L. and Corpstein, R.R., Ind.Eng.Chem. (P.D.D.), 2, (4), 310, (1963).

10. Uhl, V.W. and Gray, J.B., 'Mixing Theory and Practice', Vol.I, Academic Press, London, (1966).

11. Nienow, A.W. and Miles, D., Ind.Eng.Chem. (P.D.D.), 10, 443, (1971).

12. Bujalski, W., Ph.D. Thesis, University of Birmingham, (1987).

13. Cronin, D.G., Ph.D. Thesis, University of Birmingham, (1988).

14. Kuboi, R. and Nienow, A.W., Proc. 4th Euro. Conf. on Mixing, Holland, BHRA, Cranfield, 247, (1982).

15. Hudcova, V., Nienow, A.W. and Machon, V., CHISA 87 Prague, E6.3, (1987).

16. Smith, J.M., Warmoeskerken, M.M.C.G. and Zeef, E., A.I.Chem.E. Annual Meeting, Paper 117F, (1986).

17. Solomon, J., Ph.D. Thesis, University of London, (1980).

18. Nienow, A.W., Wisdom, D.J., Solomon, J., Machon, V. and Vlcek, J., Chem.Eng.Comm., 19, 273, (1983).

19. Calderbank, P.H. and Moo-Young, M.B., Trans.Instn.Chem.Eng., 37, 26, (1959).

20. Hickman, A.D., Ph.D. Thesis, University of Birmingham, (1985).

21. Chapman, C.M., Nienow, A.W., Cooke, M. and Middleton, J.C., Chem. Eng. Res. Des., 61, Parts (I-IV), (1983).

22. Nienow, A.W., Wisdom, D.J. and Middleton, J.C., Proc. 2nd Euro. Conf. on Mixing, Cambridge, F1-1, BHRA, Cranfield, (1977).

23. Warmoeskerken, M.M.C.G. and Smith, J.M., Proc. 4th Euro.Conf. on Mixing, Holland, G1, 237, BHRA, Cranfield, (1982).

24. Warmoeskerken, M.M.C.G. and Smith, J.M., Fluid Mixing II, I.Chem.E. Symp.Ser., no.89, p.59, (1984).

25. Nienow, A.W., Warmoeskerken, M.M.C.G., Smith, J.M. and Konno, M., Proc. 5th Euro.Conf. on Mixing, W.Germany, 25, 143, (1985).

26. van't Riet, K. and Smith, J.M., Chem.Eng.Sci., 28, 1031, (1973).

27. Kuboi, R., Nienow, A.W. and Allsford, K.V., Chem.Eng.Comm., 22, 23, (1983).

28. van't Riet, K., Ph.D. Thesis, University of Delft, (1975).

29. Warmoeskerken, M.M.C.G. and Smith, J.M., Chem.Eng.Res.Des., 67, 193, (1989).

30. Cooke, M., Middleton, J.C. and Bush, J.R, Proc. 2nd Int.Conf. on Bioreactor Fluid Dynamics, BHRA, Cranfield, (1988).

31. Saito, F., Nienow, A.W., Chatwin, S. and Moore, I.P.T. (to be published).

32. Frijlink, J.J., Kolijn, N. and Smith, J.M., Fluid Mixing II, I.Chem.E.Symp.Ser. No.89, 49, (1984).

33. Nienow, A.W., Konno, M. and Bujalski, W., Proc. 5th Euro.Conf. on Mixing, W.Germany, BHRA, Cranfield, U.K., pp.1-13, (1985).

34. Nienow, A.W., Kuboi, R., Chapman, C.M. and Allsford, K.V., Proc. Int.Conf. on Physical Modelling of Multiphase Flows, BHRA Cranfield, 417-438, (1983).

35. Bakkar, A. and van der Akkar, H.E.A., I.Chem.E.Symp.Ser. No.121, Fluid Mixing, pp.153-166, (1990).

36. McFarlane, C.M., Ph.D. Thesis, Birmingham University, (1991).

37. Oldshue, J.Y., Paper to Eng.Found.Conf. on Mixing, Henniker, U.S.A. (1987).

38. Balmer, G.J., Moore, I.P.T. and Nienow, A.W., 'Biotechnology Processes; Scale-up and Mixing', (C.S. Ho and J.Y. Oldshue, Eds), A.I.Ch.E., New York, pp.117-127, (1987).

39. Nienow, A.W. and Ulbrecht, J.J., "Mixing of Liquids by Mechanical Agitators", (Ulbrecht, J.J. and Patterson, G.K., Eds), Gordons and Breach, N.Y., 6, (1985).

40. Hocker, H., Langer, G. and Werner, U., Ger.Chem.Eng., 4, 113, (1981).

41. Kipke, K.D., International Symposium on Mixing, Mons, C6-1-21 and XC60-70, (1978).

42. Schugerl, K., Advances in Biochem.Eng., 19, 71, (1981).

43. Calderbank, P.H., Trans.Instn.Chem.Eng., 36, 443, (1958).

44. Dean, J.F. and Webb, C., Int.Conf. on Bioreactor Fluid Dynamics, Cambridge, (1986).

45. Middleton, J.C., "Mixing in the Process Industries", Ch.17, (Ed. Harnby, N., Edwards, N.F., Nienow, A.W.), Butterworths, London, (1985).

46. Machon, V., Vlcek, J. and Kudrna, V., 2nd Euro.Conf. on Mixing, Cambridge F2, (1977).

47. Kietel, G. and Onken, U., Chem.Eng.Comm., 17, (1982).

48. Oolman, T.O. and Blanch, H.W., Chem.Eng.Comm., 43, (1986).

49. Phillip, J., Procter, J.M., Niranjan, K. and Davidson, J.F., Chem. Eng.Sci., 45, 3, 651-664, (1990).

50. Machon, V., Vlcek, J., Nienow, A.W. and Solomon, J., Chem.Eng.J., 19, 67-74, (1980).

51. Warmoeskerken, M.M.C.G., Feijn, J. and Smith, J.M., I.Chem.E.Symp. Ser. No.64, Fluid Mixing, J1-J14, (1981).

52. Nienow, A.W. and Wisdom, D.J., Chem.Eng.Sci., 29, 1994, (1974).

53. Nienow, A.W., Chapman, C.M. and Middleton, J.C., Chem.Eng.J., 17, 111, (1979).

54. Mann, R., 'Gas-Liquid Contacting in Mixing Vessels', I.Chem.E.Ind. Research Fellowship Report, (1983).

55. Bailey, J.E. and Ollis, D.F., 'Biochemical Engineering Fundamentals', McGraw-Hill Book Company (1986).

56. Hixson, A.W., Gaden, E.L., Ind.Eng.Chem., 42, 1792, (1950).

57. Danckwerts, P.V., Ind.Eng.Chem., 43, No. 6, 1460, (1951).

58. Shah, Y.T., Sharma, M.M., Trans.Instn.Chem.Eng., 54, (1976).

59. Sideman, S., Hortacsu, O., Fulton, W., Ind.Eng.Chem., 58, 32, (1966).

60. Rainer, B.W., Chem.Biochem.Eng., 4, 185, (1990).

61. Calderbank, P.H., Trans.Instn.Chem.Eng., 37, (1959).

62. Mehta, V.D., Sharma, M.M., Chem.Eng.Sci., 26, 461, (1971).

63. Robinson, C.W., Wilke, C.R., A.I.Chem.E.J., 20, (1974).

64. Joshi, J.B., Kale, D.D., Chem.Eng.Comm., 3, 15, (1979).

65. Vermeulen, T., Williams, G.M., Langlois, G.E., Chem.Eng.Prog., 51, No.2, 85, (1955).

66. Lee, J.C. and Meyrick, D.L., Trans. Instn. Chem. Engrs., 48, 37, (1970).

67. Lockett, M.J. and Safekourdi, A.A., A.I.Ch.E.J., 23, No.3, 395, (1977).

68. Sridhar, T., Potter, O.E., Chem.Eng.Sci., 35, 683, (1980).

69. Kawecki, W., Reith, T., van Heuvan, J.W. and Beek, W.J., Chem.Eng. Sci., 22, 1519, (1967).

70. Landau, J., Boyle, J., Gomaa, H.G. and Al Taweel, A.M., Can.J.Chem. Eng., 55, 13, (1977).

71. Sridhar, T., Potter, O.E., Chem.Eng.Sci., 33, 1347, (1979).

72. Westerterp, K.R., van Dierendonck, L.L. and de Kraa, J.A., Chem. Eng.Sci., 18, 157, (1963).

73. van't Riet, K., Ind.Eng.Comm., 18, 357, (1979).

74. Heineken, F.G., Biotech.Bioeng., 13, 599, (1971).

75. Moo-Young, M., Blanch, H.W., Adv.Biochem.Eng., 19, 48, (1981).

76. Paca, J., Ettler, P. and Gregr, V., J.Appl.Chem.Biotech., 26, 309, (1976).

77. Zlokarnik, M., Adv.Biochem.Eng., 8, 133, (1978).

78. Judat, H., Ger.Chem.Eng., 5, 357, (1982).

79. Hickman, A.D., 6th Euro.Conf. on Mixing, Pavia, 369, (1988).

80. Ruchti, G., Dunn, I.J. and Bourne, J.R., Biotech.Bioeng., 23, 277, (1981).

81. Heineken, F.G., Biotech.Bioeng., 12, 145, (1970).

82. Linek, V. and Benes, P., Biotech.Bioeng., 19, (1977).

83. Dang, N.D.P., Karrer, D.A. and Dunn, I.J., Biotech.Bioeng., 19, 853, (1977).

84. Linek, V. and Vacek, V., Biotech.Bioeng., 19, (1977).

85. Linek, V., Vacek, V. and Benes, P., Chem.Eng.J., 34, 11, (1987).

86. Votruba, J. and Sobotka, M., Biotech.Bioeng., 18, (1976).

87. Dunn, I.J. and Einsele, A., J.Appl.Chem.Biotech., 25, 707, (1975).

88. Chapman, C.M., Gibilaro, L.G. and Nienow, A.W., Chem.Eng.Sci., 37, 891, (1982).

89. Heijnen, J.J., van't Riet, K., Wolthuis, J., Biotech.Bioeng., 22, 1945, (1980).

90. Spriet, J.A., Botterman, J.H., J.Chem.Tech.Biotechnol., 34A, 137, (1984).

91. Allsford, K.V., Ph.D. Thesis, Birmingham University, (1985).

92. Chatwin, S. and Nienow, A.W., Lab.Sci. and Technol., 19, Sept., (1985).

93. Vogel, A.I., "A text book of quantitative inorganic analysis", 3rd Ed. London, Longmans, Geen and Co. Ltd., pp.256-296, (1961).

94. Hickman, A.D., "Gas-liquid mass transfer in agitated vessels: two experimental techniques for use in fermenters", NEL, BDC/FDTP/PR07, (1989).

95. Yagi, H. and Yoshida, F., Ind.Eng.Chem. (P.D.D.), 14, no.4, (1975).

96. Nishikawa, M., Nakamura, M. and Hashimoto, K., J. of Chem.Eng. Japan, 14, no.3, (1981).

97. Ekato Sales Literature, Research Development in Mixing Technology, Ekato Ruhr-und Mischtechnik GmbH, Schopfheim.

98. Perfect, S., U.G. Research Project, Dept of Chem.Eng., The University of Birmingham, (1984).

99. Ibrahim, S., Ph.D. Thesis, The University of Birmingham, (1992).

100. Himmelsbach, W., Private Communication, K. Kipke to A.W. Nienow.

101. Kipke, K.D., Proc. 4th Euro.Conf. on Mixing, B.H.R.A., Cranfield, K1, 355, (1982).

102. Kipke, K.D., 3rd Euro.Conf. on Mixing, B.H.R.A., York, E1, 244 ,(1979).

103. Kipke, K.D., Bioreaktoreu BMFT-Statusseminar, KFA-Julich, Red.J. Gartzen, (1979).

104. Laufhutte, H.D., Mersmann, A., Chem.Eng.Technol., p 56-63, (1987).

105. Phillip, G., Forschner, P., Schneider, T., Mixing XII, Potosi, Missouri, (1989).

106. Henzler, H.J. , Chem.Ing.Tech., 54, Nr5, (1982).

107. Van de Molen, L. and Van Maanen, H.R.E., Chem.Eng.Sci., 33, 1161, (1978).

108. Singh, V., Hensler, W., Fuchs, R. and Constantinides, A., Proc.Int.Conf. Bioreactor Fluid Dynamics, BHRA, Cranfield, U.K., 231-248,(1986).

109. Glastonbury , J.R. and Levins, D.M., Trans.Instn.Chem.Engrs., 50, 32, (1972).

110. Fort, I., Podvinska, J. and Baloun, R., Coll.Czech.Chem.Commun., 34, 959, (1969).

111. Tatterson, G.B., Yuan, H.S. and Brodkey, R.S., Chem.Eng.Sci., 35, 1369, (1980).

112. Otomo, N., Nienow, A.W. and Dawson, M.K., 1st Year Report, Univ. of Birmingham, (1991).

113. Foust, A.C., Mack, D.E. and Rushton, J.H., Ind.Eng.Chem., 36, 517, (1944).

114. Smith, J.M., van't Riet, K. and Middleton, J.C., 2nd Euro.Conf. on Mixing, F4,(1977).

115. Hassan, I.T.M. and Robinson, C.W., A.I.Ch.E.J., 23, 48-56, (1977).

116. Lopes De Figuereido, M.M. and Calderbank, P.H., Chem.Eng.Sci., 34, 1333-1338, (1979).

117. Calderbank, P.H. and Figuereido, M., Int.Symp.Mixing, Mons, C3, (1978).

118. Mooyman, J.G.m, Biotech.Bioeng., 26, 180-186, (1987).

119. Legrys, G.A., Chem.Eng.Sci., 33, 83-86, (1978).

120. Zlokarnik, M., Chem.Ing.Tech.,m 47, Nr 7, 281-282, (1975).

121. Buckland, B.C., Gbewonyo, K., DiMasi, D., Hunt, G., Westerfield, G. and Nienow, A.W., Biotech.Bioeng., 31, (1988).

122. Davies, S.N., Gibilaro, L.G., Middleton, J.C., Cooke, M. and Lynch, P.M., 5th Euro.Conf. on Mixing, Wurzburg, 6, (1985).

123. Nienow, A.W. and Brocklehurst, P.A., Int.Conf. Bioreactors and Biotransformations, Gleneagles, (1987).

124. Man, K.L., McEwan, D., Working papers for the Technical Review Panel, Bioreactor Design Club, 7, (1989).

125. Crozier, D.B.A., Working papers for the Technical Review Panel, Bioreactor Design Club, N.E.L., 10, (1989).

126. Kipke, K.D., Presentation at the GVC Special Committee Conference "Mixing Operations", Konigstein, (1977).

127. Kipke, K.D., Ger.Chem.Eng., 8, 241-247, translated reprint, (1985).

128. Kipke, K.D., Chemie-Technik 13, Vol.8, pp.46-51, (1984).

129. Crozier, D.B.A., Bioreactor Project Research Symposium, N.E.L., paper 1D, (1989).

130. Gerstenberg, H., Sckuhr, P., Steiner, R., Ger.Chem.Eng., 6, 129-141, (1983).

131. Henzler, H.J., Kauling, J. , Proc. 5th Euro.Conf. on Mixing, Paper 30, 303-312, (1985).

132. Matthew Hall Engineering, Process Plant for Biotechnology, AGITATORS, PPFB/29/1987, Prepared for the Mech.Eng. and Manufacturing Technology Division of the D.T.I., (1987).

133. Hocker, H., Langer, G., Rheol. Acta., 16, 400, (1977).

134. Hocker, H., Langer, G., Werner, U., Chem. Ing. Tech., 52, 916, (1980).

135. Sittig, W., J. Chem. Tech. Biotechnol., 32, 47, (1982).

136. Griot, M., Galindo, E., Heinzle, E., Dunn, I.J., Bourne, J.R., 6th Euro. Conf. on Mixing, Pavia, (1988).

137. Ekato Sales Literature, Process Improvement in Fermentation Using the InterMIG, Ekato Ruhr- und Mischtechnik G.m.b.h., Schopfheim.

138. Rogers, G.F.C. and Mayhew, Y.R., "Thermodynamic and Transport Properties of Fluids", 3rd Ed., Oxford Basil Blackwell, (1981).

139. International Critical Tables, 3, 372, McGraw Hill, New York, (1928).

140. Wasan, D.T., Lynch, M.A., Chad, K.J. and Srinivasan, N., A.I.Ch.E.J., 18, No.5, (1972).